

DIFFUSION IMAGING AND  
TRACTOGRAPHY IN THE PAEDIATRIC  
NEUROSURGICAL POPULATION

Jonathan G Bull

MA MB BChir MRCSGlasg MRCSEng

Harold Bridges Research Fellow

(Royal College of Surgeons of England)

Imaging and Biophysics Unit

UCL Institute for Child Health

30 Guilford Street

London WC1N 1EH

*Thesis submitted for the degree of*

*MD Res*

*University College London*

*2010*

---

## DECLARATION

---

I, Jonathan Bull, confirm that the work presented in this thesis is my own and derived from original observations carried out between February 2006 and January 2008. Where information has been derived from other sources, I confirm that this has been indicated in the thesis.

*This work has been approved for submission for the degree of MD Res by University College London*

The copyright of this thesis rests with the author and no quotation from it or information derived from it may be published without the prior consent of the author.

---

## ABSTRACT

---

Diffusion MRI uses magnetic field gradients to sensitise a MR sequence to in vivo water diffusion. Application of these gradients in specific directions (20 in this work) enables a 3D representation of diffusion on a voxel basis. Quantitative diffusion measures are derived; using the voxel maximal diffusion direction and linking neighbouring voxels iteratively based on this creates a visual construct of the white matter: tractography.

It is not possible, currently, to non-invasively determine the histological nature of an intracranial tumour. We recruited paediatric patients with radiological evidence of such lesions from April 2006 to January 2008 and retrospectively to August 2003. We used diffusion MR metrics to discriminate paediatric central nervous system tumours based on existing histological diagnoses. Using apparent diffusion coefficient histograms, common posterior fossa childhood tumours were differentiated with 93% success; Primitive neuroectodermal tumours (PNET) and supratentorial atypical teratoid rhabdoid tumours (ATRT) were separated in 100% of cases. Development of these methods with a larger population may facilitate the obviation of surgical biopsy and its attendant risks.

Diffusion data was used to reconstruct the cerebellar white matter anatomy using tractography. Initially a population of normal subjects were investigated using single region of interest (ROI) analysis. DTI metrics were implemented, demonstrating the existence of white matter asymmetry where lateralisation corresponded to handedness in 17 right-handed subjects.

To assess functional significance of changes in DTI metrics; clinical cerebellar dysfunction was correlated with changes in cerebellar white matter DTI metrics in a patient population with posterior fossa tumours and with the normal population. Fractional anisotropy of the tracts was reduced in patients with tumours and clinical cerebellar signs as compared to healthy individuals.

This work demonstrates that diffusion MRI and tractography metrics may enable discrimination of paediatric CNS tumour type and are related to the functional integrity of cerebellar white matter tracts.

---

# CONTENTS

---

Declaration	2
Abstract	3
Table of Contents	4
List of Figures	9
List of Tables	11
Abstracts/Presentations/Publications	12
Acknowledgements	14
1 General Introduction	15
1.1 Conventional MRI	16
1.1.1 Basic Principles.....	16
1.1.2 Classical Theory of NMR .....	17
1.1.3 Larmor Frequency and Precession.....	19
1.1.4 Quantum Mechanical Description .....	20
1.1.5 Boltzmann distribution .....	20
1.1.6 Radiofrequency Pulses.....	21
1.1.7 Gradients and Slice Selection .....	23
1.1.8 T1 and T2 Relaxation .....	24
1.1.9 Imaging Sequences .....	27
1.2 MR Imaging of CNS Tumours	31
1.3 Paediatric CNS Intracranial Tumours	40
1.3.1 Paediatric CNS tumours Background .....	40
1.3.2 Diagnostic Imaging.....	42
1.3.3 Treatment Modalities.....	43
1.4 Cerebellar White Matter Anatomy	46
2 Diffusion MRI Theory and Applications	50
2.1 MR Diffusion Imaging	50
2.1.1 Principles & Background.....	50
2.1.2 Diffusion-Weighted Imaging.....	52

2.2	Clinical Applications of DWI in Intracranial Lesions	56
2.2.1	Diffusion-weighted imaging CNS applications.....	56
2.2.2	Diffusion-weighted imaging of intracranial Tumours.....	58
2.3	Diffusion Tensor Imaging	60
2.3.1	The Diffusion Tensor.....	61
2.3.2	Diffusion Tensor Imaging.....	64
2.3.3	Complex Diffusion Models.....	65
2.4	White Matter and Tractography	67
2.4.1	Anatomy of White Matter.....	67
2.4.2	Tractography.....	67
2.5	DTI and Tractography Applications	71
2.6	Intentions of this Study	75
3	Methodology	76
3.1	Patient Recruitment	76
3.2	Ethics and Consent	80
3.3	MRI and Diffusion Protocols	82
3.3.1	Clinical MRI Sequences.....	82
3.3.2	ADC Data Acquisition.....	84
3.3.3	DTI Data Acquisition.....	87
3.4	Calculation of the Diffusion Tensor Indices	91
3.4.1	Mean Diffusivity (MD).....	91
3.4.2	Fractional Anisotropy (FA).....	92
3.5	Study Methods of Tractography	93
3.5.1	Directional Encoded Colour Maps.....	94
3.5.2	Regions of Interest.....	94
3.5.3	Tractography Algorithm.....	95
3.5.4	Visualisation of Tractography Output.....	98
4	ADC Discrimination of Paediatric CNS Tumours	99
4.1	Introduction	99
4.2	Methods	103
4.2.1	Patients.....	103

4.2.2	MR Imaging and Image Processing.....	104
4.2.3	Statistical Analysis.....	106
4.3	Results	107
4.3.1	Mean ADCs .....	110
4.3.2	ADC Histograms: all Tumour Groups.....	117
4.3.3	ADC Histograms Posterior Fossa Tumours.....	119
4.3.4	ADC Histograms PNET versus ATRT .....	121
4.4	Discussion	123
4.4.1	Limitations.....	127
4.4.2	Conclusion .....	129
5	Posterior Fossa Tractography in Healthy Paediatric Controls	130
5.1	Introduction	131
5.1.1	DTI & Tractography in the Paediatric Population.....	131
5.1.2	Age related brain development .....	134
5.1.3	Brain Asymmetry and Handedness.....	135
5.1.4	Objectives .....	138
5.2	Methods	140
5.2.1	Patients.....	140
5.2.2	Determination of Handedness.....	140
5.2.3	MRI Data acquisition.....	141
5.2.4	Tractography Method .....	141
5.2.5	Tractography Thresholds .....	141
5.2.6	Construction of ROIs .....	143
5.2.7	Output of Tract MD, FA & Volume .....	146
5.2.8	Statistical Analysis.....	146
5.3	Results	149
5.3.1	Cerebellar Peduncular Tractography .....	150
5.3.2	Linear Regression of DTI metrics and volume with age.....	151
5.3.3	Cerebellar Peduncular Asymmetry and Handedness.....	154
5.4	Discussion	157
5.4.1	Limitations .....	159
5.4.2	Conclusion .....	161

6	Tractography in Paediatric Posterior Fossa Tumours	163
6.1	Introduction	163
6.1.1	Tractography in Neurosurgery.....	165
6.1.2	Objectives .....	169
6.2	Methods	171
6.2.1	Patients.....	171
6.2.2	MRI Data Acquisition.....	173
6.2.3	Tractography Method .....	173
6.2.4	Tractography Thresholds .....	173
6.2.5	Construction of ROIs .....	173
6.2.6	Output of Tract MD, FA and Volume .....	174
6.2.7	Statistical Analysis.....	174
6.3	Results	176
6.3.1	Descriptive Statistics of Metrics .....	181
6.3.2	Linear Regression Analyses.....	184
6.3.3	Comparisons of Group Metrics.....	185
6.4	Discussion	188
6.4.1	Limitations .....	192
6.4.2	Conclusions.....	193
7	Conclusions	194
7.1	Diffusion Imaging of Paediatric CNS Tumours	194
7.1.1	Conclusions.....	194
7.1.2	Limitations .....	197
7.1.3	Future developments.....	198
7.2	Tractography in Paediatric Neurosurgery	200
7.2.1	Conclusions.....	200
7.2.2	Limitations .....	203
7.2.3	Future applications	206
8	Appendix	209
8.1	Ethical Approval (COREC)	210
8.2	Patient Information Sheets	213

8.2.1	Parents.....	213
8.2.2	Children 5 Years or Less .....	215
8.2.3	Children 6 to 12 years .....	217
8.2.4	Children 13 years plus .....	219
8.3	Consent Forms	221
8.3.1	Parents Consent.....	221
8.3.2	Patients Assent Form .....	223
8.3.3	Patients Consent Form .....	224
8.4	Paediatric MRI Sedation Protocols	225
8.5	ADC Histogram Protocol Instructions	226
8.5.1	Dispimage Analysis Computer Protocols .....	226
8.5.2	Protocol for Drawing ADC ROIs .....	228
8.6	Tractography Protocol Instructions	229
8.6.1	DTI Analysis Computer Protocols.....	229
8.6.2	Tractography Computer Protocols.....	232
8.6.3	Batch File Instructions .....	237
8.6.4	Batch Files .....	238
8.7	Glossary	239
9	References	241



---

# LIST OF FIGURES

---

FIGURE	PAGE
1.1 Spinning proton and bar magnet.....	17
1.2 Effect of B <sub>0</sub> on the dipole moments ( $\mu$ ).....	18
1.3 Application of Radiofrequency Pulse B <sub>1</sub> .....	19
1.4 Effect of application of the RF pulse (B <sub>1</sub> ) to the magnetic moment (M).....	22
1.5 Application of Gradients resulting in frequency and phase encoding.....	24
1.6 T1 Relaxation.....	25
1.7 T2 Relaxation.....	26
1.8 PNET-Medulloblastoma.....	34
1.9 Juvenile pilocytic astrocytoma.....	35
1.10 Ependymoma.....	36
1.11 Atypical teratoid rhabdoid tumour (ATRT).....	37
1.12 Dysembryoplastic neuroepithelial tumour (DNT).....	38
1.13 Choroid plexus papilloma.....	39
1.14 Types of CNS tumours presenting to GOSH 2007.....	41
1.15 New CNS tumours by age group.....	42
1.16 Summary of treatment pathways.....	44
1.17 Connections of the Cerebellum.....	48
2.1 Diffusion weighted images; b = 0 and b = 1000 images.....	54
2.2 Eigenvectors and values as applied to an ellipsoid representation.....	62
2.3 Visual representation of the tensor in isotropic and anisotropic tissues.....	63
2.4 FA and MD Maps.....	64
2.5 Colour Maps.....	65
3.1 New tumour referral GOSH 2003 - 2007.....	79
3.2 Directional ADC Maps.....	85
3.3 A two dimensional illustration of the iterative tractography.....	97
4.1 Representative ADC maps of tumour types.....	108
4.2 Scatter plot of tumour ROI average ADC classified by tumour group.....	110
4.3 Normalised histograms averaged for all tumours within each group.....	112
4.4 Scatter plot of posterior fossa tumour type versus ADC 75 <sup>th</sup> centile.....	120
4.5 Scatter plot of skewness versus peak height for PNET and ATRT groups.....	122
5.1 Effect of changing FA threshold on tract reconstruction.....	142
5.2 ROIs superimposed onto the FA image.....	145
5.3 Tractography reconstruction of posterior fossa structures.....	150

5.4	Scatterplot of Age versus average MD .....	151
5.5	Scatterplot of Age versus average FA .....	152
5.6	Scatterplot of Age versus average sub voxel volume.....	152
5.7	Histogram of asymmetry measures of MD.....	154
5.8	Histogram of asymmetry measures of FA .....	155
5.9	Histogram of asymmetry measures of sub voxel volume.....	155
6.1	Cerebellar tracts of posterior fossa tumour case without cerebellar symptoms .	178
6.2	Cerebellar tracts of posterior fossa tumour case with cerebellar symptoms .....	179
6.3	Scatterplot of average MD and age for PFCS group .....	182
6.4	Scatterplot of average FA and age for PFCS group .....	183
6.5	Scatterplot of average sub voxel volume and age for PFCS group .....	185
6.6	Scatterplot of average MD for NC and PFCS groups .....	185
6.7	Scatterplot of average FA for NC and PFCS groups.....	186
6.8	Scatterplot of average sub voxel volume for NC and PFCS groups.....	186

---

## LIST OF TABLES

---

Table	Page
1.1 NMR characteristics of CNS tissues and CSF .....	27
1.2 Incidence of paediatric CNS tumours .....	41
3.1 Summary of project MRI sequences .....	86
3.2 Summary of DTI directions .....	89
4.1 Summary of histological diagnosis, demographics and tumour mean ADC .....	109
4.2 ANOVA testing of group average ADC values .....	111
4.3 Logistic regression analysis classification of all tumour cases .....	118
4.4 Logistic regression analysis classification of posterior fossa tumours .....	119
4.5 Logistic regression analysis classification of PNET and ATRT groups .....	121
5.1 Demographics of healthy cases .....	149
5.2 Linear regression p-values for age versus MD, FA and sub voxel volume .....	153
5.3 Descriptive statistics of asymmetry measures for MD, FA and sub voxel volume	154
5.4 One sample <i>t</i> -tests for asymmetry measures .....	156
6.1 Demographics of posterior fossa tumour group .....	177
6.2 Mean MD, FA and sub voxel volumes for NC and PFCS groups .....	181
6.3 Linear regression p-value results for MD, FA & SV volume for versus age .....	184
6.4 Two sample <i>t</i> -test results for group-wise comparisons of NC and PFCS cases ....	187

---

## ABSTRACTS / PRESENTATIONS / PUBLICATIONS

---

### **ABSTRACTS**

Tractography of Cerebellar Peduncles in Paediatric Infratentorial Tumours.

*J. G. Bull, D. E. Saunders, C. A. Clark; Proceedings of 37th Scientific Meeting of the International Society for Paediatric Neurosurgery. Childs Nervous System 2007.*

The use of ADC parameters to distinguish paediatric brain tumours. *J. G. Bull, M. D. King, D. E. Saunders, C. A. Clark; Proceedings of the ISMRM Toronto May 2008.*

Diffusion MRI and Apparent Diffusion Coefficient (ADC) in discrimination of paediatric CNS tumours. *J. G. Bull, M. D. King, D. E. Saunders, C. A. Clark; Proceedings of the SBNS Liverpool. British Journal of Neurosurgery 2008.*

### **PRESENTATIONS**

Tractography of Cerebellar Peduncles in Paediatric Infratentorial Tumours.

*J. G. Bull, D. E. Saunders, C. A. Clark; 37th Scientific Meeting of the International Society for Paediatric Neurosurgery; Liverpool 2007.*

The use of ADC parameters to distinguish paediatric brain tumours. *J. G. Bull, M. D. King, D. E. Saunders, C. A. Clark; International Society of Magnetic Resonance in Medicine Toronto May 2008.*

Diffusion MRI and Apparent Diffusion Coefficient (ADC) in discrimination of paediatric CNS tumours. *J. G. Bull, M. D. King, D. E. Saunders, C. A. Clark; SBNS Liverpool April 2008*

***SUBMITTED FOR PUBLICATION***

Discrimination of paediatric brain tumours using apparent diffusion coefficient histograms Jonathan G. Bull MA, MRCS, Martin D. King PhD, Dawn E. Saunders MD, FRCR, and Christopher A. Clark PhD. *Accepted by European Radiology*

---

## ACKNOWLEDGEMENTS

---

I am greatly indebted to my supervisor Chris Clark for his advice and guidance.

I thank John Thornton and David Plummer for assistance with UNIX programming and the functionality of DispImage and also to Ai-Wern Chung for assistance with Matlab scripts. I am grateful to David Gadian for welcoming me to his department and providing me with the opportunity to undertake this study.

There are a number of people who have made contributions to the work presented in this thesis. I have to thank Tom Barrick for his time and support in tolerating my endless questions and recurring software issues and David Atkinson for aiding in the production of a Matlab script to correct the changes in the sequence resulting from an unexpected software upgrade.

Martin King, I thank for repeatedly questioning my results and providing me with a deeper understanding of the complexities of statistical analysis. The Neuroradiologists at GOSH provided considerable amounts of time to discuss my findings and questions, in particular Kling Chong and Dawn Saunders. I also thank Kate Riney for access to some of her control data which has been analysed here.

This work would not have been possible without the financial support of Cancer Research U.K. (Ref: C8807/A3870) and particularly Martyn Coomer at the Royal College of Surgeons in the form of the award of the Harold Bridges Research Fellowship to the author.

The difficulties encountered in paediatric patient recruitment were greatly ameliorated by the nursing and medical staff of Parrot Ward at Great Ormond Street Hospital (GOSH). In particular I thank Sister Kim Phipps for access to the GOSH tumour patient database and Lindy May for help in facilitating the recruitment to this study.

The Radiology department at GOSH were instrumental in accommodating my imaging sequences despite the frequent time constraints and short notice. In particular I thank Clare Simcock for her good humour and support. When imaged on research time Tina Banks was outstandingly helpful by, on many occasions, fitting someone in at the last minute.

Finally, I would like to express my deepest gratitude to parents for their unfailing support and tolerance.

---

# 1 GENERAL INTRODUCTION

---

## CONTENTS

---

1.1	Conventional MRI	16
1.1.1	Basic Principles.....	16
1.1.2	Classical Theory of NMR.....	17
1.1.3	Larmor Frequency and Precession.....	19
1.1.4	Quantum Mechanical Description.....	20
1.1.5	Boltzmann distribution.....	20
1.1.6	Radiofrequency Pulses.....	21
1.1.7	Gradients and Slice Selection.....	23
1.1.8	T1 and T2 Relaxation.....	24
1.1.9	Imaging Sequences.....	27
1.2	MR Imaging of CNS Tumours	31
1.3	Paediatric CNS Intracranial Tumours	40
1.3.1	Paediatric CNS tumours Background.....	40
1.3.2	Diagnostic Imaging.....	42
1.3.3	Treatment Modalities.....	43
1.4	Cerebellar White Matter Anatomy	46

---

Magnetic resonance imaging (MRI) has become one of the key tools in medical imaging and this is attributable to several factors. Significantly it can be sensitised to the different properties of tissues resulting in the production of multiple different contrasts and it is completely non-invasive. These properties combined with the absence of any known biological hazard make it, in the research and clinical environments, a very valuable tool.

MRI is based on the resonance of nuclei within a material when placed in a strong magnetic field and subjected to radiofrequency (RF) pulses as stimulation. The RF pulses result in absorption and subsequent release of energy by the nuclei which produce a signal containing spatial and structural information from the material under investigation. It is from these signals that the images are reconstructed.

## 1.1 CONVENTIONAL MRI

The basis of MRI is that of nuclear magnetic resonance (NMR). This is a phenomenon describing the interaction of an externally applied magnetic field with the magnetic moment of the nucleus of an atom, whereby the nucleus absorbs radiofrequency energy and the dipole moment is tipped from equilibrium subsequently emitting energy which is quantifiable. Initially described in 1946, two groups working independently using different substrates, specifically Bloch et al looking at water in a liquid state and Purcell using solid paraffin, shared the 1952 Nobel Prize for physics. The developments of Lauterbur allowed movement from single dimension NMR spectroscopy to a second dimension of spatial organisation. Mansfield's application of gradients in the magnetic field and use of Fourier transforms allowed mathematical reconstruction of images from the MR signals; such that a research tool became a means of medical imaging in 1976.

### 1.1.1 BASIC PRINCIPLES

The phenomenon of NMR is exhibited by the entire nucleus, both protons and neutrons. The principle originates from the fact that all the particles of an atom spin on their own axis. The rotation of the nuclear particles creates a magnetic field which is described as a magnetic moment. Hence it is possible to consider these particles behaviour akin to that of miniature bar magnets. In the case of the hydrogen atom there is only a single proton ( $^1\text{H}$ ), constituting a spinning positive charge and hence it possess the greatest



magnetic moment. The interaction of the magnetic moments with an applied magnetic field generates the recorded signals.

In medical imaging signals are most frequently collected from the nuclei of hydrogen ( $^1\text{H}$ ) atoms as a consequence of their abundance in organic structures as it forms part of water molecules, for example the human brain is constituted of more than 75% (1) water. In addition it possesses the largest magnetic moment making it the most easily detected. It is also possible to obtain signals from other elements which include  $^{13}\text{C}$ ,  $^{23}\text{Na}$  and  $^{31}\text{P}$  and MR Spectroscopy is a technique which exploits this in biological imaging.  $^1\text{H}$  constitute more than 99% of all Hydrogen nuclei by comparison to  $^{13}\text{C}$  comprising approximately only 1% of all Carbon nuclei, hence furthering its preference for medical imaging.

### 1.1.2 CLASSICAL THEORY OF NMR

The spinning hydrogen nucleus (proton) has a charge associated with it and hence produces a magnetic moment or dipole which is the magnetic field emanating from the proton possessing a north and south pole (Figure 1.1).

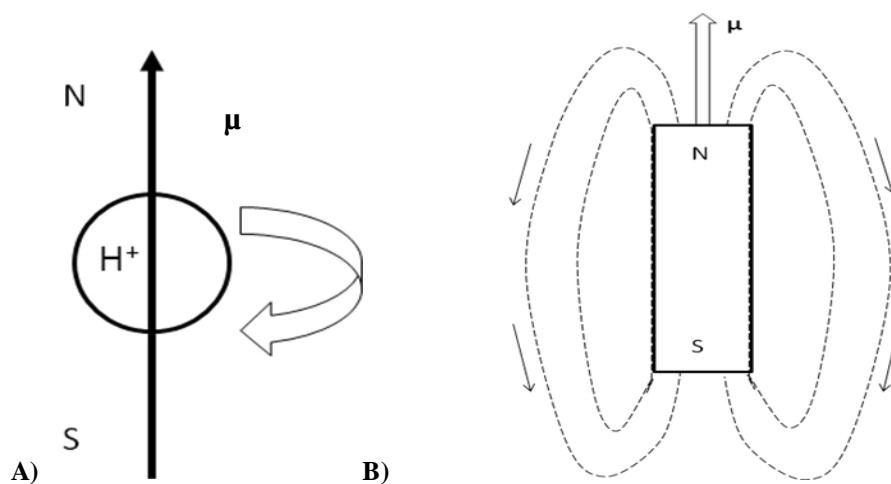
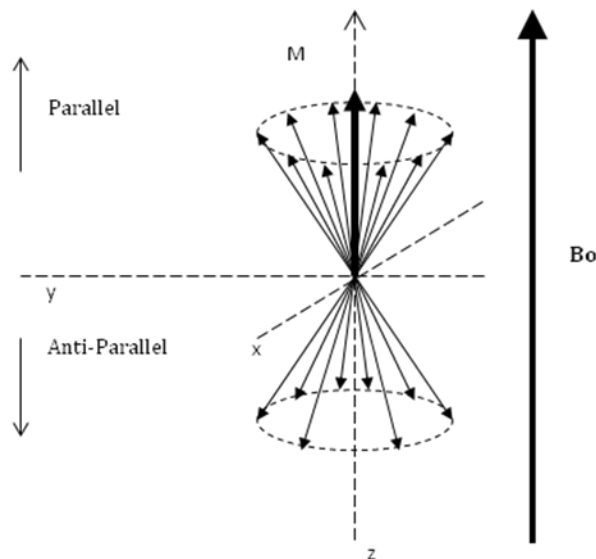


**Figure 1.1 Spinning Proton (A) and Bar magnet (B) image. Where  $\mu$  is the magnetic moment.**

---

The magnetic moment is generated from the angular momentum of the nucleus, in this case the spinning proton. It can be calculated as the product of the angular momentum and the gyro magnetic ratio, which is a descriptive value associated with each individual nucleus, hence the magnetic moment is proportional to the angular momentum.

If a proton (or any magnetic dipole) is placed in a static magnetic field  $B_0$ , acting along an axis (E.g. the z-axis) the previously randomly arranged protons will align with the  $B_0$  either parallel or anti-parallel. The combined alignment of the magnetic moments  $\mu$  can be represented as a magnetic vector  $M$  (Figure 1.2).



---

**Fig 1.2 Effect of  $B_0$  on the dipole moments ( $\mu$ ). The protons ( $\mu$ ) align parallel and antiparallel with  $B_0$  creating a net magnetic vector  $M$ .**

---

The alignment of the protons is such that a greater proportion will be aligned parallel than anti-parallel and this creates a magnetic vector  $M$  in the direction of  $B_0$ , the externally applied field. The higher the  $B_0$  field strength the greater the magnetic vector. When force is applied to  $M$  in order to overcome this equilibrium the nuclei release energy in order to return to this state of equilibrium with  $B_0$ . The signal is created from

this release of energy from the polarised nuclei and hence imaging quality increases with increasing field strength. In the case of MRI the external exerted force is in the form of a rotating radiofrequency pulse  $B_1$  typically applied perpendicular to  $B_0$ .

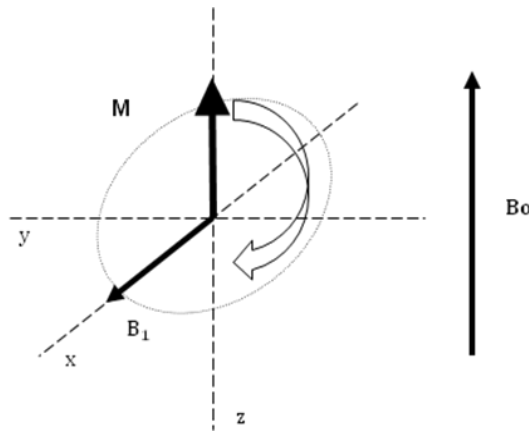


**Figure 1.3 Application of Radiofrequency Pulse  $B_1$ . The RF pulse is applied rotating perpendicular to  $B_0$ , exerting a force on the protons ( $M$ ) against  $B_0$ . It is the release of this energy which generates the NMR signal.**

---

The  $B_0$  field is represented in the  $z$  plane, by convention in the direction of the bore of the magnet and hence running cranio-caudal in the patient lying flat within the magnet.

The  $x$  and  $y$  axes are the planes of the axial slice image.

### 1.1.3 LARMOR FREQUENCY AND PRECESSION

Spinning protons, due to their angular momentum, when placed in a magnetic field  $B_0$  experience a torque perpendicular to the field and hence to the axis of their rotation.

This torque induced motion is known as precession.

The frequency of this precession changes proportionally with the strength of the magnetic field the proton experiences. The frequency of precession is known as the Larmor frequency, at a particular field strength the resonant frequency at which the nuclei absorb applied radiofrequency energy is derived from the Larmor equation:

$$\omega = \gamma B$$

Where the angular frequency of precession of the proton is  $\omega$  and  $\gamma$  is the gyromagnetic ratio or intrinsic magnetic moment which is a property of a proton (or nucleus) in a given magnetic field and  $B$  is the magnetic field strength. The frequency of precession or Larmor frequency at field strength ( $B$ ) of 1.5T is of the order 64 MHz, corresponding to the frequency of electromagnetic radio waves.

#### 1.1.4 QUANTUM MECHANICAL DESCRIPTION

In order to understand NMR both a classical physics and a compatible quantum mechanical model are useful. At the quantum level, individual proton subsets behaving in a similar fashion are isochromats. A single particle possesses its own quantum spin number proportional to its angular momentum and this determines whether it will result in NMR.

The proton ( $I = + \frac{1}{2}$ ) when placed in a magnetic field will move into one of its two preferred states and is then described as quantised. The number of states a nucleus can occupy is related to its  $I$  value and these are known as Zeeman energy levels, described by  $2I + 1$ . In the case of the proton (hydrogen nucleus) they are  $- \frac{1}{2}$  and  $+ \frac{1}{2}$ . The two states are separated by an amount of energy equal to that of the Larmor frequency. So when energy is supplied to them at the Larmor frequency (the nuclear precessional frequency) in the form of an RF pulse a transition between states can occur.

#### 1.1.5 BOLTZMANN DISTRIBUTION

In figure 1.2 it is seen that the nuclei experiencing a magnetic field  $B_0$  will precess in either a parallel or anti-parallel state. As the anti-parallel state requires more energy to

achieve it a very slight preference exists for the parallel state of approximately 1 in  $10^5$  spins, the very small differences necessitate the significant amplification of the signal. The existence of this population results from random thermal motion, providing energy and equalising the two spin states. It is the predominance of parallel spins which generates the NMR signal.

The relative numbers of each state can be described by the Boltzmann distribution:

$$\frac{N_+}{N_-} = \exp\left(-\frac{\Delta E}{kT}\right)$$

Where  $k$  is the Boltzmann constant and  $T$  is the temperature and  $N_+$  and  $N_-$  represent the parallel and anti-parallel conditions. In order to maximise the signal from the NMR experiment it is necessary to increase the proportion of nuclei in  $N_+$ . In a human body the temperature varies only by a small amount and hence with  $k$  as a constant the only means to achieve a higher signal is to input more energy through increasing  $B_0$  by using a magnet with greater field strength.

### 1.1.6 RADIOFREQUENCY PULSES

As discussed previously in order to produce the NMR signal a second magnetic field known as  $B_1$  is applied at  $90^\circ$  to  $B_0$ , this field is the radiofrequency (RF) pulse. The  $B_1$  field is applied at the Larmor frequency (the frequency at which energy transitions are possible) and imparts energy to the system causing the net magnetic vector ( $M$ ) to turn into the x-y plane, perpendicular to the plane of  $B_0$  in the z axis. The  $B_1$  field is generated by magnetic coils and the angle through which it tips the magnetic moment is known as the flip angle, this occurs at the Larmor frequency and is determined by the shape and amplitude of the RF pulse.

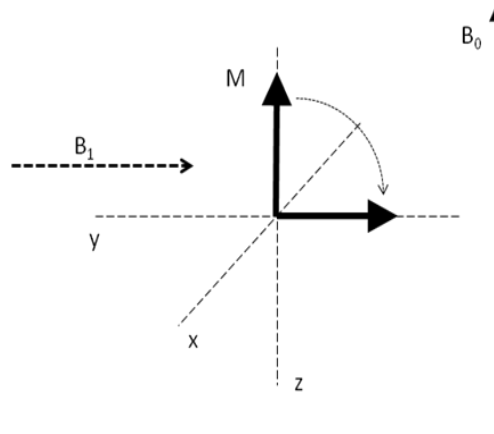


**Figure 1.4 Effect of application of the RF pulse ( $B_1$ ) to the magnetic moment ( $M$ )**

---

The RF pulse causes a redistribution of the spins between the parallel and anti-parallel states and their combined magnetisation is averaged in the x-y plane, it also focuses all the spins to be in the same phase with a strong magnetic moment in the x-y plane. Whilst it is possible to tip the spins through any angle, the x-y plane is optimal as there is no  $M_z$  component.

The RF pulse is applied then removed and the energy imparted to the system is released as the protons precessing perpendicular to the  $B_0$  field return to precess in the axis of it. This energy release produces a magnetic field which decays with time, the field induces an electric current in a receiver coil (which may or may not be the same as the transmitting coil). The signal received is relatively weak ( $\sim 10$  watts) by comparison to that transmitted in the initial RF pulse (up to 20,000 watts) and hence it must be amplified considerably. In order to protect the signal from other radiofrequencies the MR system must be shielded in a copper Faraday cage.

### 1.1.7 GRADIENTS AND SLICE SELECTION

In order to reconstruct an image, the spatial distribution of the signals must be determined. This is possible through the application of further gradients in addition to  $B_0$  and  $B_1$ . Gradients can be applied in all three axes, for example increasing the  $B_0$  linearly along its axis through the application of a gradient will result in a change in the Larmor frequency as a function of the  $z$  axis position in the material studied. The position that the nucleus occupies along the  $z$  axis will determine the frequency at which it resonates. Therefore a slice of protons perpendicular to the  $z$  axis can be excited by adjusting the RF pulse to the Larmor frequency of that slice. This is known as slice selection and the gradient is determined as  $G_z$ . Slice thickness is determined by the gradient's amplitude and the width of frequency of the RF pulse.

Once a slice is selected it is then necessary to encode the spatial information within the slice. A voxel is encoded using the application of gradients in the  $x$  ( $G_x$ ) and  $y$  ( $G_y$ ) axis and they are known as frequency and phase encoding respectively. The frequency encoding gradient is applied during signal reception, the effect being to cause the nuclear spins to resonate at different frequencies along the  $x$  axis. The phase encoding gradient has a similar function but is applied over a shorter period and results in alteration of the phase of the spin with respect to the  $y$  axis. Its application is between excitation and reception and causes the spins to precess according to the strength of magnetic field they experience as it changes along the  $y$  axis. On removal of the gradient the spins return to precess at their original frequency but at different phases. Figure 1.5 highlights the effect of the frequency and phase gradients in encoding each individual voxel such that their NMR signal is unique to their position.

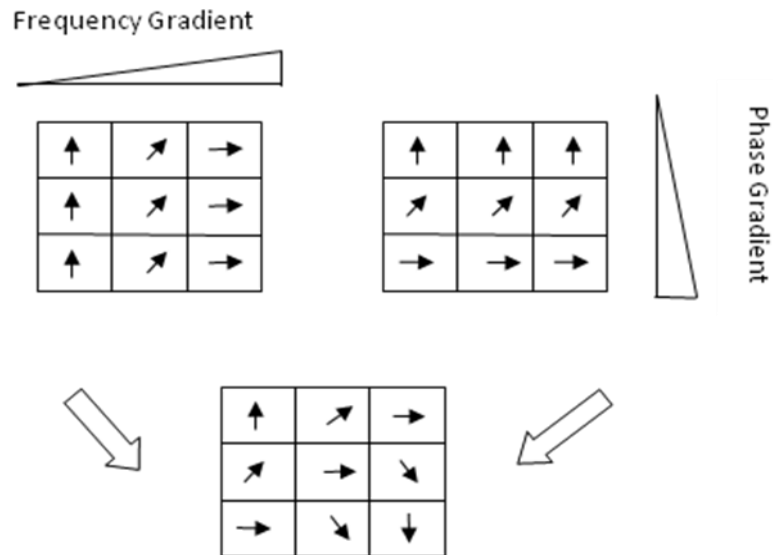


**Figure 1.5 Application of Gradients resulting in frequency and phase encoding** (Image reproduced with permission of CA Clark)

---

The construction of an image is the result of repeated excitations and read outs, the time between each of these excitations is known as the repeat time or TR.

The signals measured from the receiver coil are digitised for MR image processing and reconstruction. The frequency of the RF pulse is digitalised through a digital to analogue convertor. This digital information is stored in a data matrix called K- space using frequency and phase encoding data from the signals received. A single phase encoding step constitutes a single line of the matrix. Once the matrix has been filled a 2D Fourier transform is applied to the data in order to reconstruct the MR image, where the frequency component is extracted in the x direction and the phase component in the y direction.

### 1.1.8 T1 AND T2 RELAXATION

After the application of the RF pulse the nuclei give up their absorbed energy, known as relaxation. Two types are described; *spin lattice* (T1) and *spin-spin* (T2), which result in the nuclei resuming their original state.



The re-establishment of the dipole moment  $M$  along the  $z$  axis is achieved through  $T_1$  relaxation. The nuclei give up energy to their surroundings, known as the lattice, in order to return to its original state. The energy exchange is through the external stimulation of a protons magnetic moment and near neighbour magnetic moment, where the encountered magnetic field must be resonating at the Larmor frequency.  $T_1$  relaxation is also known as the longitudinal relaxation rate, the exponential function of the time to repeat of the RF excitatory pulse ( $TR$ ) and the  $T_1$  value describes the rate at which the magnetisation returns to the  $z$  axis ( $B_0$ ), seen in Figure 1.6.

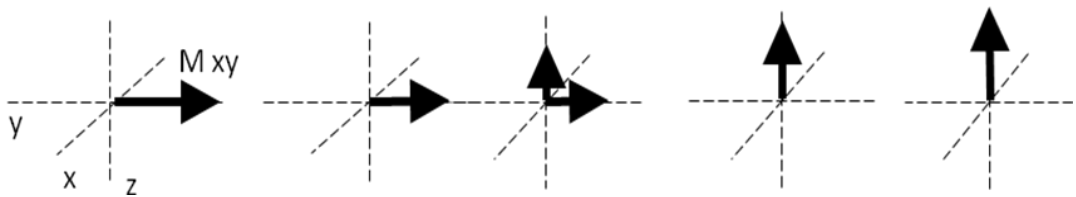


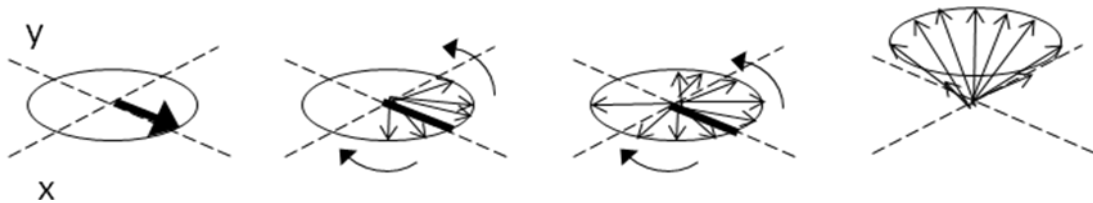
**Figure 1.6 T1 Relaxation. Exponential recovery of the magnetic moment ( $M$ ) in the  $z$  axis from the  $x$ - $y$  axis.  $T_1$  for a material is the point of maximum growth, the 63% point of the final value achieved.**

---

$T_2$  relaxation takes place in the transaxial plane occurring as the signal decays due to the individual magnetic moments dephasing in the  $x$ - $y$  plane and  $T_2$  is known as the transverse relaxation rate. Individual nuclei experiencing varying magnetic fields cause the loss of phase. This may be where nuclei experience local magnetic fields and exchange energy with adjacent nuclei at the same frequency without net energy loss from the system.

Illustrated in Figure 1.7; spins dephase in both directions in the  $x$ - $y$  plane, in a fan like motion. Where they move to the left they are travelling at a lower rate of precession than previously and in moving to the right are at a higher rate of precession. The

transverse magnetisation falls as a ratio of the T2 and the time between the initial RF pulse and the signal or echo following a second RF pulse. This is known as the time to echo or echo time (TE). As the echo time increases the signal reduces.



---

**Figure 1.7 T2 Relaxation. Decay of signal in the x-y plane as the nuclei dephase. T2 is the point of achieving 37% of full time to dephasing.**

---

It can be seen that the signal intensity from a voxel will depend on the T1 and T2 but it also depends upon the proton density (PD), although this does not change for a given material. The T1 and T2 relaxations were initially described by Bloch (2) in 1946 and it is in part through manipulation of these parameters that different contrasts can be achieved.

The material studied affects the signal intensity, for example the low proton density of bone results in low signal on a proton density-weighted image. The effect of the environment of the hydrogen nuclei is crucial, T1 relaxation is most efficient at the Larmor frequency but in the case of free water the random free movement of the nuclei exceeds the Larmor frequency and the T1 is prolonged. If water is more restricted in its movements as in white or grey matter the T1 is shortened. In the case of T2 relaxation it is most efficient in solids like bone where loss of phase is occurring due to both the effects detailed previously. When in liquids the hydrogen nuclei only dephase by

interaction with adjacent nuclei, the effect of the field fluctuations is cancelled by the random movement of the nuclei and consequently the T2 is prolonged.

It is possible to plot the values of T1 and T2 for different tissues as seen in Table 1.1. The NMR signal is dependent upon a number of properties including the proton density, the environment the nuclei being studied are found (i.e. free water or within white matter), magnetic susceptibility as well as flow where the nuclei are in blood or cerebrospinal fluid (CSF). Through manipulation of TE and TR it is possible to modify the signal intensity to weight a sequence such that signals from certain tissue types predominate. The rate of  $T_1$  relaxation is also strongly dependent on the NMR frequency, hence varies with magnetic field strength  $B$ . As a consequence measurements made on different MR machines will vary. The temperature of the tissue being imaged also affects the signal, although in vivo this is a less significant problem.

	Proton Density (relative to H <sub>2</sub> O)	T1	T2
White Matter	0.73	557	72
Grey Matter	0.85	993	87
Cerebrospinal Fluid (CSF)	1	4000	2500

*Measurements on a 1.5T MR scanner*

**Table 1.1 NMR characteristics of CNS tissues and CSF**

---

### 1.1.9 IMAGING SEQUENCES

The application of an RF pulse to a hydrogen nucleus produces a signal; this signal is known as free induction decay (FID) as a result of the magnetisation being tipped into the x-y plane. This decay in signal is due to a dephasing effect and is known as T2\*. The decay is less than the “true” T2 of the tissue as a consequence of B<sub>0</sub> field

inhomogeneities from susceptibility effects and imperfections in the magnet causing the diminution in the observed decay.

Spin echoes (SE) result from two consecutive RF pulses at  $90^\circ$  and  $180^\circ$ . They are preferred over FID's as the  $T2^*$  effects mean that the signal decays too rapidly. The  $180^\circ$  pulse refocuses the spins but also has the effect of cancelling the dephasing effect of the  $T2^*$  after the  $90^\circ$  pulse as they are mirrored following the  $180^\circ$  pulse through effectively reversing the spins. This is the method described as the spin echo (SE) sequence to remove inhomogeneities in the magnetic field (3). The result of which is that the signal is determined by the  $T2$  (which is always greater than the  $T2^*$ ). The majority of clinical MRI sequences are SE's; modification of the TE and TR allows acquisition of images weighted for  $T1$  or  $T2$ . Contrast between tissues can also be obtained through the use of a contrast material injected intravenously. Gadolinium is in common usage; it is highly paramagnetic resulting in a reduction (shortening) of the  $T1$  time of the hydrogen nuclei nearby. Its effects are useful when the blood-brain barrier in the brain is breached and the gadolinium leaks out into the tissues as may occur in the presence of a tumour. Its properties also lend it to use in the case of imaging of blood vessels in MR angiography.

One of the significant issues in MRI is the amount of time required to collect the data. The use of the fast spin echo (FSE) uses a series of refocusing pulses following the initial excitatory pulse. In contrast with the SE, multiple lines of k-space are obtained for each TR. The number of views corresponds to the number of graduations in the phase encoding direction, all of which must be obtained before image reconstruction. In the FSE sequence multiple views are recorded where the number of echoes is referred to as the echo train length (ETL) obtained before the TR; if the ETL is 2 then the imaging time would be halved and so on with increasing ETL. As the ETL increases the image

quality falls due to a fall in signal intensity at the increasing echo times. The length of the T2 also affects the FSE image quality.

In some sequences the desired effect is to null the signal from a particular material, this is the case when wishing to assess the nature of lesions near to the ventricles of the brain. In such locations the high signal provided by the CSF diminishes the ability to define periventricular lesions. Inversion recovery imaging using a  $180^\circ$  RF pulse applied prior to the rest of the sequence causes the nuclei to reverse their direction from parallel to the z-axis to anti-parallel, the nuclei then relax back to parallel at the T1 rate. This initial inversion ( $180^\circ$ ) pulse is typically followed by the first excitatory pulse ( $90^\circ$ ) of a SE or FSE, the time between which is the time to inversion (TI). The suppression of the signal from fluid is achieved using the fluid attenuated inversion recovery (FLAIR) (4) sequence through the matching of TI to the point at which there is net no longitudinal magnetisation from the fluid and hence no transverse magnetisation of the CSF.

Gradient echoes are also used as a consequence of their short acquisition times and sensitivity to materials causing distortions in the magnetic field such as haemosiderin and ferritin. The  $90^\circ$  initial RF pulse which tips the nuclear spins into the x-y plane is followed by a gradient that is the reverse of the slice-select gradient and causes a dephasing which is then followed by an opposite gradient refocusing the spins, generating an echo. The rapid acquisition of data is dependent on the use of a single RF pulse and then multiple rapidly alternating gradients. However the sequences are susceptible to image artefacts as they are sensitive to inhomogeneities caused by changes in magnetic susceptibility as occurs at the interface between tissue and air for example.

The goal of obtaining optimal images with restricted time stems from the need to maintain the imaged object in the same position for a lengthy period of time. In the case of a patient not only does the individual's tolerance of remaining still become an issue during the sequence acquisition but also so does the involuntary movement of the body such as cardiac pulsation and respiratory movements. In the context of diffusion imaging in which the sequence is intentionally sensitised to small motions, the need for fast sequences is more apparent. To this end echo planar imaging (EPI) is implemented in diffusion imaging and this is the sequence used in this work.

As described for the gradient echo sequence the readout gradient can be repeated many times, changing polarity, it is this method that is used in EPI. After each readout gradient a further phase encoding gradient is applied to determine the next view and only a single excitation pulse is used to collect all the data in k-space. This makes the imaging time much shorter. The major limitation of this method is that EPI is very susceptible to susceptibility artefacts and low signal to noise ratio.

## 1.2 MR IMAGING OF CNS TUMOURS

MRI is considered to be the optimal method for the detection of childhood tumours. Typically lesions will exhibit prolonged T1 or T2 relaxation times enabling their visualisation. The extent and location of the lesion is usually well displayed with multi-planar imaging. MRI has the advantage over CT in that images are not degraded by the presence of overlying bone, which is a particular concern in the posterior fossa. Axial and sagittal images tend to provide the most information in such cases and coronal imaging adds value particularly in supratentorial lesions. The role for CT is often as a first line investigation available out of hours at general hospitals where MRI services are not provided. CT is also useful in providing information as to the relationship to the bone which is not provided by MRI (5).

There are numerous histological types and grades of tumour seen in the CNS; frequently they have characteristic appearances on MRI. The common types of tumour are further summarised in section 1.4, specifically Astrocytomas, Primitive neuroectodermal tumours and ependymomas occur most commonly. As individual tumour types their grade can vary, providing sub-classification, which is also a marker of their aggressiveness and hence information which may determine the course of future treatment. Their appearances will differ on MRI, according to the grade and the type of lesion. Radiologists review the imaging and can provide a differential diagnosis; in effect a list of the possibilities in order of their likelihood based on their experience, results may vary from individual reviewers, prior to a surgical or other treatment intervention (6). This is discussed further in chapter 4.

In order to better characterise a lesion contrast agents are commonly used, such as Gadolinium diethylenetriaminepenta-acetic acid (DTPA). This is a paramagnetic

contrast agent which has a similar distribution following intravenous injection to the iodinated contrast media used in CT imaging. The effect of the Gadolinium is to shorten T1 times such that tissues which contain it will appear bright on T1-weighted images. Such contrast has the potential to assist in the discrimination of features such as tumour tissue from surrounding oedema or to provide inference as to the grade. Typically higher grade glioma lesions are seen to enhance heterogeneously with contrast although this is not always reliable and low grade lesions are sometimes seen to enhance (7). In addition, some small lesions may only be visualised after contrast enhancement.

The different sequences used vary from department to department and the standard tumour imaging protocol at GOSH for intracranial lesions is seen in section 3.3. The use of FLAIR imaging aids in the discrimination of lesions and associated vasogenic oedema and also aids discrimination of periventricular lesions. MRI still remains limited as a tool in determining as to what degree the tumour has invaded at a microscopic level and hence delineating the boundary between normal brain and tumour (8). MRI is also the modality of choice for the assessment of the spine in terms of tumour spread (metastases) or of primary neoplasms.

Other imaging modalities play a role in the assessment of neoplasms; positron emission tomography is helpful in providing information as to the viability or metabolic activity of tissues. This can be of particular help when following up post radiotherapy so as to discriminate viable tumour from necrotic or inactive tissue. MR spectroscopy has a role in characterising neoplasms, molecules such as choline, creatine, phosphocreatine; neurotransmitters such as glutamate; markers of metabolic activity, lactate and also *N*-acetyl aspartate; all exhibit characteristic resonant frequencies. Metabolite levels can be detected and a spectrum of frequencies created in order to describe the lesion. This



information has been used in an attempt to discriminate areas of tumour in surrounding brain and in classification of lesions (6;9-11).

The radiological appearance of the common paediatric posterior fossa lesions and their imaging characteristics are highlighted overleaf.

One of the common infratentorial tumours is primitive neuroectodermal tumour (PNET) PNET-Medulloblastoma. Typically they arise in the midline, from the cerebellar vermis in younger children and in adolescents more commonly in the cerebellar hemisphere. Radiologically they are characterised as well defined, lobulated solid masses. They may have a heterogeneous appearance with cysts and calcification within them. PNETs also occur supratentorially, although not classified as medulloblastomas, they share the same lineage. Generally they are solid in appearance with punctate areas of calcification, they are isointense to grey matter with reduced diffusion and typically they are sharply margined (6).

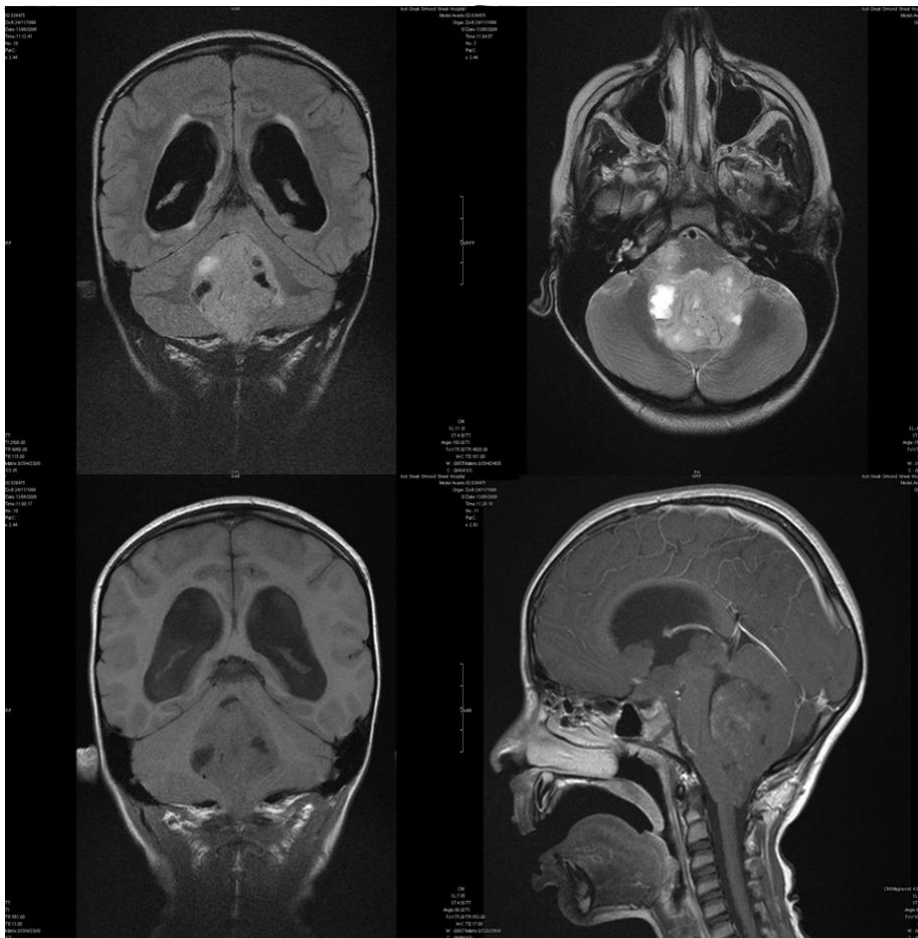


**Figure 1.8 PNET-Medulloblastoma. Coronal T2, axial FLAIR, coronal T1 and sagittal T1 with contrast.** Images show an extensive disseminated malignancy. A midline posterior fossa mass is identified which is largely poorly enhancing. There is moderate secondary obstructive hydrocephalus.

Astrocytomas can have several grades but are usually low grade, in a hemispheric or vermian location. They are usually cystic with a solid enhancing nodule, the cystic component is hyperintense on T2-weighted imaging (6).

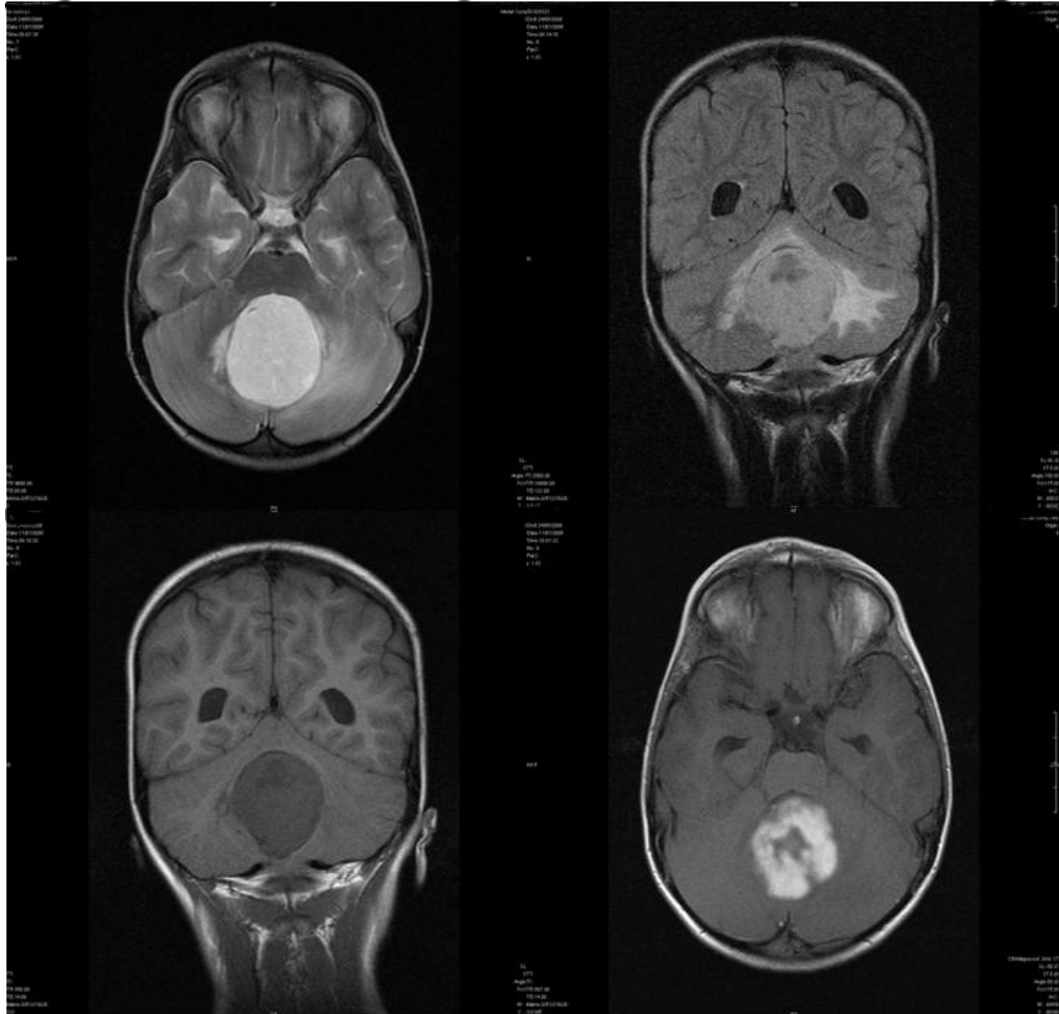


**Figure 1.9 Juvenile pilocytic astrocytoma. Axial T2, coronal flair and T1-weighted MRI, axial T1-weighted MRI with contrast.** Images show a large well demarcated mass arising from the cerebellar vermis showing heterogenous enhancement with surrounding oedema, effacement of the fourth ventricle and prominence of the lateral and third ventricles.

---

Ependymomas are often heterogeneous in appearance with mixed solid and cystic areas which display fluid levels. Approximately 50% have calcification and a low T2-weighted signal from the presence of the calcium or haemorrhage. The tumours in the posterior fossa arise from the cells lining the roof of the fourth ventricle and often extend through the outflow of the fourth ventricle via the foraminae of Magendie and Lushka (6).

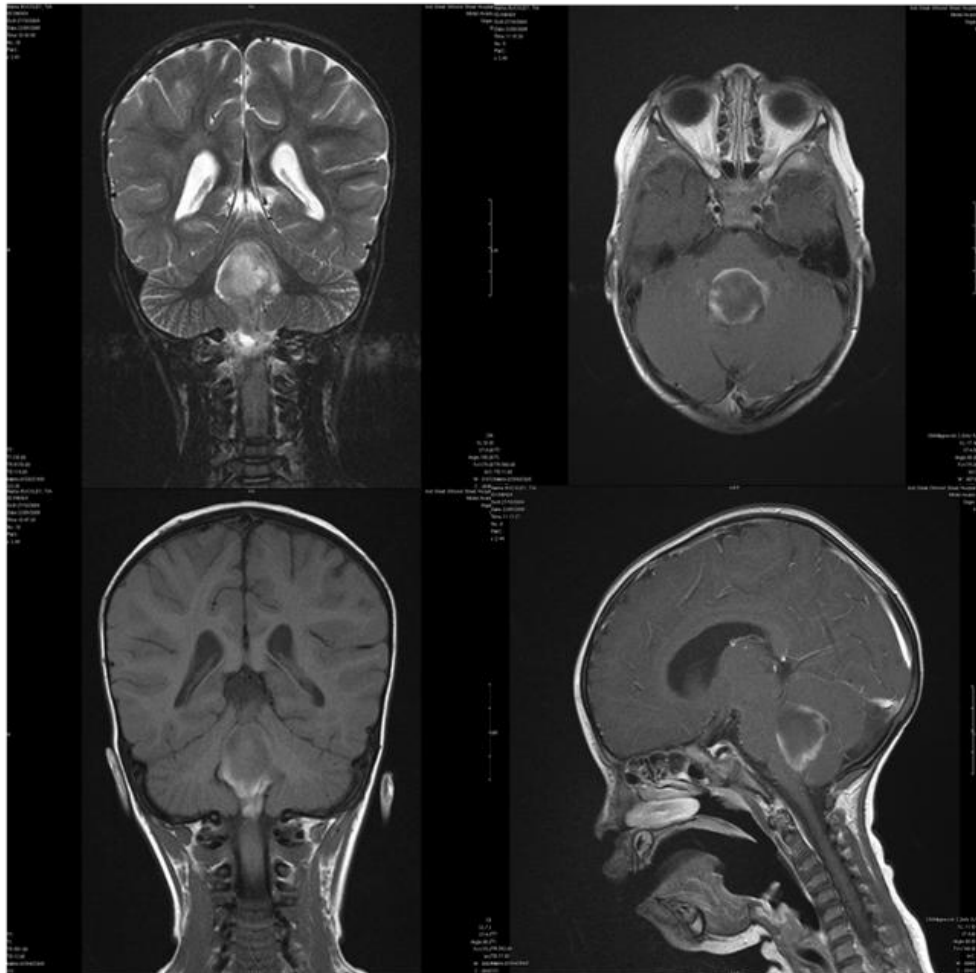


**Figure 1.10 Ependymoma. Coronal T2 and T1-weighted images, axial and sagittal T1-weighted images with contrast.** A large peripherally enhancing mass arising from the dorsal aspect of the midbrain and growing into and obstructing the fourth ventricle is seen. Haemorrhage is evident within the tumour.

---

The atypical teratoid/rhabdoid tumours may be both supra or infratentorial in location with a heterogeneous appearance typically with haemorrhage, necrosis, and cysts, enhancement is similarly heterogeneous. When infratentorial they arise from the cerebellar vermis and are not usually midline. When supratentorial, they are solid with necrotic regions which enhance heterogeneously (6).

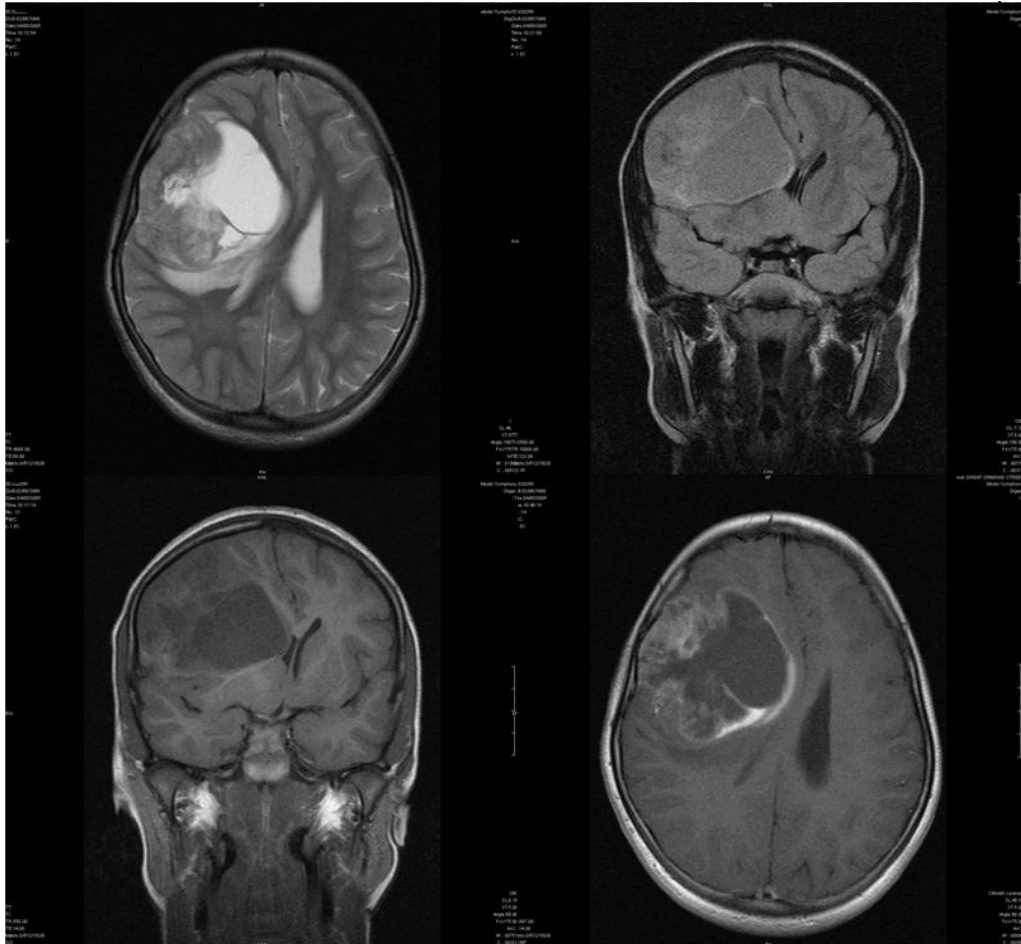


**Figure 1.11 Atypical teratoid rhabdoid tumour (ATRT). Axial T2-weighted, coronal FLAIR, coronal T1-weighted and axial T1-weighted MRI with contrast.** There is a right frontal lobe mixed cystic/necrotic and solid tumour with adjacent scalloping of the frontal bone. The peripheral solid component has signal characteristics of high cellularity. There is midline shift to the left with contralateral hydrocephalus.

---

Dysembryoplastic neuroepithelial tumours (DNTs) are low grade lesions and often present with seizures in young children. They tend to be located in the temporal lobe and also the frontal lobe. They lie, in part or entirely, in the cortex and may have poorly defined contours. They have multinodular bright signal qualities on T2-weighted MRI; they can also show remodelling of the adjacent calvarium. On T1-weighted images they are typically hypo-intense and are devoid of mass effect or associated oedema. A minority show discrete foci of nodular or ring enhancement (12).

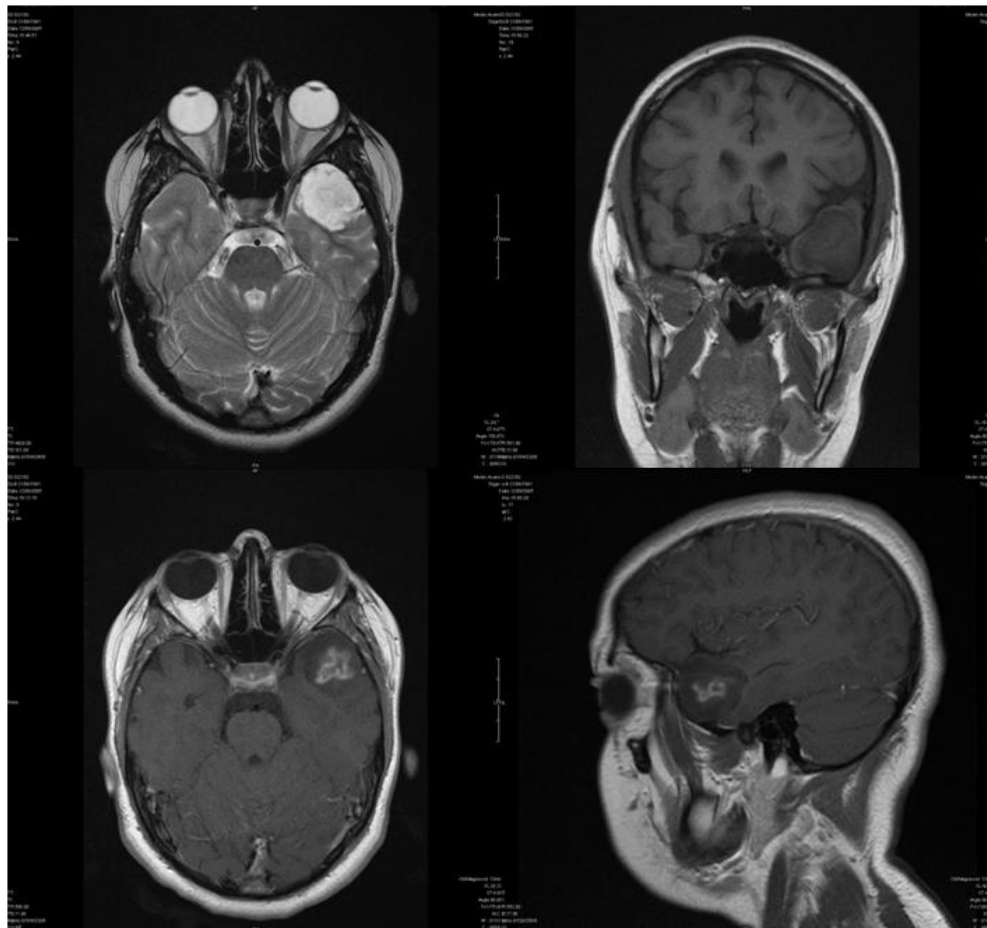


**Figure 1.12 Dysembryoplastic neuroepithelial tumour (DNT).** Axial T2-weighted, coronal T1-weighted and axial and sagittal T1-weighted MRI with contrast images. A small cortical mass with a rim enhancing central component is seen in the left anterior temporal region exerting minimal mass effect. There is expansion of the left middle cranial fossa indicating a long standing lesion. Also characteristic is the absence of white matter changes indicative of oedema.

---

Choroid plexus papillomas tend to have a papillary appearance and are intra ventricular neoplasms derived from choroid plexus epithelium, typically occurring mainly in childhood. They occur most frequently in the lateral ventricles, although they can occur in the fourth ventricle or even be multifocal. Clinically they manifest themselves due to hydrocephalus either through obstruction to cerebrospinal fluid flow or its excessive production. On T2-weighted images they appear as lobulated masses with frond like papillary projections. They may be isointense relative to the cortex and have internal hypointense foci that may represent prominent vessels. Often there is associated hydrocephalus and transependymal cerebrospinal fluid flow (13).

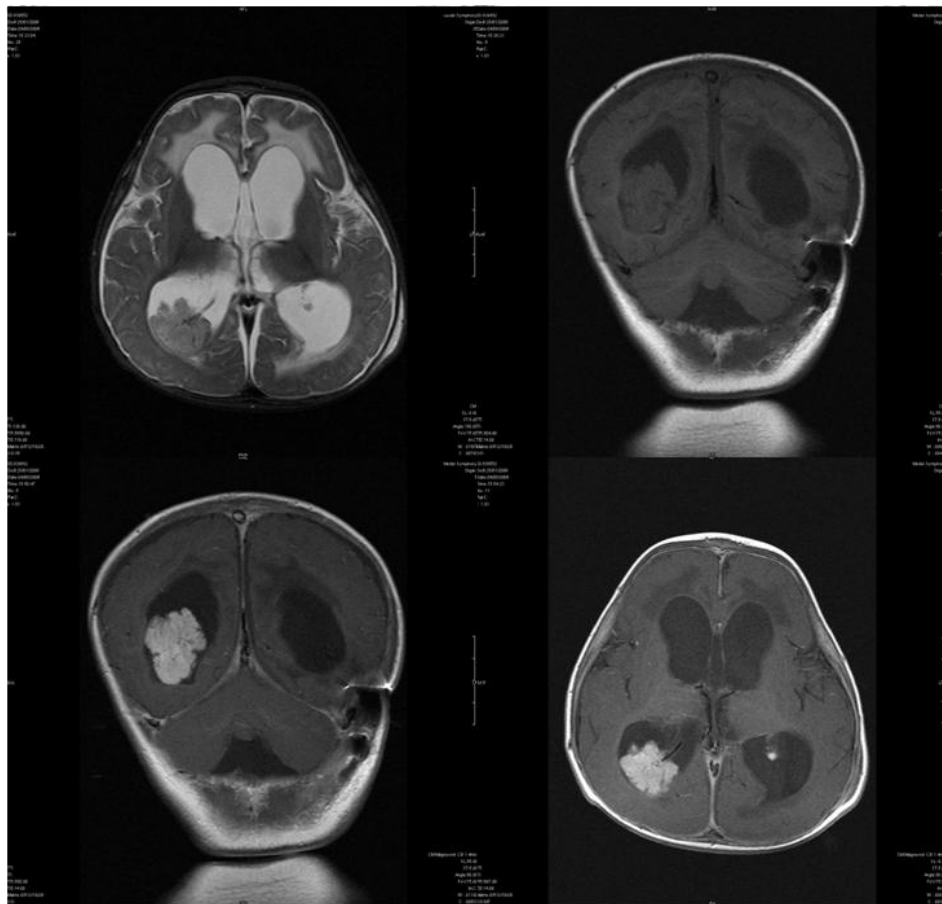


**Figure 1.13 Choroid plexus papilloma. Axial T2-weighted, coronal T1-weighted, coronal and axial T1-weighted MRI with contrast.** Imaging shows a lobulated highly vascular lesion within the right trigone which remains confined to the lateral ventricle. There are vascular flow voids associated with it likely to represent choroidal vascular supply. It enhances avidly with contrast.

## 1.3 PAEDIATRIC CNS INTRACRANIAL TUMOURS

Cancer in childhood is rare and in comparison to adult practice the majority can expect to be cured. However paediatric primary CNS tumours account for almost 20 percent of all neoplasms in children less than 15 years. They represent the second most common form of paediatric cancer exceeded only by leukaemia. In addition they represent the leading cause of death in infancy and childhood in developed countries.

### 1.3.1 PAEDIATRIC CNS TUMOURS BACKGROUND

The incidence of paediatric CNS tumours in the UK is 2-3 per 100,000 (5). Incidence in the US is reported as similar (14) and 28,000 children in the U.S. are living with the diagnosis of a primary brain tumour with 3,750 more children diagnosed each year, equating to 10 a day.

They differ from adult tumours in some important respects. A greater proportion are infratentorial and low grade gliomas tend to predominate, hemispheric high grade gliomas, whilst common in the adult population, are rare in children. Typical low grade gliomas include pilocytic astrocytomas commonly located in the posterior fossa. PNETs constitute approximately a quarter of all paediatric CNS tumours and have bimodal age distribution with peak incidences at ages 3-4 years and subsequently at 8-9 years. There are more than 130 types of paediatric CNS tumour (15) and many of them are rare and specific to children making diagnosis and treatment more of a challenge as the numbers encountered for study are often small. The type and incidence of paediatric CNS tumours from five large series are presented in Table 1.2. Similar information is shown of those cases presenting to GOSH in 2007, in figure 1.14.



Tumour	% incidence
Astrocytic tumours	47
Ependymomas	11
Medulloblastomas	19
Pineal region tumours	2
Craniopharyngiomas	6

**Table 1.2 Incidence of paediatric CNS tumours. Summary of data from 5 large series (Cohen & Duffner 1994) (16)**

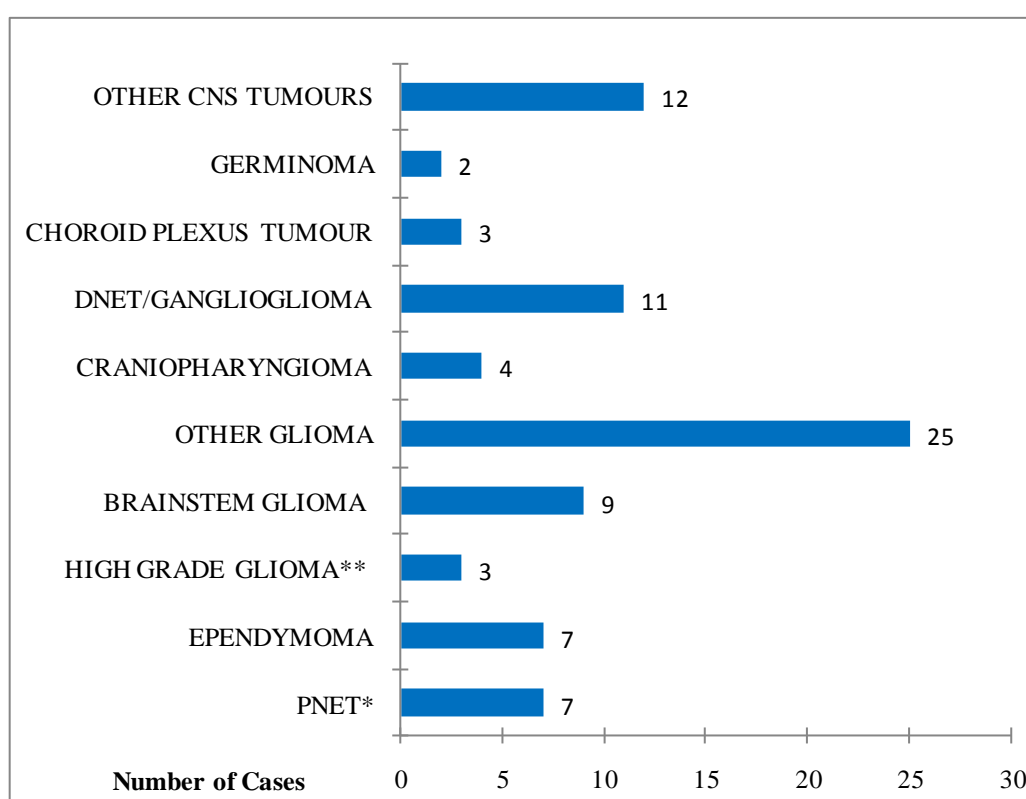


**Figure 1.14 Types of CNS Tumour presenting to GOSH in 2007 as a first diagnosis.** \*Includes PNET-Medulloblastoma & ATRT. \*\* Excludes brain stem lesions

In terms of age-related risk children less than 5 years of age have the greatest incidence of brain tumours. The National Institute of Neurological Disorders and Stoke report (17) that one third of all tumours have presented by this age, three quarters have presented by

the age of ten years. In terms of age distribution by tumour type for ages 0-3 PNET and ependymoma were commonest (11 and 7 per million respectively). Gliomas had the lowest incidence throughout infancy and peaks at age 8 and 17 (9 and 7 per million) (18). Figure 1.15 shows the distribution of ages for new tumours presenting to GOSH in 2008.

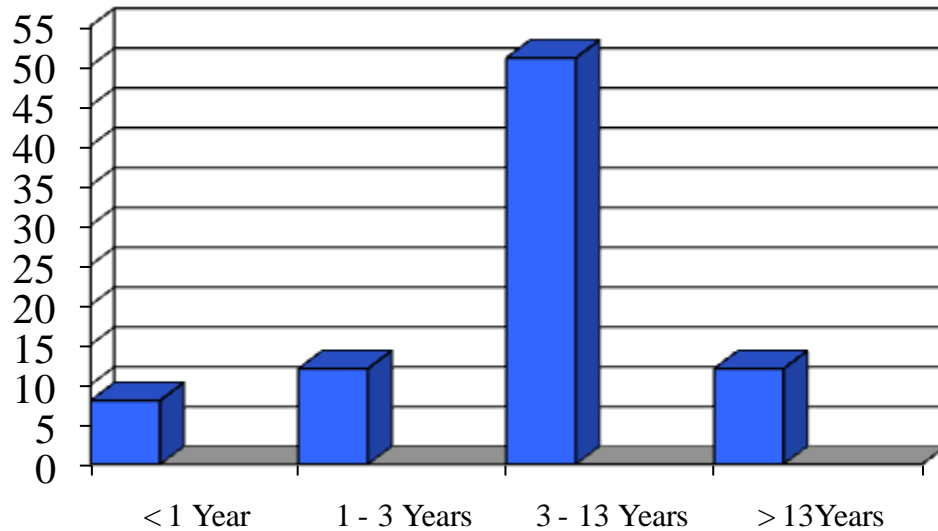


**Figure 1.15 CNS tumours presenting to GOSH in 2008 by age group**

---

In addition there has been an increase in the diagnosis of paediatric brain tumours over the last twenty years. Between 1973 and 1994, the reported incidence of childhood brain tumours increased by 35% (18). This is thought to be due to the increasing use of MRI and coincides with its introduction and development as an imaging tool.

### 1.3.2 DIAGNOSTIC IMAGING

The use of CT and MRI and typical imaging findings of the common paediatric CNS tumours investigated in this work are covered in section 1.2.

### 1.3.3 TREATMENT MODALITIES

The treatment pathways for new paediatric tumours are variable and decisions as to the correct course are taken in the context of multidisciplinary teams (5). There still remains some debate over the correct course of action in terms of surgical intervention and the decision may rest as to whether a surgical biopsy should be undertaken or whether treatment in terms of radiotherapy or chemotherapy can proceed on the basis of the presumptive diagnosis based on the clinical history, laboratory investigations and the radiological findings. The treatment pathways of the new CNS tumours presenting to our institution in 2008 is shown in Figure 1.16.

The development of dedicated paediatric neurosurgeons and the provision of intensive care beds have lead to an increase in the number of surgical cases being undertaken. The operations have become more radical and the morbidity has decreased. Of the 83 new cases at GOSH in 2008, 69 (83%) cases had histological confirmation either by biopsy, debulking or radical surgery and 22 cases had more than one procedure (typically insertion of a VP shunt) of the surgical cases 20 were diagnostic open or stereotactic biopsies. Of the 69 children who had surgery 21 went on to have radiotherapy and 24 to have chemotherapy.

The nature of the surgical intervention in an individual case depends on many factors, for example direct open diagnostic biopsy is preferred to stereotactic biopsy in very young children while remaining an option in older children (5). There exists an intention to avoid surgery and particularly biopsy with its attendant risks of morbidity and mortality where possible. Imaging can in some cases provide a satisfactory diagnosis without the need for biopsy, such as optic nerve and brainstem gliomas in children with neurofibromatosis. Germ cell tumours have quite distinct imaging

findings and in combination with raised CSF / serum markers (HCG/ $\alpha$ FP) the need for diagnostic surgical intervention obviated.

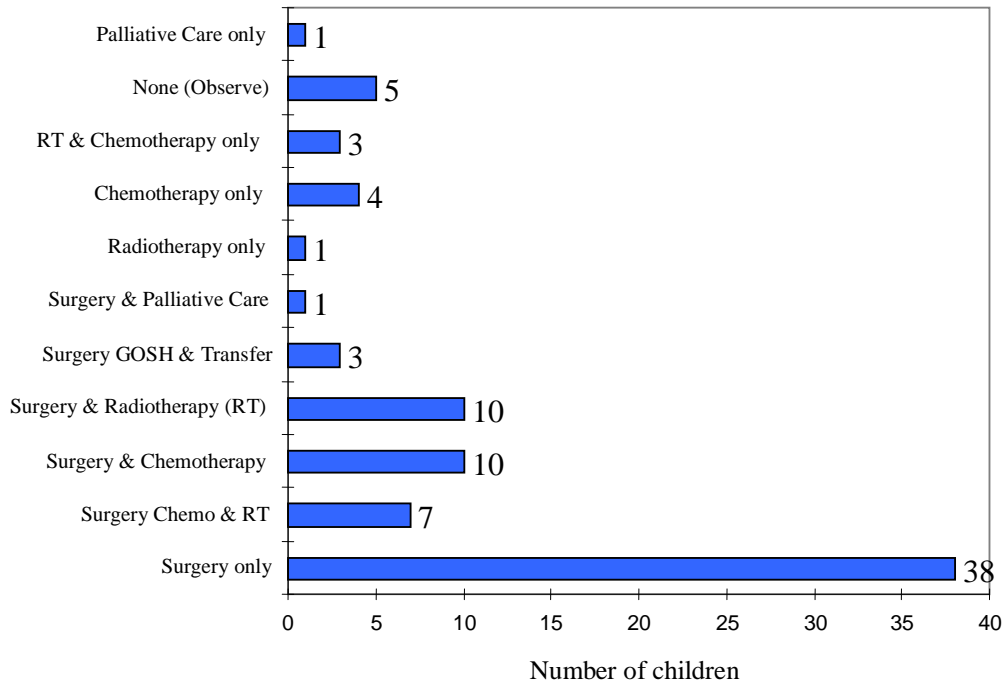


**Figure 1.16 Summary of treatment pathways. Children presenting with new CNS tumours to GOSH 2008**

---

Radiotherapy and chemotherapy are the alternative and additional treatment options when surgery alone is inadequate or not indicated due to the risks and poor prognosis from the tumour, (as in the case of atypical teratoid rhabdoid tumours ATRTs). Radiotherapy has improved greatly in terms of focusing the beam and treatment area, hence diminishing the amount of normal brain exposed, however this still poses a significant risk. Radiotherapy is not usually undertaken in children under 4-5 years for fear of the risks of long term developmental damage. Tumours with a tendency to metastasise throughout the neuraxis can warrant whole craniospinal radiotherapy, typically cases such as PNETs fall into this category.

Chemotherapy has had some success but is thought in part to be limited by the presence of the blood brain barrier which prevents water soluble drugs crossing into the brain. This has at least been the experience with adult lesions, although there appear to be more positive results in paediatric tumours (19-21).

Overall survival for children with paediatric brain tumours has improved in the past 10 to 20 years and is just over 70% (18). This is most likely due to the multidisciplinary approach with improved surgical technique, better peri-operative care, the focused use of radiotherapy and multidrug chemotherapy regimes.

Despite these improvements, survivors often suffer from lifelong side effects of treatments such as surgery, radiation and chemotherapy. They may have physical, learning and emotional difficulties that will limit the quality of their lives into adulthood. This underlines the key nature of minimising mortality and morbidity associated with treatment modalities, in the case of surgery, either the avoidance of it or the improved pre-operative planning in terms of the location of eloquent white matter tracts (22).

## 1.4 CEREBELLAR WHITE MATTER ANATOMY

The cerebellum is involved in the control of fine movement, muscle tone, balance and equilibrium. Put simply it compares that which you thought you were doing with that which you are doing, through proprioceptive feedback. The key difference from the cortex of the cerebrum in terms of circuitry is that the functions are represented ipsilaterally in the cerebellum (23). It is thought to perform a key role in motor learning of fine or complex tasks (24).

The fourth ventricle is covered by the cerebellum, the narrowed midline is the vermis and the lateral expansions form the hemispheres. It is divided into a flocculonodular lobe which is located posteriorly and a more anterior corpus cerebelli which is subdivided into an anterior and posterior lobe. The cerebellar cortex forms the outer layer and overlies a white matter core together forming the arbour vitae, at the centre of which are the cerebellar deep nuclei. These nuclei are the output areas of the cerebellum, receiving inputs from the cortex and sending projections to the thalamus, red nucleus and brainstem. The nuclei are, named medial to lateral, the fastigial, interpositus (in man it is divided into globose and emboliform) and the dentate nucleus, they are bilaterally represented (25).

The efferent and afferent connections from the cerebellum transit via three peduncles which are bilateral and contribute to the walls of the fourth ventricle. All output from the cerebellum, via the deep nuclei, passes through the superior cerebellar peduncle, although it also contains some input fibres. The middle cerebellar peduncle receives input exclusively from the pontine nuclei. The inferior cerebellar peduncle contains exclusively inputs (26).

The major afferent connections are from the vestibular system, spinal cord, inferior olive, and the cerebral cortex. The vestibular system input helps control coordination of posture and gait via the midline muscle groups and the limbs. The fibres distribute principally to the posterior vermis and hemisphere of the flocculonodular lobe transiting via the inferior cerebellar peduncle. Input from the spinal cord is via the spinocerebellar tract for the lower extremity and enters through the inferior cerebellar peduncle; the accessory cuneate nucleus providing upper limb input gives rise to cuneatocerebellar fibres. These cuneatocerebellar fibres distribute to the anterior vermis, the anterior lobe and the paravermian areas of the anterior and posterior lobes delivering proprioceptive information originating in the limbs in order to coordinate the limbs for gait and posture. In essence the vestibular, spino- and cuneatocerebellar input is ipsilateral.

The olivocerebellar fibres form a substantial part of the inferior cerebellar peduncle, pass contralaterally from the olive, and distribute to all areas of the cerebellum. The fibres are thought to deliver spinal cord sensory and supra-segmental motor input to the cerebellum. The corticopontine fibres descend from the motor areas of the cerebral cortex to synapse on the nuclei of the ipsilateral basis pontis. Once the pontocerebellar fibres have synapsed they cross and enter the cerebellum via the middle cerebellar peduncle, distributing primarily to the hemispheres of the anterior and posterior lobes. This cortico-pontocerebellar input helps regulate fine movements particularly in the distal muscles of the hand. The patterns of distribution and connections of the cerebellum are demonstrated in figure 1.17.

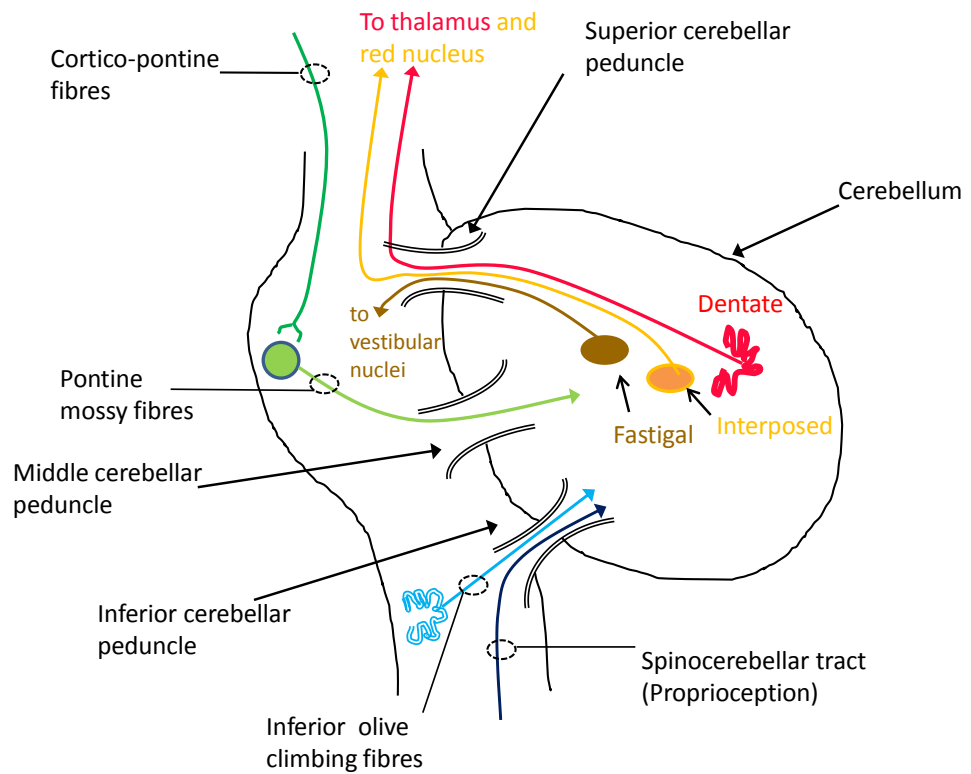


**Figure 1.17 Connections of the cerebellum. Superior, middle and inferior cerebellar peduncles**

Lesions of the cerebellum in primates, specifically removal of the cerebellum result in hypotonia or loss of muscle tone. In reversible cooling of the dentate nucleus it is seen that reaction times are slowed and that there is impairment of rapidly alternating movements, thought to be due to a delay in antagonist onset. The response to muscle load changes is impaired. In situations where load changes are expected but not predicted the muscle stretch evokes an antagonist response to limit oscillations. As a consequence of cooling the antagonist response is delayed (27). Slow movements become jerky and tracking moving targets with the hand also becomes jerky as the velocity is no longer matched whilst the subject attempts to match the position. This has



led Thach et al in 1993 (24) to suppose that the cerebellum is important in the co-ordination of multiple joint movements.

In the clinical spectrum the classical descriptions were by Gordon Holmes in 1939 (28) where he described hypotonia (loss of muscle tone), ataxia (loss of co-ordination) and deficiencies in movement distance (dysmetria), velocity and rhythm of muscle movements. In addition he described a loss of co-ordination between different muscle groups (asynergy) and associated postural abnormalities, specifically truncal ataxia. This truncal and lower limb ataxia leads to gait ataxia and difficulty standing, ataxia of the upper limbs causing decomposition of smooth movements represented as an intention tremor. When testing for the ability to perform a rapidly alternating co-ordinated movement, the force and rhythm deficits are revealed as dysdiadochokinesia. These deficits can be bilateral or if the lesion is unilateral in the cerebellum it may only produce ipsilateral symptoms (23;28-30).

---

## 2 DIFFUSION MRI THEORY AND APPLICATIONS

---

### CONTENTS

---

2.1	MR Diffusion Imaging	50
2.1.1	Principles & Background.....	50
2.1.2	Diffusion-Weighted Imaging.....	52
2.2	Clinical Applications of DWI in Intracranial Lesions	56
2.2.1	Diffusion-weighted imaging CNS applications.....	56
2.2.2	Diffusion-weighted imaging of intracranial Tumours.....	58
2.3	Diffusion Tensor Imaging	60
2.3.1	The Diffusion Tensor.....	61
2.3.2	Diffusion Tensor Imaging.....	64
2.3.3	Complex Diffusion Models .....	65
2.4	White Matter and Tractography	67
2.4.1	Anatomy of White Matter.....	67
2.4.2	Tractography.....	67
2.5	DTI and Tractography Applications	71
2.6	Intentions of this Study	75

---

### 2.1 MR DIFFUSION IMAGING

#### 2.1.1 PRINCIPLES & BACKGROUND

Diffusion-weighted imaging (DWI) as a means of providing image contrast has become established over the last 20 years. DWI is sensitive to the random microscopic movements of water molecules in tissues, these movements are intimately related to the structure of the surroundings of the molecules.

The phenomenon of MR signal attenuation in the presence of field gradients due to movement or diffusion of molecules was initially described by Carr and Purcell in 1954 (31;32). Subsequently investigation by Stejskal and Tanner (33) resulted in the publication of their pulsed gradient technique which is frequently used in modern DWI. The later development of EPI and stronger field gradients throughout the early 1990's has enabled its use as a clinical tool.

The ability of DWI to reflect the movement of water molecules in tissue offered the possibility of a unique non-invasive means of probing the tissue architecture at a cellular level. In 1990 Moseley et al (34) showed, using a cat brain stroke model, that an area of ischaemia could be identified through a reduction in the apparent diffusion coefficient (of up to 50%) at thirty minutes whilst conventional imaging showed no appreciable change. The application was then used in the investigation of acute stroke patients (35) where regions of ischaemia could be visualised within minutes of the onset of a stroke or infarct (36-42).

The basis to the MR signal loss is the underlying thermal process of diffusion; molecules undergoing random translational movements in a fluid. Diffusion can occur along a concentration gradient from a region of high to low concentration; this is known as bulk diffusion. In the presence of a uniform concentration, where no other external forces act on them, the diffusion of molecules is described statistically. A molecule moves a certain distance in a certain time; known as self-diffusion or Brownian motion. The movement is temperature dependent and affected by interactions with adjacent molecules and has been described as a random walk (36). As the movements are random there is no net change in position (i.e. no bulk diffusion) and hence the probability of moving in any direction is identical. The process is proportionally time dependent, with increasing time comes increasing distance following a Gaussian

(normal) distribution. The process is quantified by Einstein's equation (43) to give the average distance moved in a given time:

$$\langle x^2 \rangle = 2Dt$$

Where  $\langle x^2 \rangle$  is the average value for the square of the distance moved in time  $t$  and  $D$  is the diffusion coefficient. MRI is sensitive to water molecules; their diffusion due to thermal energy driven from reactions within the body provides the substrate for investigation (41;43;44).

### 2.1.2 DIFFUSION-WEIGHTED IMAGING

In an unrestricted environment the main determinants of the magnitude of diffusion include the molecule investigated and the temperature it experiences. A further variable is then the presence of impediments to movement as provided by tissue micro architecture. CSF water molecules within the ventricular system are under less constraint than the water molecules in the extracellular and intracellular environments. The differing amounts of diffusion can be used as an image contrast in MR sequences sensitive to this as demonstrated by Le Bihan et al 1986(45).

MR imaging is sensitive to movement both at the macroscopic level (respiration, cardiac pulsation) and also at the molecular level. This can manifest as image artefact or signal loss. The phase shifts due to the diffusion and resultant signal loss due to microscopic movements can be quantified but are typically small in conventional MRI, with the addition of stronger magnetic gradients the signal loss is amplified. As described by Stejskal and Tanner (33) two strong pulsed gradients were added to a spin echo sequence, symmetrically either side of the 180° refocusing pulse. In this case the first additional gradient pulse following the initial 90° radiofrequency pulse (where the

spins align along the x-axis), briefly exposes the spins along the gradient to a differing magnetic field strength. The result is a change in phase of the spins along the gradient direction. The 180° pulse is applied reversing the phase and then a second identical gradient pulse. If the spins were to remain stationary it would mean no net phase shift as the gradients are identical. The effect of the diffusion of the water molecules means that the spins do not remain stationary between the first and second refocusing gradient pulses. Hence the signal measured when the spins are under relaxation is proportional to the loss of phase of all the spins within the region (voxel) being quantified. The loss of phase results in a signal loss and is proportional to the amount of diffusion, although there is also an effect from T2 relaxation in the spin dephasing and hence both T2 and diffusion contrast are seen. Hence the greater the degree of random molecular motion the greater the signal loss (36;39).

The degree of signal loss is also affected by the duration and strength of the diffusion gradients. The degree of diffusion sensitivity of the sequence is determined by the b value (*gradient b factor*) a product of the gyromagnetic ratio, gradient strength and duration and the time between the leading edges of the pulses. The effect of different b-values on the image contrast is illustrated below (Figure 2.1). When obtaining diffusion-weighted images long echo times are necessary and the images produced are heavily T2-weighted. If a further acquisition of EPI at  $b = 0 \text{ s mm}^{-2}$  is acquired the diffusion, D, can be calculated as per the expression below;

$$\ln\left(\frac{S(b)}{S(0)}\right) = -bD$$

Where  $S(0)$  and  $S(b)$  are the signals with and without diffusion gradient both acquisitions are equally T2 weighted, its effect is removed from the calculation. When

this calculation is applied on a voxel basis a map of the diffusion coefficients is created, known as an apparent diffusion coefficient (ADC) map.

The relatively small signal loss measured can be amplified to make it more significant through the use of stronger gradients and also extended echo times. In so doing there is a significant increase in the acquisition time and also a reduction in the signal to noise ratio of the spin echo. Increased acquisition time in a spin echo sequence that is highly sensitive to molecular motion means the effects of other intrinsic biological movements (cardiac pulsations, respiration and patient movement) are more significant and degrade the image. In order to counter this, as discussed in section 1.1 a much faster sequence is implemented, typically an echo planar image, which rapidly acquires whole tissue coverage. These sequences are however prone to susceptibility artefact and poorer resolution (44;46).

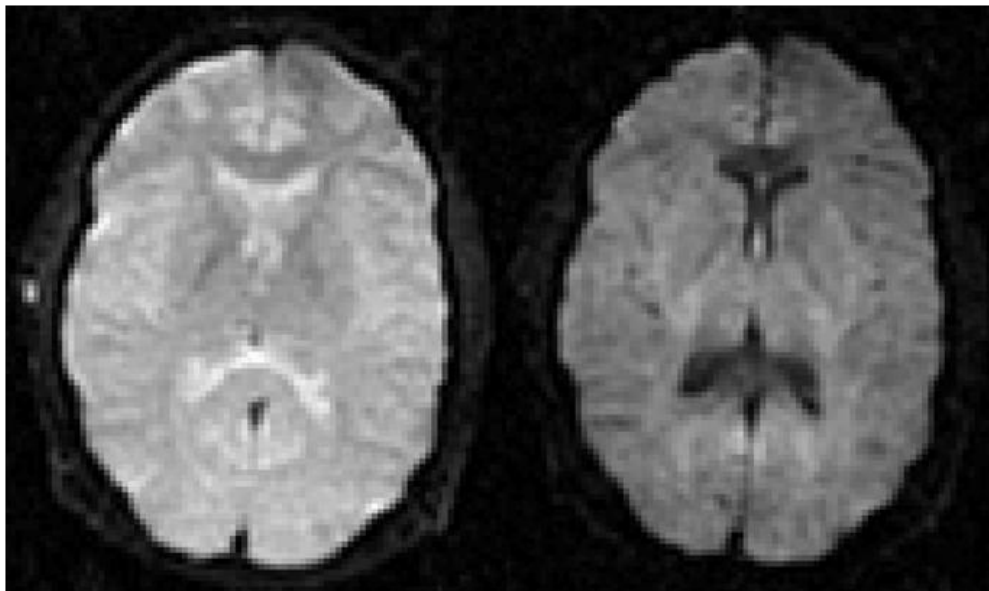


**Figure 2.1 Diffusion weighted images;  $b = 0 \text{ s mm}^{-2}$  (left) and  $b = 1000 \text{ s mm}^{-2}$  (right)**

---

In the above images it is clear that different tissues have different degrees of diffusion, as mentioned previously. In the ventricles of the brain the water molecules are

unconstrained and diffusion distance increases linearly with the square root of time. In soft tissue the water molecules are more constrained and hence diffusion is reduced, this situation has been compared to the movement of water in aqueous protein solutions (42). When the water molecules are constrained the diffusion distance is diminished even with extended time.

In a biological structure such as the brain, diffusion distances tend to be shorter than in free fluid as a consequence of the cell membrane and internal organelles and structure. However debate exists as to the determinants of diffusion in terms of the contributions of the fluid compartments on the diffusion coefficient and the effects of membranes within the tissue. The calculation of the reduced diffusion coefficient of water in a tissue as compared to that of free water was established by Nicholson and Phillips in 1981 (46;47). They also hypothesised that the effect originated from the molecules being forced around obstructions due to fibres, intracellular organelles and macromolecules. In effect the environment greatly limits the degree of diffusion and hence the use of the expression, apparent diffusion coefficient. In order to reflect that the diffusion coefficient of water has not actually changed but that the root mean displacement per unit time is diminished. The measurement of the differing amounts of impedance in structures underlies the principle of diffusion-weighted imaging (40).

The clinical applications of this contrast have increased through technical development; specifically the use of shielded gradient coils which have reduced eddy currents produced by the rapidly changing gradient pulses fundamental to diffusion-weighted imaging (40;46;47).

## 2.2 CLINICAL APPLICATIONS OF DWI IN INTRACRANIAL LESIONS

In 1981 Meerwall and Ferguson looked at the distances moved by water molecules (48) surrounded by structures with permeable membranes, their paths were seen to be tortuous through interactions with neighbouring structures. When examining such motion effects at the voxel level, in effect a more detailed investigation of the tissue structure is achieved than the apparent resolution of conventional imaging. It may follow from this that in disease processes where there may be alterations in the cellular structure as a consequence of the patho-physiology of the disease, the diffusion of water may also be changed, reflecting this.

### 2.2.1 DIFFUSION-WEIGHTED IMAGING CNS APPLICATIONS

In the brain and other living tissues the integrity of cell membranes and their function to maintain osmotic gradients is vital to the regulation of movement of water between the intra and extracellular compartments. When the blood supply and hence energy supply to cells is diminished or abolished a sequence of events takes place affecting the movement of water. Initially water diffusion is restricted secondary to cell swelling through the reduction of the extracellular volume, subsequently with loss of cell wall integrity diffusion increases (49;50). This pattern of interrupted blood supply is seen in ischaemic injury to the brain. Moseley et al in 1990 investigated imaging findings using occlusion of the carotid arteries or the middle cerebral artery in the cat to mimic the effects of an ischaemic stroke. In ischaemic regions the DWI showed hyper-intensity when the T2-weighted imaging did not from 45 minutes following the ischaemic insult, where as the T2-weighted imaging took more than 2 hours to reveal similar changes. These appearances were hypothesised as being secondary to failure of cell membranes to regulate the movement of water and its consequent accumulation in the cell



(cytotoxic oedema) causing a fall in diffusion and hence a bright signal (reduced diffusion coefficient) (34;51).

Pierpaoli et al, in 1993 (52) investigated the correlation of MR appearances with the cytological and histological findings in ischemic tissue using a photochemical model of cerebral infarction in rats. They undertook diffusion and T2-weighted MR imaging and compared appearances with light and electron microscopic findings. The T2-weighted images demonstrated vasogenic oedema but did not demonstrate differences between regions of cell damage and surrounding oedematous regions. The DWI and calculated ADC maps revealed elevated ADC in the non-ischaemic oedematous regions but in regions identified histologically as damaged or necrotic it was diminished. As the lesion progressed with time, in the core of the infarct the ADC changed from being reduced to being raised; regions subsequently identified as having cellular lysis on electron microscopy. The early identification of areas as reversible and irreversible ischaemia has the potential to better identify individuals who may benefit from further treatment in order to prevent permanent damage to that tissue (41;53;54).

The techniques application in the evaluation of acute cerebral ischaemia is well recognised (55). It has been used to distinguish between cystic or necrotic brain tumours and abscesses, where the ADC of abscesses is significantly reduced in comparison to those of tumours (56-59). This is thought to be due to the high viscosity and more cellular, purulent abscess fluid as compared to necrotic tumour and tumour cysts (60;61). The discrimination of arachnoid cysts from epidermoids has had positive results, the basis of which is thought to be that epidermoids have more complex internal structure and hence more restricted diffusion by comparison to arachnoid cysts that allow free diffusion of water (60;61).

DWI has been used in the study of multiple sclerosis plaques; diffusion was increased within plaques visualised on T2-weighted images (62;63). Subsequently apparently normal white matter regions between visible plaques have been seen to have reduced diffusivity (64). This has raised questions as to the hypothesised nature of the disease; whether it is a more diffuse rather than multifocal process.

Head injury and diffuse axonal injury have been investigated with DWI and changes similar to those seen in ischaemic stroke revealed, persisting up to 18 days post injury (65). Further studies have had conflicting results regarding changes in diffusion characteristics but when DWI is compared with conventional MRI, specifically T2-weighted fast SE, FLAIR, and T2\*-weighted gradient echo sequences, the DWI reveals the greatest number of traumatic lesions. Huismann et al in 2003 demonstrated that the DWI signal abnormalities correlated more highly with outcome as assessed by the Rankin scale and Glasgow outcome score (39).

### 2.2.2 DIFFUSION-WEIGHTED IMAGING OF INTRACRANIAL TUMOURS

Following the preliminary investigations into DWI of intracranial lesions as seen in the work of Le Bihan et al and others (45;66-69) it was shown that the diffusion coefficients of cystic components of lesions tended toward those of free water, depending upon the contents and viscosity of the fluid. This proves useful when the pyromagnetic material in the cyst shortens the T1 and T2 to the point where cystic fluid appears similar to that of solid tissue (70). This was also extended to the discrimination of cystic tumours from abscesses where the contents of the cysts differed in terms of their pyromagnetic properties (60;61;71). In the case of epidermoids the signal characteristics of the principal component, fat, made it difficult to discriminate the solid tumour from arachnoid cysts. The application of DWI highlighted the restricted diffusion in the solid

lesion as compared to the fluid comprising arachnoid cysts (68;69;72). In a further application to determine neoplastic lesions from other lesions DWI has been used by Camacho et al (73) to elucidate the difference between toxoplasmosis and cerebral lymphoma in patients with AIDS.

In terms of discrimination and determination of types of intracranial tumours several diffusion measures have been used (61;74-81). Mean diffusivity (MD) which is the ADC and also commonly, metrics derived from the enhancing and non enhancing tumour and the surrounding oedema (76;79;80;82;83). Results from these metrics have not been consistent between all groups (61;75;81;84) and this may represent different methodologies and the problems encountered with bias when using region of interest analysis.

A further development is the differentiation of tumour grade (75;77;85;86) and type (74;87), again results are variable. The most fundamental conclusions have been around the higher grade tumours which can be more densely cellular and hence have reduced diffusion (74;75;77;85;87). Similarly authors have reported that in more densely cellular tumours such as medulloblastomas (a common posterior fossa paediatric tumour) and lymphomas, the diffusion is more restricted (74;85;87). Application of diffusion tensor metrics derived from the diffusion data has also been used in discrimination of tumour type, further coverage in the adult and specifically in the paediatric intracranial tumour population is found in chapter 4.

## 2.3 DIFFUSION TENSOR IMAGING

The Gaussian distribution of water molecules moving from any starting point is dependent upon the presence of an unrestricted environment. In this case the diffusion is described as isotropic (37). As mentioned previously, the environment seen in tissues provides multiple impedances to diffusion in some directions as opposed to others and this is described as anisotropic diffusion. The impedances are provided by the cellular structures which act as physical boundaries to the movement of water molecules; this is represented in diffusion-weighted imaging as a reduction in the ADC. The cellular structure can lead to diffusion in a particular direction being more favourable than another. This is thought to be the case in the white matter of the brain with multiple parallel axons constituting the white matter tracts.

When using DWI measurements of diffusivity in different regions of the brain it is clear that the diffusion within the CSF is similar to that of free water and appears to be isotropic. In the more restricted environment of the white matter the ADC is much lower and the diffusion is anisotropic, although at a voxel level the diffusion in the gray matter is near isotropic (88).

In 1990, Moseley et al (34;34) showed that, in brain and spinal cord white matter of the cat, the amount of diffusion or diffusion coefficient measured using diffusion weighted MRI was dependent upon the direction it was measured in. The coherent arrangement of the fibres in those tissues was thought to be the cause of the anisotropy through hindrance of free movement of water in directions perpendicular to the white matter. Preference for diffusion was given to the direction perpendicular to the long axis of the axons (89).

### 2.3.1 THE DIFFUSION TENSOR

The ability of the diffusion anisotropy to characterise the tissue structure more clearly is dependent on quantification of the directionality of the diffusion. A simple scalar measurement such as the ADC does not provide a 3 dimensional representation of the anisotropy (36). The ADC only quantifies the diffusion in the form of signal loss in a single direction determined by the orientation of the diffusion sensitising gradient pulses.

In order to characterise the diffusion anisotropy more clearly the ADC can be measured in multiple unique directions and the differences compared. Skeletal muscle was the first tissue to be characterised in such a fashion by Cleveland et al in 1976 (90). Subsequently the diffusion tensor model was introduced in 1994 by Basser et al (91;92) in order to more completely describe the anisotropy.

The model proposed by Basser et al (91;92) was that of a tensor, using a symmetrical matrix of six unique elements. The basis being that the measurements of diffusion along different axes are correlated and the tensor describes this (93). The tensor takes the form of a symmetrical 3 x 3 matrix where the ADC is measured in 3 orthogonal directions and planes between them. In order to acquire the tensor the ADC must be measured in at least 6 directions through the application of at least 6 unique diffusion gradients. In addition an acquisition at  $b = 0 \text{ s mm}^{-2}$  without diffusion weighting (a T2-weighted image) is also acquired.

From this mathematical construct, a number of rotationally invariant properties can be derived. It is not necessary that the dominant direction of diffusion be aligned with any of the gradient directions but it can be derived from the calculations on a voxel basis. Specifically the trace, corresponding to the magnitude of the diffusion, is obtained.

Through a process known as diagonalisation the “dominant direction” of diffusion is calculated, known as the principal eigenvector (1) (corresponding to the direction of fastest diffusion). Further eigenvectors (2 and 3) are calculated in orthogonal planes to the principal eigenvector and the ADC’s in all these directions are known as the eigenvalues:  $\lambda_1$  (principal),  $\lambda_2$  and  $\lambda_3$ .

The inference from the principal eigenvector in tissues where fibres are orientated in a similar direction is that it will be co-aligned with the orientation of those fibres (Lin Tseng 2001, Basser 1994). Basser et al (91;94) proposed a representation of this tensor as an ellipsoid defined by the eigenvectors and eigenvalues as seen in Figure 2.2.

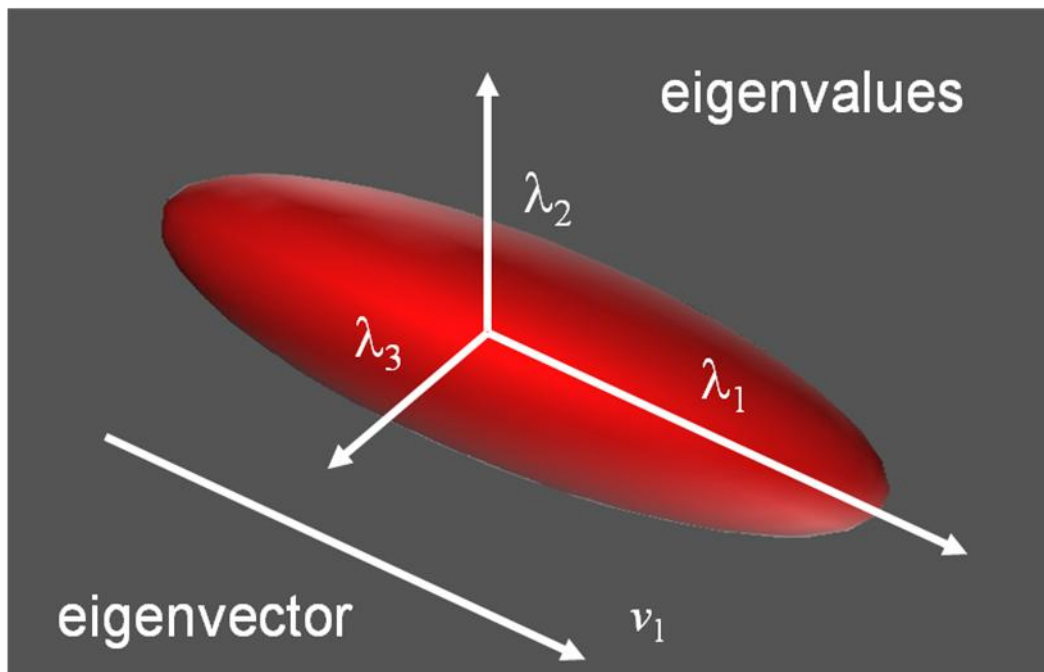


**Figure 2.2 Eigenvectors and eigenvalues as applied to an ellipsoid representation**

---

The ellipsoid representation changes appearance dependent on the equality of the eigenvalues, where the diffusion is more isotropic, as it is within the CSF the ellipsoid becomes more spherical as there is no or minimal structure. Within the more anisotropic

tissues the appearance of the ellipsoid is determined by the predominance of the principal eigenvectors. Where there is a strong principal eigenvector ( $\lambda_1 \gg \lambda_2$  and  $\lambda_3$ ) the ellipsoid is more prolate or cigar shaped. If the two major principal eigenvectors are approximately equal and greater than the third, the shape is more oblate or disc like ( $\lambda_1 \sim \lambda_2 > \lambda_3$ ) (95). The different structural representations in isotropic and anisotropic tissues are illustrated below (Figure 2.3).

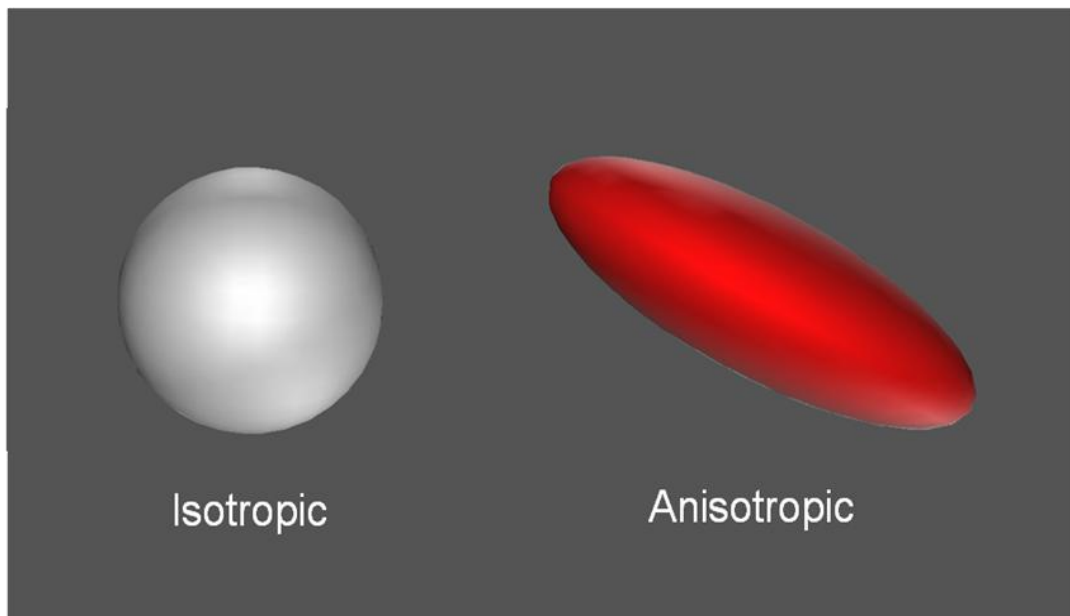


**Figure 2.3 Visual representations of the tensor in isotropic and anisotropic tissues.**

---

Various measures of diffusion anisotropy have been proposed, the rotationally invariant scalar measure, fractional anisotropy (FA) is the most common (96), its calculation is covered in chapter 3.

### 2.3.2 DIFFUSION TENSOR IMAGING

The display of tensor derived metrics such as the MD and FA is seen in Figure 2.4 below.

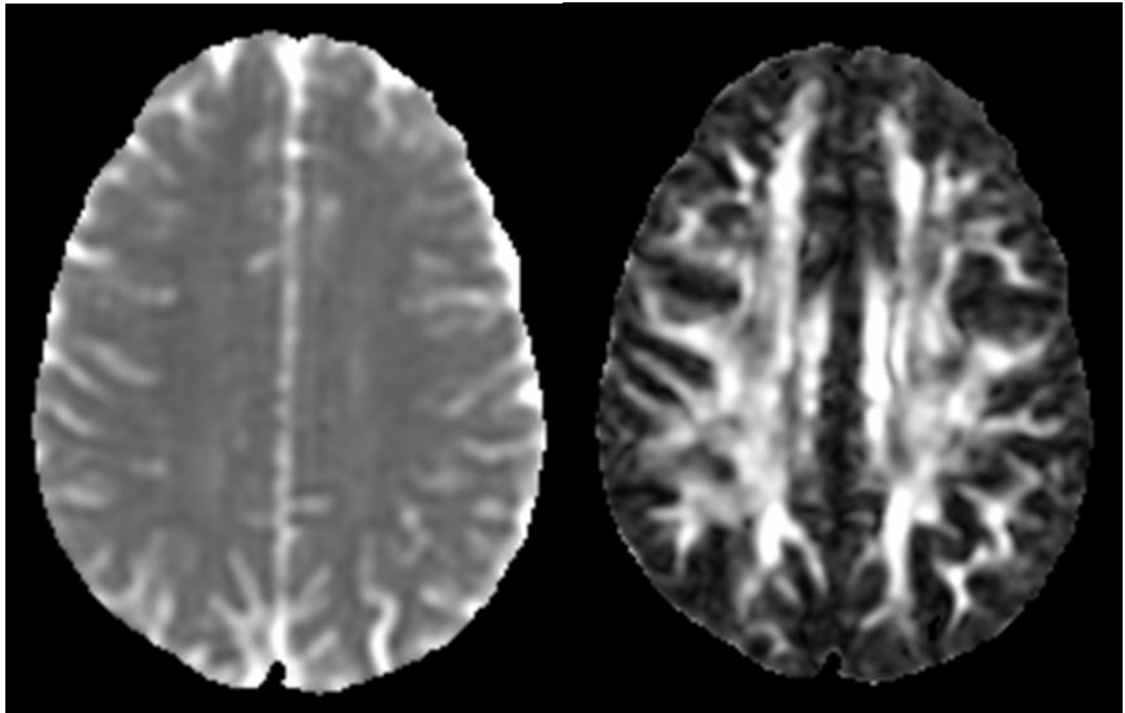


**Figure 2.4 MD (left) & FA (right) maps.** MD removes anisotropy and is rotationally invariant. FA; rotationally invariant, values from 0 to 1 and bright pixels represent high anisotropy.

---

The representation of the tensor in terms of directionality is more challenging and a solution has been the use of directionally encoded colour maps. The degree of anisotropy is reflected in the intensity of the colour and the principal eigenvector represented by the colour using the red green and blue spectrum.

Pajevic and Pierpaoli (97) developed this method and used it to show major white matter fibre tracts and their directions, in the brain, brain stem (in terms of separating the vertically oriented sensory and motor fibres and separate them from the transverse pontine fibres and cerebellar peduncles).



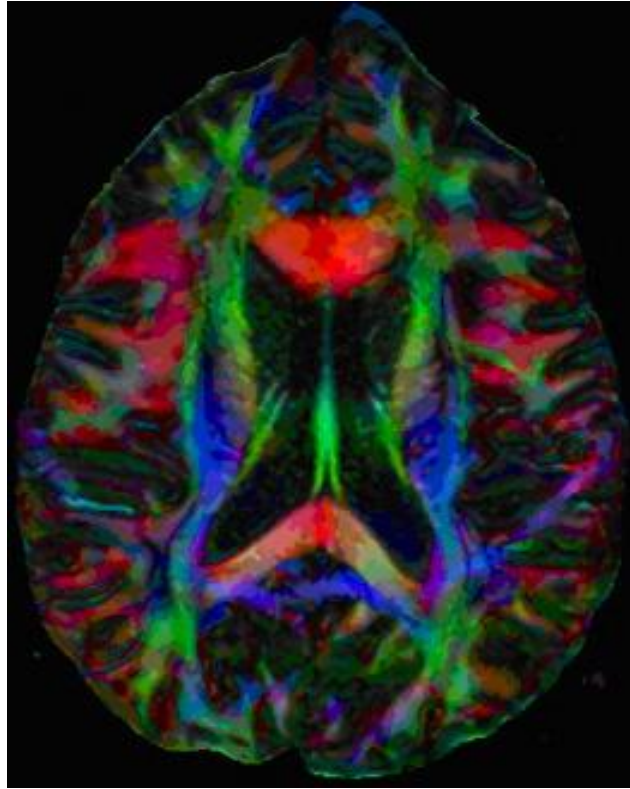


**Figure 2.5** Directionally encoded colour maps. Red, left–right direction. Blue superior–inferior direction. Green, anterior–posterior direction.

---

### 2.3.3 COMPLEX DIFFUSION MODELS

The diffusion tensor model works by providing a determination of the principal direction of diffusion and makes the assumption that the tissue microstructure is reflected by this. If the tensor shape is more prolate the fibres appear to run more coherently in a single direction. However often this will not be the case and the tensor shape is not prolate but tends to be more oblate or spherical.

The reality is that the fibres within a single voxel ( $2.5 \text{ mm}^3$ ), which is infinitely larger than the individual axons (low spatial resolution), may be travelling in several directions and intersect within the voxel such that a single orientation estimate does not truly represent the underlying structure. This situation is not uncommon as there are often multiple non-collinear fibre directions within a voxel. This could lead to tracking of

pathways that do not exist (false positive) or failing to track ones that do (false negative) (98). Barrick and Clark, 2004 (99) describe these as singularities in the tensor field, highlighting where for example the corticospinal tract running superior-inferiorly meets with fibres from the corpus callosum running from left to right and the principal direction is not truly representative.

Attempts have been made to address this problem; an improved resolution would help and also models not reliant on a Gaussian distribution have been explored (100-103). There have also been developments in the use of high angular resolution diffusion imaging (HARDI) (100) and attempts to provide processing of multi-peak diffusion profiles to accommodate crossing fibres (100;104-106).

There are other limitations to following white matter pathways in terms of being unable to determine if they are antero- or retrograde or whether it is actually functional (106;107). A study by Lawes et al 2008 (108) provided a convincing comparison of the results of white matter mapping in comparison to blunt dissection in an attempt to validate the results of the imaging. The field is continually expanding.

## 2.4 WHITE MATTER AND TRACTOGRAPHY

### 2.4.1 ANATOMY OF WHITE MATTER

The understanding of the structure of the brain has, and continues to undergo development. Investigations to determine its underlying structure were undertaken using light microscopy and staining techniques at the turn of the last century. Meynert at the end of the 19<sup>th</sup> Century theorised that there existed multiple interconnections in the brain in the form of the white matter (109). The use of Weigert myelin stain allowed Dejerine to publish an expansive anatomical atlas of images of the nervous system and specifically the white matter (110).

The freeze thaw technique further elucidated the white matter structures as it enabled their easier dissection as per the work published in 1956 by Ludwig et al (111). Further post mortem techniques have been implemented, including the use of horse radish peroxidase and radioactive tracers to follow specific neuronal tracts (112-114). All the techniques necessitated post mortem study and hence were not suitable for use in vivo in humans. However the understanding of these connections is vital to the understanding of brain function.

### 2.4.2 TRACTOGRAPHY

Diffusion tensor imaging can produce images representing the principal direction of diffusion of water molecules in vivo. This principal eigenvector is thought to represent the underlying structure of the white matter tracts in a given voxel. Initial two dimensional representations of the structures were reported using colour coded maps to represent the fibre orientations. (97;115-117). The directionally encoded colour map, where hues reflect tensor orientation and intensity is weighted by FA, provide an informative and easily interpreted summary of DTI features throughout the brain. In

combination with the accepted neuro-anatomy individual white matter pathways can be recognised (118). The demand was then created for a three dimensional representation and this was achieved through the estimation of the orientation of white matter fibres by equating their direction in which the diffusion is greatest (fastest). Applying this assumption several techniques have been proposed to map the white matter pathways through following the maximal diffusion direction from voxel to voxel, allowing an in vivo reconstruction of the connectivity of the brain (119-123).

The means by which the tracts are reconstructed, the tractography method, has been described in several ways. The earliest method; that of streamline tractography is based on the principal whereby a connection is made between adjacent points (voxels or sub-voxels) initiated from a defined start point and following the principal direction provided by the tensor at the next subsequent point in order to continue the reconstruction (119-123). This is the method used in this work.

Alternative methods in use are broadly described as probabilistic and are similar to the streamline tractography method but involve the sampling of the tensor using a probability density function over many iterations to define the probability of connection between two points in the brain image data (101;105;106). Numerous methods have been proposed for conducting probabilistic tractography. In “fast marching tractography” the propagation of a front through the directional tensor data results in a map of a distributed connectivity index (101;124). An alternate means is the Monte Carlo method, where a random walk is undertaken by a hypothetical particle. This walk is dependent upon the direction and strength of the underlying diffusion determined by the diffusion tensor, the path is halted where the particle reaches a voxel failing to satisfy, typically, an anisotropy threshold. The process is repeated and all voxels contained in the paths retained, the relative connectivity of the voxel is determined by

the frequency that a particle passes through. This is visually represented by the signal intensity the voxel displays (125-127). Such methods have been applied in order to determine the likelihood of connections between areas of the brain through a probability distribution function (44).

The streamline method uses the directional similarity of adjacent voxels in order to connect them based on the principal eigenvector. If the principal eigenvector in the adjacent voxel is sufficiently similar in orientation, the threshold for which is arbitrarily determined, they will be connected and the streamline continues propagating (120;122) in both antero and retrograde directions (128). The streamline will cease at the point where the trajectory of the principal eigenvector in the adjacent voxel or point exceeds the threshold or where the FA falls below a chosen threshold value. This is intended to ensure adequate similarity and to prevent tracking into the grey matter or the ventricles. The FA threshold also represents the degree of uncertainty over the principal eigenvector and hence when it falls the direction is becomes more uncertain (129). The means by which the principal eigenvector is determined varies with the algorithm. The algorithms can work at a voxel or subvoxel level determining the principal eigenvector at a fixed distance (vector step length). In addition the algorithms can allow the principal diffusion direction to be calculated stepwise through interpolation of either the whole tensor or the principal eigenvectors at the new co-ordinates, occurring iteratively as the streamline is constructed (119-121).

The features described: vector step length, FA threshold and angular thresholds are frequently a product of experimental investigation and the values chosen by the investigator based on previous experience.

When multiple co-orientated streamlines from this method are grouped together it is possible to conceive of reconstructions of fibre bundles (119;120), the premise being that of similarity of principal direction. However, recurrent problems exist in the demonstration of the entire distribution of a fibre pathway. Frequently other pathways or aberrant streamlines are included. The quality of the tractography reconstructions are highly dependent on the regions of interest (ROIs) defined by the investigator chosen as initiating seed regions or target regions. An ROI includes a group of voxels from which tracking can be initiated or through which the streamlines must pass in order to be included in the reconstruction (121). In the case of initiation within the ROI voxels, a single streamline is initiated from each voxel and the pathways propagated may not have similar orientations and hence multiple different fibre pathways may be created. In an effort to be more specific a second ROI can be defined, possibly to act as a start and / or end point.

An alternative method involves the use of seeding of streamlines from every voxel within the brain, known as whole brain tractography and the ROI is used to determine which seed voxels should be retained. They are the ones whose streamline reconstructions pass through the ROI. This tends to mean that a greater number of streamlines are included as the number of seed voxels is not restricted to the number contained within the ROI. The limiting factor to the placement of the ROIs is the presence of “a priori” anatomical knowledge by the user, with this in mind anatomically plausible reconstructions of the white matter tracts have been reported (105;130-134).

## 2.5 DTI AND TRACTOGRAPHY APPLICATIONS

The presence of a coherent arrangement of white matter fibres results in a pronounced diffusion anisotropy demonstrated on diffusion tensor imaging (DTI). The magnitude of the anisotropy is thought to depend on several factors including axonal density and degree of myelination (89;135). From this it is inferred that diffusion anisotropy maps (136) may be useful in the investigation of the integrity of white matter and the effect of disease on it.

The effect of myelination on diffusion anisotropy has been used to investigate effects of brain maturation and development with age. DTI has provided quantitative parameters of diffusion to be derived in order to assess tissue microstructure. The corpus callosum (a large white matter tract) has shown increasing FA and decreasing MD during childhood and adolescence and slightly slower decreases of FA and increases of MD at older ages. A study by Lebel et al in 2010 (137) reported the age at peak FA values and minimum MD values varied from 21 to 44 years. Similar results have been reported with increasing FA with age due mainly to falling perpendicular diffusivity (138). Studies directed at the development of foetal brains and effects of gestational age have drawn similar conclusions and may be related to the process of white matter myelination that occurs in development (139-142). The process of demyelination and axonal loss with age results in an increase in the extracellular space and a consequent fall in the FA and an increase in the MD (141;143).

In disease processes, stroke has been a significant avenue for the application of ADC measurements and DTI (see section 2.2). As the ADC changes through the different phases as the effects of the ischaemic injury in stroke evolve, initial increase in ADC followed by normalisation and then falling ADC are seen in specific regions in and

around the infarct (51;144-146). These measurements have allowed determination of acute and potentially salvageable regions.

Following an ischaemic insult to a region, the white matter pathways undergo a process of Wallerian degeneration resulting in loss of structure and this is detected in terms of a reduction in FA. Investigations specifically of one of the major white matter motor pathways, the corticospinal tract (CST) have shown that reduced FA in the CST following a stroke is correlated with a poorer recovery long term (147-151).

Multiple sclerosis (MS) has been investigated with respect to identifying lesions not seen on conventional MRI and assessing whether there is a correlation between radiological findings and functional assessment. Tractography has been directed at determining if the connectivity it may reveal has a correlation with disability. Assessment of the FA in lesions has shown that it is lower than in normal surrounding white matter (152). In further assessment of the CST of patients with relapsing and remitting MS with isolated motor symptoms when compared with normal individuals and those without motor symptoms the diffusion indices were reduced (153;154). These findings may elucidate an on-going process of Wallerian degeneration to explain these symptoms.

Investigations have been undertaken into the effects of chronic epilepsy on the white matter tracts. Wadjaja et al 2007, (155) showed that in patients with epilepsy and focal cortical dysplasia the white matter tracts that project to or from the malformed cortex could not be tracked, indicating a loss of directional organisation in the white matter thought to be due to the seizures or focal cortical dysplasia. The effects of temporal lobe epilepsy on memory-related structures in patients with medically intractable temporal lobe epilepsy and unilateral mesial temporal sclerosis was reviewed by Concha et al



(156) and they reported a bilateral symmetrical reduction in FA in the tractography derived fornix and the cingulum proximal to the hippocampus, possibly indicating evidence of Wallerian degeneration.

The use of tractography for the planning of epilepsy surgery in terms of the risks of complications has been studied. Powell et al (157) showed that a probabilistic method of tractography could be used to assess the position and extent of Meyer's loop (a part of the optic radiations, the resection of which results in a visual field defect) in order to predict the superior quadrantanopia that can result from resection of the anterior temporal lobe. When the preoperative right optic radiation was overlain onto the post-operative field it was evident that the white matter that had been resected had included the radiation into the temporal lobe.

The process of brain development and maturation involves increasing myelination and growth of white matter tracts. Tractography has been used to demonstrate an apparent diminution in volume of white matter projection fibres to the prefrontal cortex in cases where there is established reduction in grey matter persisting throughout adolescence (158). In the case of children presenting with developmental delay a group have looked at the corpus callosum and reported that the mid-sagittal area of the entire corpus callosum is reduced as compared to children with normal development. Similarly the white matter volumes of corresponding cortical lobes were reduced in the developmentally delayed group (159).

In the cases of development affected by pathology such as that from a vascular injury resulting in a congenital hemiparesis, there is asymmetry in the reconstructed CST (160). In conditions such as cerebral palsy, the hemisphere contralateral to the insult is seen to have a higher fibre number in the CST and corticobulbar tracts (calculated

through tractography) than that in the affected hemisphere and when compared to normal controls (161).

Neurodegenerative diseases frequently involve loss of axons in addition to the loss of cortical neurones. It has been seen that DTI can detect changes in connectivity in the brain at an early stage of the neurodegenerative process (162-164). Reduced FA has been detected in the cingulum, hippocampus, and the posterior corpus callosum of individuals who are cognitively well but have a genetic disposition to dementia (as in the case of APOE $\epsilon$ 4 carriers). In individuals with Alzheimer's disease tractography has been used to identify and localise degeneration along specific white matter paths; in transgenic mice which express excess  $\beta$ -amyloid precursor protein the reduction in diffusivity parameters was seen to correlate with the severity of the Alzheimer's disease (165).

Parkinson's disease and conditions such as multiple system atrophy or progressive supranuclear palsy have been the subject of tractography and the possibility raised of discriminating between these diseases as they result in degeneration along specific tracts. Further investigations are required to validate this (166).

## 2.6 INTENTIONS OF THIS STUDY

The literature in the adult population and to some extent in the paediatric population indicates that diffusion MRI data can provide information as to the structure of the white matter in the brain and also to probe the character and structure of lesions within the brain.

The intention of this research is to collect MRI diffusion data on paediatric subjects with CNS tumours presenting to Great Ormond Street Hospital for Children prior to and also following surgery to remove the tumour.

The specific aims of the research are to apply diffusion MRI metrics to determine the ability to discriminate between paediatric CNS tumours, through the assessment of their internal structure.

Secondly we intend to determine the practicability of our tractography algorithm for the reconstruction of the cerebellar peduncular white matter in paediatric subjects. Using these reconstructions we hope to determine their functional validity through comparison with cerebellar functional deficits and clinical signs.

The premise being to determine if it is possible to use diffusion MRI and tractography as an adjunct to the preoperative characterisation of paediatric CNS lesions and also its use for neurosurgical planning.

---

## 3 METHODOLOGY

---

### CONTENTS

---

3.1	Patient Recruitment	76
3.2	Ethics and Consent	80
3.3	MRI and Diffusion Protocols	82
3.3.1	Clinical MRI Sequences .....	82
3.3.2	ADC Data Acquisition.....	84
3.3.3	DTI Data Acquisition.....	87
3.4	Calculation of the Diffusion Tensor Indices	91
3.4.1	Mean Diffusivity (MD).....	91
3.4.2	Fractional Anisotropy (FA) .....	92
3.5	Study Methods of Tractography	93
3.5.1	Directional Encoded Colour Maps .....	94
3.5.2	Regions of Interest .....	94
3.5.3	Tractography Algorithm .....	95
3.5.4	Visualisation of Tractography Output .....	98

---

### 3.1 PATIENT RECRUITMENT

In the context of this study the patients investigated in this thesis fall into 3 groups. A group of 17 control paediatric patients recruited by Dr Kate Riney from the Department of Neurology at Great Ormond Street Hospital which formulated a pre-existing data set supplemented by five normal adult volunteers recruited by the author.

A further cohort of patients in two overlapping groups recruited from the Department of Neurosurgery at Great Ormond Street Hospital. In the case of patients where ADC data was analysed they were collected from a retrospective review from 2003 onwards, compiled using the local electronic oncology database picking out cases of histologically confirmed central nervous system tumours (CNS). To have a histological diagnosis the patients had to have undergone a surgical procedure to obtain a tissue diagnosis. The initial group consisted of a total of 289 cases (to March 2007) that had had imaging at Great Ormond Street Hospital (GOSH). The imaging was reviewed, all cases without pre-operative DWI were excluded as were cases where the imaging was corrupted by artefact or the imaging was incomplete (not all cases had all their pre-operative imaging at GOSH). This identified 55 cases initially and subsequently the author recruited individuals prospectively from March 2007 until July 2007; providing 10 further cases (total 65). The diffusion sequence formed part of the pre-operative imaging sequence for patients with newly diagnosed brain tumours who underwent further imaging at GOSH where it was required in addition to their local imaging.

A second group of patients were recruited for DTI performed on the 1.5T Siemens Avanto MRI system. This group was recruited from April 2006 (when ethical approval was obtained) until January 2008 and cases overlapped with those recruited for the ADC study. Children presenting to GOSH with a suspected diagnosis of intra-cranial central nervous system tumour identified on either CT or MRI were considered for inclusion. Only patients and families who were willing and well enough to undergo an additional DTI investigation were included. To be well enough the patient had to be able to tolerate lying flat and still for the 20 minutes required to obtain the DTI sequence if they were having an un-sedated scan. The process for this involved informed consent of the parent or guardian and the child's agreement, in the form of

assent or consent, depending on their capacity. (Copies of the patient and parent information sheets and consent forms can be seen in Appendix 8.2 and 8.3) The DTI sequence would, on occasion be done as an addition to a pre-operative MRI sequence (see chapter 3.3) necessitated for clinical management. This meant that it could be achieved in cases where sedation or general anaesthetic (GA) was required but only with considerable co-operation and tolerance from Radiographers, Anaesthetists and Radiologists. The concern being that the addition of a further 20 minutes to an already lengthy scan would diminish the ability to accommodate further patients on the MRI “list”. In patients where an un-sedated scan was possible then the DTI sequence (chapter 3.3) would be done independently and in dedicated research time paid for by Cancer Research UK or Royal College of Surgeons Grant funding. In all cases a magnetic safety questionnaire was completed by the patient or family. Where patients were unable to tolerate the scan due to restlessness, claustrophobia or symptomatology, the scan was ceased and the patients returned to the ward.

It was anticipated that it would be possible to collect between 20 and 30 patients per year from the cases referred to GOSH. The expectation being based on the referral patterns for the hospital over the preceding years reflected in the annual GOSH Neuro-Oncology report showing data up to the end of 2007, seen in figure 3.1 (data compiled by Sister Kim Phipps GOSH Research Nurse). The mean number of referrals per year over the period illustrated was seventy one.

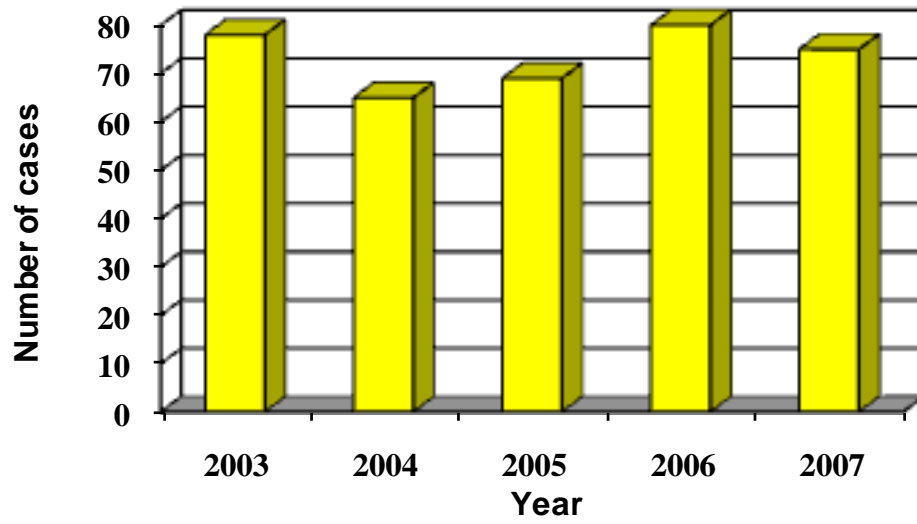


**Figure 3.1**      **New Tumour referrals GOSH 2003-2007**

---

### 3.2 ETHICS AND CONSENT

The work in this project formed two separate applications to local research ethics committees (COREC). The first was under the title of “*Development of Magnetic Resonance Tractography for Paediatric Neurosurgical operative planning*” and was approved in June of 2006. This project used an established DTI sequence, detailed in section 3.3, used in current and previous research at ICH. A subsequent application was made to the GOSH local research ethics committee in respect of “*Apparent Diffusion Coefficients characteristics may predict Neuro-oncological tumour type in a paediatric population*”. This study was approved in December 2006 and it was deemed that further informed consent was not required nor was ethical review as the imaging was performed as part of a routine clinical protocol, detailed in section 4.2. Copies of the ethical approval are seen in appendix 8.1.

In the case of the paediatric neurosurgical patients recruited to the Tractography study they were recruited to the study by the author, J G Bull, from in-patients awaiting treatment for suspected intracranial tumours. Consent was taken by the author following the local GOSH practice involving the patient themselves where they had capacity to do so in terms of assent or consent. Typically this involved consent by both the parents and the child but where this was not possible, in the very young, then consent would be obtained from the parents, as per the World Health Organisation, Declaration of Helsinki. Copies of the patient information sheets with consent and assent forms are seen in appendix 8.2 and 8.3. Where children required sedation (protocol detailed in appendix 8.4) or a general anaesthetic, the DTI imaging was obtained as an addition to a necessary clinical investigation through close liaison with the GOSH Radiology Department. No children underwent further sedation or GA procedures in order to



obtain research imaging. Where children were able to tolerate imaging awake then research DTI would be obtained on dedicated research time. Patients were scanned both pre-operatively and post-operatively where possible.

Children recruited to the DTI study were reviewed by the author with reference to the patient's clinical case notes and through the collection of the clinical history both from the patient and the parents, in conjunction with a neurological examination. Such examinations were performed immediately prior to the acquisition of the MRI / DTI sequence. All demographic data (specifically: name, date of birth, hospital number, sex, dates of imaging), history and examination findings (typically presence or absence of a neurological deficit such as degree of motor weakness, evidence of cerebellar signs and lateralisation), handedness, location of tumour and its histopathological diagnosis (determined by the GOSH Neuropathology Department) were recorded using Microsoft Excel 2003.

Patients recruited to the ADC study were deemed not to require consent and in this study the sequence was part of an established clinical protocol (detailed in section 4.2). Histopathological data was obtained from the GOSH Neuropathology Department and images were retrieved from stored hard copies by the author.

The normal cases obtained as part of the study performed by Dr Kate Riney, from 2004 to 2007, were part of an existing database extant in the Imaging and Biophysics Unit of the UCL Institute of Child Health. Their imaging was obtained using the same established DTI sequence and hence could be processed in the same fashion as the authors' neurosurgical data. Patient demographics were available for these individuals, where further information was required the author obtained this through meeting with

the individuals at the time of their recruitment as normal subjects to Dr Kate Riney's study or at subsequent telephone interview.

### 3.3 MRI AND DIFFUSION PROTOCOLS

#### 3.3.1 CLINICAL MRI SEQUENCES

The standard imaging protocol for paediatric CNS tumours undertaken on the 1.5 T Siemens' Avanto MRI system at GOSH is detailed below. Typically, where there was a possibility of spinal metastases, this would also involve imaging of the spine.

The brain imaging protocol consisted of:

- Axial T2-weighted Turbo Spin Echo (TSE)
- Coronal T2-weighted unenhanced fluid attenuated inversion recovery (FLAIR)
- Axial T1-weighted spin echo (SE)
- Sagittal T1-weighted SE
- Diffusion-weighted imaging ( $b = 0$  and  $b = 1000$ )
- Axial, coronal and sagittal gadolinium enhanced T1-weighted MRI

*Imaging time was 28.5 minutes*

The same protocol was also performed on the 1.5T Siemens Symphony system, patients requiring routine pre-operative and post-operative tumour imaging would be scanned on either system depending on availability. In the scope of this work; only DWI data was used from this scanner, all DTI data was from the Avanto system. The details of the protocols are shown in table 3.1. Specifically; the standard imaging protocol was used where data was required for clinical assessment and in so doing DWI imaging (sequence 3, Avanto or 4, Symphony; table 3.1) would be routinely collected as part of this protocol. Where clinical data was acquired on research patients then the DTI

sequence would be appended to the end of the clinical sequence above (patients were imaged on the Avanto scanner, ie sequence 2 in table 3.1), adding 16mins 24secs to the acquisition time. If clinical data was not required then the 20 direction DTI sequence would be performed on a separate occasion and a T1 3D Flash with the DWI sequence would also be acquired as per table 3.1 (ie sequences 1, 2 and 3), total imaging time 24 mins 12secs.

In terms of the patients toleration of the sequences; imaging of children necessitates further considerations in addition to those as of adult investigations. The presence of impaired consciousness and co-operation secondary to the underlying brain abnormality are compounded by the degree of development and maturity of the child. There are established protocols for determining which individuals needed either sedation (so called "*feed and wrap*"), general anaesthetic or would tolerate imaging without pharmacological assistance. Details of the protocols for sedation are found in Appendix 8.4. In general, where time allowed, DTI data could be acquired on sedated patients and patients undergoing general anaesthetic with the greatly valued co-operation of the anaesthetic and radiographic staff. In the case of patients who did not require sedation and did not need further clinical imaging, the DTI data was collected in dedicated research time. The selection of patients for this was the decision of the author in conjunction with advice from the ward staff caring for the patients and with the vital co-operation of the patient and their parents.

The DTI protocol (total time 25 minutes 10 seconds) was well tolerated by most patients but in the event that they wished to stop at any point the scan was immediately discontinued.

### 3.3.2 ADC DATA ACQUISITION

Data was obtained from imaging performed on the 1.5T Siemens Avanto (maximum magnetic field gradient strength of 40 mT m<sup>-1</sup>) or the 1.5T Magnetom Symphony (maximum magnetic field gradient strength of 30 mT m<sup>-1</sup>). A diffusion sensitised single-shot echo planar sequence was used at two b values (500 and 1000 s mm<sup>-2</sup>) subsequent to an initial b = 0 acquisition. The details of the DWI sequences are seen in Table 3.1 and discussed in section 4.2.2.

The signal intensity on diffusion-weighted images is dependent on spin density, T1, T2, TR, and TE. These factors can be eliminated to obtain pure diffusion imaging by calculating diffusion coefficient maps. Such maps are calculated by combining two or more diffusion-weighted images which are differentially sensitized to diffusion but whose other parameters, spin density, T1, T2, TR, and TE are identical. In this case a sequence ( $S_0$ ) not sensitised to diffusion ( $b = 0$ ) was combined with a diffusion sensitised sequence ( $S$ ) at  $b = 1000$ . From this it is possible to calculate a value ( $D$ ) for the diffusion in each voxel by the following equation:

$$D = \frac{1}{b} \ln \frac{S}{S_0}$$

The parametric image representing these data is called a diffusion map or apparent diffusion map (ADC). The implication of the apparent term highlights the fact that the  $D$  values obtained depend on the experimental conditions, specifically factors such as the direction of the sensitizing gradient and diffusion time. As discussed in chapter one there is considerable contrast in the ADC values obtained when the diffusion gradients are applied in different directions, this is referred to as diffusion anisotropy.

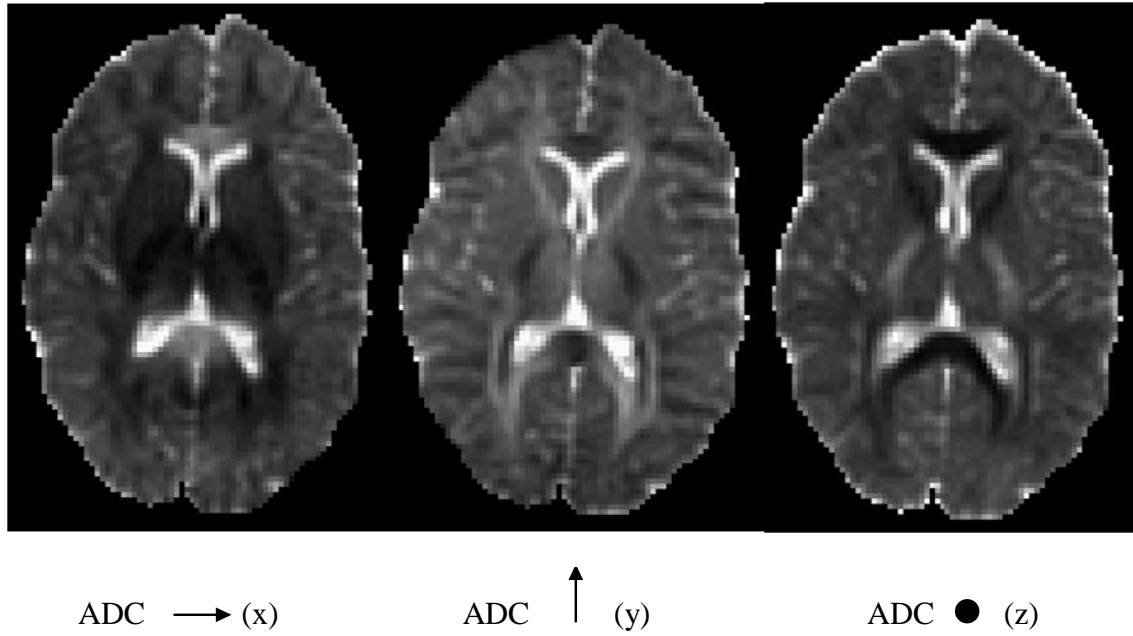


**Figure 3.2 Directional ADC maps. ADC measured in different directions results in ADC contrast.**

In order to obtain a rotationally invariant coefficient where anisotropy is removed the mean ADC is calculated. In this case we applied gradients in three orthogonal directions; ADC was calculated for each and then averaged as per the equation below.

$$ADC_{av} = \frac{ADC_x + ADC_y + ADC_z}{3}$$

This value is the mean ADC but is also known as the trace or mean diffusivity (MD); it provides a quantitative, directionally averaged evaluation of the diffusion within the voxel. The values obtained from this were used to construct the tumour mean ADC histograms.

	Sequence	Imaging Time (sec)	No. slices	Echo time (ms)	Repeat time (ms)	Thickness (mm)	Gap	Matrix	FOV	Flip	Number of b values	Number of directions
1)	3D FLASH	05:34	176	4.94	11	1	0	224 x 256	256 x 224	15	n/a	n/a
2)	DTI_20	05:28 (Repeat 3 times 16.24)	55	89	7600	2.5	0	96x 96	240	n/a	n/a	20
3)	DWI	01:04:00 (Repeat 3 times 03:12:00)	19	96	2700	5	30% (1.5mm)	128 x 128	230	n/a	0, 500, 1000	6
4)*	DWI Symphony	00:56 (Repeat 2 times 01:52)	20	107	3600	5	50% (2.5mm)	128 x 128	230	n/a	0, 500, 1000	6

**Table 3.1 Summary of Project MRI sequences.** Sequences 1, 2 and 3 were performed on the Avanto system when acquiring diffusion tensor data. Sequences 3 and 4 were performed as part of the GOSH tumour imaging protocol and were performed on the Avanto and Symphony (\*) systems respectively.

### 3.3.3 DTI DATA ACQUISITION

All DTI data was obtained from the Siemens Avanto 1.5T system with a maximum field gradient strength of  $40 \text{ mT m}^{-1}$  using a Siemens CP receive only head coil. The acquisition when performed as a standalone sequence consisted of a 3D Flash, time 5 minutes and 34 seconds, DTI sequence (16 mins 24 secs) and the DWI at  $b = 0$  and  $b = 1000$  (3 mins 12 secs). If the sequence was performed as part of a clinical brain tumour sequence the DWI was not repeated.

Mention has already been made of the fact that patient movement causes problems with the acquisition of in vivo MRI data. These issues are exacerbated in the study population due to potentially impaired consciousness secondary to underlying diagnosis but also due to their developmental age. These considerations are reflected in the use of sedation or general anaesthetic to obtain imaging in some cases. In spite of this there remains physiological movement from respiration and cardiac pulsation providing the force for blood flow. These movements can degrade the brain MR imaging quality and are particularly amplified in the acquisition of diffusion sensitised data where the sequence is attenuated particularly to microscopic movement. In order to diminish these effects, a single shot echo planar imaging (EPI) sequence (the industry standard) was used to obtain the imaging in this study. The advantage of EPI is the exceptionally rapid data acquisition, through which the effects of the physiological motion is minimalised (37).

The EPI sequence is particularly sensitive to magnetic susceptibility artefact as compared to a spin echo or a fast spin echo sequence. Such artefacts arise from ferromagnetic materials or paramagnetic / diamagnetic materials and specifically from implanted medical devices. These materials distort the linear magnetic field gradients

resulting in bright areas (misregistration) or dark areas (absence of signal) near to the magnetic material. There are regions of the head and brain where this is particularly prevalent. Specifically: adjacent to the air sinuses in the skull base, and of particular relevance in this study, in the boney posterior fossa. The artefacts result from the significant differences in the magnetic properties of the different tissues. Static field inhomogeneities can cause geometric distortions and as the EPI sequence uses diffusion sensitising gradients with high amplitude very short duration eddy currents are induced causing further distortion of the data acquired (167).

As discussed in chapter one and also covered in section 3.3.2 water diffusion follows a Gaussian distribution that is affected by the tissue structure around it. Consequently the measured rate of diffusion or diffusion coefficient “ $D$ ” will be dependent on the direction it is measured in. In DWI three gradient directions are used to estimate the trace or average diffusivity. To better describe this directionality, a diffusion tensor is used to characterise the diffusion in the tissue under examination. This could be defined by determining the values of the diffusion coefficient in the three unique orthogonal directions, the eigenvectors ( $D_{xx}$ ,  $D_{yy}$  and  $D_{zz}$ ). Although in reality the reference frame defined by the MR device may not match the reference frame of the diffusion in the tissue under examination. Hence the tensor will be described by cross terms ( $D_{xy}$ ,  $D_{xz}$  and  $D_{yz}$ ). There are only six independent values for  $D$  as a consequence of the symmetrical properties of the diffusion ( $D_{xx}$ ,  $D_{yy}$ ,  $D_{zz}$ ,  $D_{xy}$ ,  $D_{xz}$ ,  $D_{yz}$ ) (41). This model remains rather simplistic assuming a homogenous and linear diffusion pattern.

Work by Basser et al 1994 (168;169) demonstrated that to obtain these six values of  $D$  on a voxel basis it was necessary to perform a minimum of seven DWI acquisitions. In the work contained in this thesis the DTI sequence (Table 3.1) consisted of an initial single shot EPI acquisition with no diffusion gradient applied ( $b = 0$ ) and subsequent



acquisitions with diffusion sensitising gradients either side of the 180° refocusing pulse.

The gradients were individually applied in twenty directions, seen in Table 2.2.

X	Y	Z	b value ( s mm <sup>-2</sup> )
0	0	0	0
-1	0	0	1000
0	1	0	1000
0.031984	0.799591	-0.599693	1000
-0.856706	0.493831	0.148949	1000
-0.834429	0.309159	-0.456234	1000
-0.834429	-0.309159	-0.456234	1000
-0.856706	-0.493831	0.148949	1000
-0.822228	0	0.569158	1000
-0.550834	0.425872	0.717784	1000
-0.468173	0.834308	0.291108	1000
-0.515933	0.808894	-0.281963	1000
-0.39189	0.515855	-0.761785	1000
-0.478151	0	-0.878278	1000
-0.39189	-0.515855	-0.761785	1000
-0.515933	-0.808894	-0.281963	1000
-0.468173	-0.834308	0.291108	1000
-0.550834	-0.425872	0.717784	1000
-0.111012	-0.264029	0.958105	1000
-0.111012	0.264029	0.958105	1000
-0.031984	0.799591	0.599693	1000

**Table 3.2 Summary of DTI directions.** Twenty directions used for the acquisition of the DTI data in addition to the first b = 0 sequence.

As is evident from Table 3.1 the twenty direction DTI sequence was repeated 3 times and an average was calculated prior to processing in order to improve the signal to noise ratio. Work by Burdette et al 1998 (170), has shown that the most efficient estimation of  $D$  with respect to this ratio is achieved when the b values differ by  $1/D$  and in the brain this is approximately 1000 – 1500 s mm<sup>-2</sup>. In the acquisition of the DTI data the difference in the diffusion weighting (b value) was 1000 s mm<sup>-2</sup>, with the imaging acquired at b = 0 and b = 1000 s mm<sup>-2</sup>.

Further details of the sequences are found in Table 3.1. The image matrix was 96 by 96 using a 240 mm field of view and voxels were isotropic at 2.5 mm<sup>3</sup>, a total of 55 slices in total were used to ensure whole brain coverage. The images underwent realignment to remove eddy current effects as described by Haselgrove et al 1996 (171) using the AIR program (172) before the calculation of the diffusion tensor. The interleaved acquisitions were repeated three times consecutively and the magnitude data averaged off line prior to calculation of the diffusion tensor (173).

### 3.4 CALCULATION OF THE DIFFUSION TENSOR INDICES

The processing of the data following the calculation of the diffusion tensor in each voxel as per Basser et al 1994 (174) was the calculation of the mean diffusivity (MD) and the fractional anisotropy (FA) through diagonalisation of the tensor for each voxel. The exact sequence is detailed in appendix 8.6. Data taken from the MRI system was processed through a Python program and subsequently through mriCro (175) which allows Windows and Linux computers to view medical images. The DICOM images were converted to Analyze format and were exported to a Linux platform (Sun Blade 100 Sun Microsystems, Mount View, California) for processing.

Diagonalisation is a mathematical process that allows the determination of the true maximal direction and magnitude of diffusion. The necessity for this arises as the reference frame of the diffusion tensor is defined by the diffusion sensitising gradient's axis which is independent of the tissue being investigated, hence the tissue's true reference frame must be found. The result of the diagonalisation of the diffusion tensor is the calculation of the eigenvectors and eigenvalues which correspond to the vector components of the direction and the magnitude of maximal diffusion (168;169). The term for this largest eigenvalue is the principal eigenvector and is thought to be co-aligned with the local direction of fibres.

#### 3.4.1 MEAN DIFFUSIVITY (MD)

This provides a scalar measure of the amount of diffusion on a voxel basis. Its calculation has been covered in section 3.3.2, as the mean diffusivity is also known as the mean ADC or trace and is obtained by obtaining the mean of the three diffusion coefficients ( $D_{xx}$ ,  $D_{yy}$ , and  $D_{zz}$ ) which is rotationally invariant.

### 3.4.2 FRACTIONAL ANISOTROPY (FA)

A scalar representation of the degree of anisotropy was also calculated. Several indices have been used previously (34;176) based on diffusion-weighted images and ADC's measured in perpendicular directions. The limitation was that the scalar quantities were reliant on the alignment of the diffusion sensitising gradients with the structure of the tissue under investigation and may not reflect the true degree of anisotropy in the tissue. As with MD a rotationally invariant characterisation of the anisotropy is necessary and to this end the fractional anisotropy was calculated from the diagonalised tensor using the following equation. Where  $\lambda_{1-3}$  represent the principal eigenvectors of the tensor for each voxel as discussed in chapter one.

$$FA = \frac{\sqrt{(\lambda_1 - \lambda_2)^2 + (\lambda_2 - \lambda_3)^2 + (\lambda_1 - \lambda_3)^2}}{\sqrt{2}\sqrt{\lambda_1^2\lambda_2^3\lambda_3^1}}$$

The value is dimensionless, scaling between 0 and 1, where with increasing anisotropy the scalar tends to 1.

### 3.5 STUDY METHODS OF TRACTOGRAPHY

The tractography algorithm was written in the “C programming language” by Dr Tom Barrick, St George’s Hospital, London. The algorithm had evolved from work on several previous projects and involved the use of other software to process the ROIs, specifically *mriCro* (175) (<http://www.cabiatl.com/mricro/mricro/mricro.html>). The algorithm was run on a Sun work station (Sun Blade 100 Sun Microsystems, Mount View, California) and the applied method of tractography were based on the techniques originally described by Basser et al (177).

The original MR data underwent several processing steps in order to prepare it for investigation as detailed in 3.4 and as described by Clark et al 2003 (178). The “*diff\_DTI\_GE*” program was used to generate the MD, FA and also a “*\_deff*” file which was used for further tractography processing (full details in appendix 8.6.1). The “*\_deff*” file contained the DTI data and specifically the voxel-wise principal eigenvectors.

In the period the research was undertaken a change in the software on the Siemens Avanto MRI system necessitated a change in this process and a Matlab (R2007a) script written by Dr David Atkinson was inserted to modify the data to the correct format for further processing, again producing a “*\_deff*” file. This program also provided a masking feature to remove noise outside of the brain through the subtraction of all voxels with an ADC of less than  $1/15^{\text{th}}$  of the maximum ADC, mimicking that undertaken in the *diff\_DTI\_GE* program.

### 3.5.1 DIRECTIONAL ENCODED COLOUR MAPS

Once the FA, MD and \_deff files were produced, it was possible to visually assess the output to confirm that it was suitable for further processing. Colour maps of the principal eigenvectors were produced (detailed instructions in appendix 8.6.2) using the output of the tractography program. Images were coloured using the absolute value directional encoding colour (DEC) scheme of Pajevic and Pierpaoli (97). This method allows the principal eigenvectors of the individual voxels to be represented, where red represents the orientation in the left-right direction, blue the inferior-superior direction and green the anterior-posterior direction. The DEC images were viewed using mri3dX, (<http://imaging.aston.ac.uk/mri3dX/>) a freeware program for visualisation of 3D structural/functional MRI data, written by Dr Krish Singh. If the images showed the expected principal orientation of fibres understood from previous anatomical work then further processing of the data was undertaken.

### 3.5.2 REGIONS OF INTEREST

The data in the form of the MD and FA maps were transferred to a Dell work station and using mriCro, regions of interest were drawn on the FA maps, the specifics of which are discussed in section 5.2. In summary: mriCro allows the drawing of three dimensional ROIs corresponding to the predicted anatomical location of the tracts to be studied.

The ROIs schemes were used to localise structures of interest. The ROIs acted as locations where seed voxels whose streamline tracts passed through them were retained. The algorithm also provided an option to determine a second point (dual ROI) through which the tracts should pass to be retained (121). “Exclusion” ROIs could be drawn, for

example: a whole hemisphere, so as to ensure tracts were only constructed for the left or right side; or a whole brain slice so as to potentially exclude streamlines passing supra or infra-tentorially. The ROIs were overlain onto the MR image, rather than being drawn on it directly, meaning that the brain images could be viewed with or without corresponding ROIs. When ROIs were constructed they could cover areas on several slices, in effect creating a volume ROI.

Once the ROIs were drawn for an individual case they were saved and transferred back to the SUN workstation for further processing, individual ROI's were saved into the respective folder for each individual case. As part of the manual user processing it was possible to draw ROI's on several individual cases in one sitting and subsequently process them as a group using a single command through the use of batch files, (Batch file code is found in appendix 8.6.4), the detailed instructions for this are found in appendix 8.6.3.

### 3.5.3 TRACTOGRAPHY ALGORITHM

The fibre tracking method was similar to that of Basser et al 2000 (177). The tractography algorithm (detailed instructions in appendix 8.6.2) could be run at either high or low resolution, the difference being the number of voxels in the whole brain that were seeded from to construct the tracts. When used in high resolution the algorithm would seed from the centre of every voxel within the whole brain and when used in low resolution it would seed from voxels in a checker board fashion, seeding from every other voxel in a linear fashion. The low resolution method was fast but less inclusive. It was also possible to define other parameters that would allow the tracking to continue or cease, dependent on the degree of similarity to the previous calculated eigenvector.

The vector step length: the distance from the current point at which it would then resample and calculate the principal eigenvector, in this work this was 1mm. This meant that subvoxel tracking was performed.

The angle of termination: the angle at which the direction of the principal eigenvector, in consecutive vector lines, was considered to be sufficiently different to cause tracking to cease at that point.

Fractional Anisotropy (FA) threshold: the FA value at which the algorithm would consider the principal eigenvector FA to be too ill defined and results in termination of the streamline.

The specific details of the parameters used are discussed in chapter 4.

The tracking algorithm initiated seeding from the centre of all voxels and proceeded to project a streamline in a direction equivalent to the principal eigenvector at 1mm intervals from the start voxel. The subvoxel tracking was performed through interpolation of the principal direction field at the given vector step length (1 mm) through the determination of a continuous approximation of the diffusion tensor field from the discrete (voxelwise) measurements. The linear interpolation of the tensor field method has been described previously (120-122;179;180). Essentially, the process calculates the effective diffusion tensor, eigenvalues, eigenvectors and the principal direction from the tensor field at any arbitrary point within the imaged region (subvoxel) through fitting a series of mathematical functions to the image data (93).

At 1mm intervals a streamline is constructed and the tensor field sampled and the underlying diffusion tensor calculated through interpolation. It is then further extrapolated from this new point a further one millimetre along the trajectory of the newly derived



principal eigenvector and the tracking precedes iteratively through the image data. To complete the streamline, in both retrograde and orthograde directions, the algorithm must run in the two opposite directions defined by the original principal eigenvector from the centre of the seed voxel (see figure 3.3). To allow this, the algorithm continues to proceed along the direction of the underlying principal eigenvector which is in the direction most similar to the immediately previous trajectory i.e. the streamline tends to avoid returning in the direction which it has come from. Once the algorithm has been stopped and the streamline has terminated, the algorithm recommences at the seed voxel centre seed point and extrapolates along the principal eigenvector in the opposite direction.

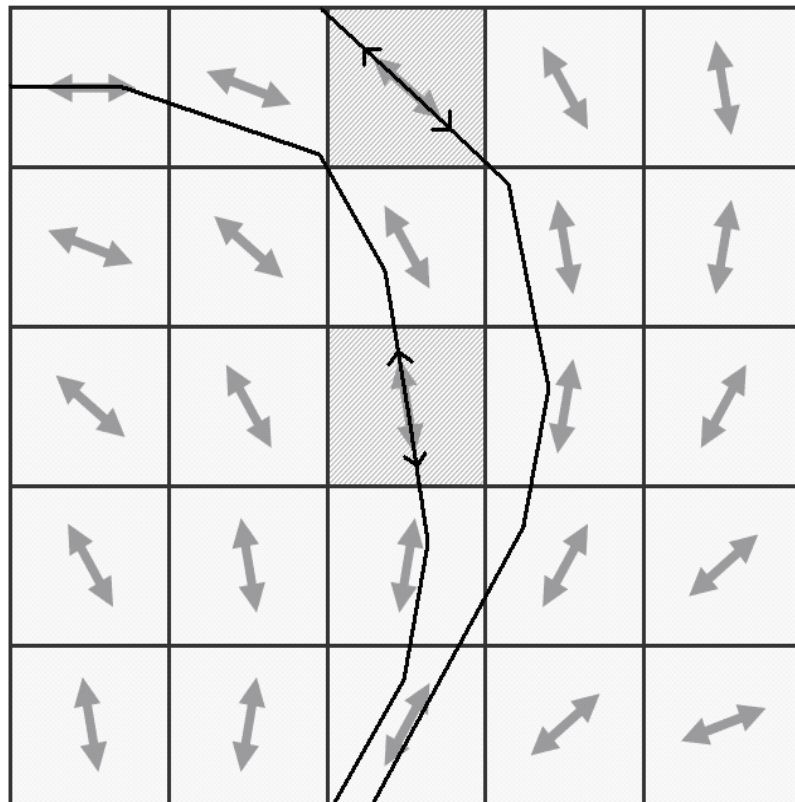


**Figure 3.3 A two dimensional illustration of the tractography algorithm. The greyed out voxels represent seed voxels from which streamlines are initiated in both directions.**

In this process the algorithm would stop and the streamline would be terminated if the FA of the interpolated tensor field was less than the FA threshold initially set. We also specified an angular threshold where the difference in streamline trajectory between two consecutive steps would terminate the streamline if it were exceeded (134;181;182). The angular threshold used in this work was 90 degrees which in effect meant that there was no angular threshold.

#### 3.5.4 VISUALISATION OF TRACTOGRAPHY OUTPUT

In order to visualise the tractography output, which used the directionally encoded colour scheme of Pajevic and Pierpaoli (97), the data was further processed so as to compress it. This was achieved with an in house program (*tractUI\_fromseed\_char*, Appendix 8.4.2), where the streamline co-ordinates used to construct the tracts were converted to a binary image. Each streamline consisted of multiple vectors with endpoints. The program determined which voxels were included in the streamline to produce a binary map which could be displayed using GeomView, an interactive 3D viewing program (<http://www.geomview.org/>). The fibre track maps were converted to 3D volume image files and viewed as overlays on T2-weighted, T1-weighted and contrast enhanced T1-weighted images in mriCro to reveal their anatomical relations to each brain and lesion being studied. The method of visual evaluation of the output and the quantitative data extracted from the tractography is discussed in chapters 5 and 6.

---

## 4 ADC DISCRIMINATION OF PAEDIATRIC CNS TUMOURS

---

### CONTENTS

---

4.1	Introduction	99
4.2	Methods	103
4.2.1	Patients.....	103
4.2.2	MR Imaging and Image Processing.....	104
4.2.3	Statistical Analysis.....	106
4.3	Results	107
4.3.1	Mean ADCs .....	110
4.3.2	ADC Histograms: all Tumour Groups.....	117
4.3.3	ADC Histograms Posterior Fossa Tumours.....	119
4.3.4	ADC Histograms PNET versus ATRT .....	121
4.4	Discussion	123

---

#### 4.1 INTRODUCTION

Accurate preoperative diagnosis is important in paediatric patients with CNS lesions, particularly as they may require different surgical approaches and have differing natural histories and outcomes (183).

Definitive histological diagnosis remains the gold standard for deciding the optimal oncological management and likely prognosis. The process of interpreting the tissue diagnosis requires light microscopy and immuno-histochemical staining of the sample.

This can take several days and requires considerable training of the interpreting pathologist. The sample can be obtained from a total resection or partial debulking or a simple biopsy. There is a mortality associated with craniotomy and tumour resection. In cases where a craniotomy is not appropriate due to the location of the lesion or the probable diagnosis is that of a lesion likely to be sensitive to radio or chemotherapy a surgical biopsy can be undertaken. This procedure still carries significant risk of morbidity (184-187) and mortality. Risks of neurological deficit are secondary to complications due to haemorrhage, cerebral oedema, seizures or infection (184). In addition there is a significant risk of a non diagnostic biopsy (8.1% in 300 cases (188)).

A non-invasive diagnosis could reduce this surgical morbidity. Several techniques have been attempted including the use of CSF and serum markers (189), dynamic contrast MRI (190), positron emission tomography and MR spectroscopy (191;192). Histological examination remains definitive but magnetic resonance imaging plays a central role in the radiological diagnosis of brain tumours (193-196). In particular, the quantitative measurement of water diffusion by gradient sensitisation (DWI) allows derivation of the ADC, enabling the investigation of tissue structure. This has been used to characterise acute infarcts and both adult and paediatric brain lesions with regard to discrimination of their nature (55;60;61;84;197;198). The ADC appears to be influenced by tumour cellularity and nuclear characteristics (85;87;199;200).

There has been some evidence of correlation of ADC with tumour grade although results have been conflicting. In general higher grade tumours are more densely cellular and it is hypothesised that it correlates inversely with ADC (61;75;84-87;198-206). Variable ADC values are seen in different components of the tumour, surrounding oedema and white matter. Cystic tumours and high grade lesions, which outgrow their

blood supply and become necrotic, may have higher ADC values due to the increased water movement within these components (207). A study looking at extra cranial mass lesions in children to determine if a relationship existed between the ADC and the histopathologic cell count found a significant relationship between cellularity and ADC but determined that cell count was likely not to be its only determinant (202).

Attempts to discriminate paediatric brain tumour types using DWI has shown useful results when using the mean ADC of tumour groups alone (197;208), or when taken in combination with age and sex (86). Production of a reliable discrimination method for new cases on these grounds alone has been elusive in part due to extensive overlap of ADC ranges between groups. In reality questions as to diagnosis are often more focused due to the different demographics of lesions. ADC values in combination with single voxel proton magnetic resonance spectroscopy (MRS) has been employed to discriminate four common posterior fossa (PF) tumours (juvenile pilocytic astrocytoma (JPA), primitive neuroectodermal tumour-medulloblastoma PNET-MB, ependymoma and glioma. 17 cases) using linear discriminant analysis which assumes multivariate normality (208). However, it was not possible to discriminate them using either the ADC or the metabolite variable alone. Recently histograms of the ADC derived from the tumour volume and surrounding peritumoural oedema have been used to discriminate adult brain tumours, specifically low-grade gliomas, astrocytomas and oligodendrogliomas (209). ADC histograms generated from regions of interest (ROIs) drawn within whole tumour volumes have been used to differentiate between oligodendroglial tumour genotypes with some preliminary success (194). A related application of the whole tumour ADC histograms has been in its use to stratify progression-free survival in bevacizumab treated patients with recurrent glioblastoma multiforme (210).

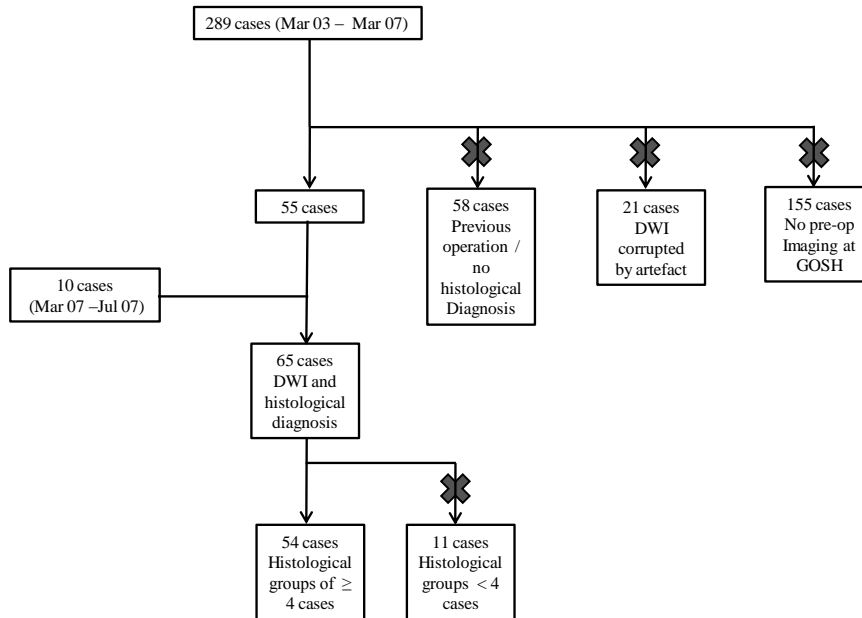
Histograms provide the frequency of occurrence of ADC values and can be determined within the entire tumour volume. Histograms of the ADC derived from both the tumour volume and surrounding peri-tumoural oedema have been used to discriminate adult brain tumours, specifically low-grade gliomas, astrocytomas and oligodendrogliomas (209).

We therefore attempted to determine whether common paediatric tumour types could be discriminated using statistical analysis (multinomial logistic regression) of ADC histogram parameters. Subsequently a more focused analysis was performed on the PF groups and then specifically we determined the ability of the technique to differentiate a rare tumour, atypical teratoid rhabdoid tumour (ATRT), from its embryological relative PNET. We addressed this as there is no established method, currently, to discriminate them pre-operatively and ATRT has a much poorer prognosis and more complex management (211-216).

## 4.2 METHODS

### 4.2.1 PATIENTS

We undertook a retrospective review from 2003 (the point at which DWI was added to the local tumour preoperative imaging protocol) specifically looking at all cases of paediatric CNS tumours with a histologically confirmed diagnosis. This was compiled from a local electronic oncology database. The initial group consisted of a total of 289 cases (to March 2007) that had had imaging at Great Ormond Street Hospital (GOSH). The imaging was reviewed, all cases without pre-operative DWI were excluded as were cases where the imaging was corrupted by artefact or the imaging was incomplete (not all cases had all their pre-operative imaging at GOSH). Initially 55 cases were identified, subsequently individuals were added prospectively from March 2007 until July 2007; providing 10 further cases (total 65). Analysis was performed on tumour groups with greater than three cases, resulting in the exclusion of 11 cases, including groups of brain stem gliomas (3), high grade gliomas (3), choroid plexus carcinomas (2) and other types of astrocytoma (3).



Flow chart of cases selected for DWI analysis

In total 54 cases were used in the study comprising: JPA (11), choroid plexus papillomas (CPP) (7), Dysembryoplastic neuroectodermal tumour (DNET) (5), ependymoma (5), PNET (22), ATRT (4). The mean age was 6.1 years and range 0.1 - 15.8 years. There were 22 females and 32 males.

#### 4.2.2 MR IMAGING AND IMAGE PROCESSING

All imaging was performed on either a 1.5 T Siemens Avanto (maximum magnetic field gradient strength of  $40 \text{ mT m}^{-1}$ ) or a 1.5T Magnetom Symphony (maximum magnetic field gradient strength of  $30 \text{ mT m}^{-1}$ ). The full tumour imaging protocol is detailed in chapter 3.2. Diffusion MRI data were obtained using a diffusion-sensitized single-shot echo planar imaging sequence. Two b values were applied of  $500 \text{ s mm}^{-2}$  and  $1000 \text{ s mm}^{-2}$  following an acquisition with  $b = 0$ . DW images were acquired with diffusion gradients applied in 3 orthogonal directions (image matrix  $128 \times 128$  and FOV  $230 \times 230 \text{ mm}$ ). The Avanto protocol acquired 19 5mm thick slices (distance factor 30%,



1.5mm) and 3 averages with a total sequence time of 64 seconds (TR 2700ms, TE 96ms). The Symphony protocol acquired 20 5mm thick slices (distance factor 50%, 2.5mm) and 2 averages with a total sequence time of 56 seconds. (TR 3600ms, TE 107ms).

All DWI data, ADC maps and  $b = 0$  images, were transferred to a Sun workstation (Sun Blade 100 Sun Microsystems, Mount View, California.) and off-line analysis was performed using DispImage (217) (UCLH Department of Medical Physics, Capper Street, London, UK).

Image analysis was performed blind to histological diagnosis, by allocating individual cases a random number reference and processing cases in sequential numerical order. ROIs were drawn around the whole tumour margin on each slice of the  $b = 0$  image on which it was evident, by the author (four years of neurosurgical experience). Areas of large cyst, identified as regions of hyper-intensity, or necrosis were excluded (208); where there was uncertainty as to the location of the margin of the tumour, that area was excluded. The whole tumour ROI volumes were transferred to the intrinsically co-registered ADC maps from which ADC histograms were generated for the entire tumour volume. In addition ADC histograms and mean ADC values were calculated for regions of normal appearing white matter (NAWM) through the use of a region in the contralateral hemisphere of similar size over the same number of slices.

The ADC histograms generated for the individual whole tumours were normalised for tumour volume (218), bin width of  $0.02 \times 10^{-3} \text{ mm}^2 \text{ s}^{-1}$  was preserved for all histograms. An in house Matlab (R2007a) script was used to extract the parameters: peak height, peak location (mode), mean ADC, 10<sup>th</sup>, 25<sup>th</sup>, 50<sup>th</sup>, 75<sup>th</sup>, 90<sup>th</sup> centile points (The X<sup>th</sup> centile point is that which has X% of the voxel values forming the histogram to the left

in the histogram) and skewness (a measure of the histogram asymmetry calculated in DispImage).

#### 4.2.3 STATISTICAL ANALYSIS

All 9 parameters were extracted from each tumour histogram and cases were grouped into specific histological tumour types. The data were analyzed using SPSS for Windows (Ver. 14. 2006. Chicago: SPSS Inc.). As part of our initial analysis in common with that of Rumboldt et al (197) we examined differences in mean ADC between tumour types using a one-way ANOVA and Tamhane's T2 post hoc multiple comparisons correction, in order to avoid assumptions of common variance.

Logistic regression (LR) analysis was performed using all 9 histogram parameters from each individual case. The first analysis of the tumour histogram data examined all the tumour groups and determined which of the histogram parameters best discriminated the tumours into their histological groups by means of a predicted classification. To achieve this all histogram variables were entered for analysis and added in a stepwise manner to allow determination of the optimal parameters for discrimination. The process was repeated to determine the differentiation of three common PF tumour types (JPA, PNET-MB, ependymoma) and the discrimination of all PNETs from ATRTs.

### 4.3 RESULTS

In order to determine possible differences in ADC values obtained on the two scanners the mean ADC of water at 18°C was measured on both systems using the same sample. There was no significant difference between the values obtained (ADC of water measured on the Avanto =  $2.276 \times 10^{-3} \text{ mm}^2 \text{ s}^{-1}$ , SD  $0.035 \times 10^{-3} \text{ mm}^2 \text{ s}^{-1}$ , range  $2.17 - 2.39 \times 10^{-3} \text{ mm}^2 \text{ s}^{-1}$  and ADC of water measured on the Symphony =  $2.245 \times 10^{-3} \text{ mm}^2 \text{ s}^{-1}$ , SD  $0.033 \times 10^{-3} \text{ mm}^2 \text{ s}^{-1}$ , range  $2.13 - 2.45 \times 10^{-3} \text{ mm}^2 \text{ s}^{-1}$  ) therefore the calculated difference between the scanners was ignored.

Representative ADC maps for each tumour type are shown in Figure 4.1 (a - f). Mean ADC of all tumour groups and NAWM together with each group's patient demographics are shown in Table 4.1. A scatter plot, by group, of each individual tumour mean ADC value is shown in Figure 4.2. Normalised ADC histograms, averaged for each group, are shown in Figure 4.3 (a - g).

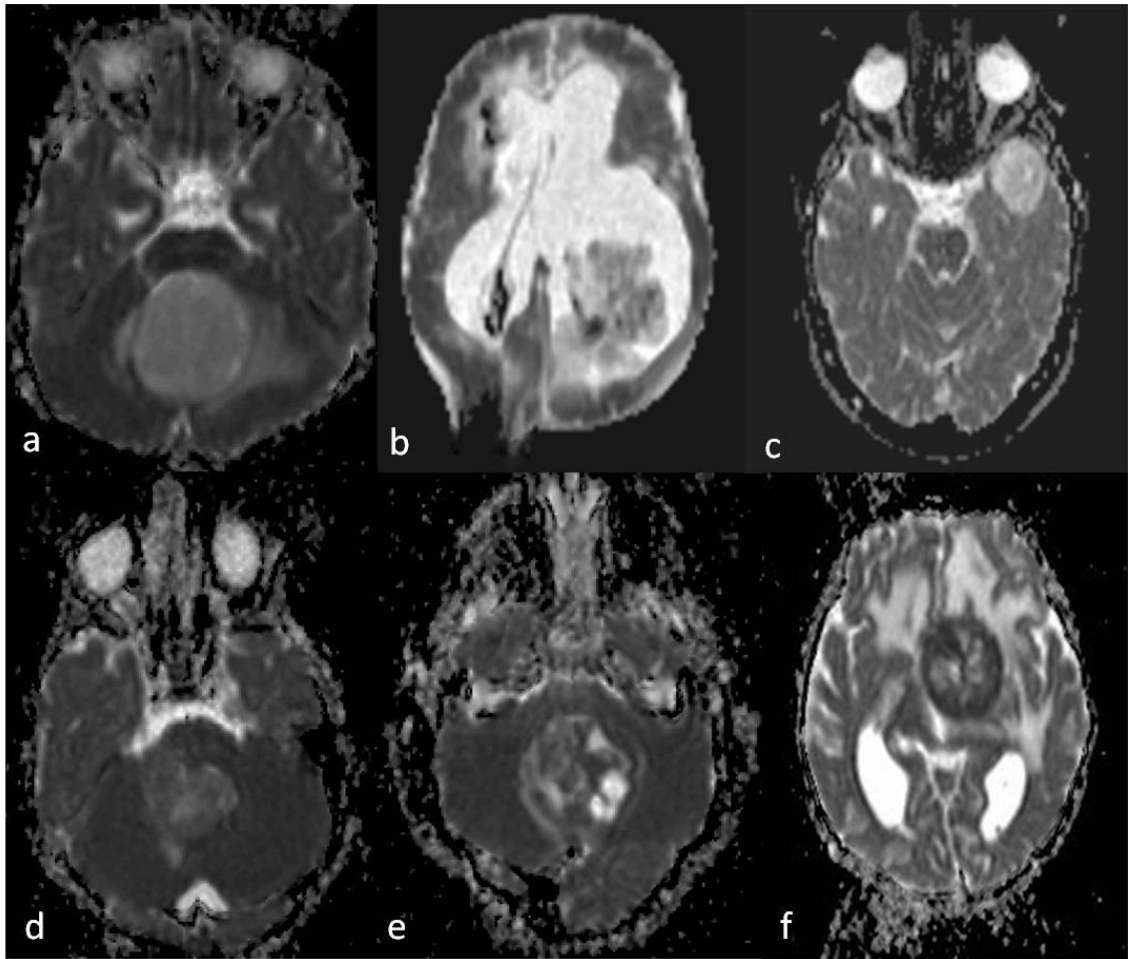


Figure 4.1 ADC maps showing the lesions investigated.

---

- a) Cerebellar juvenile pilocytic astrocytoma (JPA) with a high ADC value b) Choroid plexus papillomas within the left lateral ventricle., c) Dysembryoplastic neuroepithelial tumour in the left temporal pole d) Midline posterior fossa ependymoma e) Heterogeneous but predominantly dark midline primitive neuroectodermal tumour (medulloblastoma type, PNET- MB), f) Atypical teratoid rhabdoid tumour (ATRT) demonstrated as a supratentorial heterogeneous lesion with areas of very restricted diffusion.**

CHAPTER FOUR: ADCs IN THE DISCRIMINATION OF PAEDIATRIC CNS TUMOURS

Tumour type	N (M/F)	Age Range (Year Fraction)	Average Age (Year Fraction)	Av Age SD (Year Fraction)	Mean ADC ( $\times 10^{-3} \text{ s}^{-1} \text{ mm}^2$ )	SE	Min Av ADC ( $\times 10^{-3} \text{ s}^{-1} \text{ mm}^2$ )	Max Av ADC ( $\times 10^{-3} \text{ s}^{-1} \text{ mm}^2$ )
JPA <sup>1</sup>	11 (7/4)	2.29 - 13.85	8.91	4.72	1.837	0.051	1.609	2.135
CPP <sup>2</sup>	7 (5/2)	0.49 - 2.95	1.04	1.08	1.549	0.152	0.993	2.028
DNET <sup>3</sup>	5 (2/3)	7.74 - 15.76	13.13	3.2	1.392	0.198	1.01	2.041
Ependymoma	5 (3/2)	1.34 - 6.44	3.71	2.11	1.180	0.028	1.099	1.254
PNET <sup>4</sup> (All)	22 (16/6)	0.43 - 11.66	5.25	3.35	0.921	0.034	0.667	1.231
PNET-MB <sup>5</sup>	16 (12/4)	0.43 - 11.66	5.69	3.47	0.880	0.035	0.667	1.222
ATRT <sup>6</sup>	4 (1/3)	1.55 - 9.60	4.99	3.65	0.806	0.100	0.523	0.962
Normal WM	54 (34/20)	0.43 - 15.76	6.10	3.89	0.789	0.020	0.671	1.028

1) Juvenile Pilocytic Astrocytoma, 2) Choroid plexus papilloma, 3) Dysembryoplastic neuroepithelial tumour, 4) Primitive neuroectodermal tumour, 5) Medulloblastoma, 6) Atypical teratoid rhabdoid tumour

**Table 4.1 Summary of histological diagnosis, demographics and ADC**

### 4.3.1 MEAN ADCs

Comparisons between group means using a one-way ANOVA test and Tamhane's T2 post hoc multiple comparisons correction are shown in Table 4.2. Significant differences (at the  $p < 0.05$  level) were seen between JPAs and PNET-MBs, between JPAs and all PNETs, between JPAs and ependymomas and between JPAs and ATRTs. There were also significant differences between ependymomas and JPAs, PNETs and PNET-MBs.

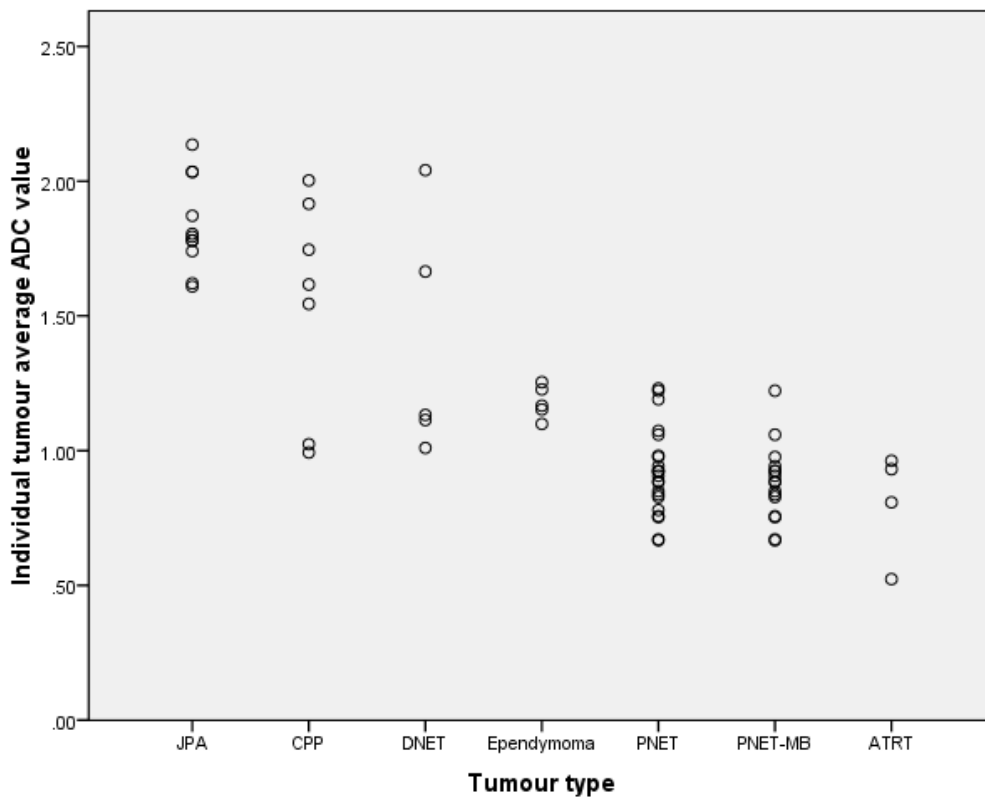


Figure 4.2 Scatter Plot of individual tumour ROI average ADCs classified by tumour group (ADC values  $\times 10^{-3} \text{ mm}^2 \text{ s}^{-1}$ )

**Significant differences on ANOVA of mean ADC of tumour groups (p Values)**

<b>Tumour Type</b>	Ependymoma	DNET <sup>1</sup>	Choroid Plexus Papilloma	Juvenile Pilocytic Astrocytoma	PNET <sup>4</sup>	PNET-MB <sup>5</sup>	ATRT <sup>6</sup>
Ependymoma		N/S	N/S	<0.0005	<0.0005	<0.0005	N/S
DNET <sup>1</sup>	N/S		N/S	N/S	N/S	N/S	N/S
CPP <sup>2</sup>	N/S	N/S		N/S	N/S	N/S	N/S
JPA <sup>3</sup>	<0.0005	N/S	N/S		<0.0005	<0.0005	0.008
PNET <sup>4</sup>	<0.0005	N/S	N/S	<0.0005		N/S	N/S
PNET-MB <sup>5</sup>	<0.0005	N/S	N/S	<0.0005	N/S		N/S
ATRT <sup>6</sup>	N/S	N/S	N/S	0.008	N/S	N/S	

1) Dysembryoplastic neuroepithelial tumour, 2) Choroid plexus papillomas, 3) Juvenile Pilocytic Astrocytoma, 4) Primitive neuroectodermal tumour, 5) Medulloblastoma 6) Atypical teratoid rhabdoid tumour

**Table 4.2 ANOVA testing of group mean ADC values for significant differences at the P < 0.05 level (N/S: not significant)**

**Figure 4.3** Normalised histograms averaged for all tumours within each group. (Note that the average histograms are for illustration; in the analysis the individual case parameters were used)

---

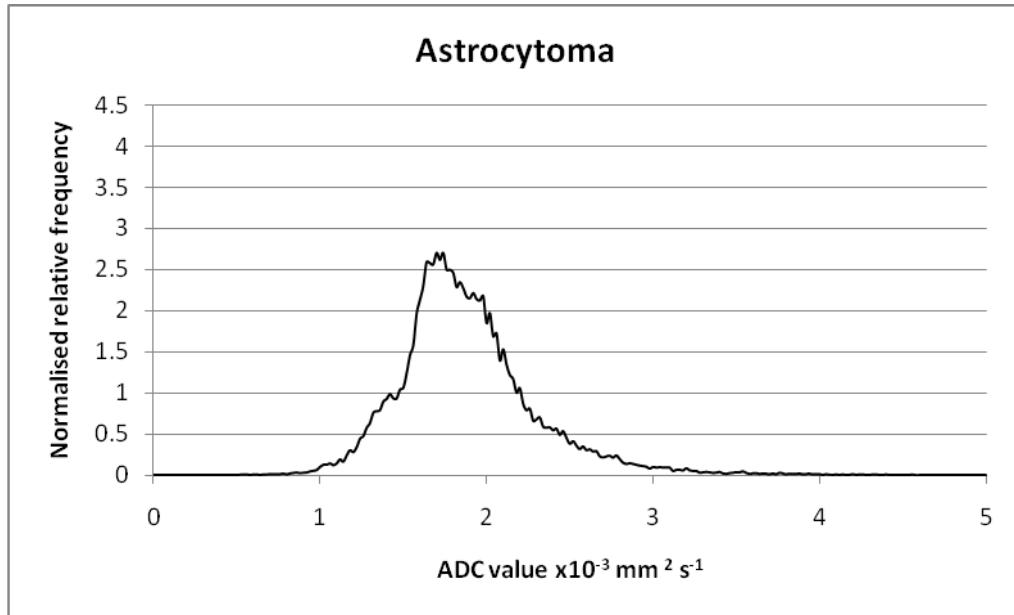


**Figure 4.3a** Juvenile pilocytic astrocytoma (JPA) normalised average histogram

---



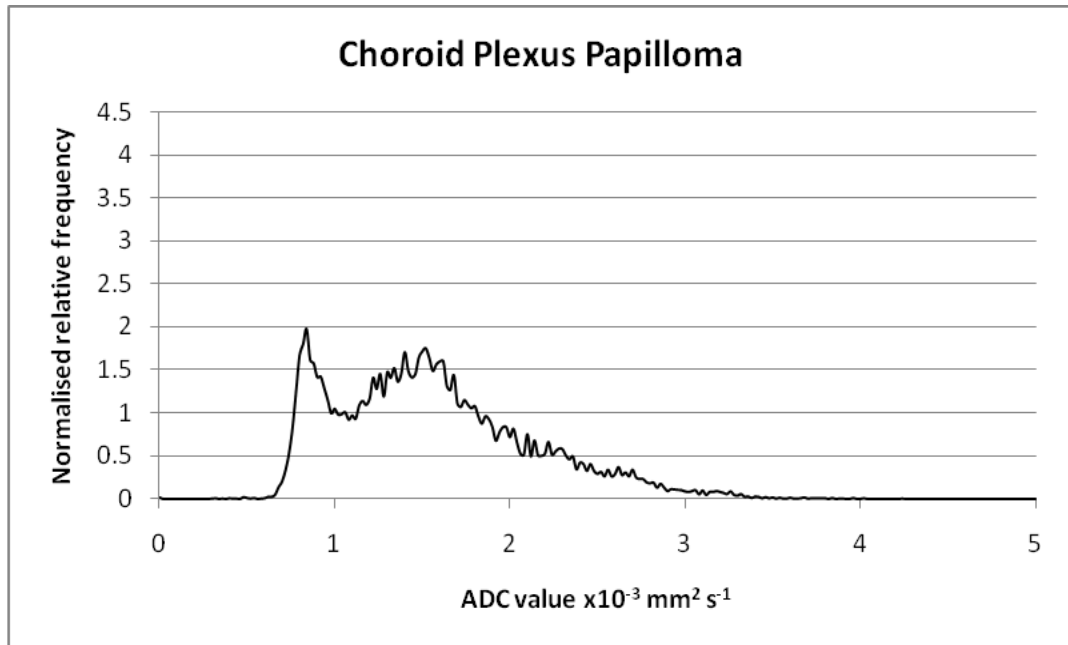


**Figure 4.3b(i) Choroid plexus papilloma normalised average histogram**

---

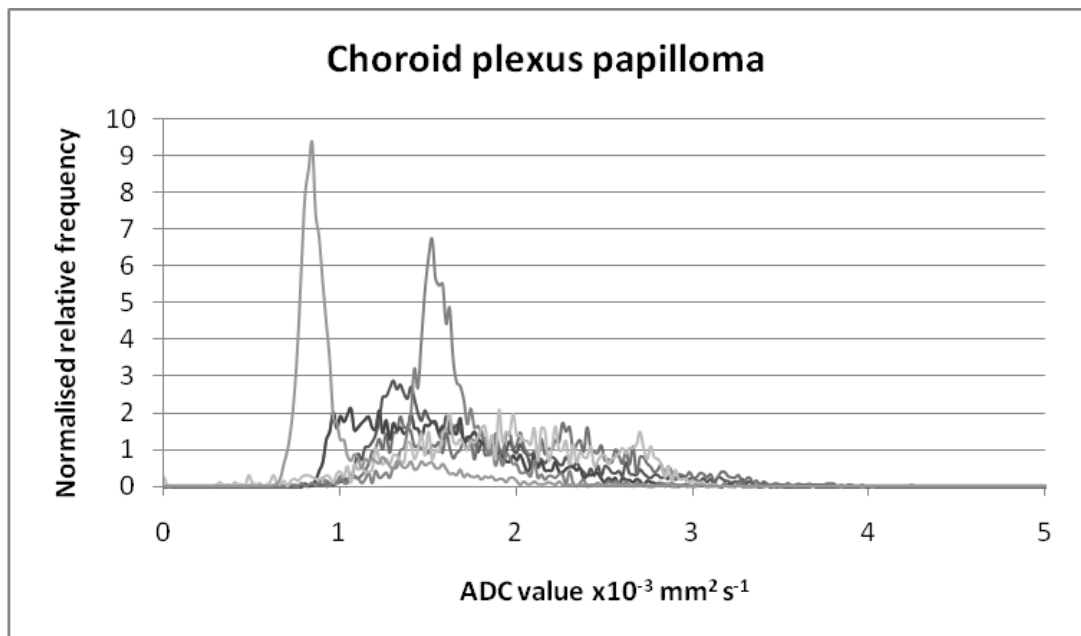


**Figure 4.3b(ii) Choroid plexus papilloma (CPP), individual normalised histograms illustrating the distortion of the average histogram due to the heterogeneity within the group.**

---

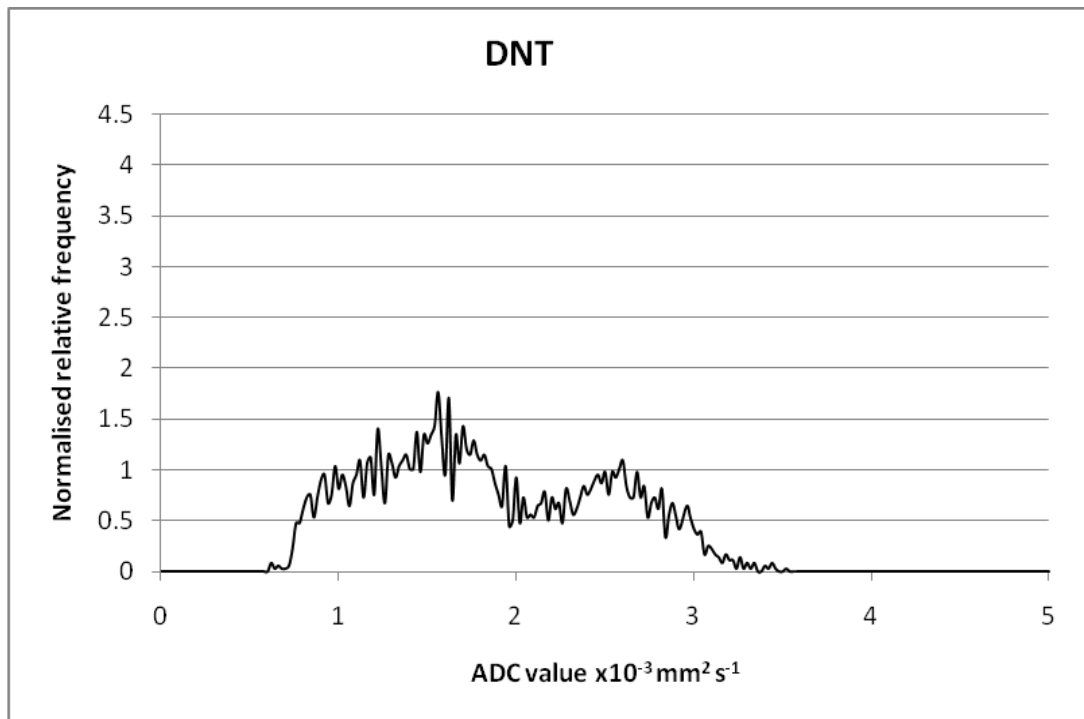


**Figure 4.3c Dysembroplastic neuroepithelial tumour (DNET) normalised average histogram.**

---

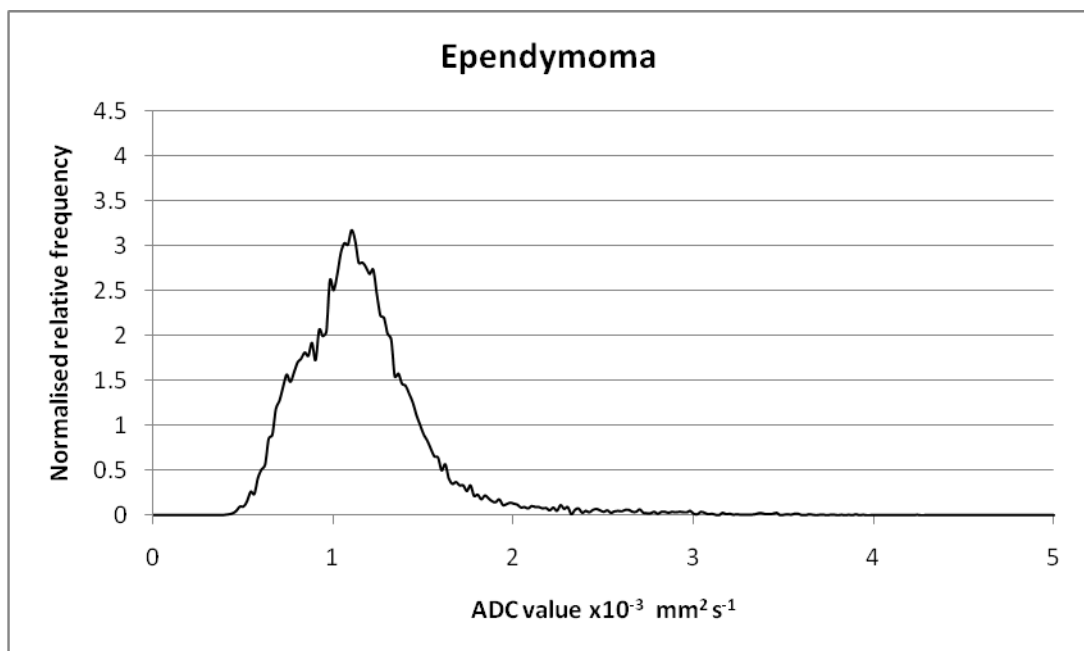


**Figure 4.3d Ependymoma normalised average histogram.**

---

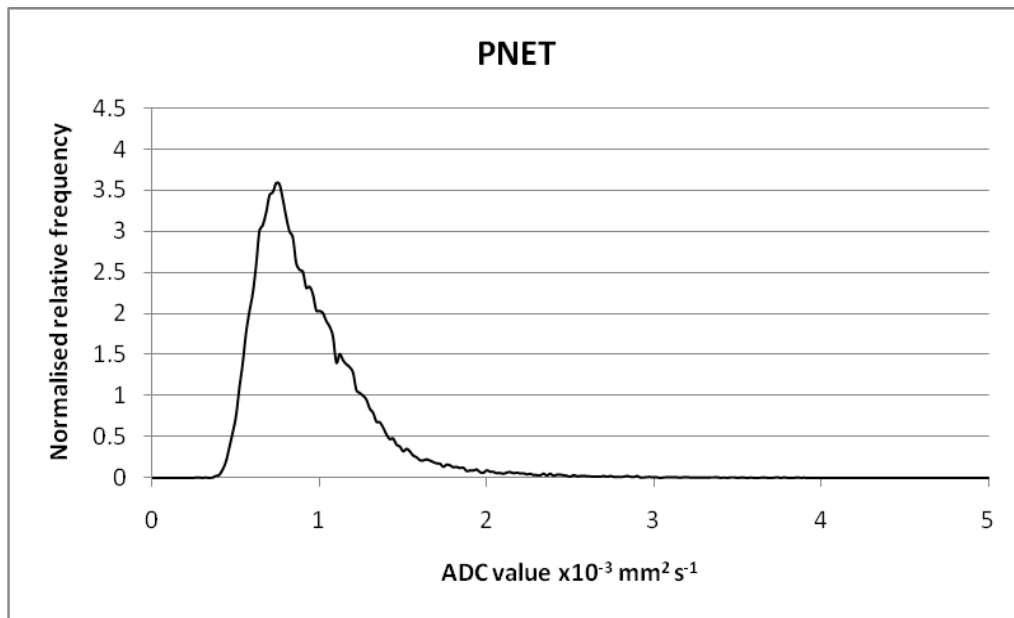


**Figure 4.3e Primitive neuroectodermal tumour (PNET) normalised average histogram.**

---

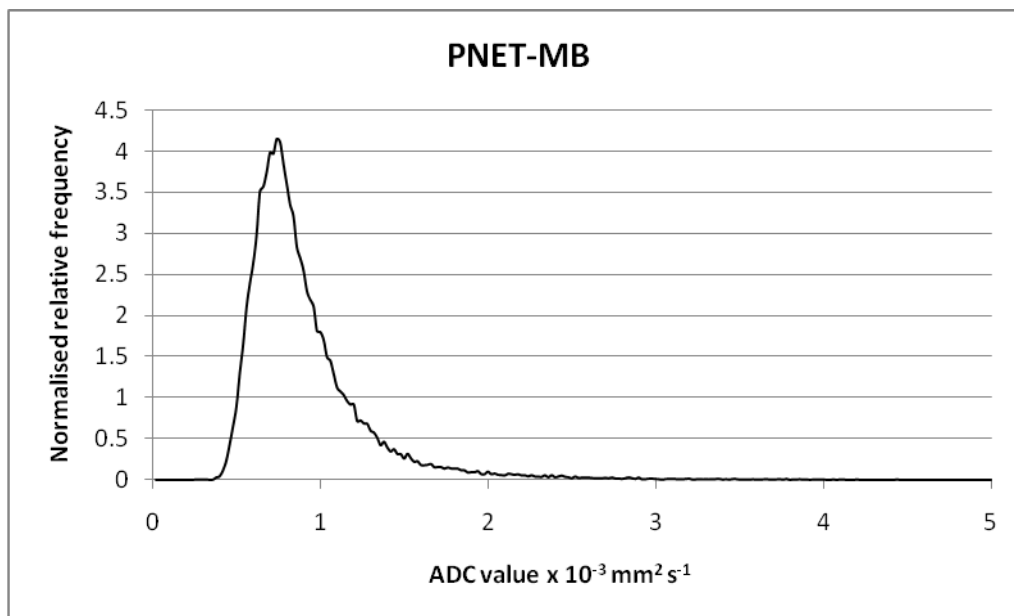


**Figure 4.3f Primitive neuroectodermal tumour–medulloblastoma (PNET-MB) normalised average ADC histogram.**

---

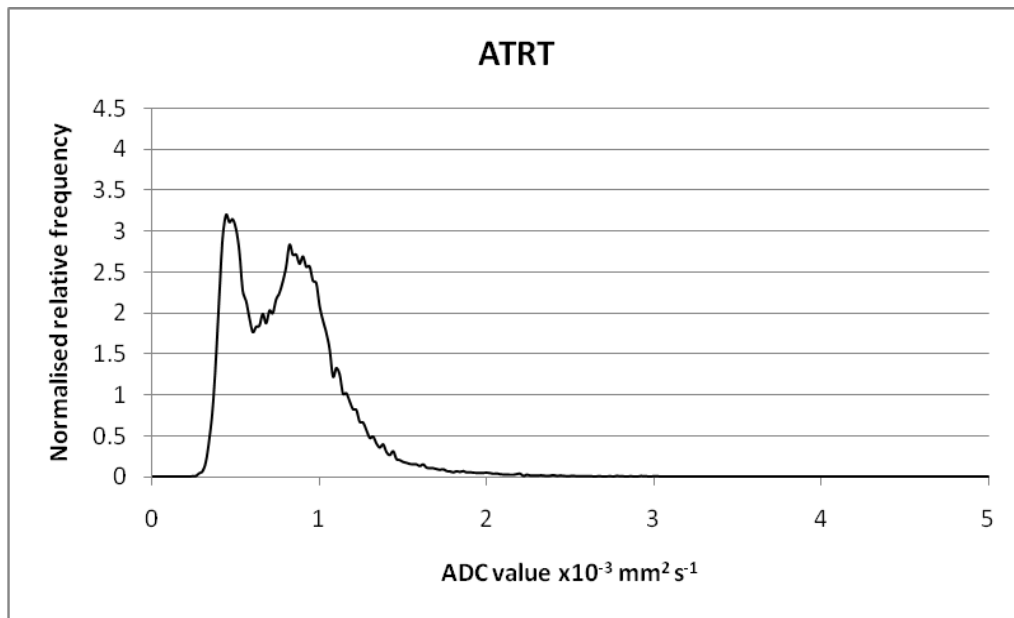


**Figure 4.3g(i) Atypical teratoid rhabdoid tumour (ATRT) normalised average Histogram.**

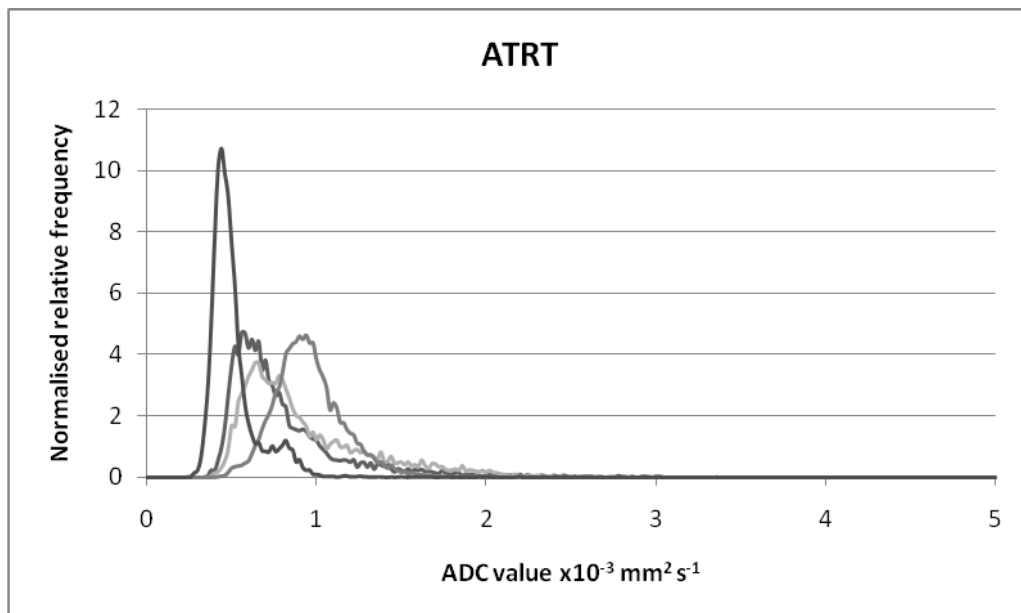


**Figure 4.3g(ii) Atypical teratoid rhabdoid tumours, individual normalised histograms highlighting that the bimodal distribution is representative of the heterogeneity within the group.**

### 4.3.2 ADC HISTOGRAMS: ALL TUMOUR GROUPS

Histogram data analysed using LR, including all tumour groups, is shown in Table 4.3. The results of this analysis show that, 74.1% (40/54) of tumours were correctly classified. This included 91% (20/22) PNETs, 82% (9/11) JPAs 80% (4/5) DNETs and 75% (3/4) ATRTs. However, no ependymomas were correctly classified (0/5) and only 57% (4/7) of CPPs were correctly identified. Peak height and the 10<sup>th</sup> centile provided the best discrimination of tumour type.

CHAPTER FOUR: ADCs IN THE DISCRIMINATION OF PAEDIATRIC CNS TUMOURS

---

Observed	Predicted Group Membership						Percent Correct	Total Correct
	Ependymoma	DNET	Choroid Plexus Papilloma	Juvenile Pilocytic Astrocytoma	PNET	ATRT		
Ependymoma	0	1	0	0	4	0	0.0%	0 / 5
DNET <sup>1</sup>	0	4	1	0	0	0	80.0%	4 / 5
CPP <sup>2</sup>	0	0	4	1	2	0	57.1%	4 / 7
JPA <sup>3</sup>	0	1	1	9	0	0	81.8%	9 / 11
PNET <sup>4</sup>	0	1	1	0	20	0	90.9%	20 / 22
ATRT <sup>5</sup>	0	0	0	0	1	3	75.0%	3 / 4
Overall Percentage	0.0%	13.0%	13.0%	18.5%	50.0%	5.6%	74.1%	40 / 54

1) Dysembryoplastic neuroepithelial tumour. 2) Choroid plexus papillomas. 3) Juvenile Pilocytic Astrocytoma. 4) Primitive neuroectodermal tumour. 5) Atypical teratoid rhabdoid tumour

**Table 4.3 Logistic regression analysis classification of all tumour cases**

---

### 4.3.3 ADC HISTOGRAMS POSTERIOR FOSSA TUMOURS

The LR of the histogram parameters of the PF tumour groups is shown in Table 4.4. The analysis showed that 94% (30/32) of the PF tumours were correctly classified. Specifically: 80% (4/5) of ependymomas, 94% (15/16) of PNET-MBs and 100% (11/11) of JPAs. The variable used to construct the model was the 75<sup>th</sup> centile value (Figure 4.4).

Observed	Predicted Group Membership			Percent Correct	Total Correct
	Ependymoma	JPA	PNET-MB		
Ependymoma	4	0	1	80	4 / 5
JPA	0	11	0	100	11 / 11
PNET-MB	1	0	15	93.75	15 / 16
Overall Percentage	15.6%	34.4%	50.0%	93.75	30 / 32

**Table 4.4 Logistic regression analysis classification of Posterior Fossa Tumours**

---

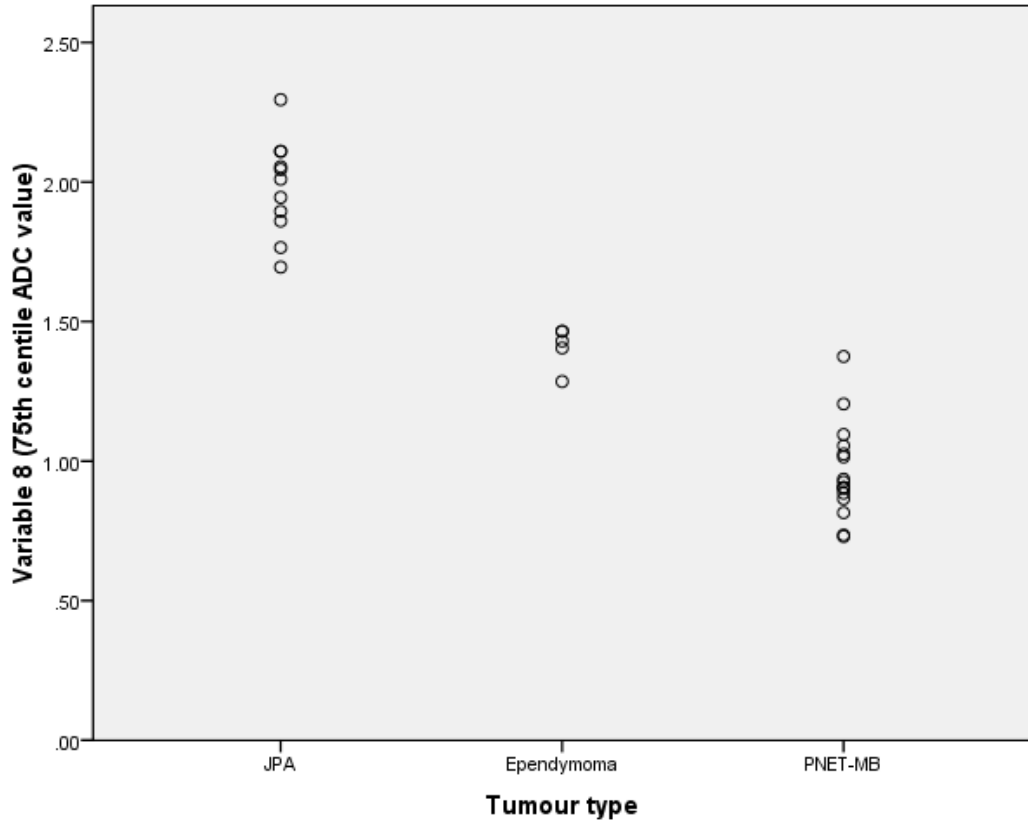


**Figure 4.4 Scatter plot of posterior fossa tumour type versus ADC 75th centile value (ADC values x 10<sup>-3</sup> mm<sup>2</sup> s<sup>-1</sup>) (The variable used to discriminate the three tumour groups in the logistic regression analysis).**



#### 4.3.4 ADC HISTOGRAMS PNET VERSUS ATRT

The LR of the histogram parameters of the PNET and ATRT groups is shown in Table 4.5. The analysis correctly classified 100% (26/26) of the tumours, specifically all 22 of the PNETs (100%) and all 4 ATRTs (100%). The variables used were the peak height and the mean ADC (Figure 4.5).

<b><u>Predicted Group Membership</u></b>				
Observed	PNET <sup>1</sup>	ATRT <sup>2</sup>	Percent Correct	Total Correct
PNET <sup>1</sup>	22	0	100.0%	22 / 22
ATRT <sup>2</sup>	0	4	100.0%	4 / 4
Overall Percentage	84.6%	15.4%	100.0%	26 / 26

---

**Table 4.5 Logistic Regression Analysis Classification of PNET and ATRT groups**

---

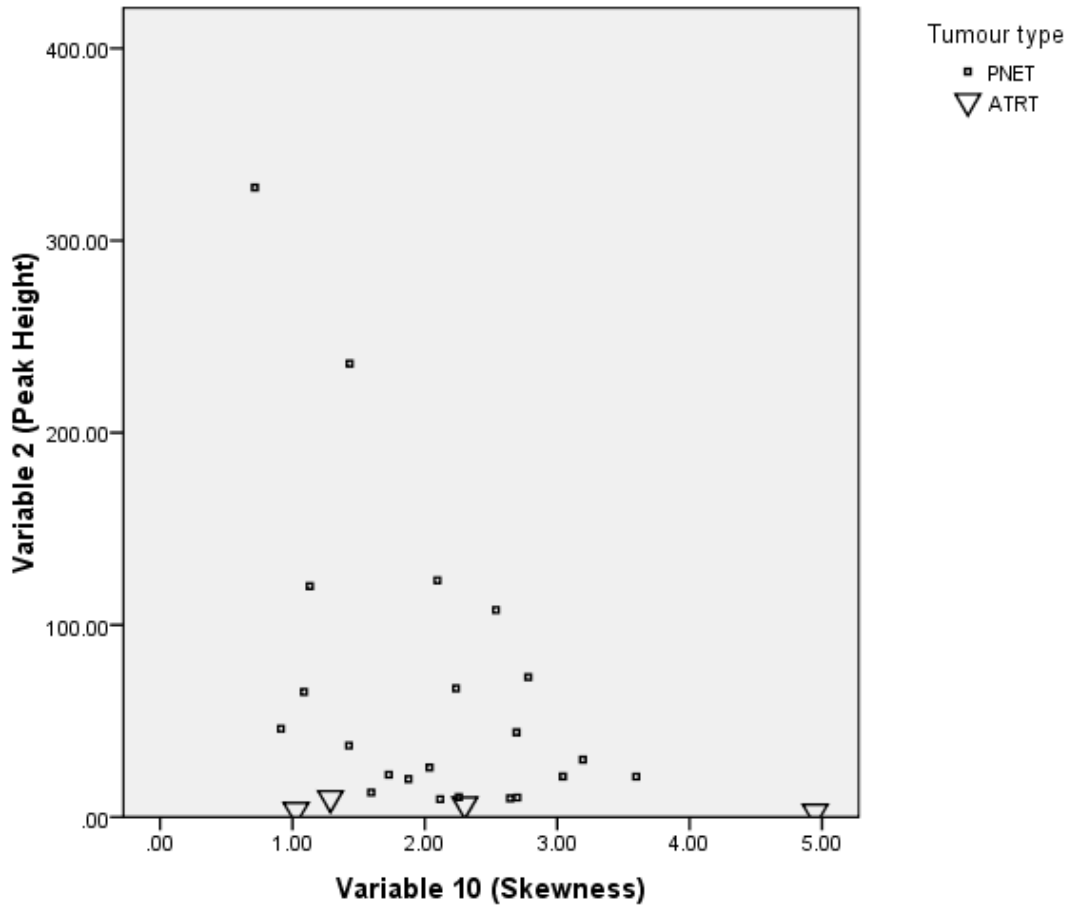


**Figure 4.5 Scatter plot of skewness (variable 10) versus peak height (variable 2) for PNET and ATRT groups.** (The variables used to discriminate ATRT and PNET groups in the logistic regression analysis).

---

## 4.4 DISCUSSION

This study attempted to discriminate paediatric brain tumours based on ADC histogram parameters alone. The most important findings in our study were the discrimination of common PF tumours with 94% reliability and ATRT from PNET with 100% accuracy.

### **Mean ADC values**

The mean ADC values for each tumour group (Table 4.1) were similar to previously published work (86;197). The values for the DNT group are lower than those reported by Yamasaki et al 2005 and are likely to reflect the heterogeneity within the tumour group (86). Values for ATRT are higher than previous studies have shown but fall within the range given in these series (197;208;214). In Rumboldt et al (197) and Koral et al's (214) series' the mean ADC for PNETs was lower than both our series and Yamasaki et al's (86) series whilst our data and the Yamasaki data were comparable. This may be because the ATRTs in previous series (197;214) were all in the PF, whilst they were supratentorial in our cohort. Gauvain et al (87) grouped all embryonal tumours (PNET and ATRT) using ADC and diffusion tensor imaging to assess tumour cellularity and obtained a mean consistent with our results.

### **Distinguishing tumour types using mean ADC**

The significant increase in the mean ADC of the JPA group compared to the PNET / PNET-MB groups and the ATRT group (Figure 4.2) reflects the histological difference between the loose stroma of the JPA from the densely packed cells seen in the small blue round cell tumour group of PNET, medulloblastoma and ATRT. The overlap of the ependymoma mean ADCs with the PNET and ATRT groups is in line with previous work on PF tumours (86;197) and ATRTs (214) and demonstrates why discrimination of individual tumours based on mean ADCs alone is hampered. Rumboldt et al (197)

proposed a lower limit of a mean ADC of  $1.40 \times 10^{-3} \text{ mm}^2 \text{ s}^{-1}$  for the JPA group and an upper limit of  $0.90 \times 10^{-3} \text{ mm}^2 \text{ s}^{-1}$  for PNET/ ATRT. The former value for JPA applies to our data but the cut off value for PNET-MB required was considerably higher at less than  $1.20 \times 10^{-3} \text{ mm}^2 \text{ s}^{-1}$  in our series.

### **ADC histograms**

It is apparent from the normalised histograms that PNET, PNET-MB and ATRT have distributions to the lower end of the ADC range, in keeping with their more densely cellular nature, as has been reported previously (87;197). The JPA group are at the higher end of the ADC range due to their loose stroma. Significant heterogeneity of the mean ADC histogram is seen within the ATRT group, Figure 4.3g (i) shows a bimodal distribution and this reflects differences between histograms within the group (Figure 4.3g (ii)). The DNT group have a broader and more flat distribution than the other groups, again reflecting a heterogeneous appearing tumour (Figure 4.3c). The bimodal distribution of the CPP group (Figure 4.3b (i)) also reflects a very heterogeneous tumour group (Figure 4.3b (ii)).

### **LR analysis all tumours**

LR of all tumour groups correctly classified 74.1% (40/54) of tumours (Table 4.3); 90% (20/22) PNETs, 82% (9/11) JPAs, 80% (4/5) DNTs and 75% (3/4) ATRTs. The failure to correctly classify any ependymomas (0/5) can be explained by the significant overlap with the PNET group. Only 57% of CPPs were correctly classified, the 3 incorrectly classified tumours were placed in 3 other groups (JPA, DNT and PNET). It may be that the broad distribution of the four DNTs in this study means that when included in the analysis other tumours are more easily classified into this group. The ependymoma that was not misclassified as a PNET was grouped with the DNTs. The variables which

provided the best discrimination were the peak height and the 10<sup>th</sup> centile. This may represent differences in cellularity, where low ADC values are associated with more densely packed tumour types and allow discrimination from tumours with more heterogenous cellularity or simply less densely cellular structure as has been seen with PNET versus juvenile pilocytic astrocytomas.

### **LR of PF tumours**

The LR analysis demonstrated that 94% of PF tumours were correctly classified (Table 4.4), 80% (4/5) of ependymomas, 94% (15/16) of PNET-MBs and 100% (11/11) of JPAs, using the 75<sup>th</sup> centile value, highlighting the additional information obtained from the histogram over and above the mean ADC (Figure 4.4). In contrast to the analysis including all the tumour groups it was possible to correctly classify 80% of ependymomas, again the incorrectly classified case was placed in the PNET group, reflecting the overlap in ADC histograms. Similarly the incorrectly classified PNET was placed with the ependymoma group.

### **LR of PNET v ATRT**

The significance of this question arises as the ATRT group are more aggressive and less susceptible to surgical and oncological treatment with a bleaker prognosis (211-213;219;220). Previous studies of this group have shown that they are radiologically very similar (220) and it wasn't until 1987 (221) that ATRTs were recognised as a separate entity histologically being defined clearly in 1996 (213). PNETs and ATRTs have been separated through immunohistochemical markers and detection of deletions and/or mutations involving the hSNF5/INI1 tumour-suppressor gene in chromosome band 22q11.2 (222-225). It would be expected that they would share a high degree of structural similarity and Rorke et al (213) notes that ATRTs have been frequently

histologically misclassified as PNET “*primarily because 70% of ATRTs contain fields indistinguishable from classic PNETs*” and this point has also been reinforced in other publications (215;226). Previous reports in the literature have used multiple parameters from the clinical history (ATRTs generally present at a younger age), tumour location (ATRTs may involve the cerebello-pontine angle) and imaging findings from T1 – weighted acquisitions with and without gadolinium enhancement (intra-tumoural haemorrhage is more common in ATRTs) (214;227;228). Koral et al (214) made comparisons of ADCs between PNET-MB (a PF tumour) and ATRTs occurring in the PF and although they were able to highlight differences in clinical history, PF location and MRI appearance it was not possible, on ADC grounds, or using all MR sequences and clinical history as a whole to reliably discriminate the tumours.

Our correct classification in 100% (26/26) of cases of PNET and ATRT uses variables of peak height and skewness. ATRTs tend to have a flatter and hence more negatively kurtosed distribution with a much lower peak height as compared to the PNET group and a wider spread of skewness (Figure 4.5) reflected in the slightly lower mean ADC of ATRT compared to PNET.

#### 4.4.1 LIMITATIONS

In common with many single-centre studies of paediatric brain tumours, our cohort is small, reflecting the relative rarity of paediatric brain tumours (approx 3-4 per 100,000 children per year, USA and UK) (229;230). ROIs were drawn on the  $b = 0$  images as these were available for all cases and formed the basis for the initial inclusion in the study. As with many studies attempting to discriminate tumours, there is no standardised method of using ROI analysis and this may allow for contradictory results due to the micro-structural heterogeneity of the tumour through exclusion of such regions in ROI selection. Recently Wang et al (231) semi-automatically subdivided tumours into four regions: central, enhancing, immediate peritumoural and distant peritumoural, using ROIs defined on contrast-enhanced T1-weighted, fluid-attenuated inversion recovery (FLAIR), fractional anisotropy and ADC images. Our approach was simpler to perform and similar to that of Tozer et al (209) although other studies have used gadolinium enhanced T1-weighted images alone (197) or combined with conventional MRI (87) or used the ADC map for ROI placement if a T1-weighted gadolinium enhanced sequence was unavailable. In distinction to these studies and following Tozer et al 2007 (209), we used whole tumour volumes (excluding cysts) and not a region of solid tumour as an ROI.

The statistical analysis used many variables to attempt to classify what is a relatively small data set with initially several different groups. It may be possible with a larger data set to employ data reduction methods such as clustering or principal component analysis in order to determine more readily which variables should be implemented in classification. Although with this data set boosting, through the use of a sequence of classifiers has proved effective. It would also be helpful with a larger data set to use

leave one out analyses in order to perform a quality control on the conclusions drawn in terms of the variables applied to achieve classification.

Clearly a multicentre study is warranted, to fully evaluate ADC histogram diagnoses as a clinical tool, where larger sample sizes, information from other sequences, the clinical history and tumour location could also be evaluated (214). In addition unusual tumours are often radiologically challenging to diagnose making it important to sample significant numbers of rare tumour types in such a study.



#### 4.4.2 CONCLUSION

Whole tumour ADC histograms provide more descriptive information reflecting a more complete coverage of the frequency of occurrence of an ADC value within the lesion. Using LR analysis ADC histogram parameters correctly classified 94% of PF tumour types and differentiated 100% of PNETs from ATRTs, which cannot be reliably differentiated on radiological and clinical grounds (214;232). ADC histograms have the potential to better predict the histological diagnosis of paediatric brain tumours, allowing better pre-operative planning and potentially reducing the need for invasive surgical biopsy. Studies with larger sample sizes, conducted on a multi-centre basis, with the inclusion of other MR data along with ADC histograms are warranted.

---

## 5 POSTERIOR FOSSA TRACTOGRAPHY IN HEALTHY PAEDIATRIC CONTROLS

---

### CONTENTS

---

5.1	Introduction	131
5.1.1	DTI & Tractography in the Paediatric Population.....	131
5.1.2	Age related brain development .....	134
5.1.3	Brain Asymmetry and Handedness.....	135
5.1.4	Objectives .....	138
5.2	Methods	140
5.2.1	Patients.....	140
5.2.2	Determination of Handedness.....	140
5.2.3	MRI Data acquisition.....	141
5.2.4	Tractography Method .....	141
5.2.5	Tractography Thresholds .....	141
5.2.6	Construction of ROIs .....	143
5.2.7	Output of Tract MD, FA & Volume .....	146
5.2.8	Statistical Analysis.....	146
5.3	Results	149
5.3.1	Cerebellar Peduncular Tractography .....	150
5.3.2	Linear Regression of DTI metrics and volume with age.....	151
5.3.3	Cerebellar Peduncular Asymmetry and Handedness.....	154
5.4	Discussion	157
5.4.1	Limitations .....	159
5.4.2	Conclusion .....	161

---

## 5.1 INTRODUCTION

### 5.1.1 DTI & TRACTOGRAPHY IN THE PAEDIATRIC POPULATION

Diffusion tensor imaging (DTI) and fibre tractography have the ability to demonstrate connectivity between regions of the brain not readily appreciable using other imaging techniques (128). Fractional anisotropy (FA) provides a quantitative measure of the micro-architecture of the white matter in vivo (233). Directionally encoded colour maps (97) and three dimensional representations of the white matter structures, tractography, (115;119) have been used to investigate both normal architecture and pathology of the white matter mainly in adults and more recently in children. Specifically conditions such as brain malformations, cerebral ischemia, multiple sclerosis, neurocutaneous syndromes, and brain tumours.

Brain malformations have been investigated looking at potentially aberrant white matter connections and the resultant clinical sequelae such as motor weakness and cognitive dysfunction (128). Their role in the investigation of malformations of cortical development, where the principal abnormalities are thought to be cortical has revealed evidence of abnormal connections both to the affected region and amongst adjacent white matter tracts (234). The evaluation of cortical dysplasia is a significant cause of intractable epilepsy and dysplastic areas can be difficult to detect using conventional imaging modalities, DTI may aid this in demonstrating the abnormal tracts leading to the cortical abnormality (235). Issues still remain to be resolved as a consequence of the limited spatial resolution of the DTI (236;237). Abnormalities of brain development such as seen in Holoprosencephaly (failure of the forebrain to divide into two separate hemispheres), Lissencephaly (236) (Absence of the normal formation of brain convolutions) and Schizencephaly (presence of congenital clefts spanning the cerebral

hemisphere) have been investigated. Abnormal white matter architecture has been demonstrated in the regions showing such abnormalities (238;239). It has also been possible to demonstrate apparently abnormal architecture throughout the brain in regions such as the brain stem and cerebellar peduncles (240;241). The corpus callosum connects homologous regions of the cortex between hemispheres. Congenital abnormalities in its development from agenesis to dysgenesis have shown alterations in the FA of the remaining fibres and tractography revealed abnormal connections. Some reports have indicated that the tractography was more helpful than conventional MRI in determining what connections existed (235) between regions of abnormality.

Idiopathic epilepsy, where cortical abnormalities are occult or undetectable using conventional imaging is being investigated in terms of white matter architectural abnormalities through DTI tractography. Changes in MD the apparent diffusion coefficient (ADC) may provide markers of changes in the white matter than can be used in the neurosurgical evaluation of cryptogenic epilepsy (242). Idiopathic epilepsy patients have also been shown to have aberrant connections between two foci of epileptiform activity in the temporal lobe and the Rolandic fissure (243). A recent publication by Duning et al, 2010 (244) has demonstrated abnormal micro-architecture in individuals with conventional MRI negative partial epilepsy.

The technique's application in the assessment of white matter damage following stroke has been evaluated in order to attempt to determine the possibilities for functional recovery and the utility of neuro-rehabilitation. It has been applied to both perinatal strokes and newborns with cerebral palsy (245;246), where the fall in FA of the corticospinal tracts has been linked to the neuro-motor outcome.

Tumours have been targeted, in order to non-invasively assess the tissue characteristics in terms of pre-operative planning for potentially malignant tumours (243;247). The FA of the tumour core and its cell density (as discussed in Chapter 4) has been associated with the malignancy of the lesion. It is thought that this may also show potential in providing a reliable target for the biopsy of such lesions.

Demyelinating diseases such as paediatric multiple sclerosis (MS) have demonstrated altered FA and apparent diffusion coefficients in what appears to be both abnormal and normal appearing white matter on conventional MR imaging (248). These changes have been an avenue in the neuroradiological assessment of disease evolution and treatment response.

Neurocutaneous syndromes such as Neurofibromatosis (249) and Tuberose sclerosis (250) demonstrate MD increases and diminution of the FA in the white matter of sufferers as compared to healthy volunteers.

Looking specifically at the posterior fossa, Salamon et al, 2007 (251) applied DTI colour maps and selective tractography (FA threshold 0.25, angular threshold less than 70°, ROIs chosen on the DTI images, no further information given) to investigate the structure (251) of the cerebellum and its connections in 24 normal subjects, in comparison to that evident on myelin stained brain sections. They were able to localise the positions of the dentate and emboliform nuclei by the location of the connecting fibres running through the peduncles, specifically the inferior, middle and superior cerebellar peduncles. They found that more anteriorly the components were mixed with afferent white matter projections following the middle cerebellar peduncle. It was also possible to visualise the white matter fibres passing through the vermis and connecting the two hemispheres. DTI tractography appeared to compliment the anatomical

information obtained from other conventional imaging modalities used to map the brain structure and they postulated it as being a future avenue in the assessment of cerebellar ataxias and congenital disorders of the cerebellum and brain stem.

Studies of DTI in the case of posterior fossa pathology have been undertaken, Widjaja et al 2006 (252) used DTI tractography to examine posterior fossa midline malformations where colour vector maps of FA were initially used in order to locate the region of interest for the tractography. This study demonstrated that in certain developmental disorders (Joubert Syndrome, rhomboencephalosynapsis) the cerebellar vermis was abnormal and that the superior cerebellar peduncles failed to decussate in the mid brain and the deep nuclei were more laterally placed.

### 5.1.2 AGE RELATED BRAIN DEVELOPMENT

In conducting a study into the white matter architecture of the brain in a paediatric population consideration has to be given to the effects of growth and inherently, to the age of the subjects under investigation. In terms of the increase in size of the brain with age, pathological post-mortem research has shown that there is generally a rapid increase in brain size until about two years after which the increase in volume is of the order of 10 to 15 percent until around age 18 (253). The changes in the white matter with development have also been investigated using diffusion metrics such as MD and FA. Saskena et al in 2008 (254) demonstrated in cerebral white matter of 21 neurologically normal children a sharp increase in FA up to 24 months and then a gradual increase to 132 months. The cerebellar white matter FA increased sharply up to 36 months and then the increase became more gradual. Measurements of MD decreased sharply in cerebral white matter up to 24 months and again were more gradual

following that. In the cerebellar white matter, an initial decrease up to 6 months was followed by a stable pattern to adulthood. Specifically in our study we were interested in the cerebellar white matter changes.

### 5.1.3 BRAIN ASYMMETRY AND HANDEDNESS

Laterality of brain function has been extensively investigated and many methods of determination of laterality or dominance tested. In general terms this relates to laterality of language function and may be determined by use of a Wada test, involving the selective anaesthesia of a specific brain hemisphere and subsequent assessment of which tasks are still possible with the functioning hemisphere. Alternatively the use of functional MRI has revealed evidence of laterality of function. Handedness is related to brain laterality in providing an indication of the dominant hemisphere where 95 to 98 % of right handed individuals are left hemisphere dominant and approximately 50% of left handed individuals are right hemisphere dominant. There exists debate as to whether handedness is as simple as left or right or both (ambidextrous) or actually represents a continuum (255). In terms of handedness distribution in the population a recent study by McManus indicated approximately 13% left handedness (256). The incidence of atypical right hemisphere language dominance in left handed individuals has led to suspicion of a systematic association between handedness and language dominance in healthy subjects. A study by Knecht et al in 2000 found the incidence of right-hemisphere language dominance increased linearly with the degree of left-handedness (257). The evidence of a dominant hemisphere has led to questions about structural asymmetry.

Gross studies of structural brain asymmetry have focused on sylvian fissure morphology due to its relation to motor function, hypothesising its development may be affected by

hand dominance (258). Its asymmetry in men and women has been studied by Wietlsen et al, 1992 (258) revealing bilateral differences in relation to handedness in men. The post-mortem study of 67 brain specimens from individuals who had previously had detailed hand preference assessments, revealed that the asymmetry existed between those that had a strong hand preference for the right and those that did not. There was in fact a bilateral morphology change in terms of the length and point at which the sylvian fissure changed direction which was diminished in those without a strong hand preference, there was no clear left right asymmetry detected.

In the cerebellum, functional asymmetry is thought to be a special characteristic of cerebellar functional organization and the cerebro-cerebellar circuitry that underlies task performance. Imaging studies using multiple modalities have demonstrated cerebellar functional asymmetry to have a relatively complex pattern and correlations may exist with practice or some neurological disorders (259). Functional laterality using functional MRI and positron emission tomography has shown ipsilateral asymmetry / laterality in the case of simple and complex motor cognitive functions (260).

In terms of structural asymmetry however, efforts have concentrated on stereoscopic assessments of the volume and have divided it into four quadrants. The evidence has pointed towards a torsional asymmetry.

Snyder et al in 1994 (261) delineated sub-regions within the cerebellum, specifically left and right divided into anterior and posterior segments. They compared 15 right handed and 8 non right handed individuals. The results indicated that for the right handed individuals the right anterior segment had a larger volume than the left. When considering the posterior segment for the right handed individuals the left posterior



segment was larger in volume than the right. They demonstrated a significant handedness effect in asymmetry or cerebellar torque when right handed as to when not.

A study by Szesko et al, 2003 (262) has shown evidence that the cerebellar asymmetry or torque reported in normal subjects is apparently reversed with patients presenting with first episode schizophrenia and postulated that this may represent some aberrant neuro-developmental process.

The paediatric population presents further challenges in investigation of laterality of function and structure, in relation to the effects of development at the age at which handedness is determined. There exists variation in this as there exists with rates of childhood development. The issue of mixed and left-handed development is itself an increasingly important aspect of research into hand dominance (256;263). Children develop at different rates, consequently may show no strong preference, in terms of writing, for one hand over the other even by the age of 5. In left-handers, it is reportedly not uncommon for this preference to be delayed until as late as the age of 7. Conversely some reports indicate that in some individuals it may be determined from as early as 2 (264).

Schooling may also have an effect; the National Curriculum provides writing skills tuition from the age of five, or earlier and this may force a premature decision in some individuals. This leads to all children being urged to choose a hand for writing from this age. There does exist the possibility that they initially start writing with one hand only subsequently to switch to the other as fine motor skills and hand-eye co-ordination develop (256;263). Current research seems to point to a genetic determinant of handedness (256) and forcing an individual to one or other side may confound the

developmental changes potentially seen in the white matter, although this may again be dependent on the plasticity of any of the white matter changes.

Many methods of testing for handedness exist; questionnaires either answered by the individual themselves or by the parents have been used (255). Validity of this method is open to debate; results may depend upon the number and depth of questioning. Other more detailed neuropsychological or behavioural assessments are undertaken with respect to the performance of specific skills in order to determine hand dominance but are beyond the scope of this work. Simple self reported handedness is considered to be unreliable in children as individuals may use different hands for different activities (255;256). In order to determine handedness Sattler (264) suggests the use of task related questions, such as which hand to brush teeth, throw a ball, hold a knife etc to draw conclusions; this was the simple method adopted in the assessments of the author. Debate over classification of results of testing remains with respect to the possibility of a spectrum and typically individuals that are left handed are not as strongly lateralised in terms of function as right handed individuals.

#### 5.1.4 OBJECTIVES

Initially to establish the threshold values that allowed the best reconstructions of the cerebellar peduncular white matter in a healthy normal paediatric population. In so doing to determine a method for the drawing of the regions of interest (ROIs) necessary for the reconstructions.

To visually assess the tractography reconstructions in terms of anatomical plausibility in comparison to established anatomy and in comparison to previously published work on tractography in the posterior fossa.

Subsequent to tract reconstructions the intention was to calculate quantitative measurements of diffusion (MD and FA) as well as tract volume in order to establish if a relationship existed with the age of the subjects studied.

Through the use of MD, FA and tract volume, the presence or absence of asymmetry of the cerebellar peduncular white matter was to be assessed.

## 5.2 METHODS

### 5.2.1 PATIENTS

Data was collected throughout 2006 and was contemporaneous to the collection of the posterior fossa data analysed in chapter 6; it was collected by Dr Kate Riney as a control group for an epilepsy project. All cases were healthy children, typically siblings of patients being investigated with epilepsy, any individuals with other possible pathology were excluded. The collection of this data had been approved by the local research ethics committee.

### 5.2.2 DETERMINATION OF HANDEDNESS

All 18 individuals or parents, where appropriate, were questioned either in person or via a telephone interview at the end of the study. All the individuals studied were over 7 years and in full time schooling at the time of scanning. A series of questions adapted from those suggested by Sattler (264) were used to determine handedness. As the information was collected after the imaging and over the phone a lengthy questionnaire was not appropriate. An aggregate score was recorded and the preference hand for the majority of activities determined whether the individual was left handed, right handed or ambidextrous.

Specifically questions were; which hand do you usually or prefer to: switch on/off lights, brush teeth, comb hair, hold a knife, use a tool (e.g. a hammer), throw a dice, pick up/count things, open window/door, throw a ball etc, draw ,paint, write.

### 5.2.3 MRI DATA ACQUISITION

The MRI data acquisition is common to all the tractography data analysed in this thesis and is described in Chapter 3.1.3 and shown specifically as the 1<sup>st</sup> and 2<sup>nd</sup> sequences in Table 3.1.

### 5.2.4 TRACTOGRAPHY METHOD

The tractography method employed is as described in Chapter 3, sections 3.3 – 3.5. The tensor was diagonalised and the MD and FA of each voxel calculated. Analysis proceeded through calculation of whole brain streamline tractography for all 17 cases; using the programs developed by Dr Tom Barrick in the “C” programming language and utilised the methods initially described by Basser et al (120).

The tractography algorithm required the determination of a continuous estimation of the diffusion tensor field based on the individual voxel measurements. This was achieved by linear interpolation of the tensor field as described in Chapter 3 (265).

### 5.2.5 TRACTOGRAPHY THRESHOLDS

The tractography program allowed the determination of several parameters in order to better reconstruct the pathways. The FA threshold was set at 0.3 for all the data analysed based on previous experiments; producing reconstructions which excluded tracts that were aberrant or not of interest whilst maintaining those that were of interest. In figure 5.1 the relaxation of the FA threshold from 0.4, allows the inclusion of the red fibres which are crossing pontine fibres and then further relaxation allows the inclusion of the blue fibres travelling superior-inferiorly which likely represent corticospinal fibres. The effect being that where the calculated FA of the interpolated tensor field was less than 0.3, tracking would be terminated. The threshold we used sufficiently

relaxed the FA threshold for termination of tracking to allow, on visual inspection, inclusion of the cerebellar peduncular white matter (the green fibres passing antero-posteriorly) as well as a small amount of the crossing pontine fibres whilst excluding extraneous pathways such as blue vertically orientated fibres. Figure 5.1, shows tract reconstructions using the directionally encoded colour convention (97) which are superimposed on FA maps of the posterior fossa. The same ROI is used at differing levels of FA threshold.

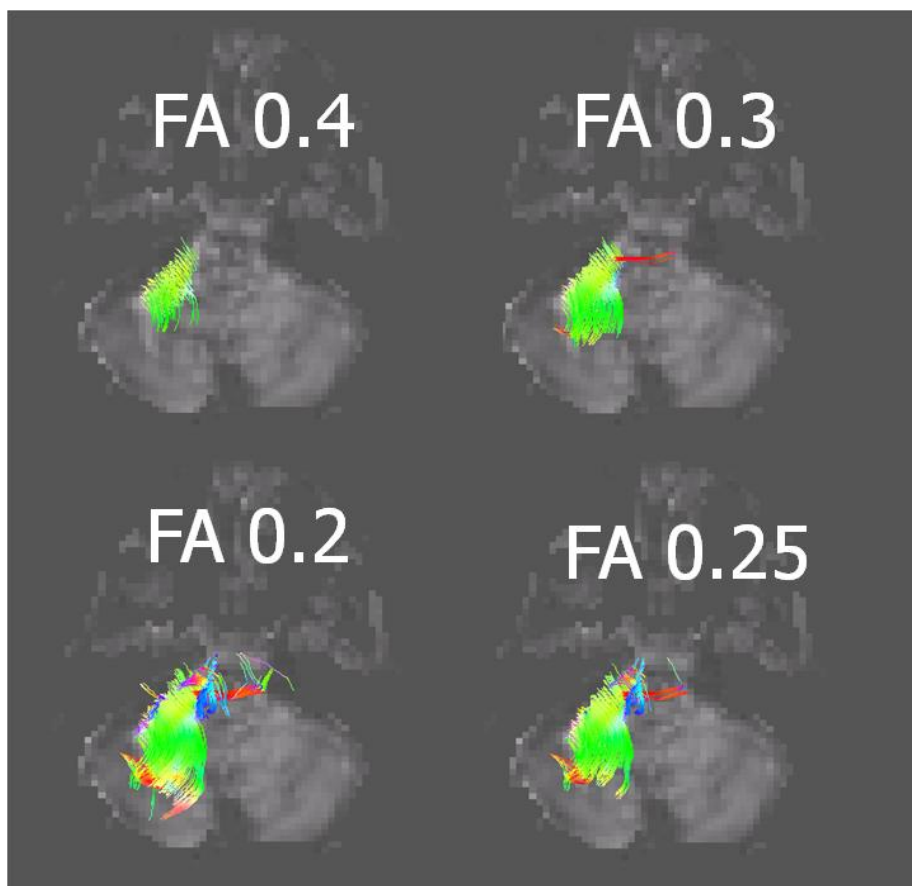


**Fig. 5.1 Effect of Changing FA threshold on tract reconstruction**

The vector step length was set at 1mm, such that whilst streamline tractography was initiated at the centre of all voxels throughout the whole brain, it would step forward or backwards at 1mm intervals such that it was able to sample at any point within a voxel. In this project the voxels were isotropic and  $2.5\text{mm}^3$ , hence the principal eigenvector

could be calculated at a subvoxel level. Subsequently the streamline would be advanced a further 1mm within the image and the principal eigenvector recalculated. The choice of step length was based on previous tractography experiments in our group.

It was possible to specify an angle of termination at which point the tracking would cease. Tracing would proceed initially in one direction from the start point and when terminated would recommence at the original start point but proceed in the opposite direction. The angle of termination chosen was  $90^\circ$ , in effect removing the angle of the subsequent eigenvector as a termination threshold. This was based on previous tractography experiments. This work had been undertaken by previous researchers in our unit and repeated by the author in an exploratory fashion in order to determine the least restrictive parameters to allow reconstructions

#### 5.2.6 CONSTRUCTION OF ROIS

The MD and FA maps were transferred to a Dell work station and using mriCro (175), regions of interest were drawn on the FA maps. Three dimensional ROIs corresponding to the predicted anatomical location of the tracts to be studied were drawn by the author in order to localise structures of interest.

Initial experiments to determine locations of ROIs utilised low resolution tracking for rapid assessment and then high resolution once the tracking from the selected ROI location appeared anatomically feasible. The low resolution method used a checkerboard approach, seeding was initiated from every other voxel where as the high resolution tracking initiated from every voxel in the image, the effect being to reduce the time taken for image analysis. Image analysis of the healthy control group was all performed using the high resolution technique. The ROIs were selected in the likely anatomical location of the cerebellar peduncular white matter and in common with the

FA threshold, the final areas chosen were those that gave the most complete reconstruction of the tracts of interest, as per the method of Clark et al 2003 (178).

The ROI acted as a selection region; where the seed voxel produced tracts that passed through the region of interest they were retained. Several methods were attempted in the initial analysis in order to determine the best reconstructions, the provision of exclusion ROIs or a second ROI was deemed not helpful.

In the analysis performed, the author was blinded to the cases in terms of handedness and drew ROI's on the regions thought to represent the cerebellar peduncular white matter region, specifically over the bright (high FA) regions lateral to the fourth ventricle of the posterior fossa. ROIs were drawn on either side for each individual case. This process was performed sequentially for each case and alternating between the left and right sides. When drawing the ROIs the author attempted to ensure that the volumes of the ROI's drawn on the image appeared visually similar. This process was then subsequently repeated for the same data in order at a later date. The result was the generation of four ROIs for each subject; two on the left and two on the right. An example of left and right ROIs drawn on a dataset are shown in Figure 5.2, below.



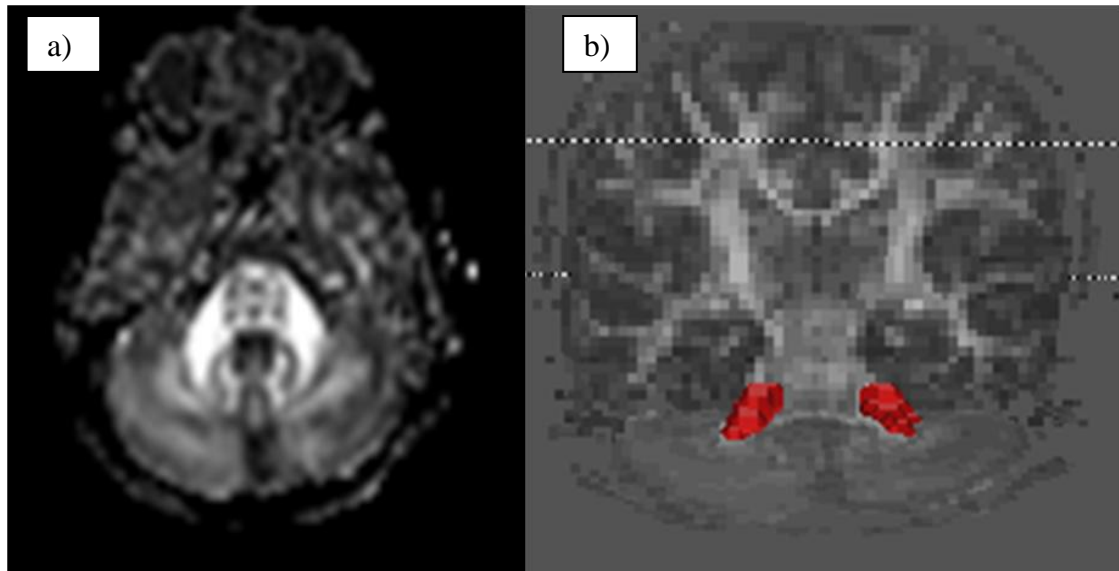


**Figure 5.2 ROIs superimposed onto the FA image (Geomview). a) High FA region adjacent to low signal IV<sup>th</sup> ventricle used as ROI. b) ROIs represented as red regions superimposed onto the FA axial and coronal slices.**

---

### 5.2.7 OUTPUT OF TRACT MD, FA & VOLUME

Following the construction of the ROIs, the ROI files were transferred to a UNIX workstation in order to produce the tract images. Tract reconstructions were visualised using “*GeomView*” (266) superimposed onto the  $b = 0$  s  $\text{mm}^{-2}$  image, in order to determine anatomical plausibility. As the FA threshold and the chosen approximate ROIs had been tested on alternative data prior to this group’s analysis, to optimise the reconstruction, it did not prove necessary to redraw the ROIs on the grounds of anatomical plausibility.

Following visual assessment of tract output, the reconstruction data was processed to calculate the volume of the tracts. Calculations were on a subvoxel basis, only the actual volume of the tract rather than the total volume of all the voxels it passed through were counted. Average FA and MD of the tract were calculated and all data were entered into excel spreadsheets (Excel 2007).

The time taken to draw the ROIs for each individual patient (left and right single cases) was approximately 5 minutes. The computational process required approximately 15 minutes for each individual case, the speed was much enhanced through the use of batch files, written by the author, in order to process multiple cases from a single command.

### 5.2.8 STATISTICAL ANALYSIS

The numerical data from an individual case comprised data for the three metrics MD, FA and sub-voxel volume. For each metric there were two individual observations for the left and two for the right. Two ROIs were used on each side in order to create replicates using the same ROI selection criteria. The two replicates were averaged for each right sided metric and each left sided metric. There were a total of 6 measurements

for each case (MD\_left, FA\_left, SV volume\_left and MD\_right, FA\_right, SV Volume\_right). All analyses were performed using SPSS for Windows (Ver. 14. 2006. Chicago: SPSS Inc.). The single left hand case did not provide sufficient information to permit an analysis allowing for left – right difference. The single case was therefore removed.

A number of linear regression analyses were performed with age as the explanatory variable and with one of the following as the dependent variable: MD, FA and sub voxel (SV) volume for both left and right sides. Regression analyses were also performed using the left-right averaged values of the three parameters (MD, FA and SV volume).

In order to circumvent some of the problems associated with repeated measures analyses we proceeded as follows:

Using individual values for each case; the structural asymmetry of the cerebellar peduncular white matter between right and left tracts was calculated for the independent measures MD, FA and SV volume. The calculation is illustrated in the equation below where “*Diff\_Stat*” refers to the scalar measure of asymmetry.

$$Diff\ Stat\ FA = \frac{(FA_R - FA_L)}{(FA_R + FA_L)}$$

This scalar measure ranges from -1 to +1 where positive values indicate asymmetry towards the right side and negative values indicate asymmetry towards the left side, a value of 0 indicates an absence of asymmetry for that case.

The data from the asymmetry scale were investigated, using a one sample *t* - test, to evaluate whether the difference in the means was equal to zero. As the study was an

exploratory one and was hypothesis generating rather than testing formal multiple comparisons analysis was not undertaken.

### 5.3 RESULTS

In total 18 cases were initially included in the group as detailed in Table 5.1. In the process of statistical evaluation the single left handed case was excluded from the analysis as constituting inadequate sample size.

The mean age of the seventeen right handed cases was 11.1 years with a range of 7.1 to 17.9, there were 10 males and 7 females.

Case	Sex	Age (Yrs)	Handedness
101	M	10.2	R
102	F	7.3	R
103	F	11.8	R
104	F	10.3	R
105	F	7.1	R
106	F	13.7	R
107	M	10.9	R
108	F	11.5	R
109	M	9.05	R
110	M	14.4	R
111	M	17.4	R
112	M	15.6	R
113	M	10.5	R
<del>114</del>	<del>F</del>	<del>8.9</del>	<del>L</del>
115	F	10.6	R
116	M	8.6	R
117	M	16.4	R
118	M	17.9	R

**Table 5.1 Demographics of healthy cases.**

(M = male, F = female, R = right, L = left. Excluded case scored through)

### 5.3.1 CEREBELLAR PEDUNCULAR TRACTOGRAPHY

In the initial investigations the FA threshold and the ROI construction method were determined. We demonstrated that using an FA of 0.3 and including the regions of high FA lateral to the IV<sup>th</sup> ventricle of the posterior fossa, it was possible to construct anatomically plausible images of the cerebellar peduncular white matter. In addition, on relaxing the FA threshold it was possible to reconstruct fibres connecting into the brain stem. An image of such reconstructions is seen in Figure 5.3, where the directional scheme of Pajevic et al (97) is used. The blue fibres represent those travelling cranio-caudally, possibly descending motor fibres or ascending sensory fibres; the red fibres likely matching the trajectory of the transverse pontine fibres seen at this level in the brainstem.

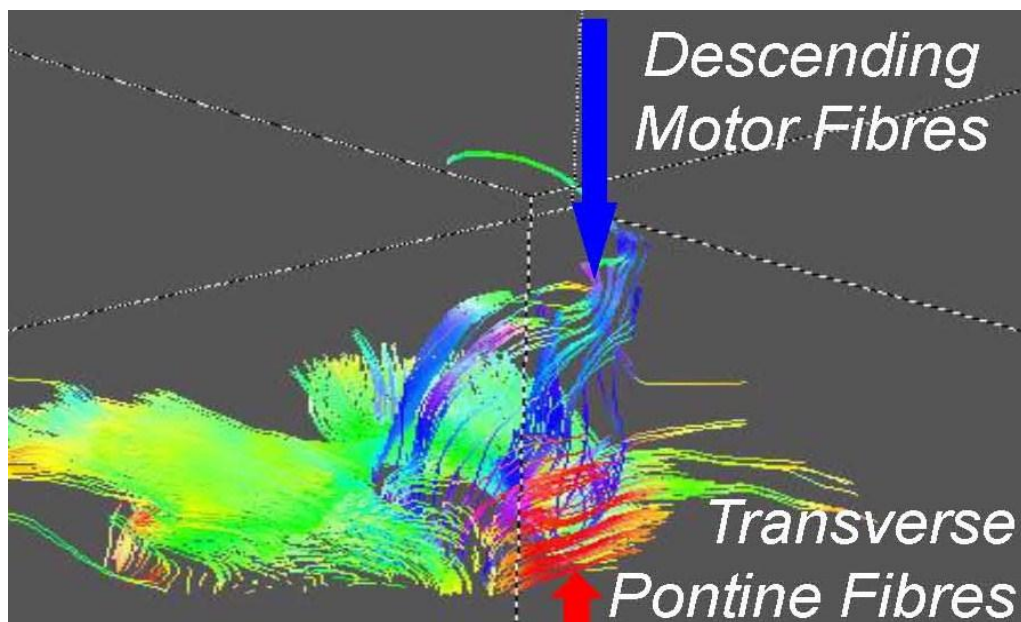


**Figure 5.3 Tractography reconstructions of posterior fossa structures**

In addition to the FA threshold effects, the selection of the ROIs was important in the determination of the reconstructions of the posterior fossa structures. Reconstruction of

the tracts without the inclusion of any of the midline structures was sought by determination of the best method for drawing the ROI prior to the analysis of this data set.

### 5.3.2 LINEAR REGRESSION OF DTI METRICS AND VOLUME WITH AGE

Scatter plots of age as the factor and the SV volume, average FA and average MD as the variable were produced. On visual inspection there does not appear to be a marked dependence on age (Below Figures 5.4 - 5.6). The single outlying value on the FA scatter plot was investigated in terms of visual inspection of the tractography reconstruction and ROIs chosen but no obvious cause could be discerned.

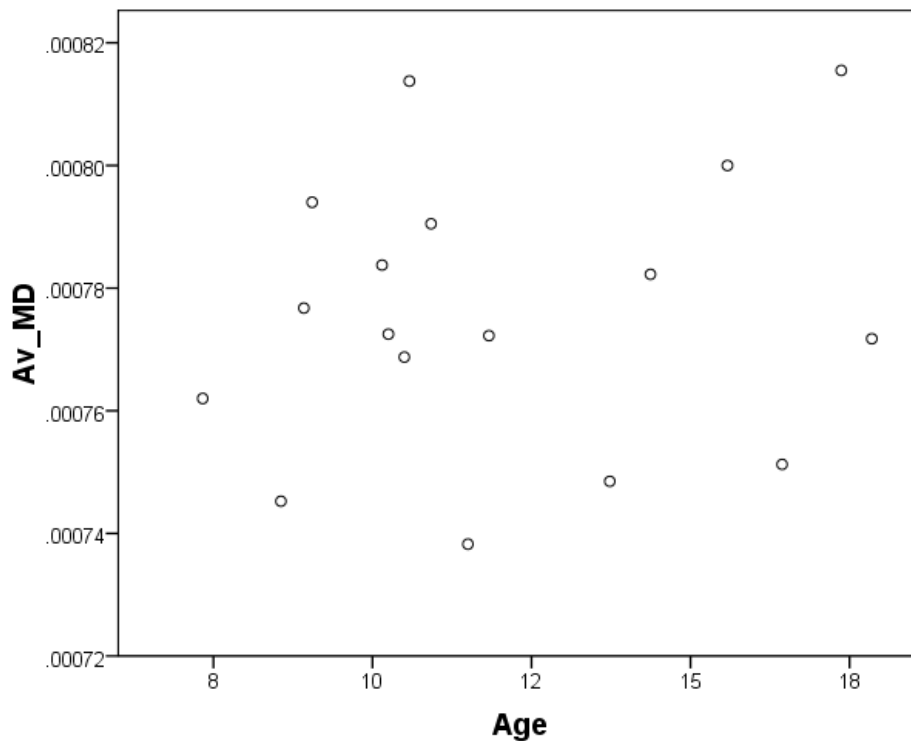


**Figure 5.4 Scatter plot of Age versus average MD (Av\_MD). (s mm<sup>-2</sup>)**

---

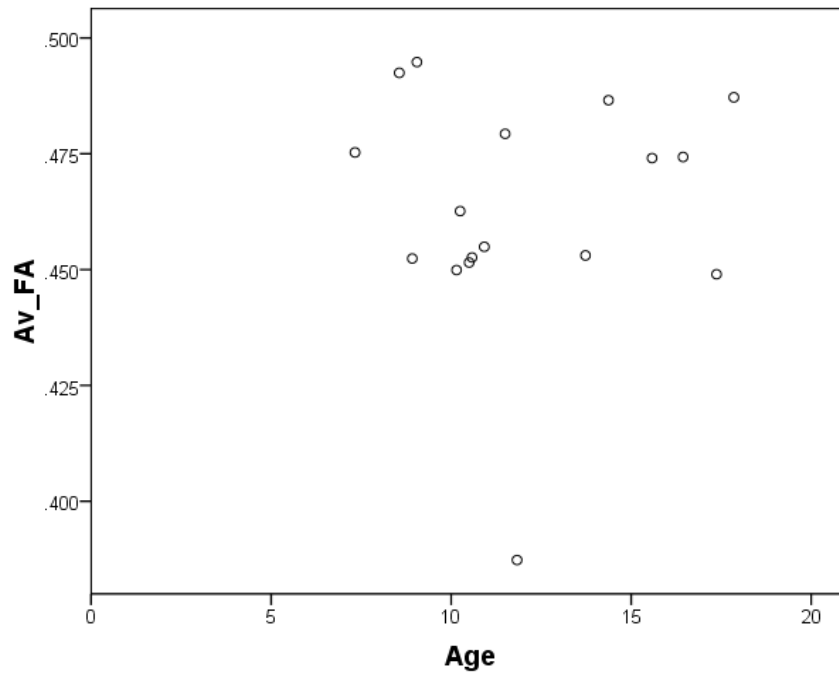


**Figure 5.5 Scatter plot of Age versus average FA (Av\_FA).**

---

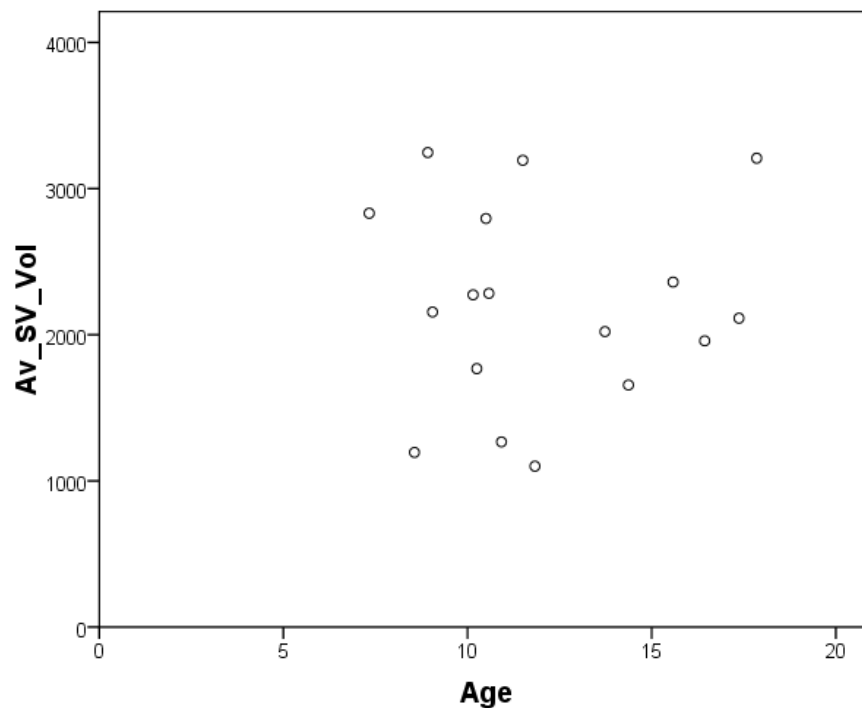


**Figure 5.6 Scatter plot of Age versus average sub-voxel volume (Av\_SV\_Vol), volume in mm<sup>3</sup>.**

---

Linear regression analyses of the left-right averaged values for MD, FA and SV volume were undertaken and similarly for the individual values of the left and right values for



the same parameters using age as the explanatory variable. The results of these analyses are shown in table 5.2.

Explanatory Variable	Dependant Variable	p-value	Significant at $p < 0.05$
Age	MD_Left	0.541	N/S
Age	MD_Right	0.183	N/S
Age	FA_Left	0.88	N/S
Age	FA_Right	0.918	N/S
Age	SV_Vol_Left	0.889	N/S
Age	SV_Vol_Right	0.942	N/S
Age	Av_MD	0.515	N/S
Age	Av_FA	0.897	N/S
Age	Av_SV_Vol	0.91	N/S

Av = average, SV\_Vol = sub voxel volume, N/S = not significant.

**Table 5.2 Linear Regression p-value results; age versus MD, FA and sub-voxel volume**

---

At the  $p < 0.05$  level the p-value result did not indicate a significant relationship between age of the subjects and the parameters of MD, FA and SV volume of the tracts for this group of healthy subjects.

### 5.3.3 CEREBELLAR PEDUNCULAR ASYMMETRY AND HANDEDNESS

The descriptive statistics mean and standard deviation for the measure of right to left asymmetry (Diff\_Stat) for the MD, FA and SV volume are shown in Table 5.3.

	N	Minimum	Maximum	Mean	Std. Deviation
Diff_Stat_MD	17	-.0507	.0323	.0034	.0187
Diff_Stat_FA	17	-.0140	.0346	.0084	.0145
Diff_Stat_SV_Vol	17	-.1326	.3837	.0692	.123

**Table 5.3 Descriptives of asymmetry measures for MD, FA & SV volume**

Histograms of the range of values for the asymmetry measures are shown in Figure 5.7 to 5.9 using only the seventeen right handed subjects.

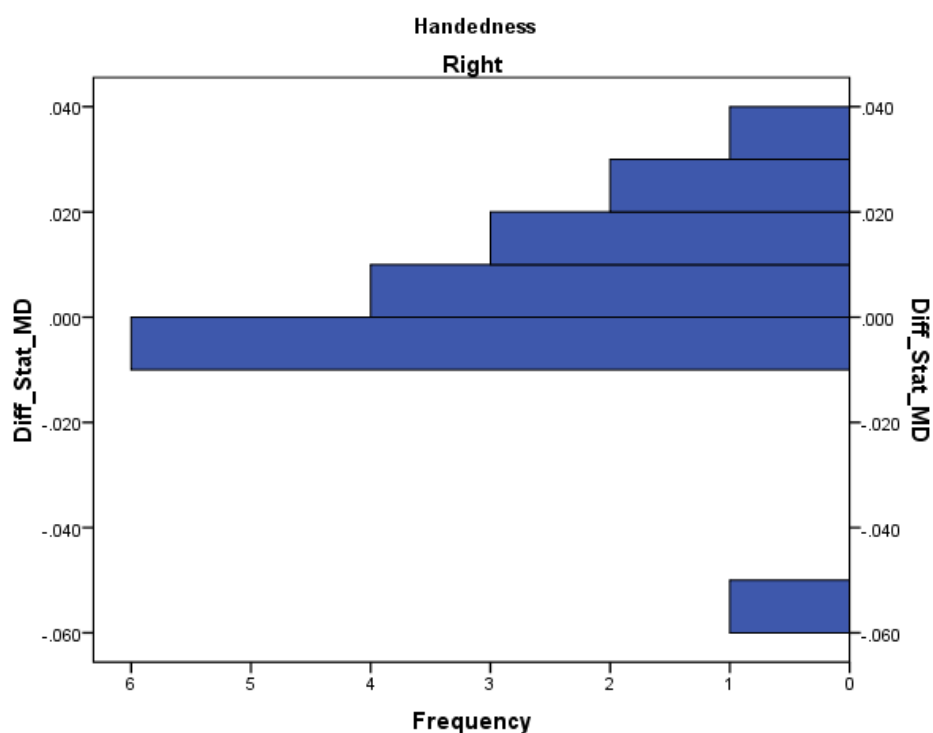


**Figure 5.7 Histogram of right-left asymmetry of MD (right handed subjects)**

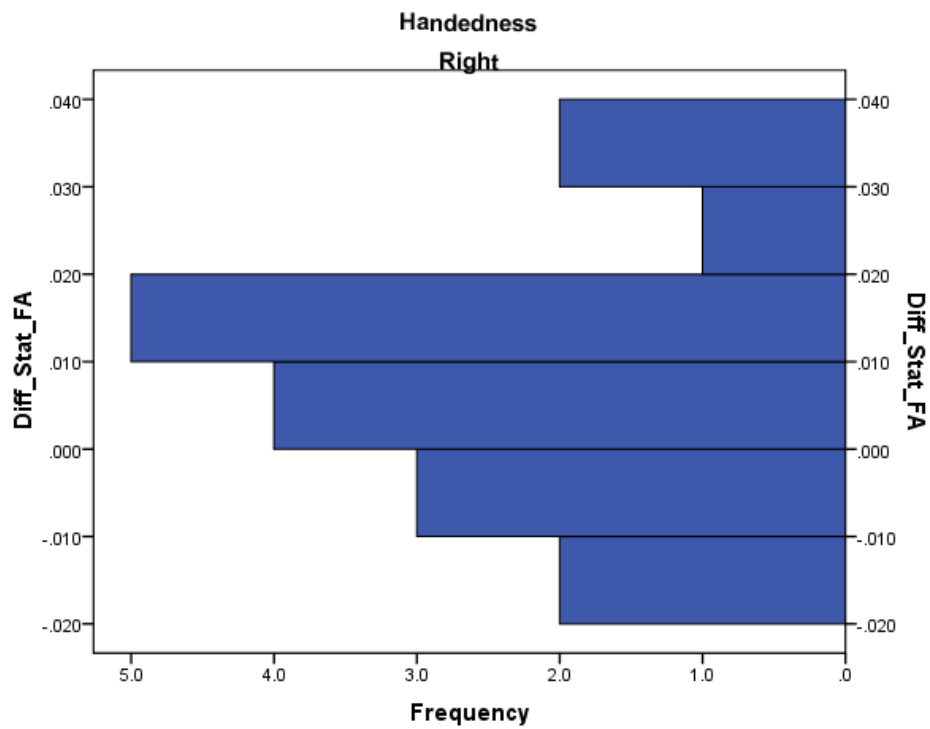


**Figure 5.8 Histogram of right-left asymmetry of FA (right handed subjects)**

---

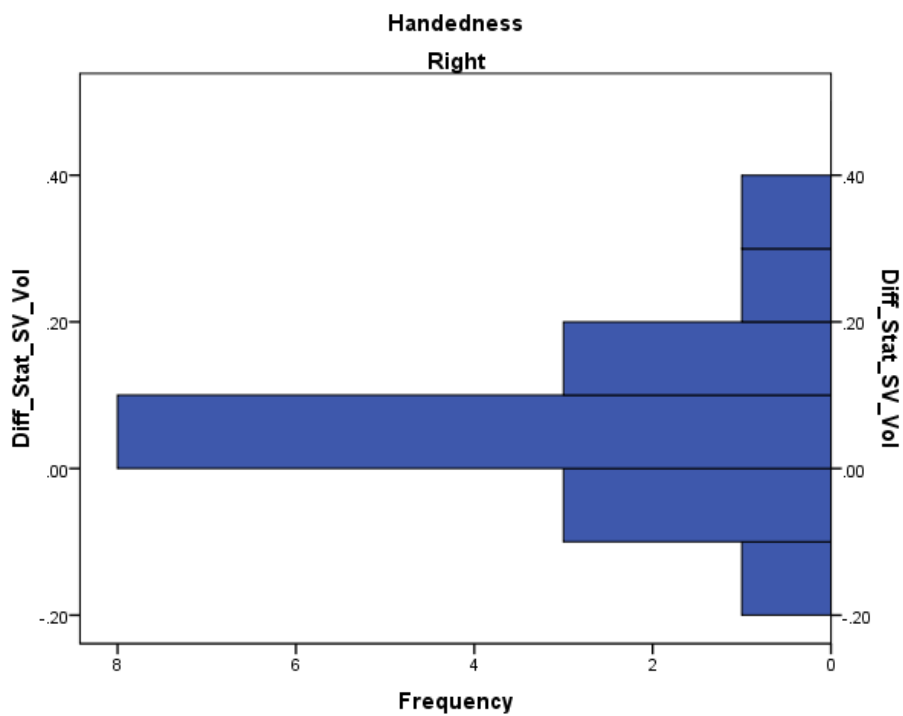


**Figure 5.9 Histogram of right-left asymmetry of sub voxel (SV) volume (right handed subjects)**

---

The asymmetry measures of the MD, FA and SV volume were investigated using a one sample *t*-test and the results with the *p* – values are tabulated below.

	t	Sig. (2-tailed)	Mean Difference	95% Confidence Interval of the Difference	
				Lower	Upper
Diff_Stat_MD	.747	N/S	.00339	-.00623	.01302
Diff_Stat_FA	2.390	.030	.00841	.00095	.01587
Diff_Stat_SV_Vol	2.318	.034	.06915	.00591	.13240

**Table 5.4 One sample *t* - test for asymmetry measures (Diff\_Stat)**  
 (*p* values significant (Sig) at the < 0.05 level).

---

The asymmetry measure (Diff\_Stat\_) is statistically significant for the FA and sub voxel volume measures, at the  $p < 0.05$  level (Table 5.4). From review of the descriptive data in Table 5.3 the inference is drawn for a positive difference indicating the right SV volume and FA are significantly greater than the left.

## 5.4 DISCUSSION

The ability to visualise the white matter tracts of the cerebellar peduncles in normal subjects was a prerequisite to investigating any changes seen in the pathological posterior fossa (PF) population discussed in Chapter 6. The algorithm's threshold values, best enabling anatomically plausible reconstructions of the PF tracts, were established. Results were consistent with the work in the adult population of Salamon et al (251). The FA threshold of 0.3 was higher than that of Salamon et al (0.25) and was without an angle termination threshold ( $70^\circ$  in the quoted work). In this process, appreciation of the anatomical location for placement of ROIs to reconstruct the white matter of the cerebellar peduncles was refined. The peduncular white matter was not subdivided into the three component groups as Salamon et al had done, although they do not clarify how they had chosen their ROIs. In this work the relatively bright regions (high FA) immediately lateral to the IV<sup>th</sup> ventricle of the PF enabled a reliable reconstruction with limited user interaction; the region had been established through experiment.

The work in this paediatric population highlighted the inability of the tractography reconstructions of the peduncles to reach to the cortex. A similar phenomenon was seen in the adult population as discussed by Salamon et al (251); it is thought that this may relate to the intervening deep cerebellar nuclei. Visual assessment of the anatomical plausibility of the tractography reconstructions with established neuro-anatomy and previously published tractography images showed the reconstructions to be similar (251).

Quantitative data was evaluated from the reconstructions of the peduncular white matter in the form of MD, FA and sub voxel volume of the tracts. It was possible to do this in all cases.

To investigate the validity of these values as measures for anatomical asymmetry a potential confounder in terms of age related changes was explored. Previous work in the paediatric population (139) has suggested that the majority of changes in white matter DTI metrics (FA and MD) occur within the first 24-36 months for FA and first 6 months for MD. In linear regression analysis of the values of mean MD, FA and sub voxel volume no significant relationship was established between the metrics and the age of the subject. This was consistent with current literature in the context of the population demographics we were investigating; the age range being from 7.1 to 17.9 years for the 17 subjects.

In assessing anatomical asymmetry of the peduncular white matter we utilised a measure of right to left asymmetry. The results of the 17 right handed individuals highlighted a statistically significant difference in the sub voxel volume and the FA values with the inference from the descriptives that the right sided tract reconstructions were larger volume and had higher FA than the left. To our knowledge this is a new finding. There was no statistically significant change in MD.

Evidence from functional and PET MRI studies have indicated a complex pattern of lateralisation or asymmetry of tasks in the cerebellum (259) and have also suggested an ipsilateral lateralisation of simple and complex motor tasks (260). It may be expected that if such ipsilateral asymmetry exists, individuals who have a strong hand preference may also have a relatively larger ipsilateral white matter volume and coherency of directionality and density, reflected in an increase in FA. This may be as a consequence

of the effects of learning and neural plasticity and has been demonstrated in internal capsule white matter of musicians (267).

Previous reports looking at volumetric analysis (stereoscopy) of the cerebellum and hand preference by Snyder et al 1996 (261), demonstrated a cerebellar torque effect where the right anterior and left posterior segments of the cerebellar hemispheres were enlarged in individuals who were right handed as compared to those who were not. This larger right anterior segment volume may be reflected in the right side cerebellar peduncular white matter having a greater volume asymmetry and higher FA on tractography and DTI metrics. Our tracking did not appear to extend past the deep nuclei into the posterior aspects of the cerebellum (See Figure 5.3); hence it was not possible to explore this phenomenon of cerebellar torque through examination of the posterior segments of the hemispheres.

#### 5.4.1 LIMITATIONS

In the tracking algorithm we used a relatively high FA threshold in keeping with other work. (251;267-270). This runs the risk of removing related white matter fibres in the attempt to also exclude aberrant tracks. The failure to track to the cerebellar cortex is also seen in adult work and may require the use of further ROIs but this is beyond the scope of this work.

The drawing of the ROIs by the author is potentially subject to bias and requires a degree of user interaction as has been found in previously published adult work (268;270-272). It is possible to question the operator's expectation of the right side tracts being relatively larger and denser and that this could be achieved through using deliberately larger ROIs. In response to this, if the region of interest were to be drawn deliberately larger; the risk is that the density and coherence of the tracts would be

reduced and hence the FA may fall to a value below the chosen threshold FA value. This was not the case in this analysis. Further more in drawing the ROIs by using an opacification technique (overlaying the ROI on the FA image) and selecting out the brightest voxels in the likely location, the remaining voxels appear relatively brighter. Such problems have been highlighted previously and are an inherent problem in the use of subjective ROIs. Whilst formal reproducibility testing of ROI's was not undertaken; the author averaged two temporally separate instances of the ROI's construction using the same construction parameters. Formal reproducibility testing would be helpful in order to ascertain the utility of the method for clinical practice, perhaps through the use of other investigators drawing ROIs or an automated system based on FA parameters and anatomical location.

The collection of the handedness data was not done contemporaneously, however all children were over the age of 7 years at the time of scanning, a point by which evidence suggests handedness has been determined (256;264). The handedness data was collected at most 10 months after the imaging had been undertaken.

The method of determining the handedness was necessarily shorter than the more in depth neuropsychological assessments. It would be worth repeating the study implementing a more robust assessment of handedness using, for example, the Crovitz scale (273) which rates which hand subjects use for many more everyday activities and answers are converted to a scale where the score determines the degree of lateralisation. There is also an account taken of the effect of education and environment favouring the use of the right hand more generally.

The small numbers used here are comparable to other published work (261) but indicate that a future study utilising a similar technique with a larger population and specifically



more non-dextral individuals (the technique of comparison in Snyder et al 1995) would be of interest. It would be of particular interest to assess cerebellar asymmetry to determine if the differences are reversed in non-dextral individuals, although this may not be the case, as mentioned earlier non-dextral individuals are frequently not as lateralised in hand function as the dextral individuals. In this analysis, a single left handed individual was considered statistically unreliable to include as a single alternative case, it is of note that the left handed case fell within the distribution of the right handed cases. It is possible that the asymmetry demonstrated may be coincidental and unrelated to hand dominance, in the context of the literature available however, it remains an important area for exploration.

#### 5.4.2 CONCLUSION

The work has defined a method to select a region of interest from which it is possible to reconstruct visually plausible cerebellar peduncular white matter tracts. Drawing of the ROI requires a relatively short period of time (approximately 2-3 minutes) now that its characteristics are defined. To our knowledge this is the first investigation of cerebellar structure in the healthy paediatric population.

These tract reconstructions have enabled the extraction of quantitative, rather than simply visual, data. MD, FA and sub voxel volume when analysed on an average basis or as separate right and left measures did not show a significant relationship with age in this population. In addition, within the auspices of the discrimination of handedness used in this study it has been possible to demonstrate a statistically significant relationship of increased FA and sub voxel volume of the reconstructed cerebellar white matter on the right side of the subject with a right hand preference.

Using the ROI method defined and in light of this exploratory study, the data suggests that formal hypothesis testing with a new and larger group of subjects analysed through a more rigorous hand dominance tool (possibly using a scale of dominance) warrants further investigation. The possibility exists of the application of this technique in assessment of paediatric patients with posterior fossa pathology. Demonstration of quantitative changes in cerebellar peduncular white matter from healthy to pathological subjects could determine whether a relationship exists between changes in the metrics and the presence and absence of signs of cerebellar disease.

---

## 6 TRACTOGRAPHY IN PAEDIATRIC POSTERIOR FOSSA TUMOURS

---

### CONTENTS

---

6.1	Introduction	163
6.1.1	Tractography in Neurosurgery.....	165
6.1.2	Objectives .....	169
6.2	Methods	171
6.2.1	Patients.....	171
6.2.2	MRI Data Acquisition.....	173
6.2.3	Tractography Method .....	173
6.2.4	Tractography Thresholds .....	173
6.2.5	Construction of ROIs .....	173
6.2.6	Output of Tract MD, FA and Volume .....	174
6.2.7	Statistical Analysis.....	174
6.3	Results	176
6.3.1	Descriptive Statistics of Metrics .....	181
6.3.2	Linear Regression Analyses.....	184
6.3.3	Comparisons of Group Metrics.....	185
6.4	Discussion	188
6.4.1	Limitations.....	192
6.4.2	Conclusions.....	193

---

### 6.1 INTRODUCTION

Neurosurgical intervention in the treatment of intracranial tumours is aimed at the ideal of complete or near complete resection. Maximal resection in children is associated with

an increased survival, particularly so in posterior fossa tumours of children (274-276) much more so than in the adult population (277). Extent of resection is balanced against risk of damage to normal brain tissue, both cortex and white matter, that may be infiltrated by tumour but remains functional. The extent of the neurological deficit, evaluated by means such as the Karnofsky score (278) relates to quality and duration of life following diagnosis. Poorer functional scores predict shorter life expectancy (277). Surgical decision making regarding a tumour, in terms of resection / debulking / biopsy, is determined by the risk to functional outcome.

In order to quantify risks to eloquent regions of the brain in surgery, techniques to determine the location of areas of such cortex have been implemented. Specifically: intra-operative mapping of the cortex (279), or functional MRI and magnetocephography (185) (280). Whilst they elucidate the location of cortical regions they do not define the underlying white matter tracts (281). Failure to preserve such connections obviates the care undertaken to preserve the cortex as functional deficits will still ensue (282;283). The risk and occurrence of deficits following surgery to treat intracranial neoplasms has determined a need to characterise the eloquent white matter connections in vivo (178;282-286). Awake craniotomy (287) with sub-cortical stimulation (288) have been useful to this end. The emergence of tractography has shown great potential to aid pre and intra-operative planning of the resection of tumours as an adjunct to the current imaging modality of choice, MRI (251;288-292). Conventional MRI provides detailed structural images of the lesions but very little localisation or data about structural integrity of eloquent white matter (178).

### 6.1.1 TRACTOGRAPHY IN NEUROSURGERY

The potential of this technique to map white matter was rapidly recognised (178;284;293) and investigations directed initially towards the motor pathways (corticospinal tracts, CST) in adults. The technique relied upon production of a ROI in the cerebral peduncles and a second one in an approximation of the motor cortex using a FA threshold as a criterion for the termination of tracking (120;121;133;134;178;182;293). The absence of a complete connection of the reconstructed pathways with the motor homunculus, appearing only to connect to the most superior cortex, raised questions over the reliability of the tracts. It was evident that they were dependent upon the subjective ROIs chosen and the FA threshold (93;281;294). In spite of this it was possible to visually reconstruct distortion or disruption of motor pathways as a result of tumour mass effect (178).

Alternatives to manual ROIs based on neuroanatomical knowledge such as cortical mapping through the use of functional MRI (293;295) (296) to locate the cortical ROIs have not resolved the incomplete reconstructions. There have been further attempts using cortical mapping in patients with glioma, with tracts reaching 16 of 27 cortical stimulation sites (297). Completeness of reconstruction has been hypothesised to be hampered by the presence of oedema surrounding the tracts, where the anisotropy is diminished and hence affects tracking (178;298) as well as the effects of crossing and bending fibres which are calculated to have a lower probability than straight fibres.

When tractography was combined with intra-operative cortical mapping, initial results were disappointing (299). This was attributed to failure to resolve crossing pathways and relatively high FA thresholds (0.3) causing underestimation of the motor tracts. More recently tractography combinations with intra-operative cortical stimulation have

been more successful (272;300;301;301-303). Similar techniques of tensor based tractography were used and improvements are likely to have stemmed from adjustments of FA threshold and experience with the tracking algorithm. Berman et al (303) determined the mean distance between sub-cortical stimulation sites and tractography-derived motor pathways was  $8.7 \pm 3.1\text{mm}$  for 16 stimulation sites in 9 patients with gliomas (303). In 40 patients planned for surgery for brain tumours near to the motor pathways Mikuni and co-authors (304) compared electro-cortical stimulation and tractography. In the majority of patients where potentials could be recorded, motor evoked potentials were elicited from the sub-cortex up to a maximum of 1 cm from the motor tract reconstructions. The authors suggest that the two techniques could be used complementarily in order to improve the outcome of surgery through the rapid identification of areas of eloquent cortex and sub-cortex (279;305-307).

The integration of tractography with intra-operative neuro-navigation has been described (272;306-308). A study by Nimsy et al (309) showed white matter tracts, specifically the internal capsule moved between - 8 to + 15mm in a 37 patient series undergoing surgery for glioma. Results reveal the significance of brain shift in the course of surgery and indicate the need for intra-operative updating of the tractography.

The optic radiations have been reconstructed using tractography; in a series of patients with arterio-venous malformations Kikuta et al (310) found incomplete post-op reconstruction of the optic pathway was associated with visual field loss. Intra-operative visual evoked potentials were compared with optic radiation tractography and were lost when the region was reached in a patient with glioblastoma (311). In an attempt to diminish the radiation exposure in patients undergoing gamma knife surgery, tractography has mapped the optic radiation and been integrated into the radio-surgical planning (269).

## Chapter Six: Tractography in Paediatric Posterior Fossa Tumours

The arcuate fasciculus, part of the language pathway connecting the frontal and temporal lobes has been investigated (312) as well as the superior longitudinal fasciculus (313). In work by Kamada et al, the arcuate fasciculus was generated in 22 patients using fMRI activation and magneto-encephalography, two cases were integrated into a neuronavigation system and the results compared with electro cortical stimulation of the area located by fMRI, stimulus locations were within 6mm of the arcuate fasciculus.

In attempts at quantitative assessments of the outputs of tractography, the FA and MD of reconstructions of the CST's have been used in the assessment of the long term outcome from stroke. Results indicated relationships between diminished average FA of the tract reconstructions (150;151;314) and poorer functional outcome scores. A study of FA of the middle cerebellar peduncle (MCP) in patients following stroke looking for reorganisation of the cerebellar connections showed evidence of reduction in FA of the MCP of the contra-lesional side to the stroke (the cerebellum supplies fibres ipsilaterally to the body, left hemisphere stroke but right sided symptoms and cerebellar peduncle). This was not FA generated from a tract average but from a ROI (315). Lui et al (316) looked at the FA of posterior fossa CST reconstructions in 30 patients with primary posterior fossa lesions, through evaluation of DTI metrics obtained from tractography of the motor tracts. In patients with well-circumscribed primary posterior fossa masses, higher MD and lower FA in the brainstem CST were associated with contralateral motor deficits.

There have been few studies in the paediatric population in part due to the lower numbers of tumours in the population (14) and the inherent difficulties presented by imaging children in terms of their ability or wish to co-operate with examination. The questions surrounding development and the degree of myelination with age have been

## Chapter Six: Tractography in Paediatric Posterior Fossa Tumours

discussed in Chapter 5. Gaetz et al (317) used magneto-encephalography and diffusion tensor tractography in paediatric brain tumour patients to map the cortico-spinal tracts. They concluded that concurrent use of MEG and tractography could be an effective tool in the pre-operative evaluation of eloquent cortex and associated white matter tracts in paediatric brain tumour patients.

The pattern of FA changes in the white matter of the cerebellar peduncles has been used to distinguish ataxia syndromes, including spinocerebellar ataxia-1 from multiple system atrophy. Prakash et al (318) looked at adult patients, assessing the types of ataxia and comparing them with qualitative and quantitative measures obtained from tractography of the cerebellar peduncles using, ROI, probabilistic and a deterministic methods. They concluded that the probabilistic method was the most reliable but all methods of tractography of the cerebellar peduncles (superior, middle and inferior) were more helpful at describing and discriminating the types of ataxia than conventional MRI techniques. Average tract FA in all patients with ataxia was decreased in all cerebellar peduncles and the reduction correlated with disease severity.



### 6.1.2 OBJECTIVES

There remain several technical problems with DTI tractography in its integration into standard clinical practice. The use of FA thresholds to remove spurious tracts whilst retaining reliable volumes measurements has remained an issue (178;319;320) (321). This work implemented a FA threshold of 0.3 which is comparable to other studies (251;299) and is a constant threshold for all the groups we are comparing.

ROI use has been described and remains problematic in terms of user interaction; the degree of a priori knowledge required and subjectivity of the choice of location (93;120;121;133;134;178;285;322). Ideally a semi-automatic method would be used to standardise this and reduce operator dependence whilst improving reproducibility, facilitating more reliable direct comparisons between groups (178) (296).

Key in the acceptance of DTI tractography in clinical practice is the functional validity of the reconstructions. Attempts have been made to correlate white matter tract integrity and the function that the tracts sub serve, this correlation is vital in showing that the reconstructions amount to more than visually pleasing representations and are functional accurate (98) (319). The accuracy of the segmentation of the structure of interest is a key question prior to making operative planning decisions based upon it (178). To this end tractography needs to be related to the presence or absence of clinical signs. Studies comparing motor pathway tractography with motor function (323-325) have been undertaken. Laundre et al (323) showed qualitatively that motor pathway (CST) appearance from tractography correlated with clinical motor examination. Kim et al (324) used a ROI placed on the region of the CST using the slice at which point the lesion was largest as well as a second to include the whole CST. The mean FA ipsilateral to the lesion was lower in the CST of those with weakness. Quantitative

## Chapter Six: Tractography in Paediatric Posterior Fossa Tumours

analysis is required as it has already been highlighted that determining if a tract is functional or not based on the degree of its visual disruption is potentially unreliable (283;310)

Our intentions were to use the ROI method described in Chapter 5 in a pathological population in order to determine if a method successful in the healthy population could be transferred and provide anatomically plausible reconstructions. If so it could allow the method to be automated and applied clinically in the future.

Further to this, the aim was to assess the functional validity of the tractography reconstructions in a paediatric pathological population. Using quantitative measures of whole tract MD, FA and volume, in paediatric patients with posterior fossa tumours and cerebellar deficits, we hoped to determine if differences in these measures could be related to the presence of clinical signs of cerebellar dysfunction through comparison with normal control subjects.

## 6.2 METHODS

Throughout the period of data collection, from April 2006 until February 2008, patients presenting with a variety of tumours were imaged. In total 39 cases were collected; it was decided to focus on the posterior fossa group for this analysis as they constituted the largest group (14) with the most uniform group of symptoms.

### 6.2.1 PATIENTS

Over the period from April 2006 until February 2008 patients presenting to the department of Neurosurgery at Great Ormond Street Hospital with a posterior fossa tumour were studied. Patients were included based on the presumptive diagnosis of a posterior fossa tumour from an MRI or more typically a CT performed at their referring hospital. Consent was sought from the patient themselves where age and competence permitted, otherwise assent was sought and formal consent obtained through the next of kin. If this was not possible the patient was excluded from the study. The study was approved by the local research ethics committee and all patients or next of kin gave formal written consent for participation.

The DTI examination was undertaken either as part of the patients clinical MR imaging or as a separate acquisition. Separate acquisitions were performed in dedicated research time when further pre-operative clinical imaging was deemed unnecessary. Separate acquisitions were only possible where the child was able to tolerate an un-sedated scan. If they required sedation or a general anaesthetic for further imaging it was not possible to justify the risks of this and they were excluded from the study. In the case of post-op imaging the DTI sequence was, in all cases, acquired as an addition to the clinical sequence. The scanning protocols are detailed in Chapter 3.3 and were identical to those of the healthy control group discussed in Chapter 5.

## Chapter Six: Tractography in Paediatric Posterior Fossa Tumours

When the imaging was performed as part of a pre-operative clinical sequence the additional DTI sequence resulted in a 20 minute extension to scanning time. Paediatric patients who were unwell or confused due to the underlying pathology did not always tolerate the whole length of the sequence and these cases were also excluded. The time pressures existing in the clinical scanning periods meant that several patients who had consented to the DTI sequence could not be accommodated.

Where possible post operative imaging was obtained; in such cases the DTI sequence was added to the post operative tumour, clinical protocol. The agreed schedule at GOSH was of imaging within 48 hours of surgery. Acquiring post operative imaging was on occasion complicated by the clinical condition of the patient such that they were not able to tolerate the additional imaging time. Next of kin, on occasion were unwilling to consent to further imaging as they felt that the patient was too unwell, although this did not apply to any of the posterior fossa cases studied here.

All patients were examined neurologically pre-operatively by the author (Neurosurgical registrar) and, where appropriate, post operatively. Examination was conducted on the same day as the imaging was obtained. The signs of cerebellar dysfunction are detailed in Chapter 1.4. Cerebellar signs were recorded in terms of presence or absence of: ataxia of gait and or trunk, past pointing / intention tremor (dysmetria) and dysdiadochokinesia. All patients studied in this group were able to walk prior to their presentation. The side of the deficit was recorded; however they were often present bilaterally being possibly more evident on one side or the other. In terms of the analysis here, we considered only their presence or absence as a group in each individual case. If the individual displayed any of the signs of cerebellar dysfunction they were classified in the positive signs group, if none of the signs were present they were classified as absent. In researching a paediatric population, when consent to the inclusion in the

study may be given by the parents, the co-operation of the individual patient could not be relied upon due to their underlying pathology or lack of desire to be examined. In this study a total of 14 patients with appropriate imaging were initially included. Of the 14 all were imaged pre-operatively. A case with imaging pre and post-op was excluded as they were unable to co-operate with clinical assessment pre and post operatively as they were too unwell. A single post operative case was excluded as the imaging was degraded due to motion artefact. In total there were 13 cases available in the final analysis, 5 with pre and post operative imaging, 8 with only pre operative imaging.

### 6.2.2 MRI DATA ACQUISITION

The MRI data acquisition is common to all the tractography data analysed in this thesis and is described in Chapter 3.1.3 and shown specifically as the 1<sup>st</sup> and 2<sup>nd</sup> sequences in Table 3.1.

### 6.2.3 TRACTOGRAPHY METHOD

The tractography method is identical to the method detailed in Chapter 5.2.3

### 6.2.4 TRACTOGRAPHY THRESHOLDS

The tractography thresholds are identical to those detailed in Chapter 5.2.4

### 6.2.5 CONSTRUCTION OF ROIS

The method of construction of the ROIs is identical to that detailed in Chapter 5.2.5. A single region of interest was drawn on the left and similarly on the right in each case. The high FA region lateral to the IV<sup>th</sup> ventricle of the posterior fossa was the region chosen. The author was blinded as to the pathology of the case in question. The visual

output of the tractography was reviewed using GeomView (266) by overlaying it on a b = 0 image to ascertain whether the reconstructions were plausible.

#### 6.2.6 OUTPUT OF TRACT MD, FA AND VOLUME

The method of output of the MD, FA and sub-voxel volume are identical to that detailed in Chapter 5.2.6. In each case analysed, values for the three metrics were output for the left and right side cerebellar peduncular white matter tract reconstructions.

#### 6.2.7 STATISTICAL ANALYSIS

In order to remove any handedness effect, identified previously (Chapter 5), the values for the left-right averaged MD, FA and sub-voxel volumes were calculated from the individual cases' left and right sided ROI values. The same process was used for the healthy normal control (NC) data from Chapter 5; again the left-right averaged values were used.

The posterior fossa data were classified into two groups; those cases that were positive for cerebellar signs (Post Fossa Cerebellar Signs, PFCS) and those that were asymptomatic, (Post Fossa No signs, PFN).

All data were tabulated in Excel (Version 2007) spread sheets. All statistical analysis was performed using SPSS for Windows (Ver. 14. 2006. Chicago: SPSS Inc.).

Scatter plots of age as the explanatory variable and left-right averaged MD, FA and sub-voxel (SV) volume as the variable were constructed for all the analysed cases. In order to statistically assess the presence or absence of an association between age and the left-right averaged MD, FA and sub SV volume of the posterior fossa tumour cases, linear regression analyses were performed for each of the three variables.

## Chapter Six: Tractography in Paediatric Posterior Fossa Tumours

The distribution of values of the left-right averaged MD, FA and SV volume was compared for the two groups of NC and PFCS using scatter plots. Group differences in the values of MD, FA and SV volume were investigated using two sample  $t$  - tests.

### 6.3 RESULTS

The data used in this analysis comprised the healthy control group used in Chapter 5 (normal controls NC) and the posterior fossa tumour group. The posterior fossa tumour group were sub divided into two groups based upon the presence (posterior fossa cerebellar signs, PFCS) or absence (posterior fossa no signs, PFN) of cerebellar clinical signs respectively.

The demographics of the NC group are seen in table 5.1; specifically the mean age of the seventeen right handed cases was 11.1 years with a range of 7.1 to 17.9, there were 10 males and 7 females.

The demographics of the posterior fossa tumour group, both those with and without cerebellar signs, are seen in table 6.1. The 13 cases with data available for analysis had a mean age of 8.8 years with a range of 2.6 to 14.7 years; there were 5 males and 8 females. Case 008 was excluded as the patient, despite being imaged was unable to cooperate with examination once at GOSH.



## Chapter Six: Tractography in Paediatric Posterior Fossa Tumours

Case	Imaging		Sex	Age	Histology	Clinical evaluation	Cerebellar Signs
	Pre Op	Post Op					
Pre_001	x		M	6.67	PNET-MB G IV	Truncal ataxia, ataxic gait, Nystagmus	Present
Pre_002	x		M	3.08	PNET-MB multi-focal	Ataxia, not walking, loss of sitting balance	Present
Post_002		x			PNET-MB Anaplastic	Ataxia worsened, loss of sitting balance	Present
Pre_003	x		F	11.67	PNET-MB G IV	Ataxia, PP, Dysdi, L>>R	Present
Pre_004	x		F	6.25	Pilocytic Astrocytoma G I	Unsteady gait, dizzy, ataxia, Cblr Si ++ L UL	Present
Post_004		x			Pilocytic Astrocytoma G I	Post op, unwell, unable to assess	X
<del>Pre_005</del>	<del>x</del>	<del>-</del>	<del>F</del>	<del>2.58</del>	<del>Ependymoma G II</del>	<del>Nausea &amp; vomiting, No Cblr signs</del>	<del>Absent</del>
Pre_006	x		M	6.75	PNET-MB Anaplastic	Headaches, ataxia UL bilaterally	Present
Post_006		x			PNET-MB Anaplastic	Post op ataxia UL bilaterally worsened	Present
Pre_007		x	F	5.83	PNET-MB Anaplastic	Gait ataxia, Dysdi	Present
Pre_008	x		M	11.5	PNET-MB, Mets Grade IV	Unwell, unable to assess	X
Post_008		x			PNET-MB, Mets Grade IV	Unwell, unable to assess	X
Pre_009	x		M	12.5	Pilocytic Astrocytoma G I	4+/5 weakness No Cblr signs	Absent
Pre_010	x		F	9.33	Pilocytic Astrocytoma G I	Dizzy, H/A, blurred vision. No FND or Cblr signs	Absent
Post_010		x			Pilocytic Astrocytoma G I	No FND / Cblr signs	Absent
Pre_011	x		F	14.67	Pilocytic Astrocytoma G I	Dysdi, PP, Gait ataxia Cblr Signs, L>R, Asp	Present
Pre_012	x		F	14.17	Ependymoma G II	Incidental finding on CT. No FND	Absent
Post_012		x			Ependymoma G II	Movement Artefact	X
Pre_013	x		F	13.17	Pilocytic Astrocytoma	Cblr signs, ataxia	Present
Pre_014	x		M	6.08	PNET-MB G IV	L UL PP, Dysdi, L LL ataxia, mild L weakness	Present

*Cblr = Cerebellar, Dysdi = dysdiadochokinesia, FND = focal neurological deficit, G = grade, PP = past pointing, UL/LL = upper / lower limb. X = Excluded from the analysis (see text)*

**Table 6.1 Demographics of posterior fossa tumour group**

The reconstructed tracts were reviewed visually as discussed previously, below are examples of reconstructions of cases with posterior fossa tumours which did not (Figure 6.1) and did (Figure 6.2) display cerebellar signs on clinical examination. Visual inspection shows the cerebellar peduncular white matter superimposed onto FA images. Visual differences in the tract reconstructions of these cases are not apparent despite the differences in symptoms, indicating the necessity for objective quantitative measures extracted from the tractography

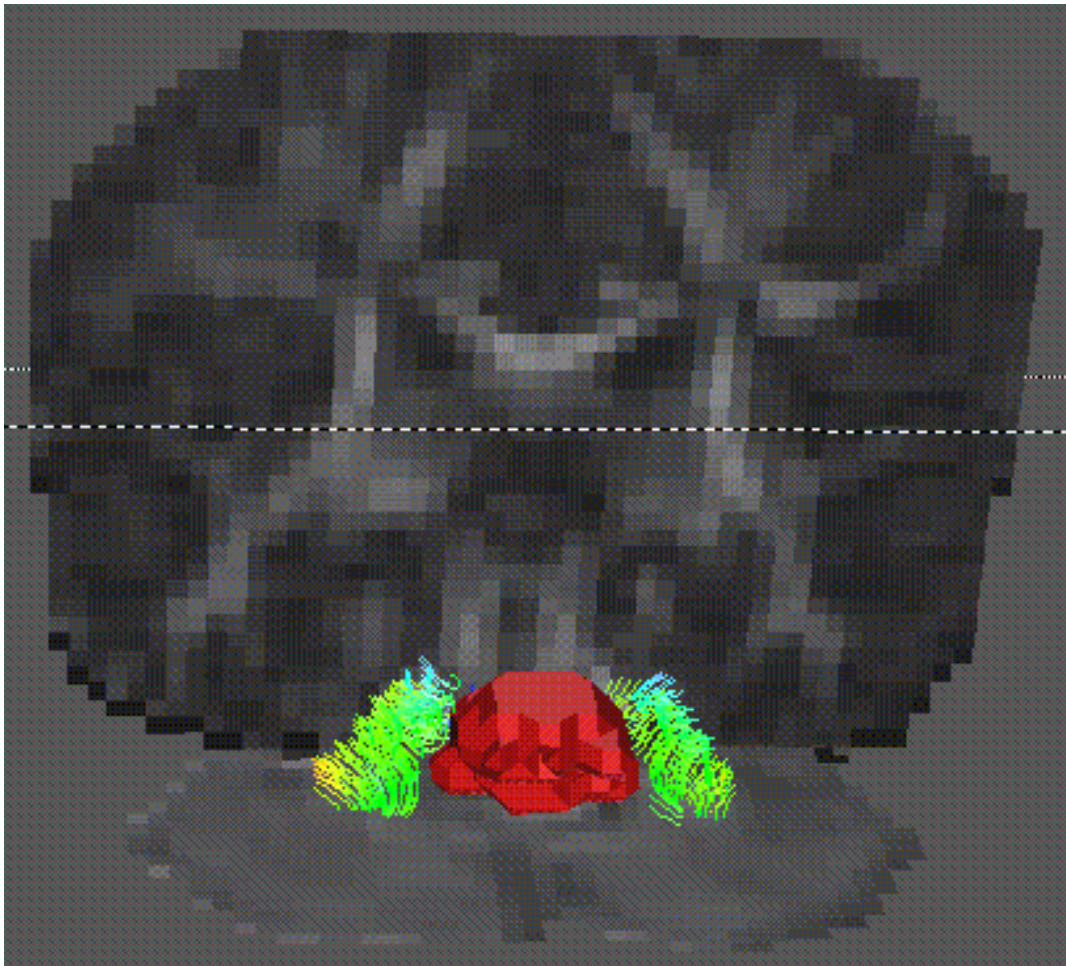


**Figure 6.1 Cerebellar tracts, posterior fossa tumour and no cerebellar signs. (PFN).**

Red area is the tumour (Ependymoma). Tracts are overlain onto axial and coronal FA slices. Green areas represent the cerebellar peduncular white matter tract reconstructions travelling antero-posteriorly. The patient had no cerebellar signs.

---

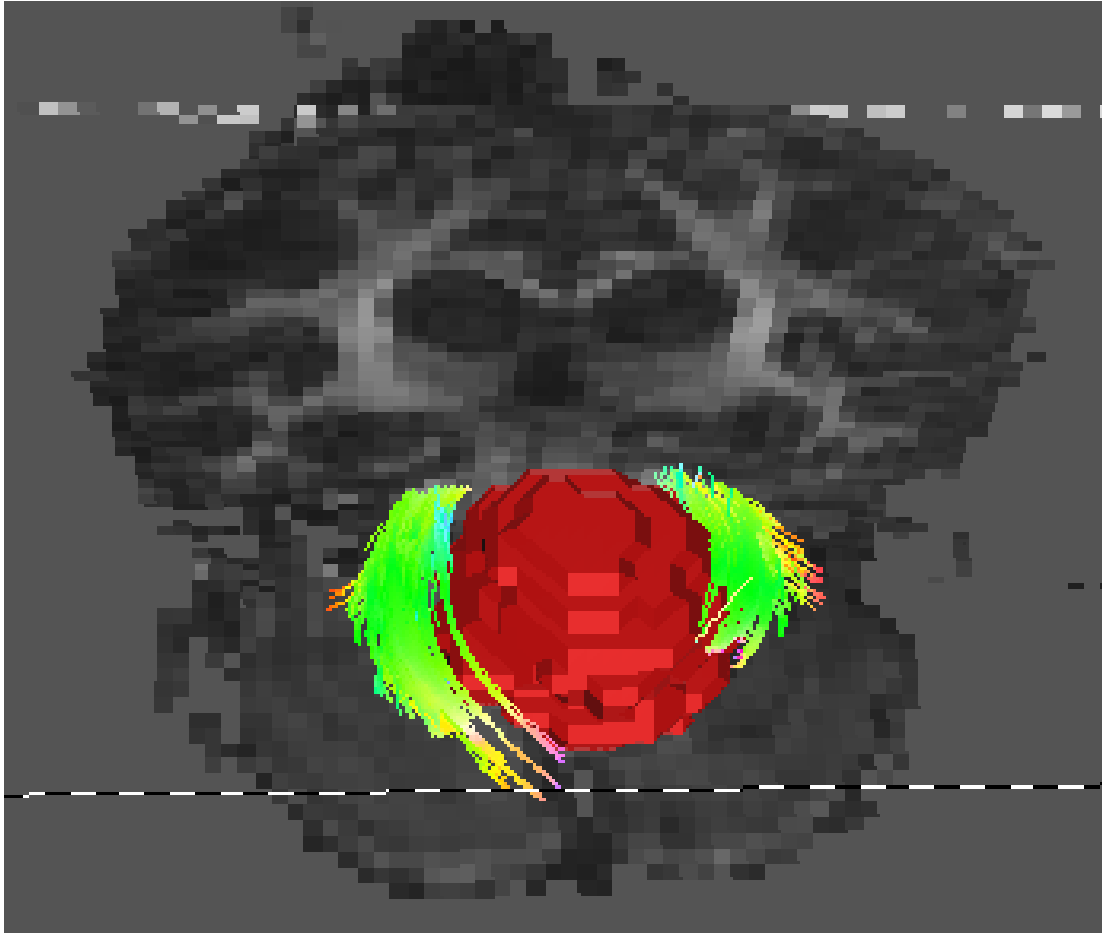


**Figure 6.2 Cerebellar tracts of posterior fossa tumour case with cerebellar signs. (PFCS)**

The red area is the tumour (Medulloblastoma). Tracts are overlain onto axial and coronal FA slices. The green areas are the tractography reconstructions of the cerebellar peduncular white matter tracts. Patient had evidence of upper limb inco-ordination, ataxia, past pointing and dysdiadochokinesia.

---

In total there were 9 cases with cerebellar signs and 4 cases without cerebellar signs at initial presentation (Pre-op). Case 005, without cerebellar signs, was 2.5 years old; 3 years is thought to be the age by which the majority of myelination has taken place. It was excluded from the analysis on the basis that any changes could potentially be ascribed to incomplete white matter development.

The group with posterior fossa tumours without cerebellar signs (PFN) consisted of only four cases and one case was excluded as detailed above hence they were deemed

too small a group for further meaningful comparative analysis. It was decided to confine comparisons to the group with posterior fossa tumours and cerebellar signs (PFCS) and the normal controls group (NC). The post operative data was analysed in terms of production of tractography reconstructions and parameters as an exploratory study. Whilst it was possible to produce tract reconstructions and extract DTI parameters from it, the data was not included in the analysis. Inclusion of this data was considered potentially unsafe with the potential for oedema and physical distortion resulting from the surgery itself causing artefactual (i.e. non structural changes) in MD and FA. It may prove useful in the future to wait a period of time (perhaps up to a month) in order to allow resolution of the oedema and haemorrhage and to reassess the cerebellar white matter. Our initial results were at least encouraging that such analyses would be possible with an appropriate data set.

## 6.3.1 DESCRIPTIVE STATISTICS OF METRICS

The left-right averaged MD, FA and sub voxel volume for the groups NC and PFCS are tabulated below along with the respective mean values and standard deviations.

Group	Variable	N	Minimum	Maximum	Mean	Std. Deviation
NC	Av_MD	17	.738	.816	.776	.0227
NC	Av_FA	17	.387	.495	.463	.025
NC	Av_SV_Vol	17	1100.50	3246.50	2201.50	687.50
PFCS	Av_MD	9	.702	.839	.778	.044
PFCS	Av_FA	9	.400	.456	.437	.0194
PFCS	Av_SV_Vol	9	775.00	4669.00	2635.28	1378.30

*NC = Normal controls, PFCS = Posterior fossa tumour cerebellar symptoms. MD:  $10^{-3} \text{ mm}^2 \text{ s}^{-1}$ , SV volume:  $\text{mm}^3$*

**Table 6.2 Mean DTI metrics for healthy control cases. (NC), posterior fossa cases with cerebellar signs (PFCS).**

Scatter plots of the PFCS using age as the factor and average MD, FA and SV volume as the variables are shown below (see Figures 6.3 – 6.5)

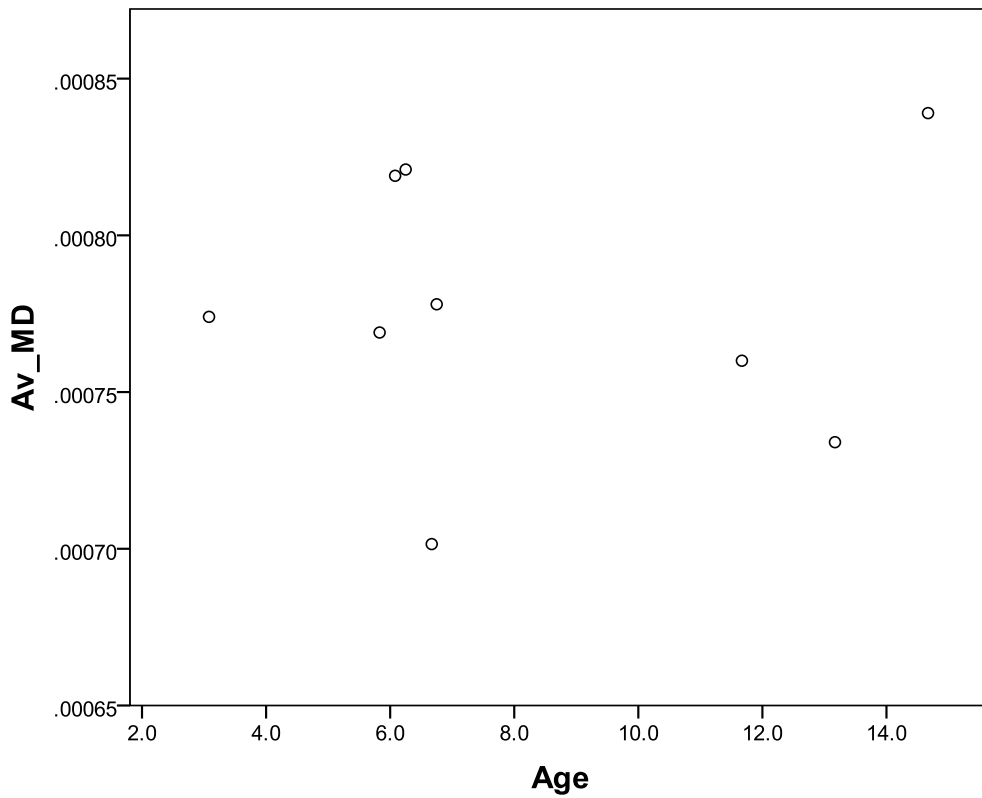


**Figure 6.3 Scatter plot of average MD ( $\text{mm}^2 \text{s}^{-1}$ ) & Age for the posterior fossa tumour cerebellar signs group (PFCS)**

---

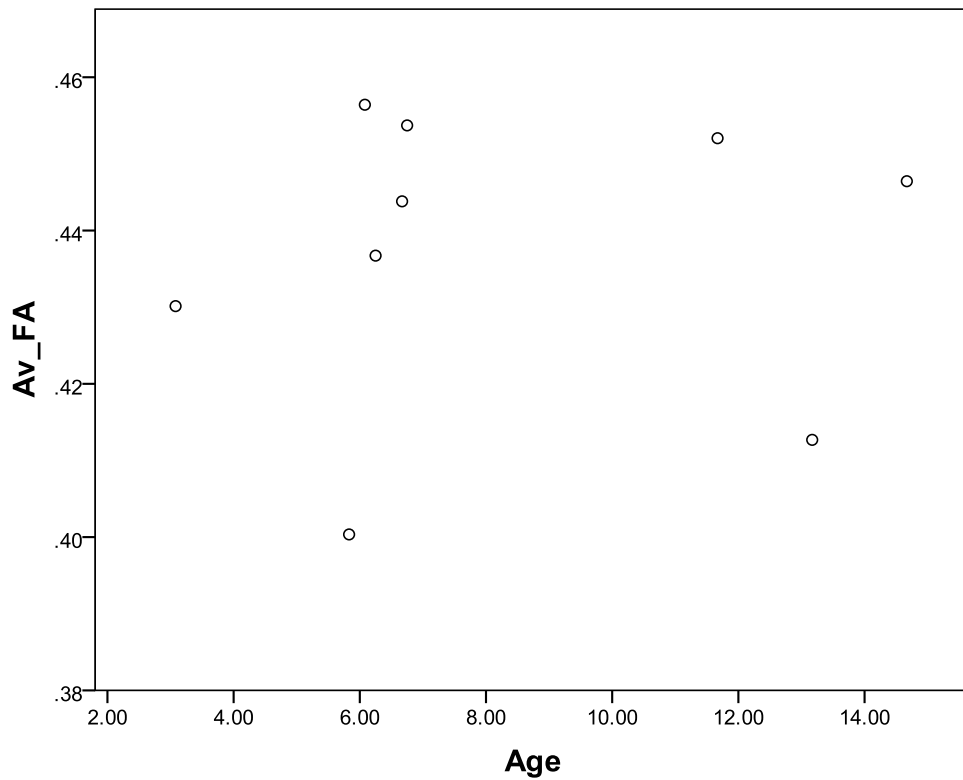


**Figure 6.4 Scatter plot of average FA and age for the PFCS group**

---

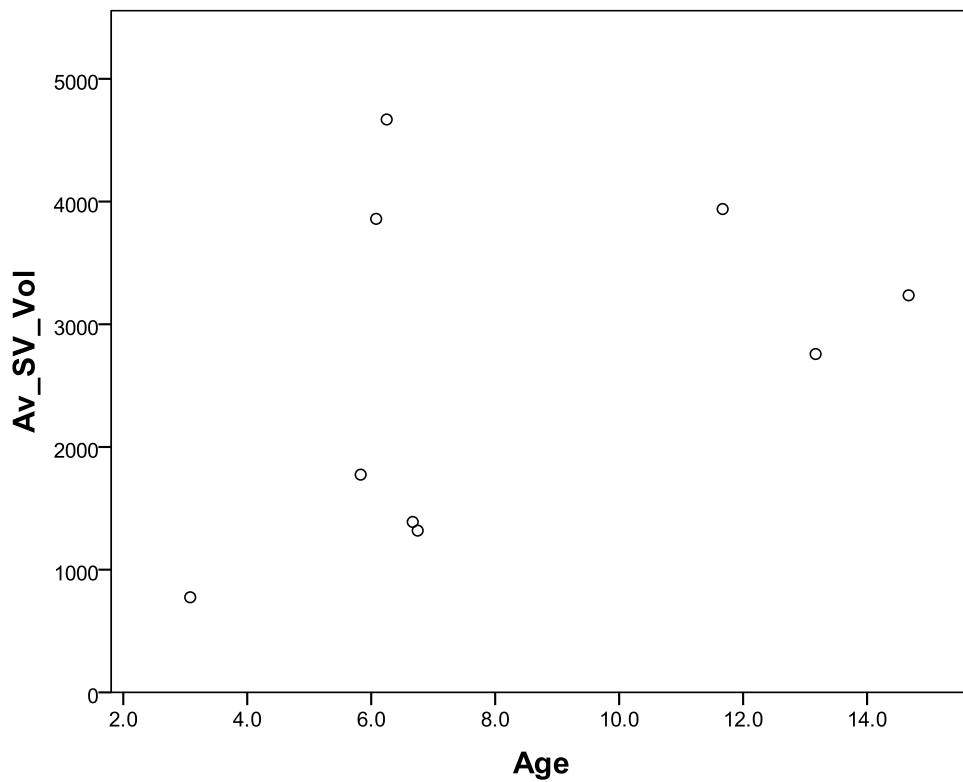


**Figure 6.5 Scatter plot of average sub voxel volume (mm<sup>3</sup>) and age for the PFCS group**

---

### 6.3.2 LINEAR REGRESSION ANALYSES

The individual cases' values of left-right averaged MD, FA and sub voxel volume for the posterior fossa group were investigated using linear regression and the results of the regression p-values are shown in table 6.3. The analysis used the 9 pre-operative cases where there were cerebellar signs at presentation. There was no evidence of a significant association between any of the metrics in this group and the age of the subject being investigated at the  $p < 0.05$  level

Independent Variable	Dependent Variable	p value	Significant at $p < 0.05$
Age	Av_MD	0.850	N/S
Age	Av_FA	0.869	N/S
Age	Av_SV_Vol	0.270	N/S

Av = average, SV\_Vol = sub voxel volume, N/S = not significant.

**Table 6.3 Linear regression p-value results, MD, FA & SV volume versus age.**

---



### 6.3.3 COMPARISONS OF GROUP METRICS

Scatter plots of the three variables of left-right averaged MD, FA and sub voxel volume are shown below using the groups of healthy cases (NC) and posterior fossa tumour cases with cerebellar signs (PFCS).

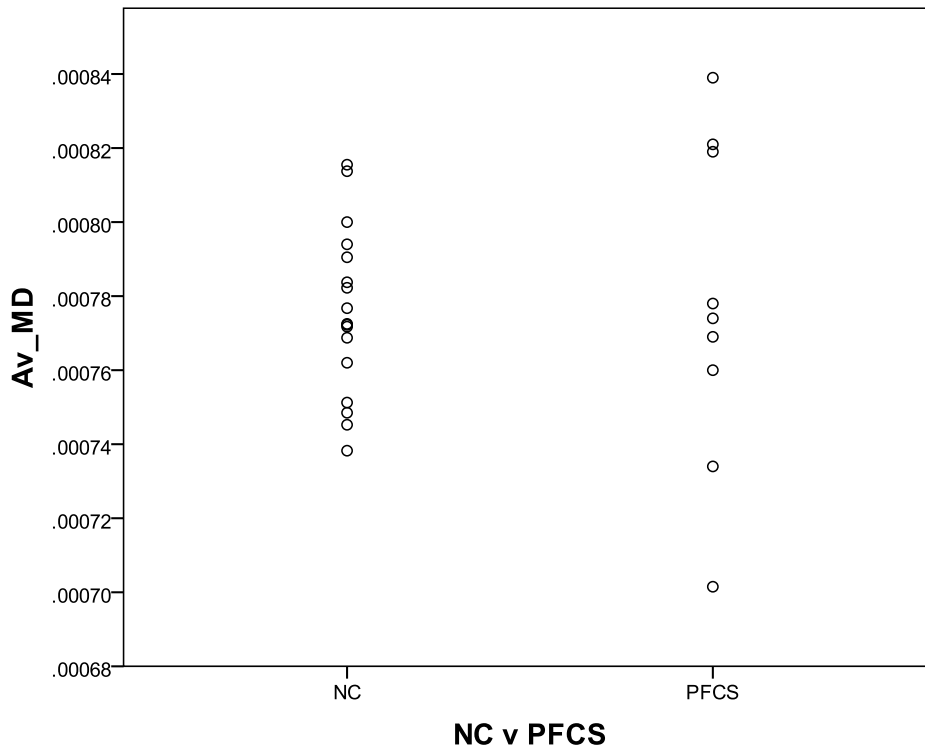


**Figure 6.6 Scatterplot of average MD (mm<sup>2</sup> s<sup>-1</sup>) for NC and PFCS**

---

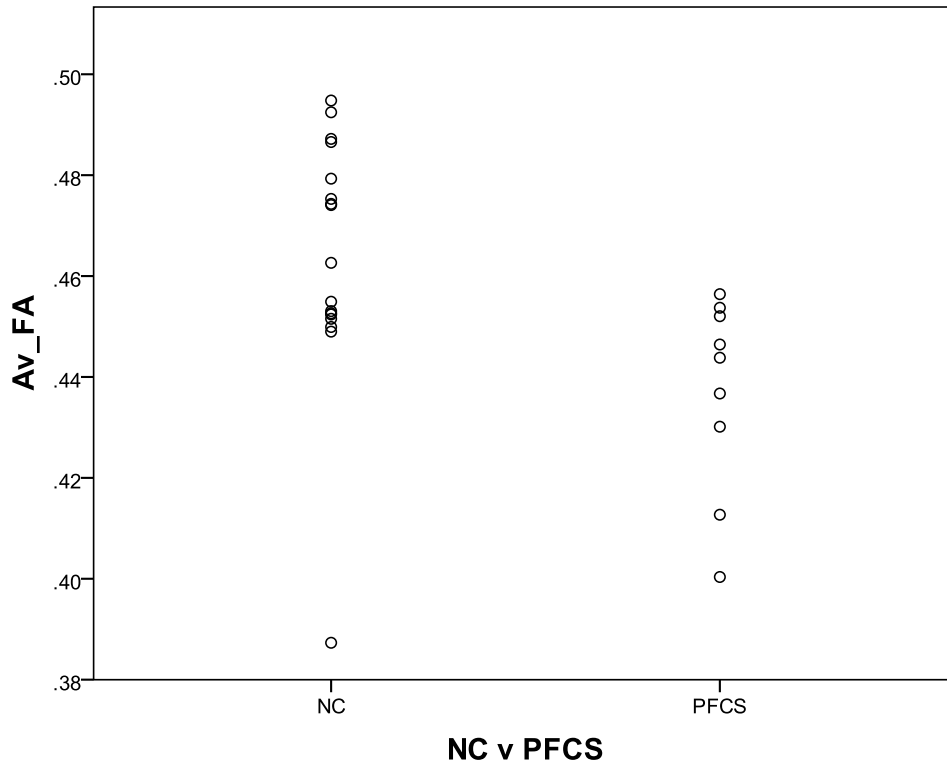


**Figure 6.7 Scatterplot of average FA for NC and PFCS**

---

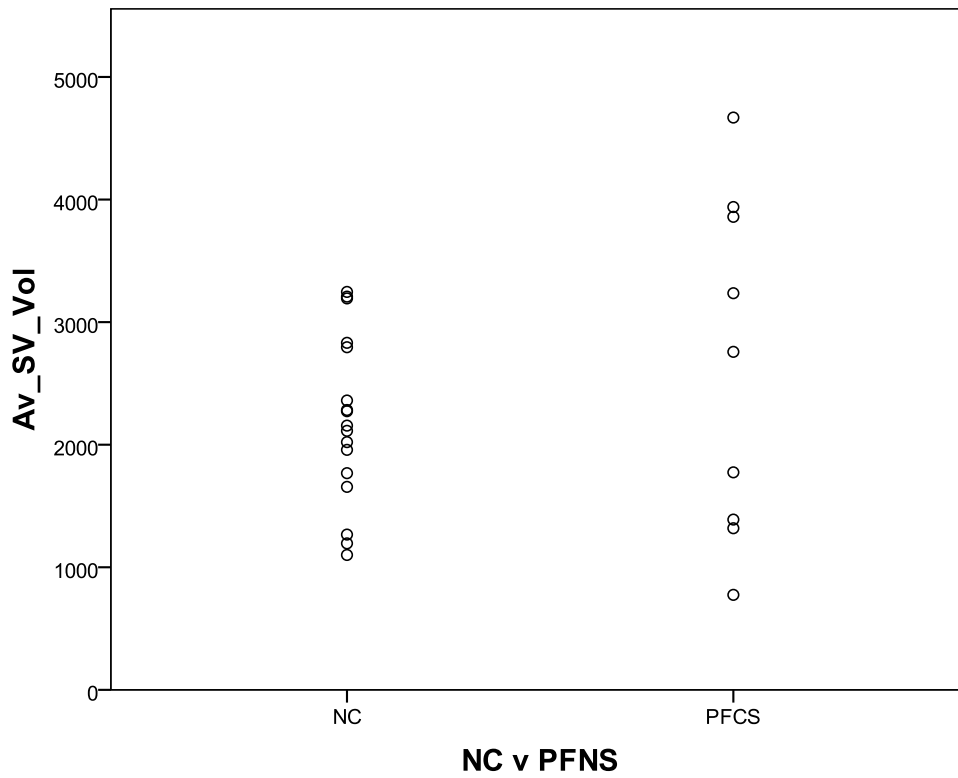


**Figure 6.8 Scatterplot of average SV volume (mm<sup>3</sup>) for NC and PFCS**

---

The scatter plots highlighted the wide spread of sub voxel volumes seen in the PFCS group as compared to the NC group. A similar wide distribution in the MD of the PFCS was observed.

The two groups NC and PFCS were compared using two sample *t* – tests of the group means. Comparisons of equality of means showed no statistically significant differences between the NC and PFCS groups in terms of MD and sub voxel volume. There was however statistically significant differences in the FA values for the two groups.

	DTI Metric / Volume	PFCS (Significance at $p < 0.05$ )
NC	Av MD	N/S
	Av FA	.012
	Av SV Volume	N/S

*NC = Normal Controls; PFCS = Posterior fossa cerebellar signs present;  
Av = average; SV = sub voxel, N/S = not significant at  $p < 0.05$ . Av\_MD  $mm^2 s^{-1}$*

**Table 6.4 Two sample *t* - tests results for group-wise comparisons of Controls with Posterior Fossa Tumour cases**

---

Average FA of PFCS was significantly different from NC; the descriptive statistics inference was that FA was lower in the PFCS group than the NC group.

## 6.4 DISCUSSION

The need to functionally validate tractography has been highlighted and attempted in several studies (283;306;307;326) (98) (323). Typically through correlation of neurological deficits with visual and quantitative changes in the white matter tract reconstructions. Intracranial tumours can result in neurological dysfunction through damage to the cerebral cortex, deep grey matter nuclei or interference with white matter tract structure and function. The effect of a tumour on white matter may occur locally via infiltration of the tract or its destruction. Effects at distance occur when the tumour's mass effect causes the tract to be distorted or compressed from its usual pathway (327). The tract may be damaged secondarily; tumour involving the cortex may result in atrophy of the associated white matter connections, a similar situation is seen following a cortical stroke; these changes are manifest as a reduction in FA and increase in MD of the associated white matter (328). Vasogenic oedema in the peritumoural white matter may lead to dysfunction of those connections, resulting in partial or complete neurological deficits. In vivo visualisation of affected tracts, using DTI tractography, raises the possibility of correlation with clinical dysfunction and hence a means of functional validation.

Validation of tractography could enable its integration into clinical practice. Increased confidence in location of eloquent white matter would enable more aggressive resection of tumours with diminished risk of morbidity; both of which are associated with a better prognosis. It could also allow more accurate planning of radiotherapy reducing the risk of radiation necrosis of eloquent pathways adjacent to the target lesion. (178) (269).

The relative paucity of studies of functional validity of tractography in the paediatric population (329) in part stems from the tumour distribution, with a greater proportion in

the posterior fossa, their lower incidence (14) as compared to adults and the additional difficulties posed by potentially lengthy data collection in a patient group who, by the nature of their disease and stage of development, may not be cooperative with investigation. Notwithstanding this, intracranial tumours in children are the second largest cause of oncological mortality in that age group and tend to be more responsive to surgical resection (230;274) than their adult counterparts.

This study looked at the association of cerebellar signs with changes in metrics of whole tract average MD, FA and sub voxel volume by comparisons of children with and without posterior fossa tumours. As compared to studies of the motor tracts, where the symptoms and signs are typically lateralised; in the posterior fossa symptoms and signs are frequently bilateral. This is due to its relatively small volume and often midline location of tumours in this region. Hence symptoms were classed as present or absent, in addition attempts at lateralisation of symptoms were open to confounding based upon the possibility of asymmetry of the peduncular white matter highlighted in Chapter 5.

Using a single ROI method defined as the high FA region immediately lateral to the IV<sup>th</sup> ventricle of the posterior fossa it was possible to consistently reconstruct the cerebellar peduncular white matter pathways in individuals with and without posterior fossa tumours.

In addressing concerns over the effect of age on DTI metrics we undertook linear regression analyses which did not demonstrate a significant relationship with age at the  $p < 0.05$  level. In the use of cases for the analysis, individuals whose age at the time of scanning were less than three years were excluded as this has been demonstrated as the age by which large changes in FA of the posterior fossa are thought to stop (330), although the MD was shown to cease undergoing significant changes after the age of six

months. The relative differences in the time periods of FA and MD changes may relate to the MD reflecting the amount of structure present and the FA the degree of cohesion of the structures present.

In comparisons of the NC with the group with the posterior fossa tumours and cerebellar signs (PFCS) group, the MD and the SV\_Volume were not shown to be significantly different. The lack of significant changes in the MD may reflect the amount of structure or tissue present in the cerebellar peduncles has not changed as a consequence of the tumour. The SV\_Volumes seen in the PFCS group were scattered over a wider range than that of the NC group although there was no statistically significant difference. This wide range may be explained by the presence of vasogenic oedema, increased extracellular fluid facilitating causing the tracts to appear larger. The wide scatter of the MD and the SV\_Volume may reflect the coincidence of swollen tracts appearing larger and the diffusivity being increased, from a visual inspection of the data, a wide spread in the MD data is similarly reflected in the SV\_Volume data spread. However on review of the data not all of the MD changes are reflected in the SV\_Volume changes. This may alternatively suggest that there are other factors influencing the distribution, not tested in this analysis (i.e. other than age).

Significant differences existed in the average FA values of tracts when the PF cerebellar signs (PFCS) group were compared to the NC group. Inference, drawn from the descriptive statistics, indicates that the FA in the PFCS was lower than in the other groups. It is possible to conclude that diminished FA of cerebellar peduncular white matter in cases of posterior fossa tumours is associated with either oedema, infiltration and/or the presence of cerebellar signs. Quantitative measures are seen to support the

functional validity of the cerebellar pathway tractography; tracts apparently damaged by intracranial tumour represented by reduced FA are found to be clinically dysfunctional.

#### 6.4.1 LIMITATIONS

While demonstrating it was possible to use a simple single ROI method to reconstruct the cerebellar white matter,(331) the algorithm required a high FA threshold in order to exclude spurious tracts, although this is similar to previously published work (178;299;302;304;332). Completeness of reconstruction remains a problem in the clinical application of these techniques, particularly where full reconstruction is important in the planning of resections (333). Completeness of reconstruction may be diminished due to falling FA secondary to white matter oedema and hence cessation of tracking as the voxel FA falls below the tracking threshold (293). FA threshold relaxation however increases the risk of inclusion of spurious tracts (320). The FA threshold limitation may be overcome with current developments in alternative tractography methods such as those utilising streamlines which select tracts on the basis of morphological similarity to an initial streamline passing through a selected voxel of interest (331).

Patient numbers in this study are relatively small, in practice this was partly complicated by patient recruitment issues as the DTI sequence was only available on one of the two MRI scanners in the GOSH radiology department and the time pressures extant dictated that not all cases recruited could be accommodated on the research scanner. Several cases were also unable to co-operate with the clinical examination as a consequence of the underlying pathology and had to be excluded.

The failure to include adequate numbers of cases where there were posterior fossa tumours and no cerebellar signs meant that it was not possible to explore the presence or absence of changes in tract metrics when no clinical signs were present. This represents a group worthy of further data collection and analysis.



#### 6.4.2 CONCLUSIONS

Using a streamline method of tractography it has been possible to reconstruct cerebellar white matter using a single ROI. This is as compared to the established published methods requiring multiple ROIs (134). Significant differences have been defined, (reduction) in the average tract FA in individuals with clinical cerebellar dysfunction as compared to normal control subjects. This illustrates that tractography can provide apparent functionally meaningful information in children with infratentorial lesions.

This functional validation supports integration of tractography into the planning of neurosurgical procedures. Pre-operative and intra-operative localisation of white matter tracts may guide surgeons towards more complete resections whilst reducing risks of neurological deficit. Significant consideration however must be given to the effect of intra-operative brain shift in the execution of such techniques (309).

---

## 7 CONCLUSIONS

---

### CONTENTS

---

7.1	Diffusion Imaging of Paediatric CNS Tumours	194
7.1.1	Conclusions.....	194
7.1.2	Limitations.....	197
7.1.3	Future developments.....	198
7.2	Tractography in Paediatric Neurosurgery	200
7.2.1	Conclusions.....	200
7.2.2	Limitations.....	203
7.2.3	Future applications.....	206

---

### 7.1 DIFFUSION IMAGING OF PAEDIATRIC CNS TUMOURS

#### 7.1.1 CONCLUSIONS

Diffusion-weighted imaging and the derived apparent diffusion coefficient (ADC) have been used to investigate tissue structure (55;60;61;84;197;198). Differences exist in terms of the intracellular and extracellular structure of different tissues and tumours, the degree of cellularity and the characteristics of tumour nuclei vary and this appears to be reflected in their ADC values (85;87;199;200).

Previous work has correlated tumour grade with ADC, higher grade tumours tending to be more densely cellular (61;75;84-87;198-206); certain features of the tumours have characteristically different ADC values, such as cystic or necrotic regions. Studies have addressed separating tumour types based on mean ADC values but overlap between groups has hampered this, although when combined with other MR methods such as

spectroscopy it has been possible to discriminate common posterior fossa tumour types using linear discriminant analysis, which assumes multivariate normality (208).

As discussed in Chapter 4, it is often possible to determine a differential diagnosis from the MR examination, clinical history and presentation of a patient. This still leaves significant uncertainty in terms of the exact identity of a lesion and hence the correct course of treatment. In the case of intracranial tumours, treatments can range from conservative management to total surgical resection. It is however unlikely that treatment will be undertaken without a diagnosis being established. Radiological reports of imaging will usually include a list of differential diagnoses and are unlikely to be definite over a diagnosis. A purely observational analysis of the reports of the cases in this study when compared to the histological diagnosis reflected this. Generally a list of differentials from most likely to least was provided and it appeared that the likelihood of the diagnosis being correct was related to the experience, in terms of years, of the reporting radiologist. frequently this will necessitate an invasive surgical biopsy with its attendant risks (184-187) and chance of non-diagnostic biopsy (188). To this end a non-invasive means of determining the nature of the lesion could be very useful.

We used a simplified ROI analysis, applied to the whole tumour volume and extracted histograms from the data to explore differences in the tumour types in our paediatric population of 56 cases, (6 common tumour types). Our hypothesis being that histograms would provide a more complete description of the ADC characteristics, as had been indicated in previous work (209). Using ADC histogram data we intended to use logistic regression, on the basis that one could not assume multivariate normality, to create a model which would allow discrimination of: initially all the tumour types and then specifically the common posterior fossa tumour types and a rarer group,

atypical teratoid rhabdoid tumours (ATRT) from primitive neuroectodermal tumours (PNET) in particular due to the differing prognosis and management (211-216).

The mean ADC values we recorded for our tumour groups were in keeping with previously published work (197;214) (214). In discriminating tumours based on mean ADC alone there existed significant overlap of the ATRT and PNET groups and the ependymoma group, the juvenile pilocytic astrocytomas (JPA) had higher mean ADC in keeping with their looser stromal architecture; these results were consistent with published literature (86;197).

Logistic regression of the ADC histogram data allowed discrimination of 74.1% of all the tumours studied: 90% (20/22) PNETs, 82% (9/11) JPAs, 80% (4/5) DNTs and 75% (3/4) ATRTs and 0% of Ependymomas (0/5). The ependymoma group had significant overlap of ADC values with other groups and was quite heterogeneous. In asking specific diagnostic questions it was possible to discriminate 80% (4/5) of ependymomas, 94% (15/16) of PNET-MBs and 100% (11/11) of JPAs, using the 75<sup>th</sup> centile ADC value from the histogram. In this case ependymomas were much more successfully classified; this may indicate that inclusion of other parameters in the model may be helpful.

A novel finding was the discrimination of ATRT from PNET in 100% of cases (4/4 and 22/22 respectively); significant as ATRT have a much bleaker prognosis and may warrant avoidance of the risks of invasive biopsy / debulking as opposed to PNET who benefit from aggressive resection. Previous studies have found such attempts at discrimination unrewarding (214).

As a methodology whole tumour ADC histograms appear to provide more descriptive information reflecting a more complete coverage of the frequency of occurrence of an

ADC value within the lesion. Using LR analysis: 94% classification of PF tumour types and 100% of PNETs from ATRTs; not currently distinguishable on MRI (214;232). Diagnostic models such as this may be able to play a role in the future neuro-radiological practice and this work indicates that it may be possible to design and implement a model capable of predicting tumour type.

### 7.1.2 LIMITATIONS

The method using whole tumour ROIs to produce ADC histograms to reflect the heterogeneity of the tumours and subsequently analysed by logistic regression has enabled discrimination of several specific tumour types in this population of 56 paediatric tumours. However there remain limitations.

The number of cases in our cohort is small but typical for data collected from a single unit in the context of the population frequency of paediatric tumours (14). In addition the number of tumour types in our group, whilst encompassing the majority of the common paediatric intracranial tumours is still limited. We asked more directed questions and our discrimination method relies on the provision of only a limited number of possibilities to the algorithm. This approach does, however reflect the clinical situation, at least partially; frequently a radiologist can determine a list of differential diagnoses and then uncertainty is restricted to a smaller group of tumour types. Clearly it would be optimal to determine a method that will allow discrimination of a more complete group of tumours.

The region of interest analysis is not a standardised method in the literature and is open to operator bias. Whilst the author who drew the ROIs was blinded to the histology of the tumour it is not always possible to be certain that the entire tumour was included in the ROI or that non-tumour areas were excluded. Fundamentally this method, by

including the whole tumour volume, was simple and less open to bias than other techniques reliant on selecting a region within the putative tumour.

A further limitation of this study is the binary logistic regression model applied to the analysis of this data. It may be that when applied to a different cohort of tumours the results may differ, we would however anticipate that they would be similar.

### 7.1.3 FUTURE DEVELOPMENTS

The use of whole tumour histograms is encouraging with this limited group of tumours. In order to appreciate the techniques application to the clinical situation a multicentre study should be undertaken over a longer period enabling a greater sample size and a broader group of pathologies. In the current MRI climate, diffusion data is being routinely collected on tumour patients and hence a simple co-ordination of this data may be possible in the near future. It is of note that the Childrens Cancer and Leukaemia Group guidelines for imaging of CNS tumours do not recommend inclusion of diffusion sequences as part of their standard assessment protocol. This study, along with others quoted, indicates that there exists diagnostic potential from the inclusion of such information and we would suggest that its inclusion in routine imaging would facilitate investigation of this potential.

The evaluation of the inclusion of other MRI data, information from the clinical history and also characteristics such as the tumour location should be integrated into the algorithm for determination of the tumour type (214). It may be possible to use other diffusion and tractography metrics such as MD, FA and volume as well MR spectroscopy and perfusion to further characterise the tumour. The diverse nature and the occurrence of rare tumours in the paediatric population demand that

significant numbers of rarer tumours are included in the sample population to make this method more applicable to the clinical environment.

ADC histograms have shown potential to better predict the histological diagnosis of paediatric brain tumours. This method could enable improved pre-operative planning in terms of deciding a location for biopsy or even diminishing the need for invasive surgical biopsy (334).

## 7.2 TRACTOGRAPHY IN PAEDIATRIC NEUROSURGERY

### 7.2.1 CONCLUSIONS

The ability to, in-vivo, reconstruct the white matter pathways in a living brain has been one of the main attractions of tractography. The possibility to apply the technique in the planning and execution of neurosurgical procedures has been a principal objective of research in this field (178;284).

Investigations in the adult population have significantly outweighed those of the paediatric population (98;335). Typically investigations have focused on the motor pathways and other eloquent pathways; there have been few anatomical studies of tractography in the posterior fossa white matter (251;318).

Currently there are limitations to the clinical application of tractography; the reliance on user defined ROIs and its inherent risk, particularly when segmentation is achieved by retaining streamlines passing through one or more ROIs. (93;120;134;182;322;336). Questions still remain over the amount of user interaction and time required to achieve the reconstructions. The uncertainty over reproducibility of the reconstructions raises doubts as to its reliability and hence integration into clinical practice.

Functional validity of the technique fundamentally determines its application to the clinical setting; tracts must not only appear to be anatomically plausible but also functionally correct (178;319). The risks of implementation without this validation were highlighted by Nimsky et al (337) and other authors have felt that the correlation with clinical findings and outcomes, ideally through quantitative measures is vital (338). To this end there have been several studies looking particularly at motor function correlation with motor pathway tractography typically in the presence of tumours and in response to white matter damage attributed to stroke (339-341). Specifically studies



have looked at the function of the CST in cases of posterior fossa tumours (342). In terms of the paediatric posterior fossa cerebellar white matter there have been anatomical studies to describe the white matter (251) and applications in the assessment of clinical conditions such as cerebellar ataxia where DTI metrics have been used to discriminate different conditions (318).

This study's intentions were to contribute to clinical validation of tractography by assessing the ability to reliably reconstruct cerebellar white matter pathways in children in health and in disease.

In the healthy paediatric population it was possible to reconstruct the cerebellar peduncular white matter, in all cases using a single ROI with an FA threshold of 0.3, which was in keeping with published literature in the reconstruction of other white matter tracts (251;271;343). Investigations of the quantitative measures of MD, FA and tract volume showed statistically significant evidence of right left asymmetry. Such asymmetry had been demonstrated with volumetric studies of the cerebellum (261). The average FA and tract volume of each side were statistically different, the inference from the descriptive statistics was that values were greater on the right than the left in this group of right handed subjects. There was no statistically significant difference in the right to left asymmetry of MD however in the 17 right handed cases in the study. The right-left lateralisation of cerebellar function has been demonstrated in other studies (260;344). The association of structural asymmetry and handedness has been postulated previously (261) and our study, which uses only right handed subjects also indicates a possible association.

It was possible to consistently reconstruct cerebellar peduncular white matter in all individuals with posterior fossa tumours using the method applied in the healthy

paediatric population. The posterior fossa tumour cases showed evidence of an association between the presence of cerebellar signs in cases with tumours and a reduced average tract FA, as compared to healthy normal cases.

It is evident that it is possible to reconstruct the cerebellar peduncular white matter using a simple single ROI in both healthy subjects and those with intracranial tumours. It required limited user interaction and the ROIs could be drawn quickly, requiring minimal anatomical knowledge; simply using the high FA regions lateral to the IV<sup>th</sup> ventricle of the posterior fossa.

The association of changes in tract FA and the presence of cerebellar signs in cases with posterior fossa tumours add further evidence pointing towards functional correlation with integrity of tractography reconstructions. However, further studies are warranted to include pathological cases without the presence of cerebellar signs in order to determine the relationship between tractography derived structural metrics of the cerebellar peduncular white matter and the presence of clinical cerebellar signs. These findings are in line with the call for rigorous assessment and investigation of tractography as a clinical tool, ahead of potential integration into neurosurgical clinical practice.

### 7.2.2 LIMITATIONS

Our results are encouraging in terms of a simple method of tractography in the paediatric population and also as a further validation of the technique as functionally meaningful. They do however only address some of the questions surrounding the advancement of tractography as a means of planning in the neurosurgical population. Whilst accepting that cerebellar white matter damage is not usually associated with as devastating and permanent functional loss as the CST or language pathways. As a proof of principal of tractography's functional validity it is significant, studies have already been published addressing recovery from cerebellar stroke and the integrity of the peduncular white matter (345). Paediatric posterior fossa tumours also represent a far greater proportion of oncological practice in the paediatric population as compared to the adult population and are hence a sensible target for investigation.

A significant factor in the quality of the tractography is the completeness of the reconstructions and this is affected by the FA thresholds. If the FA threshold is too low spurious tracts are included; if the threshold is too high, important associated tracts may be excluded (293;333). The complete and accurate description of the tract is vital if the technique is to be used for neurosurgical planning in the avoidance of damage to the white matter (321;338). In this method we used a relatively high FA threshold which may lead to the exclusion of functionally relevant tracts.

Image resolution also affects the completeness of tractography reconstructions. The exclusion of relevant white matter has been highlighted in the choice of FA threshold. The resolution of the tracts is affected by the voxel size in the image acquisition which in this study was  $2.5\text{mm}^3$  and range usually from  $1\text{-}3\text{mm}^2$ . This is considerably larger

than the diameter of individual axons and in combination with the signal to noise effects mean that reconstructions are considerably limited in their spatial resolution.

The ROI method employed, whilst simple, remains user dependent in the selection of the actual ROI. The realisation of a fully automated means of ROI selection is an important goal if tractography is to be made possible in all Neurosurgical units without dedicated physics support staff (346).

The data used in this study and many others relies on the use of a single estimation of the tensor at a given point. The assumption being that the fibres are described by a single direction. This has been highlighted as simplistic, at any point fibres from more than one direction may be crossing or merging (99). Methods are being investigated to take account of this but necessitate greater data acquisition and extended imaging times (103;106). The more complex nature of the neural architecture may in part explain the incompleteness of the tractography reconstructions seen in the CST and also in the failure to track to the cerebellar cortex in this study, although failure to track through intervening deep grey matter, such as the cerebellar deep nuclei may also play a role (346;347). In addition it is not possible to distinguish between afferent or efferent tracts or whether the tract is actually functional.

The implicit assumption that the presence or absence of symptoms is attributable to the damage to white matter pathways is open to question and the possibility that disruption of the deep cerebellar nuclei may play a role in them cannot be discounted.

Clinical cerebellar signs are diverse and cannot be described as simply as the presence or absence of hemiparesis as seen in the CST investigations. They represent a group of signs that may be attributable to different parts of the cerebellar peduncular white matter. Investigations of a group of patients with cerebellar ataxias used detailed clinical

assessments of the type of ataxia, beyond the scope of this work. They used reconstructions that they attributed to the three anatomical sub divisions of the cerebellar peduncular white matter in order to discriminate them, however they did not provide information as to how they defined the three overlapping regions of the peduncles (318). We have adopted a simplified approach using the presence or absence of symptoms to discriminate the groups in order to evaluate the functional validity of the tract reconstructions.

Specific limitations of each of the studies are further described in the relevant chapters.

### 7.2.3 FUTURE APPLICATIONS

A key issue in the relationship of the asymmetry of the cerebellum and handedness in this study is the means of definition of handedness. The initial work detailed here indicates that further investigation is warranted but should involve a more in depth neuropsychological assessment of handedness and also involve the inclusion of larger numbers of both right and left handed individuals.

The assessment of functional validity remains vital and a larger population of patients with pathology would enable more detailed investigation of the effects on the cerebellar white matter. This would be aided by more detailed neurological assessments of the individuals similar to that seen in the cases of cerebellar ataxia investigated by Prakash et al (318). This is compounded in complexity by the specialist nature of investigations in children.

As a consequence of the differing type and distribution of intracranial pathologies in children our study addressed only the cerebellar white matter. In order to continue to advance tractography as a clinical tool studies will be needed looking at all the major white matter pathways, including the visual and sensory pathways. The investigation of multiple pathways using an ROI method would be potentially time consuming and user dependant; this adds further weight to the need for automated mechanisms of whole brain tractography and selection of ROIs.

If and when functional validation is achieved, the integration of tractography into clinical practice could be potentially very helpful to neurosurgeons undertaking operations involving the resection of white matter. There still exist challenges for tractography in neurosurgical planning; when using intraoperative MRI it is clear that the need to account for brain shift in relation to the resection of tissue is an important

consideration when integrating tractography into neuronavigation systems (281;332;348;349) (326;350). It has also been proposed that virtual reality technology could be used in training with the technique in order to aid awareness of three dimensional nature of the tracts (351).

Tractography has been seen to have many potential applications and it has been used in the understanding of neurological disorders such as the white matter structural changes following stroke (98). Reviews of the current research (98) envisage the possibilities for indirect assessment of neuro-degeneration and demyelination in order to determine effectiveness of treatments and targeted therapies for these processes (245;325;340;352). The investigation of the relationship between function and structure in healthy and diseased brains shows potential; adaptive changes following stroke have hinted at possible rewiring and the degree of integrity of the pathway has been predictive of recovery of motor function (245;314;339;345;353).

In the field of functional neurosurgery tractography has been used to localise the foci for Parkinsonian symptoms and target therapies (354). It has been used to identify areas of abnormal connections or regions associated with propagation from epileptogenic foci (355). The possibility exists to define the targets for disconnection in epilepsy surgery through the combination of fMRI, EEG and tractography (355).

This study, in accordance with other studies, has shown evidence that changes in white matter tractography derived measures can be associated with clinical manifestations of the pathological condition. Tractography has allowed advances in the description and identification of the architecture of complex white matter. Future advances in image acquisition and applications at high and ultra-high fields may allow enhanced resolution imaging in the clinical setting. The results of which, should enable investigation of more

detailed anatomy and improve precision of tracing white matter pathways, possibly to elucidate in vivo intra operative tractography (326). Fundamentally an integrated approach with other developing imaging modalities such as fMRI and PET and in combination with more automated techniques may allow the integration of tractography into routine clinical practice.



---

## 8 APPENDIX

---

### CONTENTS

---

8.1	Ethical Approval (COREC)	210
8.2	Patient Information Sheets	213
8.2.1	Parents.....	213
8.2.2	Children 5 Years or Less .....	215
8.2.3	Children 6 to 12 years.....	217
8.2.4	Children 13 years plus .....	219
8.3	Consent Forms	221
8.3.1	Parents Consent.....	221
8.3.2	Patients Assent Form .....	223
8.3.3	Patients Consent Form .....	224
8.4	Paediatric MRI Sedation Protocols	225
8.5	ADC Histogram Protocol Instructions	226
8.5.1	Dispimage Analysis Computer Protocols .....	226
8.5.2	Protocol for Drawing ADC ROIs .....	228
8.6	Tractography Protocol Instructions	229
8.6.1	DTI Analysis Computer Protocols.....	229
8.6.2	Tractography Computer Protocols.....	232
8.6.3	Batch File Instructions .....	237
8.6.4	Batch Files .....	238
8.7	Glossary	239

## 8.1 ETHICAL APPROVAL (COREC)

**Great Ormond Street Hospital  
for Children NHS Trust / The  
Institute of Child Health  
Research Ethics Committee**

Institute of Child Health  
30 Guilford Street  
London  
WC1N 1EH

Tel: 020 7905 2620  
Fax: 020 7905 2201  
Email: t.austin@ich.ucl.ac.uk

19 December 2006

Dr D Saunders  
Radiology  
GOSH

Dear Dr Saunders

***Full title of project: Apparent Diffusion Coefficient characteristics may predict Neuro-oncological tumour type in a paediatric population***

Thank you for seeking the Committee's advice about the above project.

This project has been considered by the Chairman, who has advised that the project is not one that is required to be ethically reviewed under the terms of the Governance Arrangements for Research Ethics Committees in the UK.

An R&D number will be issued by the R&D Office, which will enable you to access the medical records for this project. Please contact Eleanor Rolle-Marshall in the R&D Office if you do not receive your R&D number.

Yours sincerely,

Taki Austin  
Research Ethics Coordinator

Copy to: Institute of Child Health/ Great Ormond Street Hospital R&D Office



**Joint RNOH/IOMS Research Ethics Committee**

R&D Office/ACDS  
Brockley Hill  
Stanmore  
Middlesex  
HA7 4LP

Telephone: 020 8909 5752  
Facsimile: 020 385 7151

13 June 2006

Dr Jonathan Bull MA FRCS  
Clinical Research Fellow, Radiology and Physics Unit  
Specialist Registrar Neurosurgery south Thames Rotation  
UCL Institute of Child Health  
30 Guilford Street  
London WC1N 1EH

Dear Dr Bull

**Full title of study:** Development of Magnetic Resonance Tractography for  
Paediatric Neurosurgical Operative Planning  
**REC reference number:** 06/Q0506/15

Thank you for your letter of 15<sup>th</sup> May 2006, responding to the Committee's request for further information on the above research and submitting revised documentation.

The further information has been considered on behalf of the Committee by the me.

**Confirmation of ethical opinion**

On behalf of the Committee, I am pleased to confirm a **favourable ethical opinion** for the above research on the basis described in the application form, protocol and supporting documentation.

However some of the typographical errors pointed out to you during the first review are still outstanding. I do not wish to delay your study as these do not raise any ethical issues, and I will be content if you would make these revisions and send them to Uzma Chaudhry for our record.

They are as follows:

- ✓ In two places you have called the REC the Research 'and' Ethics Committee. You need to remove the 'and'.
- ✓ In the patient information sheet for children 6-12 you need to change paragraph 6 to something along the lines of 'Some people don't like the feel of being in the scanner and if this happens the scan will be stopped.' (Otherwise it does not make sense).
- ✓ In two places the extra space in 'What will happen to me if I take part' has not been removed. (Children 6 - 12 and Children 5 or less).

**Ethical review of research sites**

The favourable opinion applies to the research sites listed on the attached form.

An advisory committee to North Central London Strategic Health Authority

**Conditions of approval**

The favourable opinion is given provided that you comply with the conditions set out in the attached document. You are advised to study the conditions carefully.

**Approved documents**

The final list of documents reviewed and approved by the Committee is as follows:

<b>Document</b>	<b>Version</b>	<b>Date</b>
Application		09 March 2006
Investigator CV	Christopher Clark	01 March 2006
Investigator CV	Jonathan Bull	
Protocol	1	01 March 2006
Covering Letter		15 May 2006
Letter from Sponsor	Emma Pendleton, GOSH & Institute of Child Health	08 March 2006
Parent Information Sheet	2/06	
Participant Information Sheet: Children 5 or less	2/06	
Participant Information Sheet: Children 6-12	2/06	
Participant Information Sheet: Children 13-15	2/06	
Participant Consent Form	1 - For parents of child participants	08 March 2006
Participant Consent Form	1 - For participants	08 March 2006
Participant Consent Form	1 - For child participants	08 March 2006
Confirmation of external Peer Review from CRUK	E-mail from Alison Mortlock	08 March 2006
Proof of funding	Angela Galpine, Cancer Research UK	25 January 2006

**Research governance approval**

The study should not commence at any NHS site until the local Principal Investigator has obtained final research governance approval from the R&D Department for the relevant NHS care organisation.

**Statement of compliance**

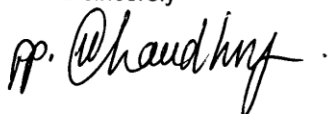
The Committee is constituted in accordance with the Governance Arrangements for Research Ethics Committees (July 2001) and complies fully with the Standard Operating Procedures for Research Ethics Committees in the UK.

06/Q0506/15

Please quote this number on all correspondence

With the Committee's best wishes for the success of this project

Yours sincerely



**Chair**

SF1 list of approved sites

An advisory committee to North Central London Strategic Health Authority

## 8.2 PATIENT INFORMATION SHEETS

### 8.2.1 PARENTS

#### UCL INSTITUTE OF CHILD HEALTH

PARENT INFORMATION SHEET  
VERSION 2/06

#### **MAPPING BRAIN CONNECTIONS IN CHILDREN WITH ABNORMAL BRAIN SCANS**

Your child is being invited to take part in a research study. Before you decide it is important for you to understand why the research is being done and what it will involve. Please take time to read the following information carefully. Talk to others about the study if you wish.

- Part 1 tells you the purpose of this study and what will happen to your child if they take part.
- Part 2 gives you more detailed information about the conduct of the study.

Ask us if there is anything that is not clear or if you would like more information. Take time to decide whether or not you wish to take part.

#### **Part 1**

##### 1. **What is the purpose of the study?**

We are looking at the connections of different parts of the brain and how they are changed when the brain's structure is altered, for example when there is an abnormal growth within it. We use a method of analysis that looks at the way water molecules move around the brain and this information is obtained using a Magnetic Resonance Image (MRI). From the information we gather we hope to be able to find ways to work out where important connections are and to minimise damage to them during surgery to remove these abnormalities

##### 2. **Why has my child been chosen?**

Your child has been chosen because their previous scan shows an abnormality which may involve one of the connections in their brain which we are interested in.

##### 3. **Does your child have to take part?**

No. It is up to your child and yourself to decide whether or not to take part. If you both agree, you will be given this information sheet to keep and you and your child (if appropriate) will be asked to sign a consent form. Your child will still be free to withdraw at any time and without giving a reason. A decision to withdraw at any time, or a decision not to take part, will not affect the standard of the care they receive.

##### 4. **What will happen to my child if I take part?**

Your doctor has decided that your child will need a Magnetic Resonance Imaging (MRI) scan to better understand what the abnormality shown on their previous scan is. If your child participates in the study the doctor will see them before their MRI scan. The MRI will take a little longer (approx 10-15mins) while the extra data for the study is collected. The scan itself is painless but it means lying flat inside a long tunnel while the machine takes the pictures of your child's brain. The only discomfort is that the scanner periodically generates noise. This effect can be minimised by the wearing of earplugs or headphones through which patients can listen to music. Some people feel claustrophobic in the scanner and if this happens the scan will be stopped.

If your child then has an operation and an MRI they will be seen again by the research doctor and the same extra information will be collected during their MRI. There will be no other tests.

##### 5. **What do I and my child have to do?**

There are no long term expectations simply that the Doctor see's your child before their MRI scan and then additional data is collected during their routine MRI scan.

(PTO)

Jonathan Bull MA MRCS  
Clinical Research Fellow, Radiology & Physics Unit  
Specialist Registrar Neurosurgery South Thames Rotation  
Trust  
UCL Institute of Child Health  
*always*  
30 Guilford Street, London WC1N 1EH  
tel: +44 (0)207 405 9200 ext 0354  
fax: +44 (0)20 7905 2358 / email jbull@ich.ucl.ac.uk  
[www.ich.ucl.ac.uk](http://www.ich.ucl.ac.uk)

UCL Institute of Child Health in  
partnership with Great Ormond Street  
Hospital for Children NHS

*The child first and*

6. **What are the side effects of any treatment received when taking part?**

There are no known risks from the use of Magnetic Resonance Imaging. The only other effect is that your child will have to spend a little more time in the MRI scanner. (approximately 10-15 minutes)

7. **What are the possible benefits of taking part?**

The study won't help your child directly but the information we get might help improve the treatment of children with abnormal brain scans similar to your own child's in the future.

8. **What if there is a problem?**

Any complaint about the way you have been dealt with during the study or any possible harm you might suffer will be addressed. The detailed information on this is given in Part 2.

9. **Will my child's taking part in the study be kept confidential?**

Yes. All the information about your participation in this study will be kept confidential. The details are in Part 2.

10. **Contact Details:**

If you have any concerns or further questions you can contact Jonathan Bull, Clinical Research Fellow, UCL Institute of Child Health, via Great Ormond Street switch board (0207 405 9200) on extension 0354.

**If the information has interested you and you are considering participation, please continue to read the additional information in Part 2 before making any decision.**

### **Part 2**

11. **What will happen if my child doesn't want to carry on with the study?**

You and your child can withdraw from the study at any point without giving a reason.

12. **What if there is a problem?**

If you or your child have a concern about any aspect of this study, you can speak with the researchers who will do their best to answer your questions (0207 405 9200 ex 0354). If you remain unhappy and wish to complain formally, you can do this through the NHS Complaints Procedure. Details can be obtained from the Great Ormond Street Hospital NHS Trust.

In the event that something goes wrong and your child is harmed during the research study there are no special compensation arrangements. If this harm is due to someone's negligence then you may have grounds for a legal action for compensation against UCL Institute of Child Health but you may have to pay your legal costs. The normal National Health Service complaints mechanisms will still be available to you.

13. **Will my child's taking part in this study be kept confidential?**

All research information collected about your child will be kept strictly confidential. Only the researchers involved in this study will have access to the data collected from this study. As standard practice all paediatric data is retained for up to 20 years.

14. **What will happen to the results of the research study?**

The results of this study will be published in scientific journals, no identifiable data will be reproduced.

15. **Who is organising and funding the research?**

Cancer Research UK provide funding, the doctors and the hospital will not receive payment for your specific involvement in this research.

16. **Who has reviewed the study?**

This study was given a favourable ethical opinion for conduct in the NHS by the Royal National Orthopaedic Hospital Local Research Ethics Committee.

**You will be given a copy of the information sheet and a signed consent form to keep.**

**Thank you for considering taking part and taking time to read this sheet.**

## 8.2.2 CHILDREN 5 YEARS OR LESS

### UCL INSTITUTE OF CHILD HEALTH

PATIENT INFORMATION SHEET. CHILDREN 5 OR LESS  
VERSION 2/06

### MAPPING BRAIN CONNECTIONS IN CHILDREN WITH ABNORMAL BRAIN SCANS

**This information sheet is designed to be read to your child**

#### **Why is this project being done?**

The research doctors are interested in looking at the brain and the way connections work between different parts of it and the rest of the body. They want to look at brain scans where there are abnormal growths especially

#### **Why me?**

The research doctors want to look at your scans because your other scans are different to normal and they want to know more about the differences

#### **Do I have to take part?**

You don't have to take part if you don't want to.

#### **What will happen to me if I take part in the research?**

- If you take part you the doctor will see you before your scan and the scan will take a little longer (about 10 -15 minutes extra).
- Sometimes people have medication before the scan which makes them sleepy and they sleep through the scan.
- Once the scans are done you won't have to have any other tests for the study

#### **Might anything else about the research upset me?**

The scan itself doesn't hurt but it means lying flat inside a long tunnel while the machine takes the pictures of your brain. The only discomfort is that scanner is noisy but you can use earplugs or listen to music through headphones while it happens.

#### **Will joining in help me?**

The study won't help you directly but the information we get might help treat young people with abnormal brain scans better in the future.

#### **Will anyone else know I'm doing this?**

Yes your details will be kept private. None of the information about you will be released and all the data will not be identifiable.

#### **What if I don't want to do the research anymore?**

If at any time you don't want to do the research anymore, just tell your parents, doctor or nurse. They will not be cross with you.

---

**Jonathan Bull MA MRCS**  
*Clinical Research Fellow, Radiology & Physics Unit*  
*Specialist Registrar Neurosurgery South Thames Rotation*  
Trust  
UCL Institute of Child Health  
*always*  
30 Guilford Street, London WC1N 1EH  
tel: +44 (0)207 405 9200 ext 0354  
fax: +44 (0)20 7905 2358 / email [jbull@ich.ucl.ac.uk](mailto:jbull@ich.ucl.ac.uk)  
[www.ich.ucl.ac.uk](http://www.ich.ucl.ac.uk)

UCL Institute of Child Health in  
partnership with Great Ormond Street  
Hospital for Children NHS

*The child first and*

**TESTS: HAVING AN MRI**



The scanner is like a huge box with a tunnel through the middle. All you have to do is lie down on a special bed, which moves into scanner. Mum and dad can stay with you. Nothing will touch you but it is very noisy!

**Any questions?**

Contact us now

Jonathan Bull Ex 0354



## 8.2.3 CHILDREN 6 TO 12 YEARS

### UCL INSTITUTE OF CHILD HEALTH

PATIENT INFORMATION SHEET. CHILDREN 6-12  
VERSION 2/06

### MAPPING BRAIN CONNECTIONS IN CHILDREN WITH ABNORMAL BRAIN SCANS

#### 1. What is research? Why is this project being done?

Research is a careful experiment to find out the answer to an important question. This project is a test to see if it is possible to map out the important connections in the brain and to see how they change when the brain has things like abnormal growths

#### 2. Why have I been asked to take part?

We are asking you to take part in this study as your previous scan shows an abnormality that may involve one of the connections that we are interested in.

In total we expect to look at about 60 children all of whom, like you, will be having a routine MRI scan.

#### 3. Did anyone else check the study is OK to do?

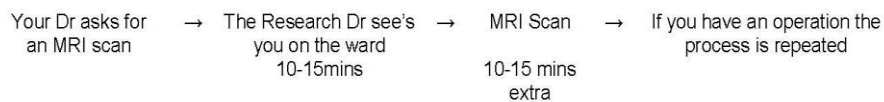
Before any research is allowed to happen, it has to be checked by a group of people called an Ethics Committee. They make sure that the research is OK to do. Your project has been checked by the **Royal National Orthopaedic Hospital Local Research and Ethics Committee**

#### 4. Do I have to take part?

No, you don't have to take part if you don't want to

#### 5. What will happen to me if I take part in the research?

- If you take part you will be seen by a doctor before your scan and the scan will take a little longer than the basic scan (about 10 -15 minutes extra).
- Sometimes people have medication before the scan which makes them sleepy and are asleep during the scan.
- Once the scans are done you won't have to have any other tests for the study
- The diagram below shows you what will happen



#### 6. Might anything else about the research upset me?

- The scan itself is painless but it means lying flat inside a long tunnel while the machine takes the pictures of your brain. The only discomfort is that scanner is noisy but you can use earplugs or listen to music through headphones during the scan.
- Some people don't like being in the scanner feel and if this happens the scan will be stopped.

#### 7. Will joining in help me?

The study won't help you directly but the information we get might help treat young people with similar abnormal brain scans more accurately and safely in the future.

**Jonathan Bull MA MRCS**  
Clinical Research Fellow, Radiology & Physics Unit  
Specialist Registrar Neurosurgery South Thames Rotation  
Trust  
UCL Institute of Child Health  
*always*  
30 Guilford Street, London WC1N 1EH  
tel: +44 (0)207 405 9200 ext 0354  
fax: +44 (0)20 7905 2358 / email jbull@ich.ucl.ac.uk  
[www.ich.ucl.ac.uk](http://www.ich.ucl.ac.uk)

UCL Institute of Child Health in  
partnership with Great Ormond Street  
Hospital for Children NHS

*The child first and*

(PTO)

**8. What if something goes wrong during the project?**

If there are any problems you can talk to the research Doctors or you want other help it can be arranged through the hospital

**9. Will my medical details be kept private if I take part? Will anyone else know I'm doing this?**

Yes your details will be kept private. None of the information about you will be released and all the data will not be identifiable.

**10. What if I don't want to do the research anymore?**

If at any time you don't want to do the research anymore, just tell your parents, doctor or nurse. They will not be cross with you.



**TESTS: HAVING AN MRI**



The scanner is like a huge box with a tunnel through the middle. All you have to do is lie down on a special bed, which moves into scanner. Mum and dad can stay with you. Nothing will touch you but it is very noisy!

**Any questions?**  
Contact us now

Jonathan Bull Ex 0354

## 8.2.4 CHILDREN 13 YEARS PLUS

## UCL INSTITUTE OF CHILD HEALTH

PATIENT INFORMATION SHEET, CHILDREN 13-15  
VERSION 2/06

**MAPPING BRAIN CONNECTIONS IN CHILDREN WITH ABNORMAL BRAIN SCANS**

- We are asking if you would agree to take part in a research project to look at the connections within the brain and how they are changed when the brain's structure is altered by, for example, abnormal growths.
- Before you decide if you want to be included it is important to understand why the research is being done and what it will involve for you. So please read this leaflet carefully. Talk about it with your family, friends, doctor or nurse if you want to.

Thank you for reading this.'

**1. Why are we doing this research?**

In order for the brain to work normally it is essential that different parts of the brain are connected to each other and that there are connections between the brain and the rest of the body. These connections enable the brain to control things like movement, speech and sight. Often these connections are affected by changes in the brain's structure due to, for example, abnormal growths. Often it is necessary to have an operation to remove these growths. When the surgeon carries out the operation they may not know exactly where all the important connections are. This can mean that not as much of the growth is removed or sometimes that the important connections are damaged. We hope to use the data from the study to map out where the important connections are and how any growth involves them. This information would be useful to surgeons to work out the best way to treat their patients in the future.

**2. What is the procedure that is being tested?**

We are using information collected from your Magnetic Resonance Imaging (MRI) scan which shows us the way that water molecules move around the brain's structure. From this information we can use a computer technique called "tractography" which analyses these water movements to map out the connections within the brain.

**3. Why have I been asked to take part?**

You have been chosen as your previous brain scan shows an abnormality which your doctors want to look at further using an MRI scan and which may involve one of the connections which we are interested in. In total we expect to look at about 60 children all of whom, like you, will be having a routine MRI scan here.

**4. Do I have to take part?**

No! It is up to you. If you do,

- your doctor will ask you to sign a form giving your consent or assent.
- you will be given a copy of this information sheet and your signed form to keep
- **you are free to stop taking part at any time during the research without giving a reason.** If you decide to stop, this will not affect the care you receive.

**5. What will happen to me if I take part?**

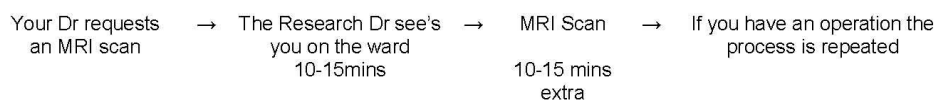
Your doctor has already decided that you need an MRI scan to better understand the abnormality on your previous scan. If you take part you will be seen by a doctor before your scan and the scan will take a little longer than your previous scan (about 10 -15 minutes extra). The MRI scan is probably different to your previous scan. The scan itself is painless but it means lying flat inside a long tunnel while the machine takes the pictures of your brain. The only discomfort is that the scanner periodically generates noise. (PTO) This effect

**Jonathan Bull MA MRCS**  
*Clinical Research Fellow, Radiology & Physics Unit*  
*Specialist Registrar Neurosurgery South Thames Rotation*  
Trust  
UCL Institute of Child Health  
*always*  
30 Guilford Street, London WC1N 1EH  
tel: +44 (0)207 405 9200 ext 0354  
fax: +44 (0)20 7905 2358 / email jbull@ich.ucl.ac.uk  
[www.ich.ucl.ac.uk](http://www.ich.ucl.ac.uk)

UCL Institute of Child Health in  
partnership with Great Ormond Street  
Hospital for Children NHS

*The child first and*

can be minimised by the wearing of earplugs or headphones through which you can listen to music. Some people feel claustrophobic in the scanner and if this happens the scan will be stopped. If you then have an operation and need an MRI afterwards the doctor will come and see you again and we will collect the extra information during your scan. There will be no other tests or visits to hospital. The diagram below shows you what will happen



### **6. What will I be asked to do?**

There are no expectations other than your agreement to take part in the study and to consent to a further brief clinical examination. The additional information is collected during your routine MRI scan

### **7. Is there anything else to be worried about if I take part?**

There are no known risks from the use of Magnetic Resonance Imaging. The main effect is that you will have to spend a little more time in the MRI scanner. (approximately 10-15 minutes)

### **8. What are the possible benefits of taking part?**

The study won't help you directly but the information we get might help treat young people with similar abnormal brain scans more accurately and safely in the future.

### **9. Contact Details:**

If you have any concerns or further questions you can contact Jonathan Bull, Clinical Research Fellow, UCL Institute of Child Health, via Great Ormond Street switch board (0207 405 9200) on extension 0354.

***Thank you for reading so far – if you are still interested, please go to Part 2:***

### **Part 2 - more detail – information you need to know if you still want to take part.**

### **10. What if there is a problem or something goes wrong?**

MRI is considered to be very safe and we do not think that there should be any significant risks from this research. If you were to be unhappy or have any questions you can contact me by phone **(0207 405 9200 ex 0354)**. If you were still unhappy formal complaints can be made through the hospital's Patient Advice and Liaison Service (PALS). Your parents will be able to help you with this.

### **11. Will anyone else know I'm doing this?**

All information which is collected about you during the course of the research will be kept strictly confidential. Any information about you which leaves the hospital will have your name and address removed so that you cannot be recognised from it.

### **12. Who is organising and funding the research?**

This research is funded by Cancer Research UK. Neither the doctors involved nor the hospital will receive any payment for your specific involvement in this research

### **13. Who has reviewed the study?**

Before any research goes ahead it has to be checked by an Ethics Committee. They make sure that the research is OK to do. Your project has been checked by the Royal National Orthopaedic Hospital Local Research Ethics Committee'

**Thank you for reading this – please ask any questions if you need to..**

## 8.3 CONSENT FORMS

### 8.3.1 PARENTS CONSENT

REC No. 04

Version 1, dated 17-Jan-10

Great Ormond Street Hospital for Children NHS Trust and Institute of  
Child Health Research Ethics Committee

**Consent Form for PARENTS OR GUARDIANS  
of Children Participating in Research Studies**

**MAPPING BRAIN CONNECTIONS IN CHILDREN WITH  
ABNORMAL BRAIN SCANS**

**NOTES FOR PARENTS OR GUARDIANS**

1. Your child has been asked to take part in a research study. The person organising that study is responsible for explaining the project to you before you give consent.
2. Please ask the researcher any questions you may have about this project, before you decide whether you wish to participate.
3. If you decide, now or at any other stage, that you do not wish your child to participate in the research project, that is entirely your right, and if your child is a patient it will not in any way prejudice any present or future treatment.
4. You will be given an information sheet which describes the research project. This information sheet is for you to keep and refer to. *Please read it carefully.*
5. If you have any complaints about the way in which this research project has been or is being conducted, please, in the first instance, discuss them with the researcher. If the problems are not resolved, or you wish to comment in any other way, please contact Emma Pendleton (R&D Office, Room 110, UCL Institute of Child Health WC1N 1EH) or if urgent, by telephone on 0207 905 2844.

**CONSENT**

I/We \_\_\_\_\_, being the parent(s)/guardian(s) of  
\_\_\_\_\_ agree that the Research Project named above has been  
explained to me to my/our satisfaction, and I/We give permission for our child to take part  
in this study. I/We have read both the notes written above and the Information Sheet  
provided, and understand what the research study involves.

**SIGNED (Parent (s)/Guardian (s) )      PRINTED      DATE**

-----  
**SIGNED (Researcher)      PRINTED      DATE**  
-----

REC No. 04

Version 1, dated 17-Jan-10

REC No. 04

Version 1, dated 17-Jan-10

**NOTES FOR THE RESEARCHER**

It is your responsibility to ensure that the parents/guardians and child (if mature enough) understand what the research project involves, both theoretically and practically. **You must allow sufficient time to do this.** You must make the judgement of whether or not the child can understand the project. Age alone is not important. Make sure that the relatives or child can contact you if they have additional questions.

A copy of this completed form must be placed in the patient's clinical records and a copy must be kept by you with the research records.

If there are any unforeseen ethical problems with this study you must inform [a representative of the sponsor] and follow this up in writing.

REC No. 04

Version 1, dated 17-Jan-10

## 8.3.2 PATIENTS ASSENT FORM

REC No. 04

Version 1, dated 23-Jan-10

Great Ormond Street Hospital for Children NHS Trust and Institute of  
Child Health Research Ethics Committee

**Assent Form for CHILDREN Participating in Research Studies**

**MAPPING BRAIN CONNECTIONS IN CHILDREN WITH**  
**ABNORMAL BRAIN SCANS**

**NOTES FOR CHILDREN**

1. You have been asked to take part in some research. The person organising that study must explain the project to you before you agree to take part.
2. Please ask the researcher any questions you like about this project, before you decide whether to join in.
3. If you decide, now or at any other time, that you do not wish to be involved in the research project, just tell us and we will stop the research. If you are a patient your treatment will carry on as it would normally.
4. You will be given an information sheet which describes the research. This information is for you to keep and refer to at any time. *Please read it carefully.*
5. If you have any complaints about the research project, discuss them with the researcher. If the problems are not resolved, or you wish to comment in any other way, please contact Emma Pendleton (R&D Office, Room 110, UCL Institute of Child Health WC1N 1EH, 0207 905 2844)

**ASSENT**

I \_\_\_\_\_ agree that the Research Project named  
above has been explained to me to my satisfaction, and I agree to take part in this study.  
I have read both the notes written above and the Information Sheet about the project, and  
understand what the research study involves.

<b>SIGNED</b>	<b>PRINTED</b>	<b>DATE</b>
-----	-----	-----
<b>SIGNED (Researcher)</b>	<b>PRINTED</b>	<b>DATE</b>
-----	-----	-----

REC No. 04

Version 1, dated 23-Jan-10

## 8.3.3 PATIENTS CONSENT FORM

REC No. 03

Version 1, dated 23-Jan-10

Great Ormond Street Hospital for Children NHS Trust and Institute of  
Child Health Research Ethics Committee

Consent Form for PARTICIPANTS in Research Studies

**MAPPING BRAIN CONNECTIONS IN CHILDREN WITH**  
**ABNORMAL BRAIN SCANS**

**NOTES FOR PARTICIPANTS**

1. You have been asked to take part in some research. The person organising that study must explain the project to you before you agree to take part.
2. Please ask the researcher any questions you like about this project, before you decide whether to join in.
3. If you decide, now or at any other time, that you do not wish to be involved in the research project, just tell us and we will stop the research. If you are a patient your treatment will carry on as normal.
4. You will be given an information sheet which describes the research. This information is for you to keep and refer to at any time. *Please read it carefully.*
5. If you have any complaints about the research project, discuss them with the researcher. If the problems are not resolved, or you wish to comment in any other way, please contact Emma Pendleton (R&D Office, Room 110, UCL Institute of Child Health WC1N 1EH) or if urgent, by telephone on 0207 905 2844 and the administration will put you in contact with her.

**CONSENT**

I \_\_\_\_\_ agree that the Research Project named  
above has been explained to me to my satisfaction, and I agree to take part in this study.  
I have read both the notes written above and the Information Sheet about the project, and  
understand what the research study involves.

**SIGNED**

**PRINTED**

**DATE**

-----

-----

-----

**SIGNED (Researcher)**

**PRINTED**

**DATE**

-----

-----

-----

REC No. 03

Version 1, dated 23-Jan-10



## 8.4 PAEDIATRIC MRI SEDATION PROTOCOLS

GREAT ORMOND STREET HOSPITAL

MRI NURSE LED SEDATION UNIT

### **SEDATION PROTOCOL:**

#### **Patient Preparation**

All patients must:

- Have hospital notes
- Be weighed
- Have local anaesthetic cream applied
- Be fasted: 4 hours for food/milk, 2 hours for clear fluids / breast milk
- Have baseline observations recorded inc. SPO2
- A metal check must be completed
- A full patient assessment should be conducted to establish suitability for sedation
- Sleep deprivation should be encouraged

Ward patients must be accompanied by a parent / guardian AND a ward nurse

#### **General Protocol**

- Small infants under 5 kgs = feed and wrap
- Co-operative children of any age: may be persuaded to lie still without sedation, please seek the assistance of play therapist (bleep 0395)
- Children with severe developmental delay, behavioural difficulties, OR over the age of 8 may need a GA
- All other patients should be considered for sedation

#### **Sedation Medications**

Under 5 kgs	-Nil, feed and wrap
5-15 kgs	-Chloral Hydrate 100mg/kg (max 1 g)
12-20 kgs	-Triclofos 100mg/kg (max 2 g) + Alimemazine 2mg/kg (max 60 mg)
20 kgs +	-Triclofos 100mg/kg (max 2g) + Alimemazine 2 mg/kg (max 60 mg)

#### **Intravenous 'Top-Up'**

To be considered if oral sedation is not effective after 45-60 minutes

IV Diazemuls 1mg/kg (max dose 20mg)

[Given slowly, in increments. Refer to PGD]

#### **Sedation Reversal**

Flumazenil 10-20 mcg/kg

#### **Audit and Record keeping**

A full history of events must be documented in the child's medical notes.

All audits for the MRI unit must be completed.

RISS should be updated with medications given and effectiveness of sedation process

August 2007

Reproduced with the permission of the Great Ormond Street Radiology Department

## 8.5 ADC HISTOGRAM PROTOCOL INSTRUCTIONS

### 8.5.1 DISPIMAGE ANALYSIS COMPUTER PROTOCOLS

#### **Original Data from scanner**

- Data retrieved as ADC and b0, b500, b1000 images from scanner, un-separated
- Scanner data processed through Python to separate files
- Use processed files to transfer to Unix
- Create folder for each Patient using # and two initials
- Create directory in GOS\_ADC\_DATA directory on Unix
- Transfer data to such

#### **xdispdc**

- On Unix terminal open directory of group of patients
- Open xdispdc (analyse as DICOM image)
- Open in prompt directory of patient E.g. >01LA
- **Select one slice and right click, opens menu, (or triple left click)**
- Select Full screen option
- NB it is possible to change the window setting of the image using the bar
- Initially there are 4 volumes of 20 images, b0, b500, b1000, b0-1000 (ADC)
- Use of ROIs on the b0 images

#### **Draw ROIs on b0 image**

- Click on regions option on the control panel
- If questioned, choose unconstrained zoom (constrained zoom picks a small area, if necessary)
- Automatic function possible, doesn't work
- Contour picks out margin
- **Use irregular option and draw around the region (NB specifics)**
- If region not accurate, erase using middle mouse button
- Care not to include extraneous areas particularly CSF
- Click on close
- Ensure that the 1<sup>st</sup> ROI drawn is the most inferior slice
- (Program later requests which slice to start from hence significance)
- Don't change the region file leave it as #initials.roi
- At the description prompt;
- Save the ROI as roi\_# where # is the number of the slice (usually from 1 to 20)
- ROI is saved, click on accept
- Now possible to draw further ROIs
- xdispdc image volumes must be continuous
- Do not use 2 ROIs on 1 slide
- Possible to join ROIs on same slice with a thin bridge roi
- Once ROIs drawn click on **store**
- *Ensure that the directory it is saved in is the same as the current Pt*

- *Saved as .roi file*

### **Working on ADC map**

- Open ADC map,
- NB triple click on mouse toggles between single and multiple images
- Open ROIs onto ADC map individually
- Ensure slice of ADC map coincides with the ROI slice number
- Accept each ROI individually
- Once all accepted
- Click on volume
- Decide on ADC image slices and in image slices prompt add the #'s of the start and end slice
- Start region prompt, add # 1, hence ROIs must be in order
- Click on Histo
- Histogram width, change bin to 5
- Save data as Histo\_#.txt in same directory
- >/home/mri/GOS\_ADC\_DATA/ASTRO/01LA/
- NB check Histogram is using all the ROIs and not just a single ROI
- (Possible to test this in the volume section by changing slice #'s and examining histogram.
- Transfer the histogram detail to PC and open in excel file.
- Data can then be interpreted in the excel file

### **Errors**

- On repeated opening of a file in xdispimage multiple copies of the data may appear.
- A file called dispdcm.idx should be deleted from the directory where the DICOM images are stored to resolve this between sessions

## 8.5.2 PROTOCOL FOR DRAWING ADC ROIS

- Outline drawn on b0 image
- Scroll through the image to visually assess the lesion
- Adjust the window level on the image to better visualise the contrast between areas of the lesion
- Using the regions tool, irregular margin option, delineate the margin
- Starting with the most inferior slice draw around the lesion on the b0 image
- Attempt to exclude areas of CSF but include cystic parts of the lesion
- Where uncertainty exists exclude the region (**Exclude cysts as per Dan Tozer paper**)
- Draw one continuous line around the lesions contour
- If greater than one ROI, link the ROIs by a narrow bridge ROI across the image
- If multiple lesions, pick the most significant lesions
- Attempt to exclude areas that appear simply oedematous
- Don't look at ADC map prior to drawing the ROI
- Once a satisfactory contour is achieved save the ROI as roi\_# of slice
- Repeat this process for each slice with the lesion apparent
- Saving each ROI with reference to its slice
- Once all ROIs drawn, save whole file as e.g. 05DM/05DM.roi
- Close the b0 image and open the ADC map
- Using the regions option, open the saved ROIs on the corresponding slice of the ADC map
- Review the ROI on the ADC image of the tumour, if acceptable click on accept
- Once all ROIs are accepted, choose volume option
- Select the slices in question and select start with roi 1
- Outputs data for mean and Standard Deviation(SD), save this as e.g. 05DM/05DM.vol
- Clicking on histo, outputs a histogram with a median
- The bin width can be adjusted, 2 is the standard width
- Save the histo under the path with the name histo\_05DM\_bin2.csv
- (csv, comma separated values, ideal for import into excel)
- This process can be repeated using the control white matter
- Data for WM is saved with the suffix \_WM
- Use the rectangular option, default. Outputs fixed size rectangle
- Place rectangle over contralateral normal WM
- Attempt to select the same slices and number to match the WM sample
- Repeat the process as above for the WM slices

## 8.6 TRACTOGRAPHY PROTOCOL INSTRUCTIONS

### 8.6.1 DTI ANALYSIS COMPUTER PROTOCOLS

#### **Original CD Data (Post co-ord change, i.e. All KR data & post Nov 06)**

- Using Matlab & “DA” program
- Open Matlab
- At the prompt edu>> cd \dti
- Edu>> edit fscript
- Modify fscript as below for each file to be processed
- Reproduce line goshdatt as many times as required for number of files
- Files will be output as \_Deff \_MD \_FA

FSCRIPT

```
% script to process Siemens DICOM files
% Copy the goshdatt line below as many times as you like, changing the
% inputs to suit.
% For each scan, place all diffusion DICOM files in one folder (there
can
% be other DICOM files in the folder and these will be ignored).
% The code will generate Analyze files and put them in a folder
% you specify with names you specify.
%
% In the example below, c:\data\MR2\AP\postop\08181833
% is the name of the folder with the DICOM diffusion files,
% postop is the stem of the files created i.e. you will get
% Analyze files called postop_FA, postop_MD and postop_Deft.
% c:\Temp is the folder where the Analyze files are written.

% You also get one other large .mat file which you can delete
% if you wish. The _FA and _MD can be read with MriCro.

goshdatt('D:\ICHData\028_FApatient_130307\03131444','FA028_D
TI','D:\ICHData\028_FApatient_130307', 15)
```

- Modify entries as required, where first part is the path to the source file with the raw data;  
'D:\ICHData\028\_FApatient\_130307\03131444'
- The second part is the name of the stem of the output,  
'FA028\_DTI'
- The final part is the destination file path where the output files will be written

'D:\ICHData\028\_FApatient\_130307'

- Now proceed to Tractography stage

### **Masking (new goshdatt.m)**

- Add a number to the call to goshdatt, setting a mask to remove the background
- The mask is all pixels in the B0 with intensity < the maximum divided by 15.
- The value is variable and could fail if there is a very bright pixel in the B0 (in which case the mask might be too aggressive and remove real tissue)
- Check the MD after processing for missing tissue.

### **Original CD Data (Pre Change of Co-ordinates i.e. pre Nov 06)**

- Make copy into folder ICH data. Create new folder in format
  - CD#\_initialsurnameDDMMYY(of scan)
  - E.g. **001\_ZZappa\_010507** (for Zappa scan on 1<sup>st</sup> May 2007)
- Open "My computer"
- E. drive, right click, "explore"
- Cut and paste original images only to folder 001\_ZZappa\_010507
- Leave numeric name unchanged

### **Reformatting ICH Data**

- Re-label with <Python> programme using "Rearrange"
- Must have created a destination folder previously (in ICH Data) (CD#\_ID\_DDMMYY)
- Name Source and Destination folder
- Destination folder format: Initials 1<sup>st</sup> & last(CD#)\_Python
- E.g.: **ZZ001\_Python**
- NOTE NUMBER OF IMAGES per volume 45 or 50
- Divide folder into the 3 Groups of Averages
- Highlight all files from 1<sup>st</sup> b0 image (0008 ep\_b0 0001.dcm)
- To last b1000 dirn 19 image 45 or 50 (0008 ep\_b1000#19 0050.dcm)
- Save as new file "**ZZ001\_Python\_Av1**" or 2 or 3
- **NB only change name up to name\_Python\_Av1**
- **Where name reads PC008\_PreOp\_Python\_Av1**
- **Only prefix up to black is changeable and this must be consistent including the name in the ICHDATA directory**

**Using MriCro to convert DICOM to Analyze**

- Convert to Analyze format using mriCro
- In mriCro. Import > Convert foreign to Analyze

Number of files: # of Volumes (20 directions & b0) x # of slices

945 = 21 x **45 or 50 (early or later scans)**

Number of volumes = # of directions + b0 image (i.e. usually 20 + 1)

- Accept all other parameters
- When prompted open "ICH data", select file format "ZZ001\_Python\_av1 or 2 or 3"
- Highlight first image
- When prompted new file name is format "**ZZ001\_mricro\_Av1**"
- Create new folder in "001\_Zappa\_010507" name "**ZZ001\_mricro\_Averages**"
- Repeat for 3 Averages
- Save all 6 analyze files (3 x Header & Images) in file "ZZ001\_mricro\_Averages"

**FA & MD maps (Unix) diff\_DTI\_GE**

- Open FTP program, ensure logged onto Sun as "mri"
- Programs and files must be put into directory **/home/mri**
- Copy the files from "ZZ001\_mricro\_Averages" into the directory
- Use programme: **diff\_DTI\_GE**
- Instructions found by \$diff\_DTI\_GE & press return
- Generic output name is format **ZZ001\_DTI**
- # Images: **3** (i.e. 3 averages)
- # b0 images: **1**
- # directions: **20**
- Direction file **encoding\_Avanto\_20.b**
- Image files **ZZ001\_mricro\_Av1 / 2 / 3** without file extensions
- Output file found in /home/mri once you have **refreshed the FTP**
- Transfer files back to folder on PC **001\_ZZappa\_010507**
- **Make copy of this file on portable hard drive**
- **Delete all transferred and produced files from Sun**
- MD & FA maps can be viewed through mriCro on PC

## 8.6.2 TRACTOGRAPHY COMPUTER PROTOCOLS

**Colour Maps**

- Working in home/mri/DATA
- **inv\_measure\_direction**
- Omit **\_deff** from file name and ignore **.img** extension instruction
- Representation type 4 (absolute value)
- Anisotropy type 2 (fractional anisotropy)
- Gamma value (amt of colour saturation) 0.8-1.25 use **1.0**
- Transfer the FA maps to home/mri/DATA
- View in mri3dX, Parameters to display Colour direction map onto FA
- **>readHDR <file name.hdr) to obtain Header info inc Image dimensions (if unknown or different from normal)**
- >zero (programme to achieve above)
- **\$zero 96 96 50 2.5 2.5 2.5 0 8 (i.e. image size, voxel size, orientation code, #of bits) Configured as zero1.img**
- **If 45 slices must reconfigure file as 45 slices e.g. zero2.img**
- >mri3dX zero1.img -3 -axial (resize doesn't work)
- mri3dX, shade-> go to files -> load new shade (should see new shade file created)
- set shade opacity to 1.0

**Creating ROI's**

- Create ROI using mriCro working on FA image of subject from which you want to work
- Save ROI as **.roi** file in mriCro
- Save ROI in SUN format (Analyze) (NB once saved as sun format (prefix "I") in front of file name)
- (NB big endian versus little endian, as Unix and PC read the program in opposite directions)
- Export ROI as analyze image to **home/mri** directory for subject
- **Each time an ROI is created, close the FA image and then reopen it afresh. If not the previous ROI will be saved in the subsequent ROI with the new ROI.**
- **Save copies of ROIs in each folder**
- Volume ROIs can be created using sequential ROIs from several slices. I.e. to segment out the peduncles of the cerebellum.
- On each change of a parameter and rerun of tractUI etc it overwrites the previous file unless the output name is changed, e.g. roi1\_1FA02 to roi1\_1FA03



### Naming format for ROI's

- **roi1\_1** or sequential number depending on the previous roi
- exclusion ROI, **roiExc\_1**
- Each set of ROIs to be saved in the `??_mri_micro_Averages` file
  
- ON UNIX MACHINE
- **>touch areas1.roi , areas2. noareas.roi** etc (touch = create file)
- (Only need to perform this **roi** , once for each subject analysis, NB save them in same directory as initial subject data)
- **nedit** (*open text file*) **areas1.roi** & (*amphisant allows program to run in background*)
- in text file type; **Image I(name of file).img**
- Save subsequent ROI's in file: **areas2.roi**
- Exclusion ROI's in file: **noareas.roi**
- Same procedure to save other ROIs,
- It is pos to save more than one ROI in each file
- EACH TIME ROI CHANGED, rerun **tractUI\_shapeFA5** and **process below**
  
- To run some tractography programs it requires whole brain tractography data, to do this leave the **areas.roi files empty** and it will calculate the values for the whole brain
- When choosing names of roi's save as **roi1\_\$1** where \$1 are sequential numbers. End up with **lroi1\_\$n.img** in batch file))

### Unix nedit function

- If editing text files on dos they must be converted to Unix format to remove any edit marks
- Transfer text file to Unix machine
- Use program **dos2unix**
- **\$ dos2unix file\_1 file\_2** (i.e. name must change)
- **Make executable (\$ chmod u+x file\_2)**

### Tractography

- For Data after 30/11/06. i.e. Processed via David Atkinson program
- Use the `tract_program1_mult` program
- In the batch file new lines of code;
- `Image_multiplier 0.000001 0.0001 $1_DTI_DeFF.img`
- `mv mult_$1_DeFF.img $1_DTI_DeFF.img`
- `mv mult_$1_DeFF.hdr $1_DTI_DeFF.hdr`
- (Allows the data to be run in the usual form)
- `Invariant_calc $1_DTI.img 1.0`

### Tractography

- NB > **tcsh**

- > tractUI\_shapeFA5
- >tractUI\_shapeFA5 <file name> <file output name E.g. .WB for whole brain or roi\_a for 1<sup>st</sup> set of ROIs)
- Parameters <vect step size (1)>
  - <angle termination in degrees (90)>
  - <high or low res, high (0)>
  - <FA or tensor shape (0)>
  - <FA or tensor threshold (0.05)>
- File used is .deff file from previous processing. But omit extension  
E.g. <JA014\_Pre\_deff> becomes <JA014\_Pre>
- > **tractUI\_shapeFA5 JA014\_Pre roi\_a 1 90 0 0 0.05**
- Takes approx 10mins
- NB when naming the output file, keep it simple as the program reduplicates the name, e.g. name it **roi1\_a** or if specific low or high res **roi1HR\_a** or for FA 0.2 and high res **roi1FA02HR\_a**
- However this information is saved in the output seed image.
- E.g. for JA014\_Pre using ROIs “a” low resolution, FA 0.22
- **JA014\_Pre\_roi\_a\_v1.0\_a90.0\_fa0.22\_seed\_roi\_255.vect**

- **Use of higher FA values to discriminate for specific tracts. Also Higher FA's speeds up the process**
- When doing initial experimental processing use the low resolution version, once happy with the FA run as high resolution to get fuller results. (slower)
- To view output use +-
  - > **tractUI\_fromseed\_char** (compresses tractography output to allow it to run on unix without crashing)
  - **tractUI\_fromseed\_char** <file name, no ext> <seed file =output of above>
    - <(1) vect step size>
    - <(90) angle term(90 = no angle)>
    - <(0) Dec or Sec, colour directions>
    - <(0) high or low resolution 0 or 1>
    - <(0) FA or tensor shape 0 or 1>
    - <(0.05) FA or tensor shape threshold>
    - <(1) ROI size threshold (1mm)
  - > **tractUI\_fromseed\_char JA014\_Pre JA014\_Pre\_roi\_a\_v1.0\_a90.0\_fa0.22\_seed\_roi\_255.vect 1 90 0 1 0 0.22 1**
  - **for a file with angle term 90, low resolution (1), FA 0.22**
  - Output is as **.vect file** (takes approx 30sec)
  - > **GeomView &**
  - Click on files and open **.vect file**
  - **Ideally displays tract**

### Production of Images with Overlay of tracts on MR slices

#### **noflood\_colour\_seg3 / noflood\_segnew4**

- NB on mriCro set size to 1mm and origin voxel to 0 (to avoid -ve values)

- Allows info at foot of mriCro panel to correspond to voxel x,y,z
- NB all Tom's programmes require whole brain tractography 1<sup>st</sup> to be performed  
(High resolution option provides this in tractUI\_shapeFA5)
- **>geomview\_isosurface** <name of .img file> <isosurface intensity (0.5)>  
<colour (as red green blue 1/0 1/0 1/0) >
- Outputs .surf file
- Surf file, slice file, tract file, load all 4 into GeomView
- Overlay tract image onto mriCro slice
- Find .vect file
- **>tract\_anatomy** <input.vect file> <image dimensions x,y,z> <voxel dimensions x,y,z>
- Use either 96, 96,50 (or 45 if 45 slices) voxel 2.5 x 2.5 x 2.5 for whole voxel
- For sub voxel (recommended) 96x2.5 = **240, 240, 125** (or **112.5**) AND **1,1,1** for 1mm<sup>3</sup> voxels
- Outputs **.tract** file
- Transfer to PC and save
- MriCro, "overlay"
- Find file and open it onto loaded image

### Use of ROIs

- Exclusion ROIs
- Can use whole slice as exclusion ROI, E.g. to avoid structures leading supratentorially. Similarly for descending structures

### tractUI\_shapeFAseedonly

- Brodman image necessary to run this
- Choose option 2 \_output.vect & \_output\_seed.img

### Zero

- **Zero** <96 96 96> <2.5 2.5 2.5> <orientation code (1)> <bit depth (8)>

### Output Slice on GeomView

- Program **output\_slice**
- output\_slice <generic.img> <x y z (co-ords of slice)> <Image colour stream> (use FA)
- Use eg **JA014\_DTI.img 0 0 14 2**
- 14 is the slice, number, to determine the slice number it is necessary to subtract  
the Z value from mriCro from the total number of slice and the remainder is the correct slice number
- program outputs file; meandiff\_ax\_40.list (for an axial slice)

### **Calculating Tract Volume, MD and FA**

- Requires output of tractUI\_fromseed\_char i.e. .vect file
- **tract\_anatomy <.vect> <size of image in mm x, y, z> <size of voxels x,y,z>**
- Image size is standard for x and y at 96 by 96 voxels
- Voxels should be isotropic, usually 2.5 x 2.5 x 2.5mm hence x and y are 240 mm x  
240mm (field of view)
- z axis depends on number of slices i.e., length is 2.5 x # of slices
- E.g.:- 45 slices, z is 2.5 x 45 = 112.5 **NB this varies from scan to scan**
- Size of voxels is done at the sub-voxel level 1 x 1 x 1 (i.e. corresponds to the dimensions picked in the tracking algorithm)
- **# tract\_anatomy .vect 240 240 112.5 1 1 1 (45 slices , 1mm voxels tracking)**
- Tract\_anatomy outputs a **\_tract.img** file
  
- To output the volume of the tract in mm<sup>3</sup>
- **tract\_volume <\_tract.img>**
- outputs .txt file (search ls \*.txt)
- open file **#cat .txt**
- **Final figure to 10 places is the volume in mm<sup>3</sup>**
- To output MD and FA, run output through tract\_stats\_TB program.

### **Snapshot (for transfer of images)**

- **sdtimage**
- snapshot screen save programme
- File menu -> snapshot
- Choose window , region, screen
- If region, use L mouse button to draw around image in question
- NB care to avoid overlapping of other windows as they will be saved as well
- Save as .tiff file in entry box
- NB there is a palette to modify the image at this stage
- Must choose file format .tiff from options
- Also **lzw** compression (assoc with the tiff file type)
- Colors; **millions**
- **Saves files into current folder**
- **FTP to PC**

### 8.6.3 BATCH FILE INSTRUCTIONS

- **tract\_program1, tract\_batch**
- (NB to open files from unix use wordpad)
- tract\_batch, tract\_program1, exist in main directory'
- command to change to directory of individual file
- ROIs must be named numerically
- For each individual (directory e.g. AD001) create the 3 ROI files in it
- areas1.roi, areas2.roi, noareas.roi

#### **tract\_batch**

- ./tract\_program1 (file-name) (number of roi's to run)
- ./tract\_program1 AD001 4
- ./tract\_program1 JD002 6 etc

#### **tract\_program1**

- Arguments written to run through whole series to output;
  - **.vect, .txt** for tract volume
  - To run with different FA values, reduplicate the file names and strings
  - Substitute in required FA values (5 points to change)
  - **Check for errors**
  - Repeat process for subsequent FA values
  - **Remain 10-15 mins to ensure running correctly**
  - Likely error is not to create the roi files in each patient directory
- 
- To include / remove terms, E.g. ROIs
  - Substitute “#” term in front of line of code concerned

#### **To run Batch file**

- Ensure all data saved for each file
- Return to /home/mri/ICHDATA or parent file
- **./tract\_batch**

## 8.6.4 BATCH FILES

```
#!/bin/csh
cd /home/mri/ICHDATA/$1
pwd
set n = 1
while ( $n <= $2 )
set str = "Image Iroi1_$.img"
echo $str>areas1.roi          # pipes output ('str') from 'echo' into areas1.roi
#set str = "Image Iroi2_$.img"
#echo $str>areas2.roi
#set str = "Image IroiExc_$.img"
#echo $str>noareas.roi
tractUI_shapeFA5 $1_DTI roi_$.n 1 90 0 0 0.2
tractUI_fromseed_char $1_DTI $1_DTI_roi_${n}_v1.0_a90.0_fa0.20_seed 1 90 0 0 0
0.2 1
tract_anatomy $1_DTI_$.n_$.n_$.n_v1.0_a90.0_fa0.20_seed_roi_255.vect 240
240 112.5 1 1 1
tract_volume $1_DTI_$.n_$.n_$.n_v1.0_a90.0_fa0.20_seed_roi_255_tract.img
tractUI_shapeFA5 $1_DTI roi_$.n 1 90 0 0 0.25
tractUI_fromseed_char $1_DTI $1_DTI_roi_${n}_v1.0_a90.0_fa0.25_seed 1 90 0 0 0
0.25 1
tract_anatomy $1_DTI_$.n_$.n_$.n_v1.0_a90.0_fa0.25_seed_roi_255.vect 240
240 112.5 1 1 1
tract_volume $1_DTI_$.n_$.n_$.n_v1.0_a90.0_fa0.25_seed_roi_255_tract.img
tractUI_shapeFA5 $1_DTI roi_$.n 1 90 0 0 0.3
tractUI_fromseed_char $1_DTI $1_DTI_roi_${n}_v1.0_a90.0_fa0.30_seed 1 90 0 0 0
0.3 1
tract_anatomy $1_DTI_$.n_$.n_$.n_v1.0_a90.0_fa0.30_seed_roi_255.vect 240
240 112.5 1 1 1
tract_volume $1_DTI_$.n_$.n_$.n_v1.0_a90.0_fa0.30_seed_roi_255_tract.img
tractUI_shapeFA5 $1_DTI roi_$.n 1 90 0 0 0.4
tractUI_fromseed_char $1_DTI $1_DTI_roi_${n}_v1.0_a90.0_fa0.40_seed 1 90 0 0 0
0.4 1
tract_anatomy $1_DTI_$.n_$.n_$.n_v1.0_a90.0_fa0.40_seed_roi_255.vect 240
240 112.5 1 1 1
tract_volume $1_DTI_$.n_$.n_$.n_v1.0_a90.0_fa0.40_seed_roi_255_tract.img
echo $n
@ n = $n + 1
echo $1 completed
end
unset $n
```

## 8.7 GLOSSARY

ADC	Apparent diffusion coefficient
ATRT	Atypical teratoid rhabdoid tumours
B	Magnetic field strength
Cblr	Cerebellar
CNS	Central nervous system
CPP	choroid plexus papillomas
CSF	Cerebro-spinal fluid
CST	Corticospinal tract
DEC	Directionally encoded colour
DNT	Dysembryoplastic neuroepithelial tumours
DNT	Dysembryoplastic neuroepithelial tumours
DPTA	diethylenetriaminepenta-acetic acid
DTI	Diffusion tensor imaging
DWI	Diffusion weighted imaging
Dysdi	Dysdiadochokinesia
EPI	Echo planar imaging
ETL	Echo train length
FA	Fractional anisotropy
FID	Free induction decay
FLAIR	Fluid attenuation inversion recovery
FND	Focal neurological deficit
FSE	Fast spin echo
G	Grade
GA	General anaesthetic
GOSH	Great Ormond Street Hospital
$G_{x,y,z}$	Gradient
HCG	Human chorionic gonadotrophin
I	Zeeman energy level
JPA	Juvenile Pilocytic astrocytoma
LL	Lower limb
LR	Logistic regression
M	Magnetic field vector
MD	Mean diffusivity
MRI	Magnetic resonance imaging
MRS	Magnetic resonance spectroscopy
MS	Multiple sclerosis
N/S	Not significant
NAWM	Normal appearing white matter
NC	Normal controls
NMR	Nuclear magnetic resonance
PD	Proton Density
PF	Posterior fossa
PFCS	Post Fossa Cerebellar Signs
PFN	Post Fossa No signs

PNET	Primitive neuroectodermal tumours
PNET-MB	primitive neuroectodermal tumour-medulloblastoma
PP	Past pointing
Pre-op	Pre-operative
RF	Radio frequency
ROI	Region of interest
ROI	Region of interest
S <sub>0</sub>	Signal with no diffusion gradient
S <sub>1</sub>	Signal with diffusion gradient
SE	Spin Echo
TE	Time to echo
TI	Time to inversion
TR	Time to relaxation
UL	Upper limb
αFP	Alpha feto-protein



---

## 9 REFERENCES

---

### Reference List

- (1) McIlwain HaBHS. Biochemistry and the Central Nervous system. Edinburgh: Churchill Livingstone; 1985.
- (2) Bloch F. Nuclear Induction. Physical Review 1946;70((7-8)):460.
- (3) Hahn EL. Spin Echoes. Physical Review 1950;70:460.
- (4) DeCoene D. MR of the brain using fluid-attenuated inversion recovery (FLAIR) pulse sequences. American Journal of Neuroradiology 2010;13:1555-64.
- (5) Plowman PN, Brada M. Paediatric brain tumours. Br Med Bull 1996 October;52(4):802-17.
- (6) Rao P. Role of MRI in paediatric neurooncology. Eur J Radiol 2008 November;68(2):259-70.
- (7) Chaichana KL, McGirt MJ, Niranjan A, Olivi A, Burger PC, Quinones-Hinojosa A. Prognostic significance of contrast-enhancing low-grade gliomas in adults and a review of the literature. Neurol Res 2009 November;31(9):931-9.
- (8) Apuzzo ML, Chandrasoma PT, Cohen D, Zee CS, Zelman V. Computed imaging stereotaxy: experience and perspective related to 500 procedures applied to brain masses. Neurosurgery 1987 June;20(6):930-7.
- (9) Astrakas LG, Zurakowski D, Tzika AA, Zarifi MK, Anthony DC, De GU, Tarbell NJ, Black PM. Noninvasive magnetic resonance spectroscopic imaging biomarkers to predict the clinical grade of pediatric brain tumors. Clin Cancer Res 2004 December 15;10(24):8220-8.
- (10) Tzika AA, Astrakas LG, Zarifi MK, Petridou N, Young-Poussaint T, Goumnerova L, Zurakowski D, Anthony DC, Black PM. Multiparametric MR assessment of pediatric brain tumors. Neuroradiology 2003 January;45(1):1-10.
- (11) Tzika AA, Cheng LL, Goumnerova L, Madsen JR, Zurakowski D, Astrakas LG, Zarifi MK, Scott RM, Anthony DC, Gonzalez RG, Black PM. Biochemical characterization of pediatric brain tumors by using in vivo and ex vivo magnetic resonance spectroscopy. J Neurosurg 2002 June;96(6):1023-31.
- (12) Ostertun B, Wolf HK, Campos MG, Matus C, Solymosi L, Elger CE, Schramm J, Schild HH. Dysembryoplastic neuroepithelial tumors: MR and CT evaluation. AJNR Am J Neuroradiol 1996 March;17(3):419-30.

- (13) McEvoy AW, Harding BN, Phipps KP, Ellison DW, Elsmore AJ, Thompson D, Harkness W, Hayward RD. Management of choroid plexus tumours in children: 20 years experience at a single neurosurgical centre. *Pediatr Neurosurg* 2000 April;32(4):192-9.
- (14) CBTRUS. 2007-2008 PRIMARY BRAIN TUMORS IN THE UNITED STATES STATISTICAL REPORT 2000-2004. 2008.
- (15) Louis DN, Ohgaki H, Wiestler OD, Cavenee WK, Burger PC, Jouvet A, Scheithauer BW, Kleihues P. The 2007 WHO classification of tumours of the central nervous system. *Acta Neuropathol* 2007 August;114(2):97-109.
- (16) Packer RJ, Boyett JM, Zimmerman RA, Albright AL, Kaplan AM, Rorke LB, Selch MT, Cherlow JM, Finlay JL, Wara WM. Outcome of children with brain stem gliomas after treatment with 7800 cGy of hyperfractionated radiotherapy. A Childrens Cancer Group Phase I/II Trial. *Cancer* 1994 September 15;74(6):1827-34.
- (17) National Cancer Institute. *Cancer Risks and Rates*. National Cancer Institute; 1996.
- (18) Gurney JG SMBG. *Miscellaneous intra-cranial and intraspinal neoplasms*. National Cancer Institute; 2001.
- (19) Hargrave D. Paediatric high and low grade glioma: the impact of tumour biology on current and future therapy. *Br J Neurosurg* 2009 August;23(4):351-63.
- (20) Moreno L, Bautista FJ, Zacharoulis S. Outcome of teenagers and young adults with ependymoma: the Royal Marsden experience. *Childs Nerv Syst* 2009 September;25(9):1047-52.
- (21) Merchant TE, Li C, Xiong X, Kun LE, Boop FA, Sanford RA. Conformal radiotherapy after surgery for paediatric ependymoma: a prospective study. *Lancet Oncol* 2009 March;10(3):258-66.
- (22) Nimsy C, Ganslandt O, Kober H, Buchfelder M, Fahlbusch R. Intraoperative magnetic resonance imaging combined with neuronavigation: a new concept. *Neurosurgery* 2001 May;48(5):1082-9.
- (23) Nitschke MF, Kleinschmidt A, Wessel K, Frahm J. Somatotopic motor representation in the human anterior cerebellum. A high-resolution functional MRI study. *Brain* 1996 June;119 ( Pt 3):1023-9.
- (24) Thach WT, Perry JG, Kane SA, Goodkin HP. Cerebellar nuclei: rapid alternating movement, motor somatotopy, and a mechanism for the control of muscle synergy. *Rev Neurol (Paris)* 1993;149(11):607-28.
- (25) Kandel E SJJT. *Principles of Neural Science*. 4th Edition ed. New York: McGraw-Hill; 2000.
- (26) Voogd J, Glickstein M. The anatomy of the cerebellum. *Trends Neurosci* 1998 September;21(9):370-5.

- (27) Vilis T, Hore J. Central neural mechanisms contributing to cerebellar tremor produced by limb perturbations. *J Neurophysiol* 1980 February;43(2):279-91.
- (28) Holmes G. The cerebellum of man. *Brain* 1939;62:1-30.
- (29) Albus JS. A theory of cerebellar function. *Math Biosci* 1971;10:25-61.
- (30) Marr D. A theory of cerebellar cortex. *J Physiol* 1969;202:437-70.
- (31) Carr HY, . Effects of diffusion on free precession in nuclear magnetic resonance experiments. *Physics Review* 2010;94:630-8.
- (32) Purcell E. Resonance absorption by nuclear magnetic momnets in a solid. *Physical Review* 1946;69(37).
- (33) Stejskal EO, Tanner TJ. Spin diffusion measurements: spin echoes in the presence of a time dependant field gradient. *J Chem Phys* 1965;42:2880-92.
- (34) Moseley ME, Cohen Y, Kucharczyk J, Mintorovitch J, Asgari HS, Wendland MF, Tsuruda J, Norman D. Diffusion-weighted MR imaging of anisotropic water diffusion in cat central nervous system. *Radiology* 1990 August;176(2):439-45.
- (35) Baird AE, Warach S. Magnetic resonance imaging of acute stroke. *J Cereb Blood Flow Metab* 1998 June;18(6):583-609.
- (36) Cercignani M, Horsfield MA. The physical basis of diffusion-weighted MRI. *J Neurol Sci* 2001 May 1;186 Suppl 1:S11-S14.
- (37) Dong Q, Welsh RC, Chenevert TL, Carlos RC, Maly-Sundgren P, Gomez-Hassan DM, Mukherji SK. Clinical applications of diffusion tensor imaging. *J Magn Reson Imaging* 2004 January;19(1):6-18.
- (38) Horsfield MA, Jones DK. Applications of diffusion-weighted and diffusion tensor MRI to white matter diseases - a review. *NMR Biomed* 2002;15(7-8):570-7.
- (39) Huisman TAGM. Diffusion-weighted imaging: basic concepts and application in cerebral stroke and head trauma. *Eur Radiol* 2003 October;13(10):2283-97.
- (40) Le Bihan D, Turner R, Douek P, Patronas N. Diffusion MR imaging: clinical applications. *AJR Am J Roentgenol* 1992 September;159(3):591-9.
- (41) Le Bihan D, Mangin JF, Poupon C, Clark CA, Pappata S, Molko N, Chabriat H. Diffusion tensor imaging: concepts and applications. *J Magn Reson Imaging* 2001 April;13(4):534-46.
- (42) Luybaert R, Boujraf S, Sourbron S, Osteaux M. Diffusion and perfusion MRI: basic physics. *Eur J Radiol* 2001 April;38(1):19-27.
- (43) Einstein A. About the movement of suspended particles in liquid at rest as required by the molecular theory of heat. *Annals of Physics* 1905;322:549-60.

- (44) Parker GJ. Analysis of MR diffusion weighted images. *Br J Radiol* 2004;77 Spec No 2:S176-S185.
- (45) Le Bihan D, Breton E, Lallemand D, Grenier P, Cabanis E, Laval-Jeantet M. MR imaging of intravoxel incoherent motions: application to diffusion and perfusion in neurologic disorders. *Radiology* 1986 November;161(2):401-7.
- (46) Turner R, Le Bihan D, Maier J, Vavrek R, Hedges LK, Pekar J. Echo-planar imaging of intravoxel incoherent motion. *Radiology* 1990 November;177(2):407-14.
- (47) Nicholson C, Phillips JM. Ion diffusion modified by tortuosity and volume fraction in the extracellular microenvironment of the rat cerebellum. *J Physiol* 1981 December;321:225-57.
- (48) vonMeerwall E, Ferguson RD. Interpreting pulsed-gradient spin-echo diffusion experiments with permeable membranes. *The Journal of Chemical Physics* 1981 June 15;74(12):6956-9.
- (49) Warach S, Chien D, Li W, Ronthal M, Edelman RR. Fast magnetic resonance diffusion-weighted imaging of acute human stroke. *Neurology* 1992 September;42(9):1717-23.
- (50) Warach S, Gaa J, Siewert B, Wielopolski P, Edelman RR. Acute human stroke studied by whole brain echo planar diffusion-weighted magnetic resonance imaging. *Ann Neurol* 1995 February;37(2):231-41.
- (51) Moseley ME, Kucharczyk J, Mintorovitch J, Cohen Y, Kurhanewicz J, Derugin N, Asgari H, Norman D. Diffusion-weighted MR imaging of acute stroke: correlation with T2-weighted and magnetic susceptibility-enhanced MR imaging in cats. *AJNR Am J Neuroradiol* 1990 May;11(3):423-9.
- (52) Pierpaoli C, Righini A, Linfante I, Tao-Cheng JH, Alger JR, Di CG. Histopathologic correlates of abnormal water diffusion in cerebral ischemia: diffusion-weighted MR imaging and light and electron microscopic study. *Radiology* 1993 November;189(2):439-48.
- (53) Sorensen AG, Buonanno FS, Gonzalez RG, Schwamm LH, Lev MH, Huang-Hellinger FR, Reese TG, Weisskoff RM, Davis TL, Suwanwela N, Can U, Moreira JA, Copen WA, Look RB, Finklestein SP, Rosen BR, Koroshetz WJ. Hyperacute stroke: evaluation with combined multisection diffusion-weighted and hemodynamically weighted echo-planar MR imaging. *Radiology* 1996 May;199(2):391-401.
- (54) Lutsep HL, Albers GW, DeCrespigny A, Kamat GN, Marks MP, Moseley ME. Clinical utility of diffusion-weighted magnetic resonance imaging in the assessment of ischemic stroke. *Ann Neurol* 1997 May;41(5):574-80.
- (55) Rowley HA, Grant PE, Roberts TP. Diffusion MR imaging. Theory and applications. *Neuroimaging Clin N Am* 1999 May;9(2):343-61.

- (56) Ebisu T, Tanaka C, Umeda M, Kitamura M, Naruse S, Higuchi T, Ueda S, Sato H. Discrimination of brain abscess from necrotic or cystic tumors by diffusion-weighted echo planar imaging. *Magn Reson Imaging* 1996;14(9):1113-6.
- (57) Desprechins B, Stadnik T, Koerts G, Shabana W, Breucq C, Osteaux M. Use of diffusion-weighted MR imaging in differential diagnosis between intracerebral necrotic tumors and cerebral abscesses. *AJNR Am J Neuroradiol* 1999 August;20(7):1252-7.
- (58) Guzman R, Barth A, Lovblad KO, El-Koussy M, Weis J, Schroth G, Seiler RW. Use of diffusion-weighted magnetic resonance imaging in differentiating purulent brain processes from cystic brain tumors. *J Neurosurg* 2002 November;97(5):1101-7.
- (59) Nadal DL, Herlidou S, de MG, Gondry-Jouet C, Le GD, Deramond H, Idy-Peretti I. Differential MRI diagnosis between brain abscesses and necrotic or cystic brain tumors using the apparent diffusion coefficient and normalized diffusion-weighted images. *Magn Reson Imaging* 2003 July;21(6):645-50.
- (60) Schaefer PW, Grant PE, Gonzalez RG. Diffusion-weighted MR imaging of the brain. *Radiology* 2000 November;217(2):331-45.
- (61) Castillo M, Mukherji SK. Diffusion-weighted imaging in the evaluation of intracranial lesions. *Semin Ultrasound CT MR* 2000 December;21(6):405-16.
- (62) Christiansen P, Gideon P, Thomsen C, Stubgaard M, Henriksen O, Larsson HB. Increased water self-diffusion in chronic plaques and in apparently normal white matter in patients with multiple sclerosis. *Acta Neurol Scand* 1993 March;87(3):195-9.
- (63) Larsson HB, Thomsen C, Frederiksen J, Stubgaard M, Henriksen O. In vivo magnetic resonance diffusion measurement in the brain of patients with multiple sclerosis. *Magn Reson Imaging* 1992;10(1):7-12.
- (64) Droogan AG, Clark CA, Werring DJ, Barker GJ, McDonald WI, Miller DH. Comparison of multiple sclerosis clinical subgroups using navigated spin echo diffusion-weighted imaging. *Magn Reson Imaging* 1999 June;17(5):653-61.
- (65) Liu AY, Maldjian JA, Bagley LJ, Sinson GP, Grossman RI. Traumatic brain injury: diffusion-weighted MR imaging findings. *AJNR Am J Neuroradiol* 1999 October;20(9):1636-41.
- (66) Le Bihan D, Breton E, Lallemand D, Aubin ML, Vignaud J, Laval-Jeantet M. Separation of diffusion and perfusion in intravoxel incoherent motion MR imaging. *Radiology* 1988 August;168(2):497-505.
- (67) Chien D, Buxton RB, Kwong KK, Brady TJ, Rosen BR. MR diffusion imaging of the human brain. *J Comput Assist Tomogr* 1990 July;14(4):514-20.
- (68) Tsuruda JS, Chew WM, Moseley ME, Norman D. Diffusion-weighted MR imaging of the brain: value of differentiating between extraaxial cysts and epidermoid tumors. *AJNR Am J Neuroradiol* 1990 September;11(5):925-31.

- (69) Tsuruda JS, Chew WM, Moseley ME, Norman D. Diffusion-weighted MR imaging of the brain: value of differentiating between extraaxial cysts and epidermoid tumors. *AJR Am J Roentgenol* 1990 November;155(5):1059-65.
- (70) Le Bihan D, Douek P, Argyropoulou M, Turner R, Patronas N, Fulham M. Diffusion and perfusion magnetic resonance imaging in brain tumors. *Top Magn Reson Imaging* 1993;5(1):25-31.
- (71) Schaefer PW. Applications of DWI in clinical neurology. *J Neurol Sci* 2001 May 1;186 Suppl 1:S25-S35.
- (72) Tien RD, Felsberg GJ, Lirng JF. Variable bandwidth steady-state free-precession MR imaging: a technique for improving characterization of epidermoid tumor and arachnoid cyst. *AJR Am J Roentgenol* 1995 March;164(3):689-92.
- (73) Camacho DLA, Smith JK, Castillo M. Differentiation of toxoplasmosis and lymphoma in AIDS patients by using apparent diffusion coefficients. *AJNR Am J Neuroradiol* 2003 April;24(4):633-7.
- (74) Guo AC, Cummings TJ, Dash RC, Provenzale JM. Lymphomas and high-grade astrocytomas: comparison of water diffusibility and histologic characteristics. *Radiology* 2002 July;224(1):177-83.
- (75) Kono K, Inoue Y, Nakayama K, Shakudo M, Morino M, Ohata K, Wakasa K, Yamada R. The role of diffusion-weighted imaging in patients with brain tumors. *AJNR Am J Neuroradiol* 2001 June;22(6):1081-8.
- (76) Krabbe K, Gideon P, Wagn P, Hansen U, Thomsen C, Madsen F. MR diffusion imaging of human intracranial tumours. *Neuroradiology* 1997 July;39(7):483-9.
- (77) Filippi CG, Edgar MA, Ulug AM, Prowda JC, Heier LA, Zimmerman RD. Appearance of meningiomas on diffusion-weighted images: correlating diffusion constants with histopathologic findings. *AJNR Am J Neuroradiol* 2001 January;22(1):65-72.
- (78) Horska A, Ulug AM, Melhem ER, Filippi CG, Burger PC, Edgar MA, Souweidane MM, Carson BS, Barker PB. Proton magnetic resonance spectroscopy of choroid plexus tumors in children. *J Magn Reson Imaging* 2001 July;14(1):78-82.
- (79) Sinha S, Bastin ME, Whittle IR, Wardlaw JM. Diffusion tensor MR imaging of high-grade cerebral gliomas. *AJNR Am J Neuroradiol* 2002 April;23(4):520-7.
- (80) Bastin ME, Sinha S, Whittle IR, Wardlaw JM. Measurements of water diffusion and T1 values in peritumoural oedematous brain. *Neuroreport* 2002 July 19;13(10):1335-40.
- (81) Provenzale JM, McGraw P, Mhatre P, Guo AC, DeLong D. Peritumoral brain regions in gliomas and meningiomas: investigation with isotropic diffusion-weighted MR imaging and diffusion-tensor MR imaging. *Radiology* 2004 August;232(2):451-60.

- (82) Lu S, Ahn D, Johnson G, Cha S. Peritumoral diffusion tensor imaging of high-grade gliomas and metastatic brain tumors. *AJNR Am J Neuroradiol* 2003 May;24(5):937-41.
- (83) Maier SE, Mamata H, Mulkern RV. Characterization of normal brain and brain tumor pathology by chi-squares parameter maps of diffusion-weighted image data. *Eur J Radiol* 2003 March;45(3):199-207.
- (84) Stadnik TW, Chaskis C, Michotte A, Shabana WM, van RK, Luypaert R, Budinsky L, Jellus V, Osteaux M. Diffusion-weighted MR imaging of intracerebral masses: comparison with conventional MR imaging and histologic findings. *AJNR Am J Neuroradiol* 2001 May;22(5):969-76.
- (85) Sugahara T, Korogi Y, Kochi M, Ikushima I, Shigematu Y, Hirai T, Okuda T, Liang L, Ge Y, Komohara Y, Ushio Y, Takahashi M. Usefulness of diffusion-weighted MRI with echo-planar technique in the evaluation of cellularity in gliomas. *J Magn Reson Imaging* 1999 January;9(1):53-60.
- (86) Yamasaki F, Kurisu K, Satoh K, Arita K, Sugiyama K, Ohtaki M, Takaba J, Tominaga A, Hanaya R, Yoshioka H, Hama S, Ito Y, Kajiwara Y, Yahara K, Saito T, Thohar MA. Apparent diffusion coefficient of human brain tumors at MR imaging. *Radiology* 2005 June;235(3):985-91.
- (87) Gauvain KM, McKinstry RC, Mukherjee P, Perry A, Neil JJ, Kaufman BA, Hayashi RJ. Evaluating pediatric brain tumor cellularity with diffusion-tensor imaging. *AJR Am J Roentgenol* 2001 August;177(2):449-54.
- (88) Chenevert TL, Brunberg JA, Pipe JG. Anisotropic diffusion in human white matter: demonstration with MR techniques in vivo. *Radiology* 1990 November;177(2):401-5.
- (89) Beaulieu C. The basis of anisotropic water diffusion in the nervous system - A technical review. *NMR Biomed* 2002;15(7-8):435-55.
- (90) Cleveland GG. Nuclear magnetic resonance measurements of skeletal muscle. Anisotropy of the diffusion coefficient of the intracellular water. *Biophys J* 1976;16:1043-53.
- (91) Basser PJ, Mattiello J, LeBihan D. Estimation of the effective self-diffusion tensor from the NMR spin echo. *J Magn Reson B* 1994 March;103(3):247-54.
- (92) Basser PJ, Mattiello J, LeBihan D. MR diffusion tensor spectroscopy and imaging. *Biophys J* 1994 January;66(1):259-67.
- (93) Catani M, Howard RJ, Pajevic S, Jones DK. Virtual in vivo interactive dissection of white matter fasciculi in the human brain. *Neuroimage* 2002 September;17(1):77-94.
- (94) Basser PJ. Inferring microstructural features and the physiological state of tissues from diffusion-weighted images. *NMR Biomed* 1995;8(7-8):333-44.
- (95) Westin CF, Maier SE, Mamata H, Nabavi A, Jolesz FA, Kikinis R. Processing and visualization for diffusion tensor MRI. *Med Image Anal* 2002 June;6(2):93-108.

- (96) Basser PJ, Pierpaoli C. Microstructural and physiological features of tissues elucidated by quantitative-diffusion-tensor MRI. *J Magn Reson B* 1996 June;111(3):209-19.
- (97) Pajevic S, Pierpaoli C. Color schemes to represent the orientation of anisotropic tissues from diffusion tensor data: application to white matter fiber tract mapping in the human brain. *Magn Reson Med* 1999 September;42(3):526-40.
- (98) Ciccarelli O, Catani M, Johansen-Berg H, Clark C, Thompson A. Diffusion-based tractography in neurological disorders: concepts, applications, and future developments. *Lancet Neurol* 2008 August;7(8):715-27.
- (99) Barrick TR, Clark CA. Singularities in diffusion tensor fields and their relevance in white matter fiber tractography. *Neuroimage* 2004 June;22(2):481-91.
- (100) Frank LR. Characterization of anisotropy in high angular resolution diffusion-weighted MRI. *Magn Reson Med* 2002;47(6):1083-99.
- (101) Tournier JD, Calamante F, Gadian DG, Connelly A. Diffusion-weighted magnetic resonance imaging fibre tracking using a front evolution algorithm. *Neuroimage* 2003 September;20(1):276-88.
- (102) Tournier JD, Calamante F, Gadian DG, Connelly A. Direct estimation of the fiber orientation density function from diffusion-weighted MRI data using spherical deconvolution. *Neuroimage* 2004 November;23(3):1176-85.
- (103) Tuch DS, Reese TG, Wiegell MR, Wedeen VJ. Diffusion MRI of Complex Neural Architecture. *Neuron* 2003;40(5):885-95.
- (104) Alexander DC. Multiple-fiber reconstruction algorithms for diffusion MRI. *Ann N Y Acad Sci* 2005;1064:113-33.
- (105) Behrens TEJ, Woolrich MW, Jenkinson M, Johansen-Berg H, Nunes RG, Clare S, Matthews PM, Brady JM, Smith SM. Characterization and Propagation of Uncertainty in Diffusion-Weighted MR Imaging. *Magn Reson Med* 2003;50(5):1077-88.
- (106) Behrens TEJ, Berg HJ, Jbabdi S, Rushworth MFS, Woolrich MW. Probabilistic diffusion tractography with multiple fibre orientations: What can we gain? *Neuroimage* 2007;34(1):144-55.
- (107) Johansen-Berg H, Behrens TEJ. Just pretty pictures? What diffusion tractography can add in clinical neuroscience. *Curr Opin Neurol* 2006;19(4):379-85.
- (108) Lawes INC, Barrick TR, Murugam V, Spierings N, Evans DR, Song M, Clark CA. Atlas-based segmentation of white matter tracts of the human brain using diffusion tensor tractography and comparison with classical dissection. *Neuroimage* 2008;39(1):62-79.
- (109) Meynert T. *Psychiatrie. Klinik der Erkrankungen des Vorderhirns.* Germany: 1884.
- (110) Dejerine J. *Anatomie des Centres Nerveux.* Paris: Rueff et Cie; 1895.



- (111) Ludwig E. Atlas Cerebri Humani. Basel: Karger; 1956.
- (112) Heimer J. Neuro-anatomical Tract-Tracing Methods. New York: Plenum; 1981.
- (113) Heimer J. Neuro-anatomical Tract-Tracing Methods: Recent Progress. New York: Plenum; 1989.
- (114) Cowan W. The use of Axonal Transport for Studies of Neuronal Connectivity. Amsterdam: Elsevier; 1975.
- (115) Basser PJ. Inferring microstructural features and the physiological state of tissues from diffusion-weighted images. *NMR Biomed* 1995;8(7-8):333-44.
- (116) Pajevic S, Pierpaoli C. Color schemes to represent the orientation of anisotropic tissues from diffusion tensor data: application to white matter fiber tract mapping in the human brain. *Magn Reson Med* 2000 June;43(6):921.
- (117) Coremans J, Luypaert R, Verhelle F, Stadnik T, Osteaux M. A method for myelin fiber orientation mapping using diffusion-weighted MR images. *Magn Reson Imaging* 1994;12(3):443-54.
- (118) Makris N, Worth AJ, Sorensen AG, Papadimitriou GM, Wu O, Reese TG, Wedeen VJ, Davis TL, Stakes JW, Caviness VS, Kaplan E, Rosen BR, Pandya DN, Kennedy DN. Morphometry of in vivo human white matter association pathways with diffusion-weighted magnetic resonance imaging. *Ann Neurol* 1997 December;42(6):951-62.
- (119) Basser PJ. Fiber-Tractography via diffusion tensor MRI (DT-MRI). Berkeley, CA 1998.
- (120) Basser PJ, Pajevic S, Pierpaoli C, Duda J, Aldroubi A. In vivo fiber tractography using DT-MRI data. *Magn Reson Med* 2000 October;44(4):625-32.
- (121) Conturo TE, Lori NF, Cull TS, Akbudak E, Snyder AZ, Shimony JS, McKinstry RC, Burton H, Raichle ME. Tracking neuronal fiber pathways in the living human brain. *Proc Natl Acad Sci U S A* 1999;96(18):10422-7.
- (122) Jones DK, Horsfield MA, Simmons A. Optimal strategies for measuring diffusion in anisotropic systems by magnetic resonance imaging. *Magn Reson Med* 1999 September;42(3):515-25.
- (123) Poupon C, Mangin J, Clark CA, Frouin V, Regis J, Le Bihan D, Bloch I. Towards inference of human brain connectivity from MR diffusion tensor data. *Med Image Anal* 2001 March;5(1):1-15.
- (124) Parker GJM, Haroon HA, Wheeler-Kingshott CAM. A framework for a streamline-based probabilistic index of connectivity (PICO) using a structural interpretation of MRI diffusion measurements. *J Magn Reson Imaging* 2003;18(2):242-54.
- (125) Koch MA, Norris DG, Hund-Georgiadis M. An investigation of functional and anatomical connectivity using magnetic resonance imaging. *Neuroimage* 2002 May;16(1):241-50.

- (126) Lazar M, Alexander AL. An error analysis of white matter tractography methods: synthetic diffusion tensor field simulations. *Neuroimage* 2003 October;20(2):1140-53.
- (127) Pajevic S, Aldroubi A, Basser PJ. A continuous tensor field approximation of discrete DT-MRI data for extracting microstructural and architectural features of tissue. *J Magn Reson* 2002 January;154(1):85-100.
- (128) Melhem ER, Mori S, Mukundan G, Kraut MA, Pomper MG, van Zijl PC. Diffusion tensor MR imaging of the brain and white matter tractography. *AJR Am J Roentgenol* 2002 January;178(1):3-16.
- (129) Jones DK, Williams SCR, Gasston D, Horsfield MA, Simmons A, Howard R. Isotropic resolution diffusion tensor imaging with whole brain acquisition in a clinically acceptable time. *Hum Brain Mapp* 2002;15(4):216-30.
- (130) Catani M, Howard RJ, Pajevic S, Jones DK. Virtual in vivo interactive dissection of white matter fasciculi in the human brain. *Neuroimage* 2002 September;17(1):77-94.
- (131) Mori M, Crain BJ, Chacko VP, Van Zijl PCM. Three-dimensional tracking of axonal projections in the brain by magnetic resonance imaging. *Ann Neurol* 1999;45(2):265-9.
- (132) Mori S, Oishi K, Faria AV. White matter atlases based on diffusion tensor imaging. *Curr Opin Neurol* 2009 August;22(4):362-9.
- (133) Stieltjes B, Kaufmann WE, van Zijl PC, Fredericksen K, Pearlson GD, Solaiyappan M, Mori S. Diffusion tensor imaging and axonal tracking in the human brainstem. *Neuroimage* 2001 September;14(3):723-35.
- (134) Wakana S, Jiang H, Nagae-Poetscher LM, van Zijl PC, Mori S. Fiber tract-based atlas of human white matter anatomy. *Radiology* 2004 January;230(1):77-87.
- (135) Beaulieu C, Does MD, Snyder RE, Allen PS. Changes in water diffusion due to Wallerian degeneration in peripheral nerve. *Magn Reson Med* 1996;36(4):627-31.
- (136) Papadakis NG, Murrills CD, Hall LD, Huang CL, Adrian CT. Minimal gradient encoding for robust estimation of diffusion anisotropy. *Magn Reson Imaging* 2000 July;18(6):671-9.
- (137) Lebel C, Caverhill-Godkewitsch S, Beaulieu C. Age-related regional variations of the corpus callosum identified by diffusion tensor tractography. *Neuroimage* 2010 April 1.
- (138) Verhoeven JS, Sage CA, Leemans A, Van HW, Callaert D, Peeters R, De CP, Lagae L, Sunaert S. Construction of a stereotaxic DTI atlas with full diffusion tensor information for studying white matter maturation from childhood to adolescence using tractography-based segmentations. *Hum Brain Mapp* 2010 March;31(3):470-86.
- (139) Saksena S, Husain N, Malik GK, Trivedi R, Sarma M, Rathore RS, Pandey CM, Gupta RK. Comparative evaluation of the cerebral and cerebellar white matter development in pediatric age group using quantitative diffusion tensor imaging. *Cerebellum* 2008;7(3):392-400.

- (140) Qiu D, Tan LH, Zhou K, Khong PL. Diffusion tensor imaging of normal white matter maturation from late childhood to young adulthood: voxel-wise evaluation of mean diffusivity, fractional anisotropy, radial and axial diffusivities, and correlation with reading development. *Neuroimage* 2008 June;41(2):223-32.
- (141) Deary IJ, Bastin ME, Pattie A, Clayden JD, Whalley LJ, Starr JM, Wardlaw JM. White matter integrity and cognition in childhood and old age. *Neurology* 2006 February 28;66(4):505-12.
- (142) Snook L, Paulson LA, Roy D, Phillips L, Beaulieu C. Diffusion tensor imaging of neurodevelopment in children and young adults. *Neuroimage* 2005 July 15;26(4):1164-73.
- (143) Willette AA, Bendlin BB, McLaren DG, Canu E, Kastman EK, Kosmatka KJ, Xu G, Field AS, Alexander AL, Colman RJ, Weindruch RH, Coe CL, Johnson SC. Age-related changes in neural volume and microstructure associated with interleukin-6 are ameliorated by a calorie-restricted diet in old rhesus monkeys. *Neuroimage* 2010 July 1;51(3):987-94.
- (144) McCabe C, Gallagher L, Gsell W, Graham D, Dominiczak AF, Macrae IM. Differences in the evolution of the ischemic penumbra in stroke-prone spontaneously hypertensive and Wistar-Kyoto rats. *Stroke* 2009 December;40(12):3864-8.
- (145) Bhagat YA, Emery DJ, Shuaib A, Sher F, Rizvi NH, Akhtar N, Clare TL, Leatherdale T, Beaulieu C. The relationship between diffusion anisotropy and time of onset after stroke. *J Cereb Blood Flow Metab* 2006 November;26(11):1442-50.
- (146) Moseley ME, Cohen Y, Mintorovitch J, Chileuitt L, Shimizu H, Kucharczyk J, Wendland MF, Weinstein PR. Early detection of regional cerebral ischemia in cats: comparison of diffusion- and T2-weighted MRI and spectroscopy. *Magn Reson Med* 1990 May;14(2):330-46.
- (147) Konishi J, Yamada K, Kizu O, Ito H, Sugimura K, Yoshikawa K, Nakagawa M, Nishimura T. MR tractography for the evaluation of functional recovery from lenticulostriate infarcts. *Neurology* 2005 January 11;64(1):108-13.
- (148) Pierpaoli C, Barnett A, Pajevic S, Chen R, Penix LR, Virta A, Basser P. Water diffusion changes in Wallerian degeneration and their dependence on white matter architecture. *Neuroimage* 2001 June;13(6 Pt 1):1174-85.
- (149) Ward NS, Newton JM, Swayne OBC, Lee L, Thompson AJ, Greenwood RJ, Rothwell JC, Frackowiak RSJ. Motor system activation after subcortical stroke depends on corticospinal system integrity. *Brain* 2006;129(3):809-19.
- (150) Cho SH, Kim SH, Choi BY, Cho SH, Kang JH, Lee CH, Byun WM, Jang SH. Motor outcome according to diffusion tensor tractography findings in the early stage of intracerebral hemorrhage. *Neurosci Lett* 2007;421(2):142-6.
- (151) Cho SH, Kim DG, Kim DS, Kim YH, Lee CH, Jang SH. Motor outcome according to the integrity of the corticospinal tract determined by diffusion tensor tractography in the early stage of corona radiata infarct. *Neurosci Lett* 2007;426(2):123-7.

- (152) Rovaris M, Gass A, Bammer R, Hickman SJ, Ciccarelli O, Miller DH, Filippi M. Diffusion MRI in multiple sclerosis. *Neurology* 2005;65(10):1526-32.
- (153) Lin F, Yu C, Jiang T, Li K, Chan P. Diffusion tensor tractography-based group mapping of the pyramidal tract in relapsing-remitting multiple sclerosis patients. *American Journal of Neuroradiology* 2007;28(2):278-82.
- (154) Pagani E, Filippi M, Rocca MA, Horsfield MA. A method for obtaining tract-specific diffusion tensor MRI measurements in the presence of disease: Application to patients with clinically isolated syndromes suggestive of multiple sclerosis. *Neuroimage* 2005;26(1):258-65.
- (155) Widjaja E, Blaser S, Miller E, Kassner A, Shannon P, Chuang SH, Snead III OC, Raybaud CR. Evaluation of subcortical white matter and deep white matter tracts in malformations of cortical development. *Epilepsia* 2007;48(8):1460-9.
- (156) Concha L, Beaulieu C, Gross DW. Bilateral limbic diffusion abnormalities in unilateral temporal lobe epilepsy. *Ann Neurol* 2005;57(2):188-96.
- (157) Powell HWR, Parker GJM, Alexander DC, Symms MR, Boulby PA, Wheeler-Kingshott CAM, Barker GJ, Koepp MJ, Duncan JS. Abnormalities of language networks in temporal lobe epilepsy. *Neuroimage* 2007;36(1):209-21.
- (158) Giorgio A, Watkins KE, Douaud G, James AC, James S, De SN, Matthews PM, Smith SM, Johansen-Berg H. Changes in white matter microstructure during adolescence. *Neuroimage* 2008 January 1;39(1):52-61.
- (159) Cascio C, Styner M, Smith RG, Poe MD, Gerig G, Hazlett HC, Jomier M, Bammer R, Piven J. Reduced relationship to cortical white matter volume revealed by tractography-based segmentation of the corpus callosum in young children with developmental delay. *Am J Psychiatry* 2006 December;163(12):2157-63.
- (160) Huppi PS, Dubois J. Diffusion tensor imaging of brain development. *Semin Fetal Neonatal Med* 2006 December;11(6):489-97.
- (161) Thomas B, Eyssen M, Peeters R, Molenaers G, Van HP, De CP, Sunaert S. Quantitative diffusion tensor imaging in cerebral palsy due to periventricular white matter injury. *Brain* 2005 November;128(Pt 11):2562-77.
- (162) Borroni B, Brambati SM, Agosti C, Gipponi S, Bellelli G, Gasparotti R, Garibotto V, Di Luca M, Scifo P, Perani D, Padovani A. Evidence of white matter changes on diffusion tensor imaging in frontotemporal dementia. *Arch Neurol* 2007;64(2):246-51.
- (163) Catani M, Piccirilli M, Cherubini A, Tarducci R, Sciarra T, Gobbi G, Pelliccioli G, Petrillo SM, Senin U, Mecocci P. Axonal injury within language network in primary progressive aphasia. *Ann Neurol* 2003;53(2):242-7.
- (164) Catani M. Diffusion tensor magnetic resonance imaging tractography in cognitive disorders. *Curr Opin Neurol* 2006;19(6):599-606.

- (165) Song SK, Kim JH, Lin SJ, Brendza RP, Holtzman DM. Diffusion tensor imaging detects age-dependent white matter changes in a transgenic mouse model with amyloid deposition. *Neurobiol Dis* 2004;15(3):640-7.
- (166) Nilsson C, Markenroth Bloch K, Brockstedt S, Långström J, Widner H, Larsson EM. Tracking the neurodegeneration of parkinsonian disorders - A pilot study. *Neuroradiology* 2007;49(2):111-9.
- (167) Bammer R, Acar B, Moseley ME. In vivo MR tractography using diffusion imaging. *Eur J Radiol* 2003 March;45(3):223-34.
- (168) Basser PJ, Mattiello J, LeBihan D. Estimation of the effective self-diffusion tensor from the NMR spin echo. *J Magn Reson B* 1994 March;103(3):247-54.
- (169) Basser PJ, Mattiello J, LeBihan D. MR diffusion tensor spectroscopy and imaging. *Biophys J* 1994 January;66(1):259-67.
- (170) Burdette JH, Elster AD, Ricci PE. Calculation of apparent diffusion coefficients (ADCs) in brain using two-point and six-point methods. *J Comput Assist Tomogr* 1998 September;22(5):792-4.
- (171) Haselgrove JC, Moore JR. Correction for distortion of echo-planar images used to calculate the apparent diffusion coefficient. *Magn Reson Med* 1996 December;36(6):960-4.
- (172) Woods RP, Cherry SR, Mazziotta JC. Rapid automated algorithm for aligning and reslicing PET images. *J Comput Assist Tomogr* 1992;16(4):620-33.
- (173) Clark CA, Barrick TR, Murphy MM, Bell BA. White matter fiber tracking in patients with space-occupying lesions of the brain: A new technique for neurosurgical planning? *Neuroimage* 2003;20(3):1601-8.
- (174) Basser PJ, Mattiello J, LeBihan D. Estimation of the effective self-diffusion tensor from the NMR spin echo. *J Magn Reson B* 1994 March;103(3):247-54.
- (175) Rorden C. MRICro. <http://www.mricro.com>.
- (176) Douek P, Turner R, Pekar J, Patronas N, Le Bihan D. MR color mapping of myelin fiber orientation. *J Comput Assist Tomogr* 1991 November;15(6):923-9.
- (177) Basser PJ, Pajevic S, Pierpaoli C, Duda J, Aldroubi A. In vivo fiber tractography using DT-MRI data. *Magn Reson Med* 2000 October;44(4):625-32.
- (178) Clark CA, Barrick TR, Murphy MM, Bell BA. White matter fiber tracking in patients with space-occupying lesions of the brain: a new technique for neurosurgical planning? *Neuroimage* 2003 November;20(3):1601-8.
- (179) Jones DK, Simmons A, Williams SC, Horsfield MA. Non-invasive assessment of axonal fiber connectivity in the human brain via diffusion tensor MRI. *Magn Reson Med* 1999 July;42(1):37-41.

- (180) Poupon C, Clark CA, Frouin V, Regis J, Bloch I, Le Bihan D, Mangin J. Regularization of diffusion-based direction maps for the tracking of brain white matter fascicles. *Neuroimage* 2000 August;12(2):184-95.
- (181) Mori S, Frederiksen K, van Zijl PC, Stieltjes B, Kraut MA, Solaiyappan M, Pomper MG. Brain white matter anatomy of tumor patients evaluated with diffusion tensor imaging. *Ann Neurol* 2002 March;51(3):377-80.
- (182) Mori S, Kaufmann WE, Davatzikos C, Stieltjes B, Amodei L, Fredericksen K, Pearlson GD, Melhem ER, Solaiyappan M, Raymond GV, Moser HW, van Zijl PC. Imaging cortical association tracts in the human brain using diffusion-tensor-based axonal tracking. *Magn Reson Med* 2002 February;47(2):215-23.
- (183) Becker LE. Pathology of pediatric brain tumors. *Neuroimaging Clin N Am* 1999 November;9(4):671-90.
- (184) Lunsford LD, Martinez AJ. Stereotactic exploration of the brain in the era of computed tomography. *Surg Neurol* 1984 September;22(3):222-30.
- (185) Hall WA, Liu H, Martin AJ, Truwit CL. Comparison of stereotactic brain biopsy to interventional magnetic-resonance-imaging-guided brain biopsy. *Stereotact Funct Neurosurg* 1999;73(1-4):148-53.
- (186) Field M, Witham TF, Flickinger JC, Kondziolka D, Lunsford LD. Comprehensive assessment of hemorrhage risks and outcomes after stereotactic brain biopsy. *J Neurosurg* 2001 April;94(4):545-51.
- (187) Bernstein M, Parrent AG. Complications of CT-guided stereotactic biopsy of intra-axial brain lesions. *J Neurosurg* 1994 August;81(2):165-8.
- (188) Soo TM, Bernstein M, Provias J, Tasker R, Lozano A, Guha A. Failed stereotactic biopsy in a series of 518 cases. *Stereotact Funct Neurosurg* 1995;64(4):183-96.
- (189) Zheng PP, Hop WC, Sillevius Smitt PA, van den Bent MJ, Avezaat CJ, Luider TM, Kros JM. Low-molecular weight caldesmon as a potential serum marker for glioma. *Clin Cancer Res* 2005 June 15;11(12):4388-92.
- (190) Ludemann L, Grieger W, Wurm R, Budzisch M, Hamm B, Zimmer C. Comparison of dynamic contrast-enhanced MRI with WHO tumor grading for gliomas. *Eur Radiol* 2001;11(7):1231-41.
- (191) Wong TZ, van der Westhuizen GJ, Coleman RE. Positron emission tomography imaging of brain tumors. *Neuroimaging Clin N Am* 2002 November;12(4):615-26.
- (192) Howe FA, Barton SJ, Cudlip SA, Stubbs M, Saunders DE, Murphy M, Wilkins P, Opstad KS, Doyle VL, McLean MA, Bell BA, Griffiths JR. Metabolic profiles of human brain tumors using quantitative in vivo <sup>1</sup>H magnetic resonance spectroscopy. *Magn Reson Med* 2003 February;49(2):223-32.
- (193) Sartor K. MR imaging of the brain: tumors. *Eur Radiol* 1999;9(6):1047-54.

- (194) Jenkinson MD, Du Plessis DG, Walker C, Smith TS. Advanced MRI in the management of adult gliomas. *Br J Neurosurg* 2007 December;21(6):550-61.
- (195) Hartmann M, Heiland S, Sartor K. [Functional MRI procedures in the diagnosis of brain tumors: Perfusion- and diffusion-weighted imaging]. *Rofo* 2002 August;174(8):955-64.
- (196) Essig M, Weber MA, von Tengge-Kobligk H, Knopp MV, Yuh WT, Giesel FL. Contrast-enhanced magnetic resonance imaging of central nervous system tumors: agents, mechanisms, and applications. *Top Magn Reson Imaging* 2006 April;17(2):89-106.
- (197) Rumboldt Z, Camacho DL, Lake D, Welsh CT, Castillo M. Apparent diffusion coefficients for differentiation of cerebellar tumors in children. *AJNR Am J Neuroradiol* 2006 June;27(6):1362-9.
- (198) Higano S, Tamura H, Mugikura S, Umetsu A, Takahashi S. [Usefulness of MR diffusion imaging for evaluating brain tumors]. *Nippon Hoshasen Gijutsu Gakkai Zasshi* 2004 October;60(10):1351-60.
- (199) Gupta RK, Cloughesy TF, Sinha U, Garakian J, Lazareff J, Rubino G, Rubino L, Becker DP, Vinters HV, Alger JR. Relationships between choline magnetic resonance spectroscopy, apparent diffusion coefficient and quantitative histopathology in human glioma. *J Neurooncol* 2000 December;50(3):215-26.
- (200) Guo AC, Cummings TJ, Dash RC, Provenzale JM. Lymphomas and high-grade astrocytomas: comparison of water diffusibility and histologic characteristics. *Radiology* 2002 July;224(1):177-83.
- (201) Kan P, Liu JK, Hedlund G, Brockmeyer DL, Walker ML, Kestle JR. The role of diffusion-weighted magnetic resonance imaging in pediatric brain tumors. *Childs Nerv Syst* 2006 November;22(11):1435-9.
- (202) Humphries PD, Sebire NJ, Siegel MJ, Olsen OE. Tumors in pediatric patients at diffusion-weighted MR imaging: apparent diffusion coefficient and tumor cellularity. *Radiology* 2007 December;245(3):848-54.
- (203) Gupta RK, Sinha U, Cloughesy TF, Alger JR. Inverse correlation between choline magnetic resonance spectroscopy signal intensity and the apparent diffusion coefficient in human glioma. *Magn Reson Med* 1999 January;41(1):2-7.
- (204) Eis M, Els T, Hoehn-Berlage M, Hossmann KA. Quantitative diffusion MR imaging of cerebral tumor and edema. *Acta Neurochir Suppl (Wien)* 1994;60:344-6.
- (205) Calvar JA, Meli FJ, Romero C, Calcagno ML, Yanez P, Martinez AR, Lambre H, Taratuto AL, Sevlever G. Characterization of brain tumors by MRS, DWI and Ki-67 labeling index. *J Neurooncol* 2005 May;72(3):273-80.
- (206) Bulakbasi N, Guvenc I, Onguru O, Erdogan E, Tayfun C, Ucoz T. The added value of the apparent diffusion coefficient calculation to magnetic resonance imaging in the differentiation and grading of malignant brain tumors. *J Comput Assist Tomogr* 2004 November;28(6):735-46.

- (207) Server A, Kulle B, Maehlen J, Josefsen R, Schellhorn T, Kumar T, Langberg CW, Nakstad PH. Quantitative Apparent Diffusion Coefficients in the Characterization of Brain Tumors and Associated Peritumoral Edema. *Acta Radiol* 2009 May 15;1-8.
- (208) Schneider JF, Confort-Gouny S, Viola A, Le FY, Viout P, Bennathan M, Chapon F, Figarella-Branger D, Cozzone P, Girard N. Multiparametric differentiation of posterior fossa tumors in children using diffusion-weighted imaging and short echo-time (1)H-MR spectroscopy. *J Magn Reson Imaging* 2007 October 29.
- (209) Tozer DJ, Jager HR, Danchaivijitr N, Benton CE, Tofts PS, Rees JH, Waldman AD. Apparent diffusion coefficient histograms may predict low-grade glioma subtype. *NMR Biomed* 2007 February;20(1):49-57.
- (210) Pope WB, Kim HJ, Huo J, Alger J, Brown MS, Gjertson D, Sai V, Young JR, Tekchandani L, Cloughesy T, Mischel PS, Lai A, Nghiemphu P, Rahmanuddin S, Goldin J. Recurrent glioblastoma multiforme: ADC histogram analysis predicts response to bevacizumab treatment. *Radiology* 2009 July;252(1):182-9.
- (211) Fenton LZ, Foreman NK. Atypical teratoid/rhabdoid tumor of the central nervous system in children: an atypical series and review. *Pediatr Radiol* 2003 August;33(8):554-8.
- (212) Chen ML, McComb JG, Krieger MD. Atypical teratoid/rhabdoid tumors of the central nervous system: management and outcomes. *Neurosurg Focus* 2005 June 15;18(6A):E8.
- (213) Rorke LB, Packer RJ, Biegel JA. Central nervous system atypical teratoid/rhabdoid tumors of infancy and childhood: definition of an entity. *J Neurosurg* 1996 July;85(1):56-65.
- (214) Koral K, Gargan L, Bowers DC, Gimi B, Timmons CF, Weprin B, Rollins NK. Imaging characteristics of atypical teratoid-rhabdoid tumor in children compared with medulloblastoma. *AJR Am J Roentgenol* 2008 March;190(3):809-14.
- (215) Arslanoglu A, Aygun N, Tekhtani D, Aronson L, Cohen K, Burger PC, Yousem DM. Imaging findings of CNS atypical teratoid/rhabdoid tumors. *AJNR Am J Neuroradiol* 2004 March;25(3):476-80.
- (216) Chen YW, Wong TT, Ho DM, Huang PI, Chang KP, Shiau CY, Yen SH. Impact of radiotherapy for pediatric CNS atypical teratoid/rhabdoid tumor (single institute experience). *Int J Radiat Oncol Biol Phys* 2006 March 15;64(4):1038-43.
- (217) Plummer D. DispImage a display and analysis tool for medical images. Proceedings of study group on artificial intelligence in radiology. *Riv Neuroradiol* 1992;5:489-95.
- (218) Tofts PS DGD. Histograms: measuring subtle diffuse disease. In *Quantitative MRI of the Brain*. Tofts PS (ed.). Wiley: Chichester, 2003; 581-610. In: Tofts PS e, editor. *Quantitative MRI of the Brain*. Wiley: Chichester; 2003. p. 581-610.
- (219) Athale UH, Duckworth J, Odame I, Barr R. Childhood atypical teratoid rhabdoid tumor of the central nervous system: a meta-analysis of observational studies. *J Pediatr Hematol Oncol* 2009 September;31(9):651-63.



- (220) Hilden JM, Meerbaum S, Burger P, Finlay J, Janss A, Scheithauer BW, Walter AW, Rorke LB, Biegel JA. Central nervous system atypical teratoid/rhabdoid tumor: results of therapy in children enrolled in a registry. *J Clin Oncol* 2004 July 15;22(14):2877-84.
- (221) Lefkowitz IB. Atypical teratoid rhabdoid tumor of infancy: definition of an entity. *Annals of Neurology* 22, 448-449. 1987. 20-11-2009.  
Ref Type: Abstract
- (222) Bruch LA, Hill DA, Cai DX, Levy BK, Dehner LP, Perry A. A role for fluorescence in situ hybridization detection of chromosome 22q dosage in distinguishing atypical teratoid/rhabdoid tumors from medulloblastoma/central primitive neuroectodermal tumors. *Hum Pathol* 2001 February;32(2):156-62.
- (223) Lopez-Gines C, Cerda-Nicolas M, Kepes J, Donat J, Gil-Benso R, Llombart-Bosch A. Complex rearrangement of chromosomes 6 and 11 as the sole anomaly in atypical teratoid/rhabdoid tumors of the central nervous system. *Cancer Genet Cytogenet* 2000 October 15;122(2):149-52.
- (224) Biegel JA, Fogelgren B, Zhou JY, James CD, Janss AJ, Allen JC, Zagzag D, Raffel C, Rorke LB. Mutations of the INI1 rhabdoid tumor suppressor gene in medulloblastomas and primitive neuroectodermal tumors of the central nervous system. *Clin Cancer Res* 2000 July;6(7):2759-63.
- (225) Judkins AR, Mauger J, Ht A, Rorke LB, Biegel JA. Immunohistochemical analysis of hSNF5/INI1 in pediatric CNS neoplasms. *Am J Surg Pathol* 2004 May;28(5):644-50.
- (226) Burger PC, Yu IT, Tihan T, Friedman HS, Strother DR, Kepner JL, Duffner PK, Kun LE, Perlman EJ. Atypical teratoid/rhabdoid tumor of the central nervous system: a highly malignant tumor of infancy and childhood frequently mistaken for medulloblastoma: a Pediatric Oncology Group study. *Am J Surg Pathol* 1998 September;22(9):1083-92.
- (227) Zuccoli G, Izzi G, Bacchini E, Tondelli MT, Ferrozzi F, Bellomi M. Central nervous system atypical teratoid/rhabdoid tumour of infancy. CT and mr findings. *Clin Imaging* 1999 November;23(6):356-60.
- (228) Niwa T, Aida N, Tanaka M, Okubo J, Sasano M, Shishikura A, Fujita K, Ito S, Tanaka Y, Kigasawa H. Diffusion-weighted imaging of an atypical teratoid/rhabdoid tumor of the cervical spine. *Magn Reson Med Sci* 2009;8(3):135-8.
- (229) Smith MA, Freidlin B, Ries LA, Simon R. Trends in reported incidence of primary malignant brain tumors in children in the United States. *J Natl Cancer Inst* 1998 September 2;90(17):1269-77.
- (230) Arora RS, Alston RD, Eden TO, Estlin EJ, Moran A, Birch JM. Age-incidence patterns of primary CNS tumors in children, adolescents, and adults in England. *Neuro Oncol* 2009 August;11(4):403-13.
- (231) Wang S, Kim S, Chawla S, Wolf RL, Zhang WG, O'Rourke DM, Judy KD, Melhem ER, Poptani H. Differentiation between glioblastomas and solitary brain metastases using diffusion tensor imaging. *Neuroimage* 2009 February 1;44(3):653-60.

- (232) Meyers SP, Khademian ZP, Biegel JA, Chuang SH, Korones DN, Zimmerman RA. Primary intracranial atypical teratoid/rhabdoid tumors of infancy and childhood: MRI features and patient outcomes. *AJNR Am J Neuroradiol* 2006 May;27(5):962-71.
- (233) Rollin N, Guyotat J, Streichenberger N, Honnorat J, Tran M, V, Cotton F. Clinical relevance of diffusion and perfusion magnetic resonance imaging in assessing intra-axial brain tumors. *Neuroradiology* 2006 March;48(3):150-9.
- (234) Gross DW, Bastos A, Beaulieu C. Diffusion tensor imaging abnormalities in focal cortical dysplasia. *Can J Neurol Sci* 2005 November;32(4):477-82.
- (235) Lee SK, Kim DI, Kim J, Kim DJ, Kim HD, Kim DS, Mori S. Diffusion-tensor MR imaging and fiber tractography: a new method of describing aberrant fiber connections in developmental CNS anomalies. *Radiographics* 2005 January;25(1):53-65.
- (236) Rollins N, Reyes T, Chia J. Diffusion tensor imaging in lissencephaly. *AJNR Am J Neuroradiol* 2005 June;26(6):1583-6.
- (237) Rollins NK. Clinical applications of diffusion tensor imaging and tractography in children. *Pediatr Radiol* 2007 August;37(8):769-80.
- (238) Albayram S, Melhem ER, Mori S, Zinreich SJ, Barkovich AJ, Kinsman SL. Holoprosencephaly in children: diffusion tensor MR imaging of white matter tracts of the brainstem--initial experience. *Radiology* 2002 June;223(3):645-51.
- (239) Hahn JS, Barnes PD, Clegg NJ, Stashinko EE. Septopreoptic Holoprosencephaly: A Mild Subtype Associated with Midline Craniofacial Anomalies. *AJNR Am J Neuroradiol* 2010 May 20.
- (240) Sarikaya B. MR tractography of schizencephaly. *Diagn Interv Radiol* 2009 December 16.
- (241) Widjaja E, Geibprasert S, Blaser S, Rayner T, Shannon P. Abnormal fetal cerebral laminar organization in cobblestone complex as seen on post-mortem MRI and DTI. *Pediatr Radiol* 2009 August;39(8):860-4.
- (242) Rugg-Gunn FJ, Eriksson SH, Symms MR, Barker GJ, Thom M, Harkness W, Duncan JS. Diffusion tensor imaging in refractory epilepsy. *Lancet* 2002 May 18;359(9319):1748-51.
- (243) Bhardwaj RD, Mahmoodabadi SZ, Otsubo H, Snead OC, III, Rutka JT, Widjaja E. Diffusion tensor tractography detection of functional pathway for the spread of epileptiform activity between temporal lobe and Rolandic region. *Childs Nerv Syst* 2010 February;26(2):185-90.
- (244) Duning T, Kellinghaus C, Mohammadi S, Schiffbauer H, Keller S, Ringelstein EB, Knecht S, Deppe M. Individual white matter fractional anisotropy analysis on patients with MRI negative partial epilepsy. *J Neurol Neurosurg Psychiatry* 2010 February;81(2):136-9.

- (245) Eliassen JC, Boespflug EL, Lamy M, Allendorfer J, Chu WJ, Szaflarski JP. Brain-mapping techniques for evaluating poststroke recovery and rehabilitation: a review. *Top Stroke Rehabil* 2008 September;15(5):427-50.
- (246) Khong PL, Tse C, Wong IY, Lam BC, Cheung PT, Goh WH, Kwong NS, Ooi GC. Diffusion-weighted imaging and proton magnetic resonance spectroscopy in perinatal hypoxic-ischemic encephalopathy: association with neuromotor outcome at 18 months of age. *J Child Neurol* 2004 November;19(11):872-81.
- (247) Kinoshita M, Hashimoto N, Goto T, Kagawa N, Kishima H, Izumoto S, Tanaka H, Fujita N, Yoshimine T. Fractional anisotropy and tumor cell density of the tumor core show positive correlation in diffusion tensor magnetic resonance imaging of malignant brain tumors. *Neuroimage* 2008 October 15;43(1):29-35.
- (248) Vishwas MS, Chitnis T, Pienaar R, Healy BC, Grant PE. Tract-based analysis of callosal, projection, and association pathways in pediatric patients with multiple sclerosis: a preliminary study. *AJNR Am J Neuroradiol* 2010 January;31(1):121-8.
- (249) van Engelen SJ, Krab LC, Moll HA, de Goede-Bolder A, Pluijm SM, Catsman-Berrevoets CE, Elgersma Y, Lequin MH. Quantitative differentiation between healthy and disordered brain matter in patients with neurofibromatosis type I using diffusion tensor imaging. *AJNR Am J Neuroradiol* 2008 April;29(4):816-22.
- (250) Piao C, Yu A, Li K, Wang Y, Qin W, Xue S. Cerebral diffusion tensor imaging in tuberous sclerosis. *Eur J Radiol* 2009 August;71(2):249-52.
- (251) Salamon N, Sicotte N, Drain A, Frew A, Alger JR, Jen J, Perlman S, Salamon G. White matter fiber tractography and color mapping of the normal human cerebellum with diffusion tensor imaging. *J Neuroradiol* 2007 May;34(2):115-28.
- (252) Widjaja E, Blaser S, Raybaud C. Diffusion tensor imaging of midline posterior fossa malformations. *Pediatr Radiol* 2006 June;36(6):510-7.
- (253) Voigt J, Pakkenberg H. Brain weight of Danish children. A forensic material. *Acta Anat (Basel)* 1983;116(4):290-301.
- (254) Saksena S, Husain N, Malik GK, Trivedi R, Sarma M, Rathore RS, Pandey CM, Gupta RK. Comparative evaluation of the cerebral and cerebellar white matter development in pediatric age group using quantitative diffusion tensor imaging. *Cerebellum* 2008;7(3):392-400.
- (255) Beaton AA. The nature and determinants of Handedness. In: Richard J. Davidson, Kenneth Hugdahl, editors. *The Asymmetrical Brain*. Cambridge, MA: MIT Press; 2003.
- (256) McManus C. *Right Hand, Left Hand*. London: Weidenfeld & Nicolson; 2002.
- (257) Knecht S, Deppe M, Dräger B, Bobe L, Lohmann H, Ringelstein E, Henningsen H. Language lateralization in healthy right-handers. *Brain* 2000 January;123 ( Pt 1):74-81.

- (258) Witelson SF, Kigar DL. Sylvian fissure morphology and asymmetry in men and women: bilateral differences in relation to handedness in men. *J Comp Neurol* 1992 September 15;323(3):326-40.
- (259) Hu D, Shen H, Zhou Z. Functional asymmetry in the cerebellum: A brief review. *Cerebellum* 2007 August 13;1-10.
- (260) Kawashima R, Matsumura M, Sadato N, Naito E, Waki A, Nakamura S, Matsunami K, Fukuda H, Yonekura Y. Regional cerebral blood flow changes in human brain related to ipsilateral and contralateral complex hand movements--a PET study. *Eur J Neurosci* 1998 July;10(7):2254-60.
- (261) Snyder PJ, Bilder RM, Wu H, Bogerts B, Lieberman JA. Cerebellar volume asymmetries are related to handedness: a quantitative MRI study. *Neuropsychologia* 1995 April;33(4):407-19.
- (262) Szeszko PR, Gunning-Dixon F, Ashtari M, Snyder PJ, Lieberman JA, Bilder RM. Reversed cerebellar asymmetry in men with first-episode schizophrenia. *Biol Psychiatry* 2003 March 1;53(5):450-9.
- (263) Warren E, McKinlay I. Handedness in children at school entry: does the 'Mesker test' provide a valid method for testing writing handedness? *Child Care Health Dev* 1993 March;19(2):127-43.
- (264) Johanna B.Sattler. *Das linkshändige Kind in der Grundschule*. Munich: Auer; 2009.
- (265) Aldroubi A, Basser PJ. Reconstruction of vector and tensor fields from sampled discrete data. In: L.W.Baggett and D.R.Larson, editor. *Contemporary Mathematics*. Providence: 1999. p. 1-15.
- (266) Geomview [computer program]. Geometry Center, University of Minnesota, MI, USA; 2006.
- (267) Han Y, Yang H, Lv YT, Zhu CZ, He Y, Tang HH, Gong QY, Luo YJ, Zang YF, Dong Q. Gray matter density and white matter integrity in pianists' brain: a combined structural and diffusion tensor MRI study. *Neurosci Lett* 2009 July 31;459(1):3-6.
- (268) Itoh D, Aoki S, Maruyama K, Masutani Y, Mori H, Masumoto T, Abe O, Hayashi N, Okubo T, Ohtomo K. Corticospinal tracts by diffusion tensor tractography in patients with arteriovenous malformations. *J Comput Assist Tomogr* 2006 July;30(4):618-23.
- (269) Maruyama K, Kamada K, Shin M, Itoh D, Masutani Y, Ino K, Tago M, Saito N. Optic radiation tractography integrated into simulated treatment planning for Gamma Knife surgery. *J Neurosurg* 2007;107(4):721-6.
- (270) Yamada K, Kizu O, Mori S, Ito H, Nakamura H, Yuen S, Kubota T, Tanaka O, Akada W, Sasajima H, Mineura K, Nishimura T. Brain fiber tracking with clinically feasible diffusion-tensor MR imaging: initial experience. *Radiology* 2003 April;227(1):295-301.
- (271) Kikuta KI, Takagi Y, Nozaki K, Hanakawa T, Okada T, Miki Y, Fushimi Y, Fukuyama H, Hashimoto N. Early experience with 3-T magnetic resonance

- tractography in the surgery of cerebral arteriovenous malformations in and around the visual pathway. *Neurosurgery* 2006;58(2):331-7.
- (272) Okada T, Mikuni N, Miki Y, Kikuta KI, Urayama SI, Hanakawa T, Fushimi Y, Yamamoto A, Kanagaki M, Fukuyama H, Hashimoto N, Togashi K. Corticospinal tract localization: Integration of diffusion-tensor tractography at 3-T MR imaging with intraoperative white matter stimulation mapping - Preliminary results. *Radiology* 2006;240(3):849-57.
- (273) CROVITZ HF, ZENER K. A group-test for assessing hand- and eye-dominance. *The American journal of psychology* 1962;75:271-6.
- (274) Wisoff JH, Boyett JM, Berger MS, Brant C, Li H, Yates AJ, Guire-Cullen P, Turski PA, Sutton LN, Allen JC, Packer RJ, Finlay JL. Current neurosurgical management and the impact of the extent of resection in the treatment of malignant gliomas of childhood: a report of the Children's Cancer Group trial no. CCG-945. *J Neurosurg* 1998 July;89(1):52-9.
- (275) Rutkowski S. Current treatment approaches to early childhood medulloblastoma. *Expert Rev Neurother* 2006 August;6(8):1211-21.
- (276) Schneider JH, Jr., Raffel C, McComb JG. Benign cerebellar astrocytomas of childhood. *Neurosurgery* 1992 January;30(1):58-62.
- (277) Lacroix M, Abi-Said D, Fournay DR, Gokaslan ZL, Shi W, DeMonte F, Lang FF, McCutcheon IE, Hassenbusch SJ, Holland E, Hess K, Michael C, Miller D, Sawaya R. A multivariate analysis of 416 patients with glioblastoma multiforme: prognosis, extent of resection, and survival. *J Neurosurg* 2001 August;95(2):190-8.
- (278) Karnofsky D&BJ. The Clinical Evaluation of Chemotherapeutic Agents in Cancer. In: MacLeod CM, editor. *Evaluation of Chemotherapeutic Agents*. Columbia Univ Press; 1949. p. 196.
- (279) Duffau H. Lessons from brain mapping in surgery for low-grade glioma: Insights into associations between tumour and brain plasticity. *Lancet Neurology* 2005;4(8):476-86.
- (280) Guggisberg AG, Honma SM, Findlay AM, Dalal SS, Kirsch HE, Berger MS, Nagarajan SS. Mapping functional connectivity in patients with brain lesions. *Ann Neurol* 2008 February;63(2):193-203.
- (281) Parmar H, Sitoh YY, Yeo TT. Combined magnetic resonance tractography and functional magnetic resonance imaging in evaluation of brain tumors involving the motor system. *J Comput Assist Tomogr* 2004 July;28(4):551-6.
- (282) Nimsy C, Fujita A, Ganslandt O, von KB, Fahlbusch R. Volumetric assessment of glioma removal by intraoperative high-field magnetic resonance imaging. *Neurosurgery* 2004 August;55(2):358-70.
- (283) Nimsy C, Ganslandt O, Hastreiter P, Wang R, Benner T, Sorensen AG, Fahlbusch R. Preoperative and intraoperative diffusion tensor imaging-based fiber tracking in glioma surgery. *Neurosurgery* 2005;56(1):130-7.

- (284) Mori S, Frederiksen K, Van Zijl PCM, Stieltjes B, Kraut MA, Solaiyappan M, Pomper MG. Brain white matter anatomy of tumor patients evaluated with diffusion tensor imaging. *Ann Neurol* 2002;51(3):377-80.
- (285) Mori S, Van Zijl PCM. Fiber tracking: Principles and strategies - A technical review. *NMR Biomed* 2002;15(7-8):468-80.
- (286) Witwer BP, Moftakhar R, Hasan KM, Deshmukh P, Haughton V, Field A, Arfanakis K, Noyes J, Moritz CH, Meyerand ME, Rowley HA, Alexander AL, Badie B. Diffusion-tensor imaging of white matter tracts in patients with cerebral neoplasm. *J Neurosurg* 2002 September;97(3):568-75.
- (287) Serletis D, Bernstein M. Prospective study of awake craniotomy used routinely and nonselectively for supratentorial tumors. *J Neurosurg* 2007 July;107(1):1-6.
- (288) Eisner W, Burtscher J, Bale R, Sweeney R, Koppelstatter F, Golaszewski S, Kolbitsch C, Twerdy K. Use of neuronavigation and electrophysiology in surgery of subcortically located lesions in the sensorimotor strip. *J Neurol Neurosurg Psychiatry* 2002 March;72(3):378-81.
- (289) Sanghvi DA. Recent advances in imaging of brain tumors. *Indian J Cancer* 2009 April;46(2):82-7.
- (290) Mechtler L. Neuroimaging in neuro-oncology. *Neurol Clin* 2009 February;27(1):171-201, ix.
- (291) Armstrong TS, Cohen MZ, Weinberg J, Gilbert MR. Imaging techniques in neuro-oncology. *Semin Oncol Nurs* 2004 November;20(4):231-9.
- (292) Youmans J. *Neurological Surgery*. 1995.
- (293) Holodny AI, Ollenschleger MD, Liu WC, Schulder M, Kalnin AJ. Identification of the corticospinal tracts achieved using blood-oxygen-level-dependent and diffusion functional MR imaging in patients with brain tumors. *AJNR Am J Neuroradiol* 2001 January;22(1):83-8.
- (294) Mori H, Abe O, Aoki S, Masumoto T, Yoshikawa T, Kunimatsu A, Hayashi N, Ohtomo K. Hemorrhagic brain metastases with high signal intensity on diffusion-weighted MR images. A case report. *Acta Radiol* 2002 November;43(6):563-6.
- (295) Nimsy C, Ganslandt O, Kober H, Moller M, Ulmer S, Tomandl B, Fahlbusch R. Integration of functional magnetic resonance imaging supported by magnetoencephalography in functional neuronavigation. *Neurosurgery* 1999 June;44(6):1249-55.
- (296) Parmar H, Sitoh YY, Yeo TT. Combined magnetic resonance tractography and functional magnetic resonance imaging in evaluation of brain tumors involving the motor system. *J Comput Assist Tomogr* 2004 July;28(4):551-6.
- (297) Berman JI, Berger MS, Mukherjee P, Henry RG. Diffusion-tensor imaging-guided tracking of fibers of the pyramidal tract combined with intraoperative cortical stimulation mapping in patients with gliomas. *J Neurosurg* 2004;101(1):66-72.

- (298) Wu JS, Zhou LF, Hong XN, Mao Y, Du GH. [Role of diffusion tensor imaging in neuronavigation surgery of brain tumors involving pyramidal tracts]. *Zhonghua Wai Ke Za Zhi* 2003 September;41(9):662-6.
- (299) Kinoshita M, Yamada K, Hashimoto N, Kato A, Izumoto S, Baba T, Maruno M, Nishimura T, Yoshimine T. Fiber-tracking does not accurately estimate size of fiber bundle in pathological condition: initial neurosurgical experience using neuronavigation and subcortical white matter stimulation. *Neuroimage* 2005 April 1;25(2):424-9.
- (300) Kinoshita M, Hashimoto N, Goto T, Yanagisawa T, Okita Y, Kagawa N, Kishima H, Tanaka H, Fujita N, Shimosegawa E, Hatazawa J, Yoshimine T. Use of fractional anisotropy for determination of the cut-off value in 11C-methionine positron emission tomography for glioma. *Neuroimage* 2009 April 1;45(2):312-8.
- (301) Mikuni N, Okada T, Enatsu R, Miki Y, Hanakawa T, Urayama SI, Kikuta K, Takahashi JA, Nozaki K, Fukuyama H, Hashimoto N. Clinical impact of integrated functional neuronavigation and subcortical electrical stimulation to preserve motor function during resection of brain tumors. *J Neurosurg* 2007;106(4):593-8.
- (302) Mikuni N, Okada T, Enatsu R, Miki Y, Urayama SI, Takahashi JA, Nozaki K, Fukuyama H, Hashimoto N. Clinical significance of preoperative fibre-tracking to preserve the affected pyramidal tracts during resection of brain tumours in patients with preoperative motor weakness. *J Neurol Neurosurg Psychiatry* 2007;78(7):716-21.
- (303) Berman JI, Berger MS, Chung SW, Nagarajan SS, Henry RG. Accuracy of diffusion tensor magnetic resonance imaging tractography assessed using intraoperative subcortical stimulation mapping and magnetic source imaging. *J Neurosurg* 2007 September;107(3):488-94.
- (304) Mikuni N, Okada T, Nishida N, Taki J, Enatsu R, Ikeda A, Miki Y, Hanakawa T, Fukuyama H, Hashimoto N. Comparison between motor evoked potential recording and fiber tracking for estimating pyramidal tracts near brain tumors. *J Neurosurg* 2007;106(1):128-33.
- (305) Keles GE, Lundin DA, Lamborn KR, Chang EF, Ojemann G, Berger MS. Intraoperative subcortical stimulation mapping for hemispherical peritumoral gliomas located within or adjacent to the descending motor pathways: Evaluation of morbidity and assessment of functional outcome in 294 patients. *J Neurosurg* 2004;100(3):369-75.
- (306) Beppu T, Inoue T, Kuzu Y, Ogasawara K, Ogawa A, Sasaki M. Utility of three-dimensional anisotropy contrast magnetic resonance axonography for determining condition of the pyramidal tract in glioblastoma patients with hemiparesis. *J Neurooncol* 2005;73(2):137-44.
- (307) Yu CS, Li KC, Xuan Y, Ji XM, Qin W. Diffusion tensor tractography in patients with cerebral tumors: a helpful technique for neurosurgical planning and postoperative assessment. *Eur J Radiol* 2005 November;56(2):197-204.

- (308) Hlatky R, Jackson EF, Weinberg JS, McCutcheon IE. Intraoperative neuronavigation using diffusion tensor MR tractography for the resection of a deep tumor adjacent to the corticospinal tract. *Stereotact Funct Neurosurg* 2005;83(5-6):228-32.
- (309) Nimsy C, Ganslandt O, Hastreiter P, Wang R, Benner T, Sorensen AG, Fahlbusch R. Intraoperative diffusion-tensor MR imaging: shifting of white matter tracts during neurosurgical procedures--initial experience. *Radiology* 2005 January;234(1):218-25.
- (310) Kikuta K, Takagi Y, Nozaki K, Hanakawa T, Okada T, Miki Y, Fushimi Y, Fukuyama H, Hashimoto N. Early experience with 3-T magnetic resonance tractography in the surgery of cerebral arteriovenous malformations in and around the visual pathway. *Neurosurgery* 2006 February;58(2):331-7.
- (311) Kamada K, Todo T, Masutani Y, Aoki S, Ino K, Takano T, Kirino T, Kawahara N, Morita A. Combined use of tractography-integrated functional neuronavigation and direct fiber stimulation. *J Neurosurg* 2005;102(4):664-72.
- (312) Henry RG, Berman JI, Nagarajan SS, Mukherjee P, Berger MS. Subcortical pathways serving cortical language sites: Initial experience with diffusion tensor imaging fiber tracking combined with intraoperative language mapping. *Neuroimage* 2004;21(2):616-22.
- (313) Kamada K, Todo T, Masutani Y, Aoki S, Ino K, Morita A, Saito N. Visualization of the frontotemporal language fibers by tractography combined with functional magnetic resonance imaging and magnetoencephalography. *J Neurosurg* 2007;106(1):90-8.
- (314) Moller M, Frandsen J, Andersen G, Gjedde A, Vestergaard-Poulsen P, Ostergaard L. Dynamic changes in corticospinal tracts after stroke detected by fibretracking. *J Neurol Neurosurg Psychiatry* 2007 June;78(6):587-92.
- (315) Kim J, Lee SK, Lee JD, Kim YW, Kim DI. Decreased fractional anisotropy of middle cerebellar peduncle in crossed cerebellar diaschisis: diffusion-tensor imaging-positron-emission tomography correlation study. *AJNR Am J Neuroradiol* 2005 October;26(9):2224-8.
- (316) Lui YW, Law M, Chacko-Mathew J, Babb JS, Tuvia K, Allen JC, Zagzag D, Johnson G. Brainstem corticospinal tract diffusion tensor imaging in patients with primary posterior fossa neoplasms stratified by tumor type: a study of association with motor weakness and outcome. *Neurosurgery* 2007 December;61(6):1199-207.
- (317) Gaetz W, Scantlebury N, Widjaja E, Rutka J, Bouffet E, Rockel C, Dockstader C, Mabbott D. Mapping of the cortical spinal tracts using magnetoencephalography and diffusion tensor tractography in pediatric brain tumor patients. *Childs Nerv Syst* 2010 June 8.
- (318) Prakash N, Hageman N, Hua X, Toga AW, Perlman SL, Salamon N. Patterns of fractional anisotropy changes in white matter of cerebellar peduncles distinguish spinocerebellar ataxia-1 from multiple system atrophy and other ataxia syndromes. *Neuroimage* 2009 August;47 Suppl 2:T72-T81.



- (319) Holodny AI, Schwartz TH, Ollenschleger M, Liu WC, Schulder M. Tumor involvement of the corticospinal tract: diffusion magnetic resonance tractography with intraoperative correlation. *J Neurosurg* 2001 December;95(6):1082.
- (320) Field AS, Alexander AL, Wu YC, Hasan KM, Witwer B, Badie B. Diffusion tensor eigenvector directional color imaging patterns in the evaluation of cerebral white matter tracts altered by tumor. *J Magn Reson Imaging* 2004 October;20(4):555-62.
- (321) Wu YC, Field AS, Chung MK, Badie B, Alexander AL. Quantitative analysis of diffusion tensor orientation: theoretical framework. *Magn Reson Med* 2004 November;52(5):1146-55.
- (322) Wakana S, Caprihan A, Panzenboeck MM, Fallon JH, Perry M, Gollub RL, Hua K, Zhang J, Jiang H, Dubey P, Blitz A, van Zijl P, Mori S. Reproducibility of quantitative tractography methods applied to cerebral white matter. *Neuroimage* 2007;36(3):630-44.
- (323) Laundre BJ, Jellison BJ, Badie B, Alexander AL, Field AS. Diffusion tensor imaging of the corticospinal tract before and after mass resection as correlated with clinical motor findings: preliminary data. *AJNR Am J Neuroradiol* 2005 April;26(4):791-6.
- (324) Kim CH, Chung CK, Kim JS, Jahng TA, Lee JH, Song IC. Use of diffusion tensor imaging to evaluate weakness. *J Neurosurg* 2007 January;106(1):111-8.
- (325) Reich DS, Zackowski KM, Gordon-Lipkin EM, Smith SA, Chodkowski BA, Cutter GR, Calabresi PA. Corticospinal tract abnormalities are associated with weakness in multiple sclerosis. *AJNR Am J Neuroradiol* 2008 February;29(2):333-9.
- (326) Nimsy C, Ganslandt O, Merhof D, Sorensen AG, Fahlbusch R. Intraoperative visualization of the pyramidal tract by diffusion-tensor-imaging-based fiber tracking. *Neuroimage* 2006;30(4):1219-29.
- (327) Jellison BJ, Field AS, Medow J, Lazar M, Salamat MS, Alexander AL. Diffusion tensor imaging of cerebral white matter: a pictorial review of physics, fiber tract anatomy, and tumor imaging patterns. *AJNR Am J Neuroradiol* 2004 March;25(3):356-69.
- (328) Wieshmann UC, Clark CA, Symms MR, Franconi F, Barker GJ, Shorvon SD. Anisotropy of water diffusion in corona radiata and cerebral peduncle in patients with hemiparesis. *Neuroimage* 1999 August;10(2):225-30.
- (329) Gaetz W, Scantlebury N, Widjaja E, Rutka J, Bouffet E, Rockel C, Dockstader C, Mabbott D. Mapping of the cortical spinal tracts using magnetoencephalography and diffusion tensor tractography in pediatric brain tumor patients. *Childs Nerv Syst* 2010 June 8.
- (330) Boujraf S, Luypaert R, Shabana W, De ML, Sourbron S, Osteaux M. Study of pediatric brain development using magnetic resonance imaging of anisotropic diffusion. *Magn Reson Imaging* 2002 May;20(4):327-36.

- (331) Clayden JD, Bastin ME, Storkey AJ. Improved segmentation reproducibility in group tractography using a quantitative tract similarity measure. *Neuroimage* 2006 November 1;33(2):482-92.
- (332) Berman JI, Berger MS, Mukherjee P, Henry RG. Diffusion-tensor imaging-guided tracking of fibers of the pyramidal tract combined with intraoperative cortical stimulation mapping in patients with gliomas. *J Neurosurg* 2004 July;101(1):66-72.
- (333) Akai H, Mori H, Aoki S, Masutani Y, Kawahara N, Shibahara J, Ohtomo K. Diffusion tensor tractography of gliomatosis cerebri: fiber tracking through the tumor. *J Comput Assist Tomogr* 2005 January;29(1):127-9.
- (334) Albright AL, Packer RJ, Zimmerman R, Rorke LB, Boyett J, Hammond GD. Magnetic resonance scans should replace biopsies for the diagnosis of diffuse brain stem gliomas: a report from the Children's Cancer Group. *Neurosurgery* 1993 December;33(6):1026-9.
- (335) Spalice A, Nicita F, Papetti L, Ursitti F, Di BC, Parisi P, Ruggieri M, Iannetti P. Usefulness of diffusion tensor imaging and fiber tractography in neurological and neurosurgical pediatric diseases. *Childs Nerv Syst* 2010 June 16.
- (336) Clark CA, Werring DJ. Diffusion tensor imaging in spinal cord: Methods and applications - A review. *NMR Biomed* 2002;15(7-8):578-86.
- (337) Nimsky C, Ganslandt O, Fahlbusch R. Implementation of fiber tract navigation. *Neurosurgery* 2006 April;58(4 Suppl 2):ONS-303.
- (338) Field AS, Alexander AL. Diffusion tensor imaging in cerebral tumor diagnosis and therapy. *Top Magn Reson Imaging* 2004 October;15(5):315-24.
- (339) Jang SH, Ahn SH, Sakong J, Byun WM, Choi BY, Chang CH, Bai D, Son SM. Comparison of TMS and DTT for predicting motor outcome in intracerebral hemorrhage. *J Neurol Sci* 2010 March 15;290(1-2):107-11.
- (340) Yin H, Cheng SH, Zhang J, Ma L, Gao Y, Li D, Lim CC. Corticospinal tract degeneration in amyotrophic lateral sclerosis: a diffusion tensor imaging and fibre tractography study. *Ann Acad Med Singapore* 2008 May;37(5):411-5.
- (341) Ludeman NA, Berman JI, Wu YW, Jeremy RJ, Kornak J, Bartha AI, Barkovich AJ, Ferriero DM, Henry RG, Glenn OA. Diffusion tensor imaging of the pyramidal tracts in infants with motor dysfunction. *Neurology* 2008 November 18;71(21):1676-82.
- (342) Lui YW, Law M, Chacko-Mathew J, Babb JS, Tuvia K, Allen JC, Zagzag D, Johnson G. Brainstem corticospinal tract diffusion tensor imaging in patients with primary posterior fossa neoplasms stratified by tumor type: a study of association with motor weakness and outcome. *Neurosurgery* 2007 December;61(6):1199-207.
- (343) Yamada K, Kizu O, Ito H, Kubota T, Akada W, Goto M, Takada A, Konishi J, Sasajima H, Mineura K, Mori S, Nishimura T. Tractography for arteriovenous malformations near the sensorimotor cortices. *AJNR Am J Neuroradiol* 2005 March;26(3):598-602.

- (344) Hu D, Shen H, Zhou Z. Functional asymmetry in the cerebellum: a brief review. *Cerebellum* 2008;7(3):304-13.
- (345) Hong JH, Jang SH. The usefulness of DTI for estimating the state of cerebellar peduncles in cerebral infarct. *NeuroRehabilitation* 2010 January 1;26(4):299-305.
- (346) Ciccarelli O, Catani M, Johansen-Berg H, Clark C, Thompson A. Diffusion-based tractography in neurological disorders: concepts, applications, and future developments. *Lancet Neurol* 2008 August;7(8):715-27.
- (347) Ciccarelli O, Parker GJM, Toosy AT, Wheeler-Kingshott CAM, Barker GJ, Boulby PA, Miller DH, Thompson AJ. From diffusion tractography to quantitative white matter tract measures: A reproducibility study. *Neuroimage* 2003;18(2):348-59.
- (348) Schonberg T, Pianka P, Hendler T, Pasternak O, Assaf Y. Characterization of displaced white matter by brain tumors using combined DTI and fMRI. *Neuroimage* 2006 May 1;30(4):1100-11.
- (349) Staempfli P, Reischauer C, Jaermann T, Valavanis A, Kollias S, Boesiger P. Combining fMRI and DTI: A framework for exploring the limits of fMRI-guided DTI fiber tracking and for verifying DTI-based fiber tractography results. *Neuroimage* 2008;39(1):119-26.
- (350) Nimsy C, Ganslandt O, Hastreiter P, Wang R, Benner T, Sorensen AG, Fahlbusch R. Preoperative and intraoperative diffusion tensor imaging-based fiber tracking in glioma surgery. *Neurosurgery* 2007 July;61(1 Suppl):178-85.
- (351) Lo CY, Chao YP, Chou KH, Guo WY, Su JL, Lin CP. DTI-based virtual reality system for neurosurgery. Conference proceedings : Annual International Conference of the IEEE Engineering in Medicine and Biology Society IEEE Engineering in Medicine and Biology Society Conference 2007;2007:1326-9.
- (352) Siewert B, Patel MR, Mueller MF, Gaa J, Darby DG, Poser CM, Wielopolski PA, Edelman RR, Warach S. Brain lesions in patients with multiple sclerosis: detection with echo-planar imaging. *Radiology* 1995 September;196(3):765-71.
- (353) Johansen-Berg H. Structural Plasticity: Rewiring the Brain. *Curr Biol* 2007;17(4).
- (354) Aravamuthan BR, Muthusamy KA, Stein JF, Aziz TZ, Johansen-Berg H. Topography of cortical and subcortical connections of the human pedunculo-pontine and subthalamic nuclei. *Neuroimage* 2007;37(3):694-705.
- (355) Hamandi K, Powell HWR, Laufs H, Symms MR, Barker GJ, Parker GJM, Lemieux L, Duncan JS. Combined EEG-fMRI and tractography to visualise propagation of epileptic activity. *J Neurol Neurosurg Psychiatry* 2008;79(5):594-7.